Structural Geology Applied to Fractured Aquifer Characterization

Amélia João Fernandes, Alain Rouleau and Eurípedes do Amaral Vargas Junior

THE **GROUNDWATER** PROJECT

Structural Geology Applied to Fractured Aquifer Characterization

The Groundwater Project

i

Amélia João Fernandes

Senior Researcher
Environmental Research Institute
São Paulo, São Paulo, Brazil

Alain Rouleau

Professor Emeritus
University of Québec at Chicoutimi
Chicoutimi, Québec, Canada

Eurípedes do Amaral Vargas Jr.

Associate Professor
Catholic University and
Federal University of Rio de Janeiro
Rio de Janeiro, Rio de Janeiro, Brazil

Structural Geology Applied to
Fractured Aquifer Characterization

The Groundwater Project
Guelph, Ontario, Canada

Version 3, April 2023

Groundwater-Project (GW-Project) works are copyrighted and can be downloaded for free from gw-project.org↗. Anyone may use and share gw-project.org↗ links to download GW-Project's work. It is neither permissible to make GW-Project documents available on other websites nor to send copies of the documents directly to others. Kindly honor this source of free knowledge that benefits you and all those who want to learn about groundwater.

Please consider signing up for the GW-Project mailing list to stay informed about new book releases, events, and ways to participate in the GW-Project. When you sign up for our email list it helps us build a global groundwater community. Sign up↗.

Dedication

This book is dedicated to students and professionals who have or will put effort in learning and building knowledge on structural geology and its application to the characterization of aquifers, as well as to small and large communities that have to rely on fractured aquifers to supply their water needs.

Table of Contents

vii

The Groundwater Project Foreword

At the United Nations (UN) Water Summit held on December 2022, delegates agreed that statements from all major groundwater-related events will be unified in 2023 into one comprehensive groundwater message. This message will be released at the UN 2023 Water Conference, a landmark event that will bring attention at the highest international level to the importance of groundwater for the future of humanity and ecosystems. This message will bring clarity to groundwater issues to advance understanding globally of the challenges faced and actions needed to resolve the world's groundwater problems. Groundwater education is key.

The 2023 World Water Day theme *Accelerating Change* is in sync with the goal of the Groundwater Project (GW-Project). The GW-Project is a registered Canadian charity founded in 2018 and committed to the advancement of groundwater education as a means to accelerate action related to our essential groundwater resources. To this end, we create and disseminate knowledge through a unique approach: the democratization of groundwater knowledge. We act on this principle through our website gw-project.org/↗, a global platform, based on the principle that

"Knowledge should be free, and the best knowledge should be free knowledge." Anonymous

The mission of the GW-Project is to promote groundwater learning across the globe. This is accomplished by providing accessible, engaging, and high-quality educational materials—free-of-charge online and in many languages—to all who want to learn about groundwater. In short, the GW-Project provides essential knowledge and tools needed to develop groundwater sustainably for the future of humanity and ecosystems. This new type of global educational endeavor is made possible through the contributions of a dedicated international group of volunteer professionals from diverse disciplines. Academics, consultants, and retirees contribute by writing and/or reviewing the books aimed at diverse levels of readers from children to high school, undergraduate, and graduate students or professionals in the groundwater field. More than 1,000 dedicated volunteers from 127 countries and six continents are involved—and participation is growing.

Hundreds of books will be published online over the coming years, first in English and then in other languages. An important tenet of GW-Project books is a strong emphasis on visualization; with clear illustrations to stimulate spatial and critical thinking. In future, the publications will also include videos and other dynamic learning tools. Revised editions of the books are published from time to time. Users are invited to propose revisions.

We thank you for being part of the GW-Project Community. We hope to hear from you about your experience with the project materials, and welcome ideas and volunteers!

The GW-Project Steering Committee

January 2023

viii

Foreword

More than half the global population lives where fresh groundwater occurs in fractured rock, either near the surface or as aquifers beneath unconsolidated material. *Structural Geology Applied to Fractured Aquifer Characterization* presents a geological perspective on the fractures and the fracture networks in rock with a focus on groundwater. This book is important because the literature about fractured rock hydrogeology is sparse relative to that of unconsolidated deposits and karst. Groundwater in fractured rock is more complex and it is expensive to install boreholes for investigations, consequently information about fractured aquifers is limited.

This book uses structural geology to understand fractures and fracture networks. As such, to fully benefit from this book, the reader needs some knowledge of structural geology as provided in an introductory course or textbook. The authors explain how to take an organized approach to visual observations at rock outcrops, illustrated by abundant photographs and conceptual diagrams to encourage spatial thinking. Information about fracture architecture is essential for understanding rock porosity and permeability based on borehole observations and hydraulic tests. In addition to combined interpretation of fractures mapped on outcrops with borehole observations and tests, use of aerial photographs and Google Earth observations of lineaments on the land surface provide information on structural geology to better locate water wells in bedrock.

The authors of this book have conducted applied research in structural geology, rock mechanics, and groundwater in fracture networks over decades and in many countries. Dr. Amélia Fernandes is a research geologist at the Institute of Geology of the Regional Government of São Paulo State in Brazil who lectures at the Geosciences Institute, University of São Paulo, Brazil. Dr. Alain Rouleau is a Professor Emeritus of the Department of Earth Sciences, University of Québec at Chicoutimi, Canada, with a career in hydrogeology with emphasis on fractured rock. Dr. Eurípedes Vargas Jr. is a professor in the Department of Civil Engineering, Catholic University of Rio de Janeiro, Brazil, where he teaches and conducts experimental research on rock mechanics with emphasis on the hydromechanics of fractured media. Their combination of expertise and experience gives readers a unique view of groundwater in fractured rock.

John Cherry, The Groundwater Project Leader

Guelph, Ontario, Canada, December 2022

Preface

The study of fractured (hard rock) aquifers is increasingly pressing because they occupy vast areas of all continents, and the dependence on this type of aquifer for water supply is growing fast. In hard rocks, groundwater flows through void spaces that are present in fractures that form a connected network; its characterization requires knowledge of structural geology and rock mechanics. This book shows how these disciplines reveal the logical organization of a fracture network and helps to build more realistic conceptual models of groundwater systems.

The ability of hard rocks to supply water depends on the fracture connectivity and transmissivity, which are related to the size and orientation of fractures, as well as the width of the opening between fracture walls (i.e., aperture). These characteristics are constrained by the principles of structural geology and rock mechanics. This book provides insight regarding questions such as: How does the geometry of different fracture types influence fracture aperture and connectivity? How do tectonic regimes (compressive, extensional and strike slip) influence the general configuration of a fracture network? How does the brittle deformation history of a region affect the architecture and connectivity of the fracture system? How does the current in-situ stress field affect the aperture of fractures?

Different rock types such as sedimentary, volcanic, metamorphic and intrusive rocks have their own typical discontinuities and previously existing structures. These influence how the in-situ stresses contribute to developing their fracture network architectures. Conceptual models of fracture networks, their connectivity, and preferential groundwater flow pathways in different geological settings are presented and explained.

The heterogeneous distribution of fracture porosity in hard rock aquifers pose significant scientific and methodological challenges. One way of overcoming difficulties is to, when possible, conduct detailed fracture surveys on large rock exposures and apply the fundamental principles of structural geology and rock mechanics to develop a conceptual model of the fracture system. Such surveys provide an essential two- and three-dimensional complement to borehole data revealing the fracture-network geometry. As more surveys are conducted, knowledge on how fracture systems affect the groundwater flow and transport properties of rocks will gradually be expanded.

Acknowledgments

We deeply appreciate the thorough and useful reviews of and contributions to this book by the following individuals:

- ❖ Thomas Doe, Principal, Golder, a subsidiary of Williams Sale Partnership (WSP); Affiliate Instructor, Department of Civil and Environmental Engineering, University of Washington;
- ❖ Jonathan Munn, Postdoctoral Fellow, G360 Institute for Groundwater Research, University of Guelph, Guelph, Ontario, Canada;
- ❖ Marco Antonellini, Associate Professor, Department of Biological, Geological, and Environmental Sciences, University of Bologna, Bologna, Emilia-Romagna, Italy;
- ❖ Anton Lukas, Ph.D. Candidate, Institute for Groundwater Studies, University of the Free State, Bloemfontein, South Africa;
- ❖ Roger H. Morin, Research Scientist, United States Geological Survey, Denver, Colorado (retired), now living in Maine, USA;
- ❖ Derek Elsworth, Professor, Earth and Mineral Sciences, The Pennsylvania State University, Pennsylvania, USA.

1 Introduction

Knowledge of rock mechanics and structural geology reveals the logic underlying the organization of a fracture network in both space and time. This knowledge makes it apparent that the network is not random. Conceptual models of fracture networks based on rock mechanics and structural geology are able to predict fracture character and distribution that are closer to reality than networks developed by generating random fracture fields using statistical measurements.

The flow of groundwater, or any fluid, in rocks whose main permeability is due to the voids associated with fractures, depends on the configuration of the connected fracture network, as well as on the opening variable width (aperture) of the fracture voids within the network.

The connected fracture network and apertures are constrained by geological and mechanical factors, which bestow certain geometric characteristics to the network, as shown schematically in Figure 1.

CONSTRAINING FACTOR	FRACTURE NETWORK CHARACTERISTICS
1) Brittle deformation history: succession in time of fracture generation phases	- Number of fracture sets - Persistence (length) of the fractures in each set - Interaction between fractures and degree of connectivity - Aperture of the fractures in each set
2) Orientation and magnitude of the tectonic stresses at each deformational phase	- Orientation of the fracture sets - Deformation intensity - Type of fractures generated, whether joints (larger aperture) or faults (tighter)
3) Type of rock affected by the deformation: massive or with previously existing structures (e.g., foliation)	- Fracture network with distinct architectures - Density and continuity of fracture sets parallel to existing structures tend to be larger, and connectivity greater

Figure 1 - Geological and mechanical factors (left) constrain geometric fracture network characteristics (right).

This book is divided into multiple sections. Section 1 defines fractured aquifers and presents the reasons why they have to be studied. Sections 2 and 3 summarize the fundamentals of rock mechanics and structural geology in a way that intends to facilitate understanding the relationships between causes (constraining factors) and effects (associated characteristics). Those two sections allow the following questions to be answered:

- Under what conditions are joints and faults generated? Can they be generated at the same time? What are the implications in terms of variation in aperture and the degree of connectivity?
- What characteristics allow the identification of fractures that were generated during the same <u>tectonic event</u>⌐?
- Why are some fractures more continuous (persistent) than others?
- How and why do different lithological types impose different characteristics on fracture networks and, consequently, variations in the degree of connection and in the groundwater flow properties?
- How does the deformation history influence the groundwater flow properties?

In Section 4 models of fracture networks in different geological contexts (sedimentary rocks, volcanic rocks, metamorphic and igneous rocks, and <u>fault zones</u>⌐) are presented, along with the main consequences for the architecture of the connected network and presence of preferential groundwater flow paths. The relevance of understanding the role of the lithological types is that, given a geological map of sufficient detail, important predictions can be made about characteristics of the fracture network in each geological unit. This allows forecasts to be made, which is significant because one of the greatest difficulties in studying fractured aquifers is the inference of the fracture network geometry in places where it is not possible to collect data directly.

Section 5 is intended to highlight hydrogeological characteristics (e.g., hydraulic conductivity, transmissivity, and preferential groundwater flow pathways) of conceptual fracture network models in the geological settings of sedimentary, volcanic, igneous, and metamorphic rocks based on case studies.

We conclude by expressing our desire that this book will inspire and motivate practitioners to carry out structural geology surveys that provide a sound basis for a better hydrogeological characterization of a site or a region.

1.1 What is a Fractured Aquifer?

Fractured aquifers are geological materials of low <u>primary permeability</u>⌐ in which groundwater flow takes place mainly through voids bounded by fracture faces (Domenico & Schwartz, 1990; Freeze & Cherry, 1979; Singhal & Gupta, 2010). These voids, which are

much better connected than matrix pores, are commonly called fracture porosity and can constitute an effective conduit for groundwater flow.

Medium- to high-grade metamorphic and intrusive igneous rocks are geological materials in which groundwater flow takes place almost exclusively through fracture porosity. Groundwater flow in fractures is also significant in fine-grained sedimentary rocks (Figure 2), where fracture flow often constitutes the most important flow conduit. In these lithologies, such as shale, some limestones and well-cemented sandstones, the intergranular system of the rock matrix is poorly connected. Sedimentary rocks usually bear both fracture and intergranular permeability.
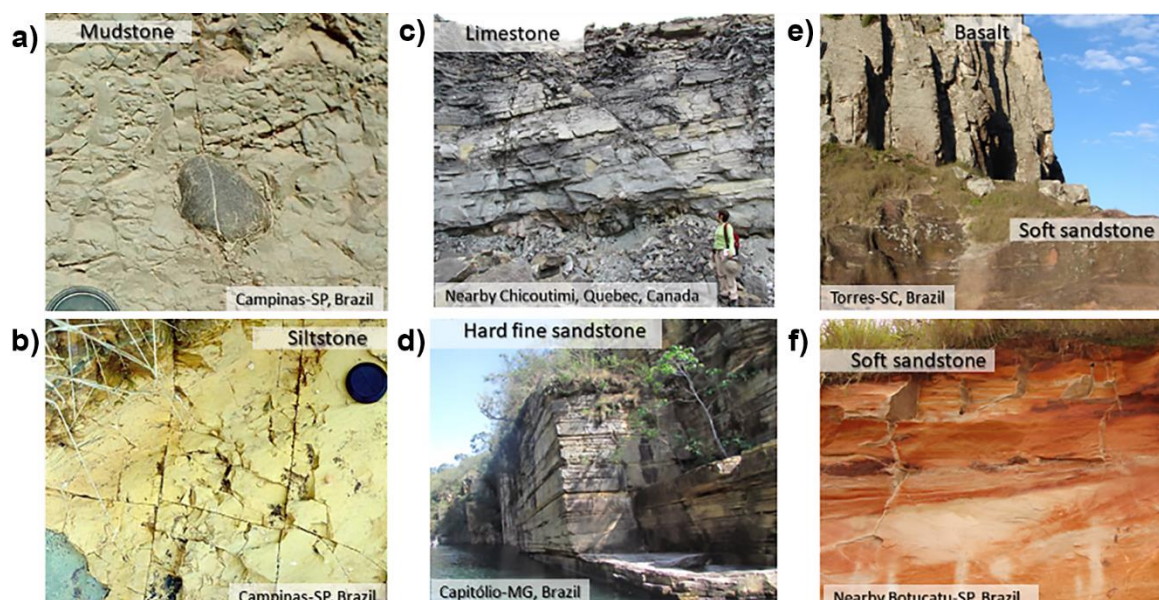
Figure 2 - Fracture flow may be significant in sedimentary rocks, mainly the ones with fine texture (silt, clay) such as mudstone (a), siltstones (b), some limestones (c), as well as hard sandstones (d). In poorly cemented sandstones (e,f), fractures may be absent or appear only in hardened portions of the formation. In (e) the dense fractures in the basalt (top) do not propagate into the sandstone (bottom). In (f) the fractures in the sandstone have propagated only to a limited depth. On the other hand, the fractures in the hard fine sandstone (d) are dense and persistent (photographs a, b, d, e, f: Amélia Fernandes; photograph c: Alain Rouleau).

As shown in Figure 3, small fracture apertures, ranging from 0.01 to 0.05 mm, are much more frequent (Van Golf Racht, 1982, in Domenico & Schwartz, 1990). Fracture aperture values typically show a skewed distribution, as most of them are indeed small. However, the few large-aperture fractures are significant for providing the overall transmissivity and preferential pathways through the rock mass. A density of one fracture per meter, considering the most frequent aperture range of 0.01 to 0.05 mm, renders hydraulic conductivity (K) values from $\sim 10^{-8}$ to $\sim 10^{-6}$ m/s.
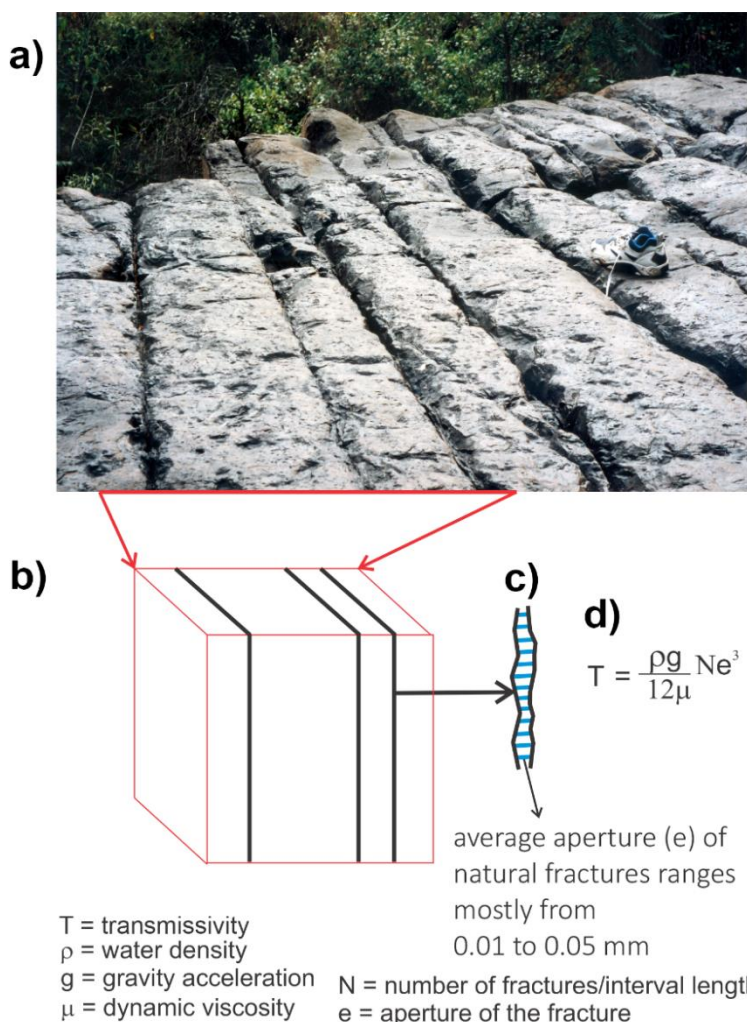
Figure 3 - Hydraulic conductivity of an interval of a rock mass containing a number of idealized fractures. a) Vertical fractures in a limestone. b) Representation of vertical fractures in a block diagram of the rock mass. c) Small apertures, ranging from 0.01 to 0.05 mm, are the most frequent (Van Golf Racht, 1982, in Domenico & Schwartz, 1990). d) Cubic law equation (Snow, 1968), which is used to calculate the flow through a section of rock mass perpendicular to the fractures. Considering the density (*N*) of just one fracture/meter, the most frequent apertures (*e*) provide hydraulic conductivities (*K*) ranging from ~10^{-8} to ~10^{-6} m/s.

As shown in Figure 4, *K* values for fractured igneous and metamorphic rocks vary by five orders of magnitude, from 10^{-8} to 10^{-4} m/s, the greater being a response to the presence of the less frequent but larger apertures. The values are similar to those obtained in field tests by many authors (e.g., Rouleau et al., 1996; Shapiro et al., 2007; Parker et al., 2018). Most aperture determinations come from hydraulic tests in wells, where transmissivity is measured and the cubic law is used to calculate the so-called hydraulic aperture. The hydraulic aperture is the opening width of an ideal fracture between smooth and parallel walls that would produce the measured transmissivity. Thus, the value approaches the effective mechanical aperture. Unfractured crystalline rocks have extremely

4

The GROUNDWATER PROJECT   © The Authors   Free download from gw-project.org

Anyone may use and share gw-project.org links. Direct distribution of the book is strictly prohibited.

low *K* values comparable to those of shale and clay (Freeze & Cherry, 1979) as shown in Figure 4a. Rock cores used in laboratory tests are small samples usually devoid of the fractures observed on rock exposures. Thus, in those tests, the calculated K values are similar to the ones of unfractured crystalline rocks (Figure 4b).
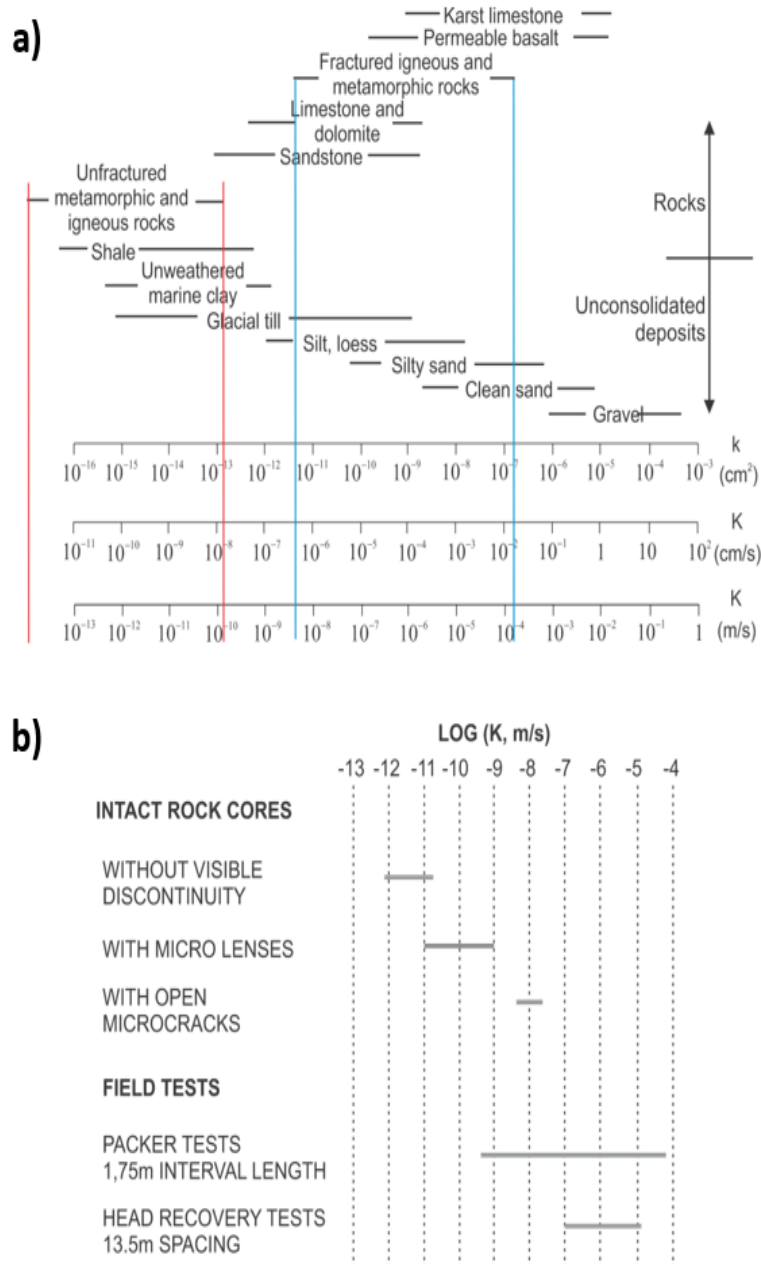
Figure 4 - a) Values of permeability (*k*) and hydraulic conductivity (*K*) for different geological materials. *K* values for the fractured igneous and metamorphic rocks (between the blue lines) vary by five orders of magnitude. Unfractured crystalline rocks have extremely low *K* values comparable to those of shale and clay (modified from Freeze & Cherry, 1979). b) Hydraulic conductivity of a fractured orthoquartzite formation, estimated at laboratory and field scales (modified from Rouleau et al., 1996).

1.2 Why Should We Study Fractured Aquifers?

Crystalline and other low primary permeability and porosity rocks occupy large areas of all continents where groundwater plays an important role in supplying populations, as well as economic activities, as discussed in Section 1.4. Thus, to determine groundwater sustainability, the production potential of these aquifers needs to be studied. In addition, the numerous cases of contamination of fractured aquifers by human activities, especially in industrial and urban areas, need to be assessed to protect public health. Understanding fracture network properties is critical for assessing and predicting contaminant transport through fractured rock aquifers. A substantial body of knowledge has been produced by Parker and collaborators (e.g., Parker et al. 2018) that reports on diffusion from fractures into the rock matrix (e.g., Wanner et al., 2018). Contaminated groundwater represents a water resource that has been lost, or is not available for most uses for a long time; preventive measures need to be taken to avoid this loss. Such needs have been exacerbated by the expansion of urban areas and polluting activities throughout regions supplied by contaminated, fractured aquifers. These anthropogenic activities considerably increase the demand for water supply, thus the motivation for studying fractured media is more pressing. Other relevant applications of fractured-aquifer knowledge are related to geotechnical engineering, mineral/oil extraction, and risk evaluation of natural disasters (e.g., landslides), as well as, over the last 40 years, disposal of radioactive waste. All these activities can cause or facilitate groundwater contamination. Geotechnical engineering works can be affected by terrain instability due to groundwater flow coupled with modifications in the landscape. Examples of fractured aquifers that face a critical situation, due to the scarcity of water supply and/or the existence of extensive cases of contamination by highly harmful substances to health, are provided in Section 1.4.

1.3 Are Fracture Systems Predictable?

While the needs are pressing, the scientific and methodological challenges for characterizing fractured aquifers are substantial. Anyone who has ever read something about fractured aquifers has certainly come across an initial statement such as: fractured media are (extremely) complex due to their inherent heterogeneity and resulting unpredictability. This heterogeneity controls the groundwater flow field. Especially in crystalline rocks such as granites and gneisses, a common first impression is that the fracture network is random, as there are fractures with several different orientations. Given this, it is natural to ask the following questions:

- Are the fractures organized in a logical way?
- Is it possible to unravel this logical organization so it makes physical sense?
- What will be the implications of this organization for the flow of groundwater in fractured aquifers?

6

In answering the above questions, two types of theoretical fundamentals must be used. They are:

1.   rock mechanics, which control the initiation and propagation of fractures; and,
2.   structural geology, which describes conditions in the Earth's crust where deformation occurs.

A structural geologist investigates the <u>fracture sets</u>↳ based on field data, as well as the spatial and temporal relationships between these sets, that is, the evolution of the deformation over time. Even when the fracture networks are highly heterogeneous, a representative fracture survey quantitatively samples the characteristic orientations (sets), sizes and other fracture properties. However, a structural geology investigation, along with the application of rock mechanics principles, provides a better understanding of how fractures were formed throughout the deformation history; this history has important implications for assessing connectivity and apertures.

A great advantage of structural geology surveys based on data collected from outcrops is their relatively low cost. Thus, it is recommended that research on fractured aquifers should make the most of data collected from outcrops to develop realistic conceptual models. In addition to proposing a fracture network conceptual model, such studies also provide a qualitative, or semi-quantitative, classification of each fracture set with respect to groundwater flow potential based on evidence of flow along fractures observed on the outcrops. Conceptual fracture networks that include the classification of each fracture set, with regard to their potential for carrying groundwater flow, can be called hydro-structural conceptual models. Such models can be used to optimize (and reduce costs of) subsequent expensive research methods such as drilling, core logging and well testing.

1.4 Groundwater from Hard Rocks has a Major Role for Water Supply

A simplified map of global groundwater resources (Figure 5) shows the distribution of three major aquifer types. The tan areas of generally low permeability correspond to typical fractured aquifers formed of relatively old, fractured, crystalline rocks. The green areas represent complex aquifers with both intergranular and fracture porosity. The blue areas contain major regional aquifers composed of sedimentary rocks having significant intergranular porosity, as well as old volcanic rocks and low-permeability sedimentary rocks where flow is controlled by fracture porosity. Fracture flow is important in most bedrock aquifers, from rocks with low primary permeability to major regional aquifer systems.
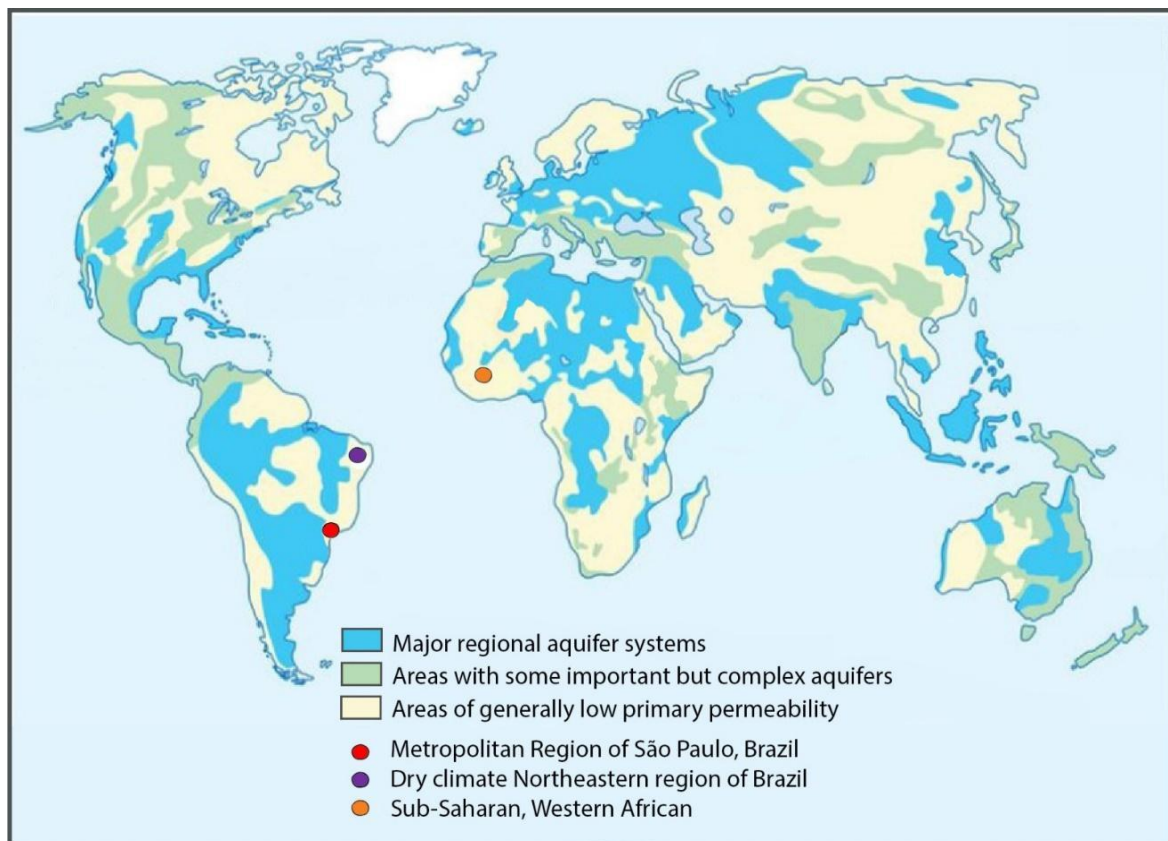
Figure 5 - Simplified map of the three major types of global aquifers (after Whymap.org). The tan (yellowish) areas consist of rocks of generally low primary permeability and are typically fractured aquifers. Location indicators highlight three regions discussed in the text with strong dependence on fractured aquifers for water supply: a red marker for the Metropolitan Region of São Paulo, Brazil, a purple marker for the dry climate region in northeastern Brazil and an orange marker for sub-Saharan, western Africa.

Asia's aquifers are mostly low primary permeability rocks. Fractured hard rock aquifers such as granite, gneiss, metamorphic rocks, and basaltic lava flows occupy 67 percent of India's territory, and they outcrop in vast areas across the African continent (Zektser & Everett, 2004). Many of the highly populated areas in India are underlain by hard, fractured-rock aquifers, and the groundwater available from these rocks is the only source of water supply for the basic needs of millions of people (Zektser & Everett, 2004). Vast areas of South America, mostly in Brazil, are underlain by Precambrian crystalline basement rocks.

Figure 5 shows the location of three examples of regions that have a significant or strong dependence on fractured aquifers for water supply, namely, the Metropolitan Region of São Paulo (Figure 6), the northeastern region of Brazil (Figure 7) and sub-Saharan Africa (Figure 8). The Metropolitan Region of São Paulo in southeastern Brazil is inhabited by about 22 million people; its central portion lies on a sedimentary basin and the densely urbanized area has been, for some decades, expanding over fractured aquifers of crystalline Precambrian rocks. Public water supply is provided by surface water reservoirs, although thousands (around 12,000) of mostly private wells complement the water needs. Even

8

though the water supply crisis caused by the 2013–2015 drought emphasized the importance of groundwater resources in meeting supply demands, contamination of shallow and deep aquifers (sedimentary and crystalline rocks, respectively) in large industrial areas has resulted in the shutdown of numerous wells and threatens public health and water security.
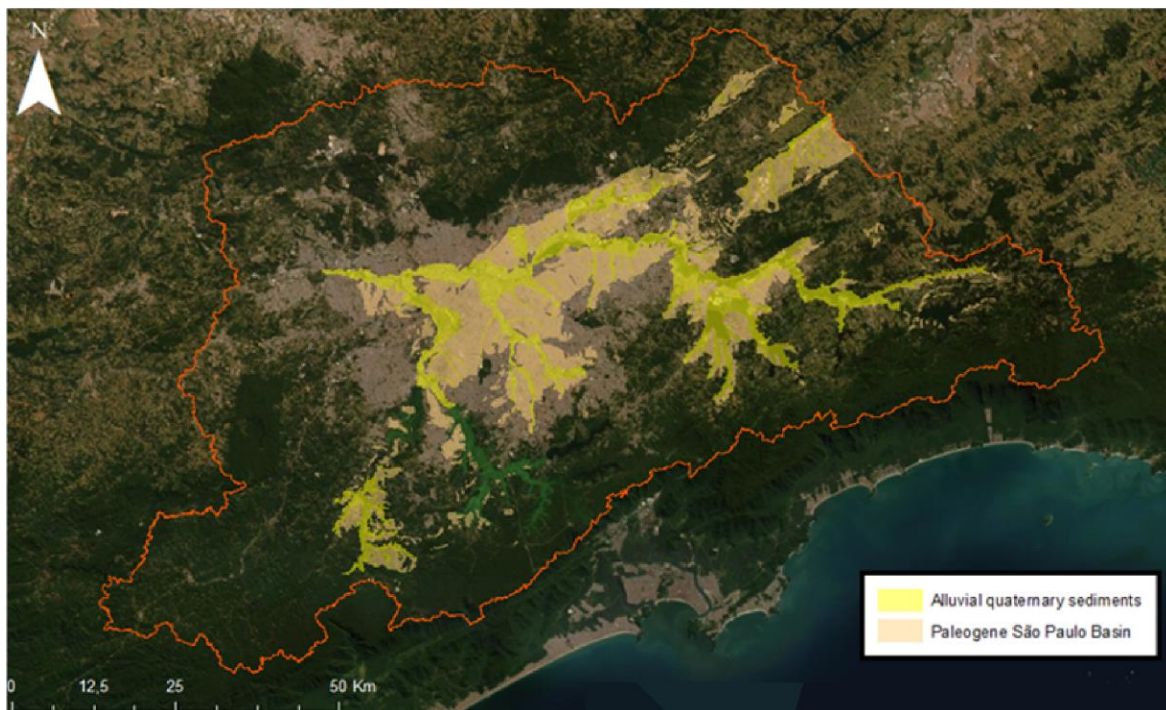
Figure 6 - Metropolitan Region of São Paulo Brazil (delimited by the red contour line): 22 million inhabitants in a very dense urbanized area (yellow and orange areas) that is expanding over crystalline Precambrian rocks (image from ArcGis, geological map from Riccomini & Coimbra, 1992).

The arid northeastern region of Brazil (Figure 7) covers 1 million km^2 and overlies Precambrian crystalline basement rocks. The six-year-long drought from 2012 to 2017 resulted in a water supply crisis. Groundwater, already an important resource, became even more relevant to supply the 27 million inhabitants (12 percent of Brazil's total population) of the region. In one state (Ceará), more than 7,000 wells were drilled between 2015 and 2019. Choosing well locations was challenging, as many were non-productive or yielded saline water. Groundwater exploration nonetheless had to proceed due to the critical need for water resources.

Figure 7 - Dry climate in northeastern region of Brazil where 27 million inhabitants depend on groundwater that comes from crystalline basement rocks (Folha de São Paulo↗).

In sub-Saharan Africa, where more than 75 million people live in regions prone to desertification (Zektser & Everett, 2004), fractured crystalline and metasedimentary rocks constitute an important reservoir of water supply for the human population (Figure 8). The largest cities are often located near the few large rivers, but most small cities and villages rely solely on groundwater for domestic and agricultural purposes. The bedrock is mostly overlain by a layer of saprolite (weathered bedrock), which is often of low permeability due to the presence of clay as a weathering product. Groundwater can be extracted by wells drilled down to the bedrock and intersecting transmissive fractures. Another way of tapping groundwater is to dig large diameter holes through the saprolite to depths below the water table. The volume of the dug hole below the water table provides a reservoir of water that can fill up overnight for extraction during the day. This traditional approach has been used over decades and is mostly limited to subsistence agriculture.

Figure 8 - Artisanal water well dug through the saprolite layer on top of crystalline bedrock in Burkina Faso, sub-Saharan Africa (photograph: Alain Rouleau).

2   Where and How are Fractures Formed?

This section presents basic theories about conditions that cause fracture formation and propagation. Fractures are produced by *brittle deformation*—permanent change in rock or soil due to cracks—that takes place at relatively shallow depths, where the rock mass is subjected to stresses that exceed certain magnitudes. We briefly describe the sources of these stresses and present a widely-accepted criterion that determines the types of fractures that will form. Finally, we explain how fluid pressure can trigger fracture formation, even when the magnitude of stresses is not high enough to cause fracture formation.

2.1 Crustal Level: Brittle versus Ductile Deformation

Metamorphic and intrusive igneous rocks, which make up most typical crystalline aquifers, are generated at depth under high temperature and pressure. Under such conditions, rocks are deformed in a *ductile manner* by flowing (rather than breaking) when in a solid state (Davis et al., 2011); this is called ductile deformation. In addition, *pervasive structures*, such as *foliation* (planar structure formed by mineral orientation), are developed. Some of these crystalline rocks are eventually uplifted to the earth surface, which is why these rocks crop out at the surface throughout vast areas.

During uplift, rocks move to shallower levels in the crust where temperature and confining pressures are gradually lower. Under these conditions the deformation becomes brittle and under certain stress magnitudes the rock breaks. The uplift process, from depths of tens of kilometers to the surface, takes place over geologic time. The rocks may undergo a succession of deformation phases associated with different tectonic events that generate structures compatible with the temperature and pressure conditions existing at each depth.

- Metamorphic foliations and tight folds are ductile structures generated at great depths; they are the oldest in the deformational history of the rocks. They are not by themselves relevant to groundwater circulation because there are no pores associated with them. However, these structures create *mechanical anisotropy*—anisotropy means different properties in different directions—in rock units. This may influence the geometry of the fracture system that will be generated later, as described in Section 3.4.

- Shear zones↴, formed at depths greater than 10 to 15 km under ductile deformation↴, are composed of a series of strongly foliated rocks called mylonites↴ (Figure 9). Their development process does not, by itself, generate porosity.

- Faults, along with minor faults and joints, are generated under brittle deformation and are formed at crustal levels shallower than 10 to 15 km (Davis et al., 2011). It is the latest deformation that takes place during uplift. Generally,

faults create secondary porosity and permeability within the rocks (Figure 9). This is discussed in detail in section 4.1.4.
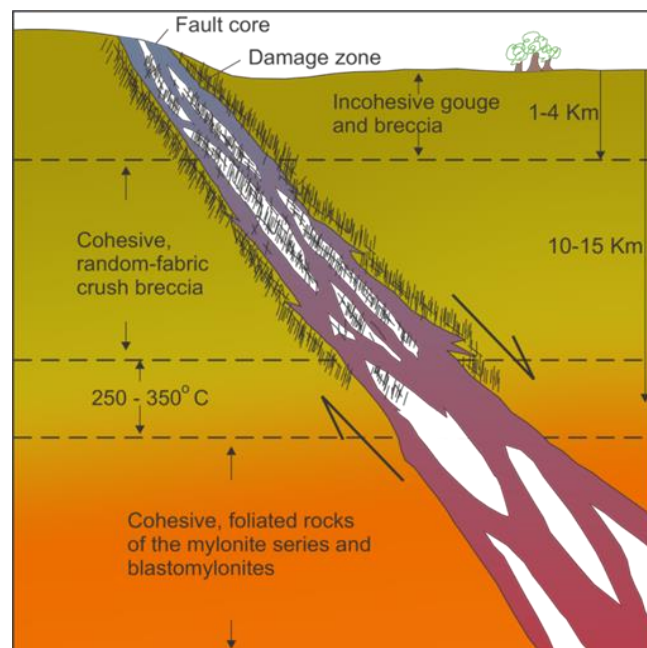
Figure 9 - Crustal levels and the materials formed at fault zones from shallower to deeper depths: incohesive breccia, cohesive random-fabric breccia, and foliated mylonitic rock. Fractures are formed by brittle deformation at shallow depths of less than 10–15 km (modified from Sibson, 1977).

Although ductile structures (such as foliation) do not produce porosity, they usually influence the fracture network configuration because they are commonly reactivated during brittle deformation (section 3.4). An important implication is that rocks with foliation, veins, and other previous anisotropies, will tend to have a denser fracture network and a higher transmissivity, as detailed in Section 3.5.

2.2 Terminology: Types of Fractures

The generic term, fracture, refers to any surface produced by brittle deformation. Basic fracture types are presented in Figure 10 and field examples are provided in Figure 11 and Figure 12. A fracture is any planar or sub-planar (gently wavy or irregular) discontinuity characterized by reduced or lost cohesion; in this type of deformation, rocks or minerals are broken. The two basic types of deformation producing fractures are opening and shearing; there is a third type that results of the combination of the two basic types.

- *Opening or extension fractures* show displacement perpendicular to the fracture surfaces (Figure 10a). Joint is the term usually used for extension fractures whose movement can be detected only by close examination. Extension fractures can be infilled by minerals (Figure 11) or by rocks; the latter is the

result of magma cooling. In the former case, the extension joint is called a vein, and in the latter, a dike. The term *fissure* is also used in the literature, but typically for open joints (Fossen, 2016).

- S*hear fractures* have displacement of the slip type, that is, the movement is parallel to the fracture walls (Figure 10b and Figure 12). Fossen (2016), page 121, states that '*The term shear fracture is used for fractures with small (mm- to dm-scale) displacements, while the term fault is more commonly restricted to discontinuities with larger offsets.*'

- *Hybrid fractures* combine both types of displacement; that is, sliding (shear) and opening (extension).

In fracture mechanics, the displacement/propagation of fractures is classified into Modes I, II, and III (Figure 10). In Mode I, opening (extension) occurs; the displacement is perpendicular to the fracture surfaces (Figure 10a). In Modes II (sliding mode) and III (tearing mode), the displacement is parallel to the fracture surface. This shear can be perpendicular (Mode II) or parallel (Mode III) to the edge of the fracture (Figure 10b) and occur along different parts of the same shear fracture (Fossen, 2016).
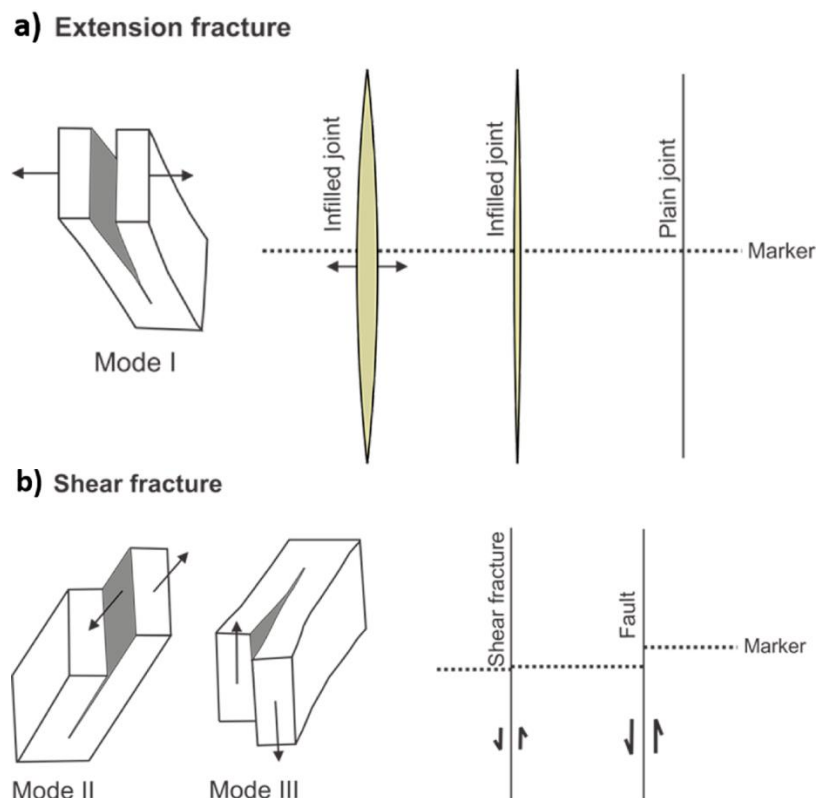
Figure 10 - The term fracture is generic for any discontinuity formed by brittle deformation. There are two basic types of fractures: a) joints (extension fractures) which can be infilled or barren; and, b) faults (shear fractures) with slip parallel to fracture surface. The marker (dotted line) indicates the presence (b) or the absence (a) of shear. In fracture mechanics fractures are classified into Modes I, II and III.
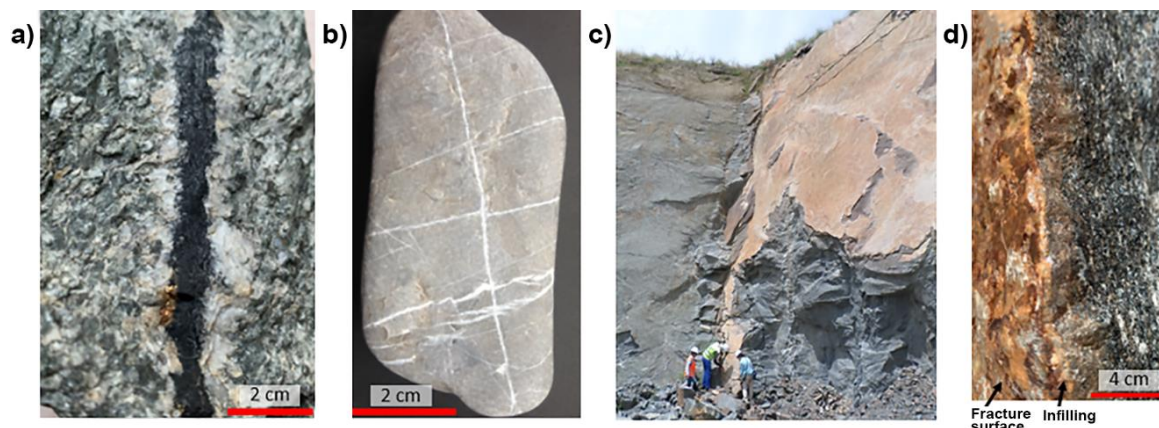
Figure 11 - Examples of veins (i.e., infilled joints that are formed by the opening mode perpendicular to a tensile stress. The infillings themselves are a demonstration of the opening mode, as it is needed to make room for the vein minerals. a) Massive granite with black infilling. b) Limestone pebble with fractures infilled by calcite. c) Two fracture faces in gneiss. The fracture to the left is gray and has no infilling, whereas the one to the right is brown and has an infilling of brown and white minerals. d) A detail of the brownish fracture face and of the brown and white infilled minerals. Just beside the infilling, the rock changes its color, likely due to chemical reaction with hot and saline water from which the infilled minerals were crystalized (photographs: Amélia Fernandes; c-d: Barra Mansa, Rio de Janeiro, Brazil).

Figure 12 - Example of shear fracture cutting through sandstone bedding. In this case, the shear fracture is a normal fault (as discussed in Section 3.1). The offset is deduced from the relative displacement of the orange/red layers, and the sense of shear is shown by the arrows (photograph: Ricardo Hirata, nearby Tegucigalpa, Honduras).

2.3 Sources of In-Situ Stress and Differential Stress

The in-situ state of stress in a rock mass is generally the sum of the gravitational and tectonic stress components (e.g., Zang & Stephansson, 2009). The former is derived from the weight of the overlying rock mass at a given depth. The so-called lithostatic stress is the reference state that results solely from the gravitational component. The tectonic stress

15

component, may partly result from remnant stresses due to paleotectonic events, but the dominant component is the active tectonic stress due to present-day deformation of the Earth's crust. The origin of the active tectonic stresses at a given location can be derived from first-, second-, and third-order factors (Zoback et al., 1989; Heidbach et al., 2007). The relative displacement of tectonic plates is a first-order stress factor; it is of global scale. The bending of plates and <u>isostatic compensation</u>⌐ that lead to erosion and deposition processes (Zoback et al., 1989) are second-order factors (regional scale). Fault-scale stresses are a third-order factor lying between regional and local scale (Heidbach et al., 2007). Apart from gravity, only the tectonic stresses can reach a regional significance. Other stress components have large standard deviations in orientation and magnitude (Zang et al., 2009). One example is the effect of the Earth's topography near the surface. In mountainous regions, the presence of a number of nearby steep slopes can cause notably variable in-situ stresses; examples of this condition are provided in Section 4.2.

Stresses are more commonly anisotropic than isotropic and vary with orientation (Figure 13a,b). The stress field can be described by an ellipsoid whose axes, perpendicular to each other, represent the minimum (σ_3), intermediate (σ_2) and maximum (σ_1) principal stresses (Figure 13c). These stresses act in planes orthogonal to each other, and the shear stress on these planes is zero. Figure 13a represents the lithostatic reference state, in which the stresses are derived solely from the gravitational component; this defines a stable condition, that is, the differential stress ($\sigma_1 - \sigma_3$) is not large enough to produce deformation. The differential stress necessary to generate fractures must exceed a certain magnitude, which in general can be met when there is a tectonic component (Figure 13b), as discussed in Section 2.4. However, existing fluid pressures that give rise to the so-called effective stresses may lead to the generation of fractures in situations where the differential stress alone is not large enough to cause the formation of fractures; this is explained in Section 2.5.
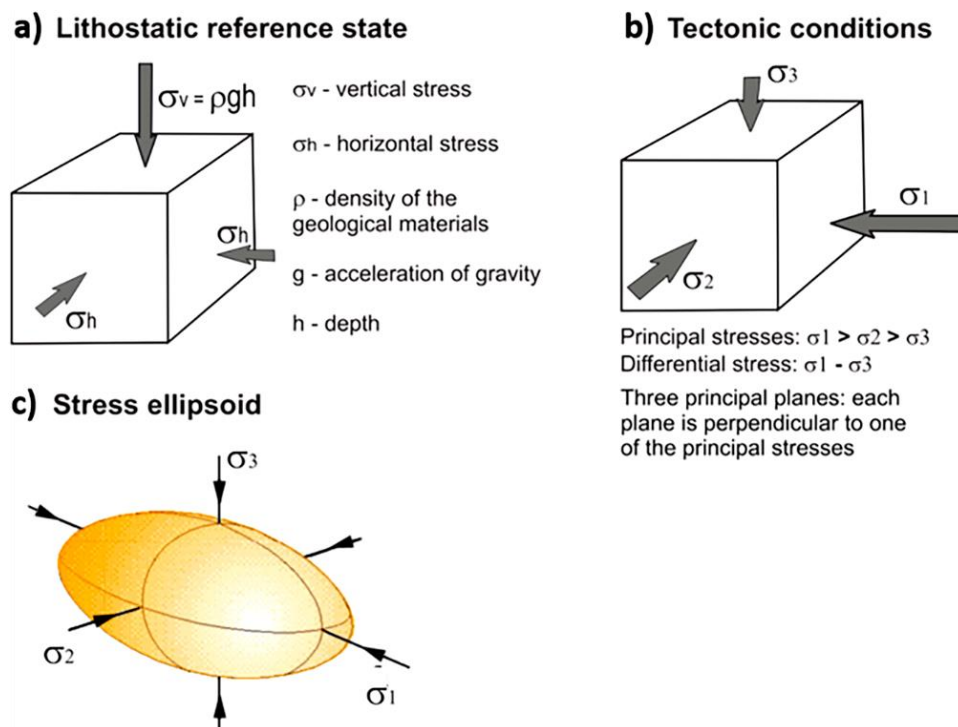
Figure 13 - Subsurface stress. a) In the lithostatic reference state, the vertical stress (σ_v) is the weight of the rock column and the horizontal stress (σ_h) is equal to fraction of the σ_v; its magnitude depends on the mechanical properties of the rock. b) Under tectonic conditions, the three orthogonal stresses are called principal stresses, in which σ_1 is the maximum principal stress, σ_2 the intermediate principal stress, and σ_3 the minimum principal stress. They act on three orthogonal planes that have no shear stress. Failure takes place when the differential stress exceeds a certain value. c) The stress ellipsoid is a three-dimensional representation of the stress vectors acting on all planes within the rock.

2.4 Stress Magnitude and Fracture Types

The magnitudes of the individual stress components control how the fractures initiate and propagate by shear or by opening modes. This relationship can be elegantly expressed by the Mohr circle↳ that is illustrated in the Mohr diagram↳ (Figure 14). Thorough descriptions of it can be found in textbooks on structural geology (Price & Cosgrove, 1990; Ramsay & Hubber, 1987; Fossen, 2016; and Davis et al., 2011, among others), and on rock mechanics (Jaeger & Cook, 1979; Goodman, 1989; Hudson & Harrison, 1997). In this book we use the convention that compressive stresses are positive and tensile stresses are negative.
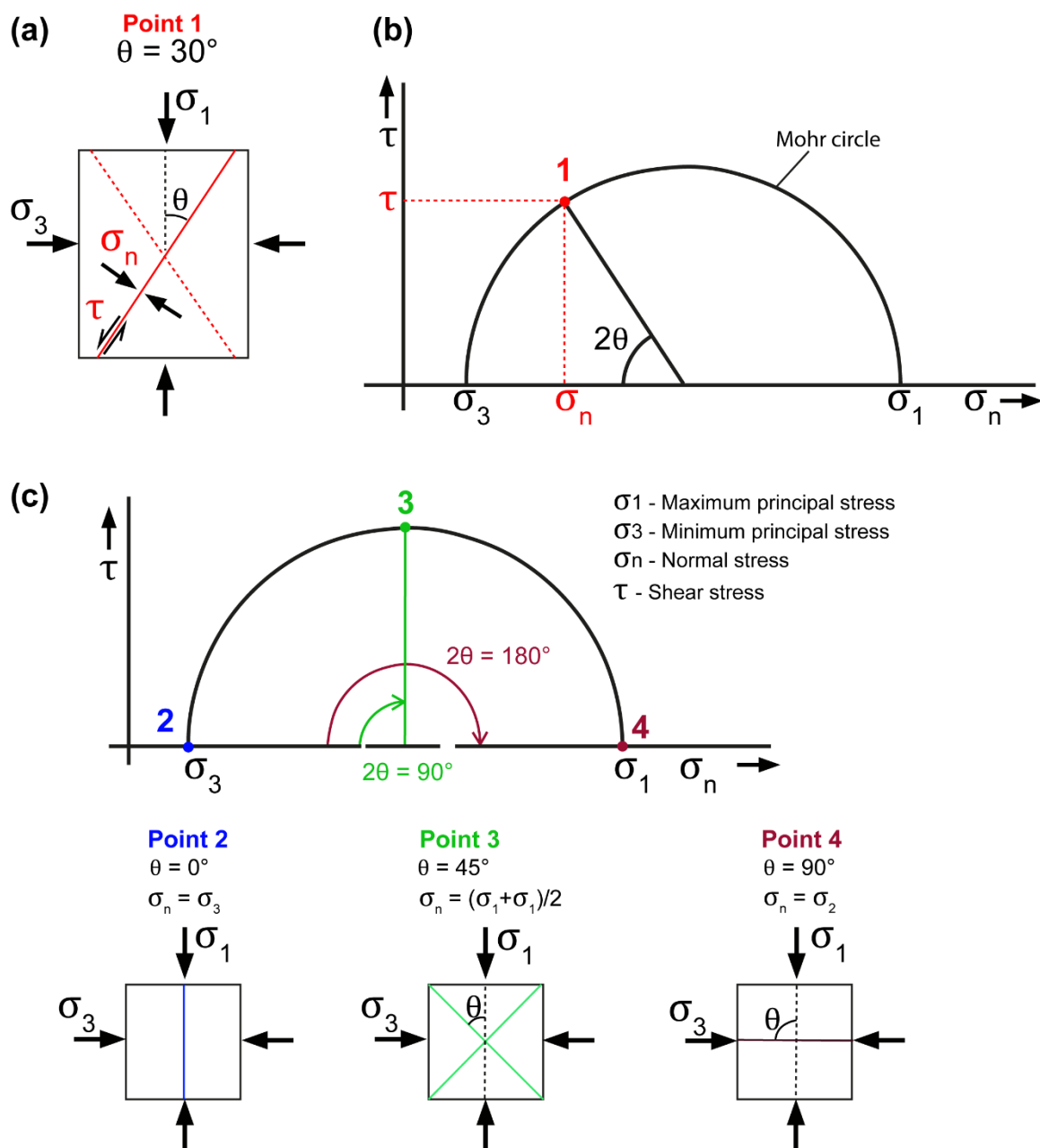
Figure 14 - Mohr circle and Mohr diagram showing how the magnitudes of the principal stresses, σ_1 and σ_3, are related to the shear and normal stresses that act on any plane at a given angle from σ_1. a) Under certain values of compressive σ_1 and σ_3 stresses, a conjugate pair of shear fractures (stippled and continuous red lines) that undergo a critical state of shear (τ) and normal stress (σ_n) is formed. Each shear fracture makes an angle θ of approximately 30° with σ_1. b) The Mohr circle diagram relates σ_1 and σ_3 with the normal stress (σ_n) and shear stress (τ) (x and y axes, respectively). At the stress state represented by Point 1, a pair of conjugate shear fractures is generated. These fractures make an angle of 30° with σ_1, as shown in part a. c) Points 2, 3 and 4 represent stress states that do not generate fractures; they are just meant to show how planes with a specific θ angle with σ_1 have specific locations (points) in the Mohr circle. Any state of stress, acting on any plane, with a specific angular relationship with σ_1 and σ_3, can be represented as a point in the Mohr circle; points 2, 3 and 4 are examples. Point 2 represents a plane perpendicular to σ_3 (the normal stress, σ_n, is equal to σ_3) and, consequently, parallel to σ_1. Point 3 represents conjugate planes that make an angle of 45° with σ_1. Therefore, as shown in the Mohr circle, 2θ is equal to 90°. Point 4 represents a plane that is perpendicular to σ_1 ($\sigma_n = \sigma_1$). This image is based on Cosgrove & Hudson (2016).

18

2.4.1 Shear Fracture

Planes perpendicular to the principal stresses have no shear stress. Planes that are not perpendicular to the principal stresses have normal stresses (σ_n) and shear stresses (τ) that are a function of the maximum and minimum principal stresses, σ_1 and σ_3. The values of σ_n and τ vary with the orientation of the plane, defined as an angle θ from the direction of σ_1. Plotting σ_n versus τ delineates the Mohr circle in the Mohr diagram. Each point in the Mohr circle represents the state of stress in planes that have an angle θ with σ_1 (Figure 15).
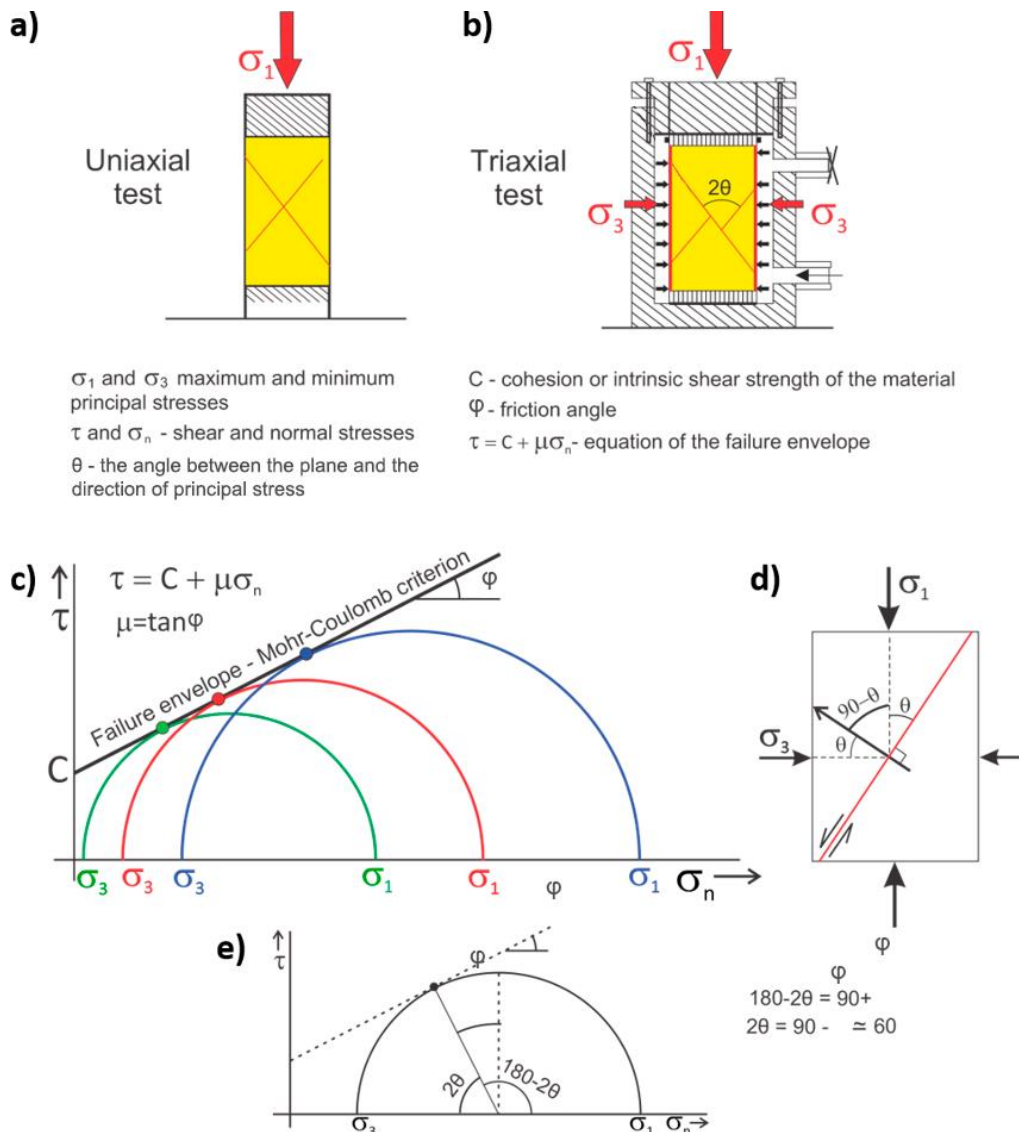
Figure 15 - Schematics of a) uniaxial (no lateral confinement) and b) triaxial (with lateral confinement) as based on Price & Cosgrove (1990) laboratory experiments, in which natural materials (soils and rocks) are subject to a specific amount of compression. Failure occurs at different combinations of specific values of σ_1 and σ_3. c) Laboratory experiments demonstrate that the points on the Mohr circles that represent conditions at which failure (fracturing) occurs, are aligned along a straight line with a specific y-intercept *C*. d) The slope of the line (φ) usually varies from 25° to 40°, which implies that 2θ ranges from 65° to 50°. In a), b) and d) the red diagonal lines represent the shear fracture planes.

A shear fracture is formed when a state of critical stress, defined by the values of τ and σ_n, acts on a plane. Shear fractures, or faults, are mostly formed as conjugate pairs, and each shear fracture makes an angle θ of approximately 30° with σ_1 (Figure 15a).

Experimental analyses carried out through uniaxial and triaxial compression tests (Figure 15a,b) define the combinations of σ_1 and σ_3 values and the differential stresses ($\sigma_1 - \sigma_3$) necessary to promote the generation of a new fracture (failure). Figure 15c shows the Mohr-Coulomb <u>failure envelope</u>⌐, which is defined by a line that is tangent to the Mohr circles. The tangent points (i.e., the points of the Mohr circle that touch the failure envelope) represent the stress states that lead to failure along specific planes. The slope of the linear failure envelope is the friction angle (φ).

The value of the shear stress at a zero normal stress (intersection of the y axis with the failure envelope) is called cohesion (C); this represents the material's intrinsic shear strength, such as that produced by cementation in sedimentary rocks. Cohesion and friction angle are the two parameters that define the Mohr-Coulomb failure criterion. The friction angle (φ) has a very well-defined relationship with θ (Figure 15e). The angle 2θ shown in Figure 15e, and measured from the direction of σ_3, is equal to $90 - \varphi$. Assuming for example a typical value of $\varphi = 30°$, the acute angle between the two conjugate shear fractures formed under this condition would be equal to 60°. The angle θ, measured from σ_3 in the Mohr circle, is also the angle between σ_1 and the generated shear fracture (Figure 14). Structural geology books in general use this notation; however, in soil and rock mechanics textbooks, θ is defined as being the angle between σ_1 and the normal to the fracture plane.

Figure 16 represents the conjugate faults (or shear fractures) that make an angle 2θ of approximately 60° with one another (Figure 16b) and 30° with σ_1 (Figure 16c). The shear along the faults is noticeable by the offset of the two adjacent and parallel lines in Figure 16c. Conjugate faults are repeatedly associated in space, with important implications for the connection between fractures, as discussed in Section 2.6.
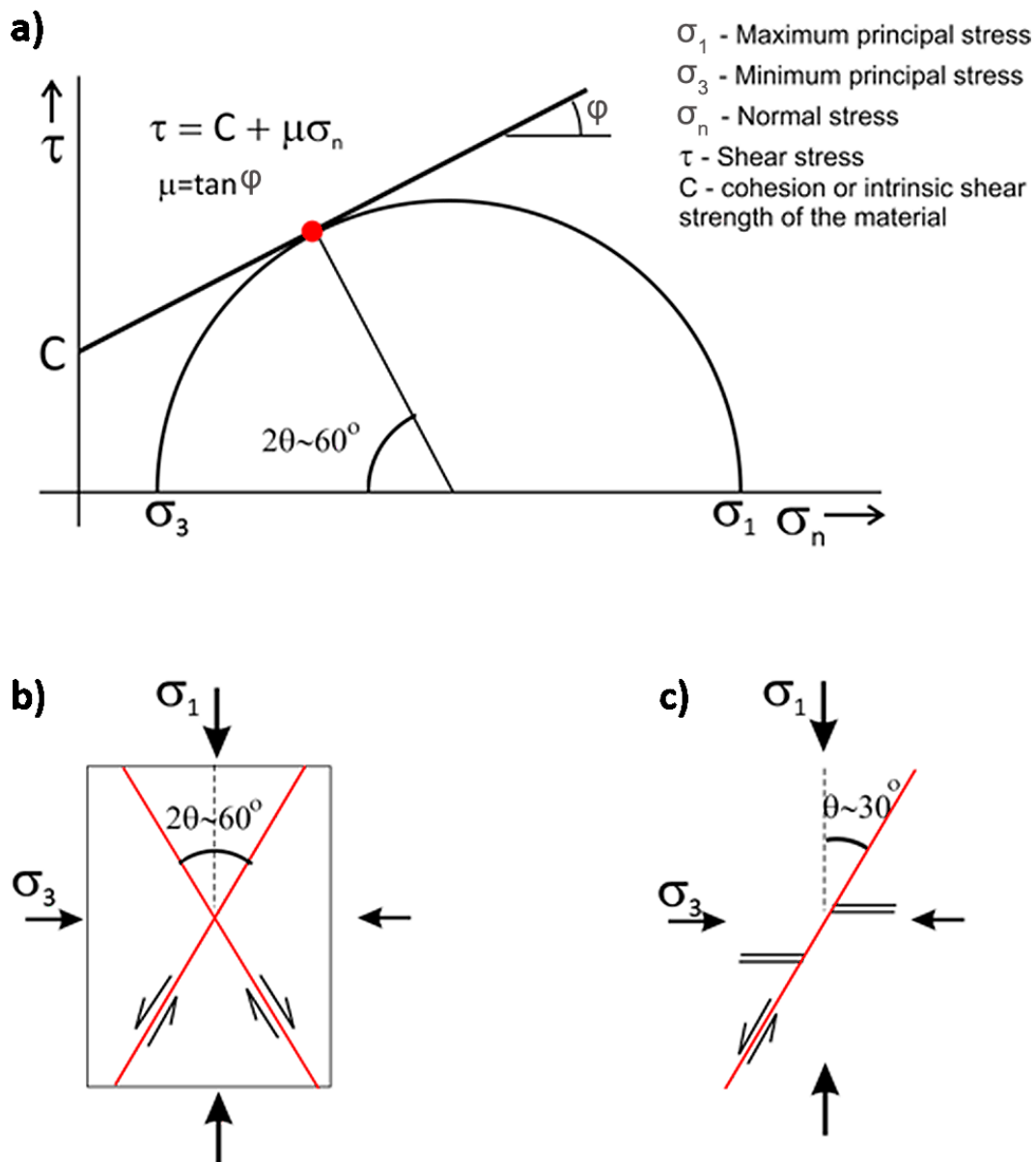
Figure 16 - Stress state associated with the formation of conjugate shear fractures. a) Mohr circle; the red point is represented in part b. b) The conjugate shear fractures make an angle 2θ of 60° with one another and 30° (θ) with σ_1. c) The shear along the fractures is noticeable by the offset of the two close parallel lines (modified from Price & Cosgrove, 1990).

2.4.2 Extension Fracture

Extension fractures (joints) are perpendicular to the lowest principal stress σ_3 and are formed when σ_3 is tensile (negative) and equal to the tensile strength (T) of the rock (Figure 17); this strength varies with lithology and is determined through laboratory experiments.
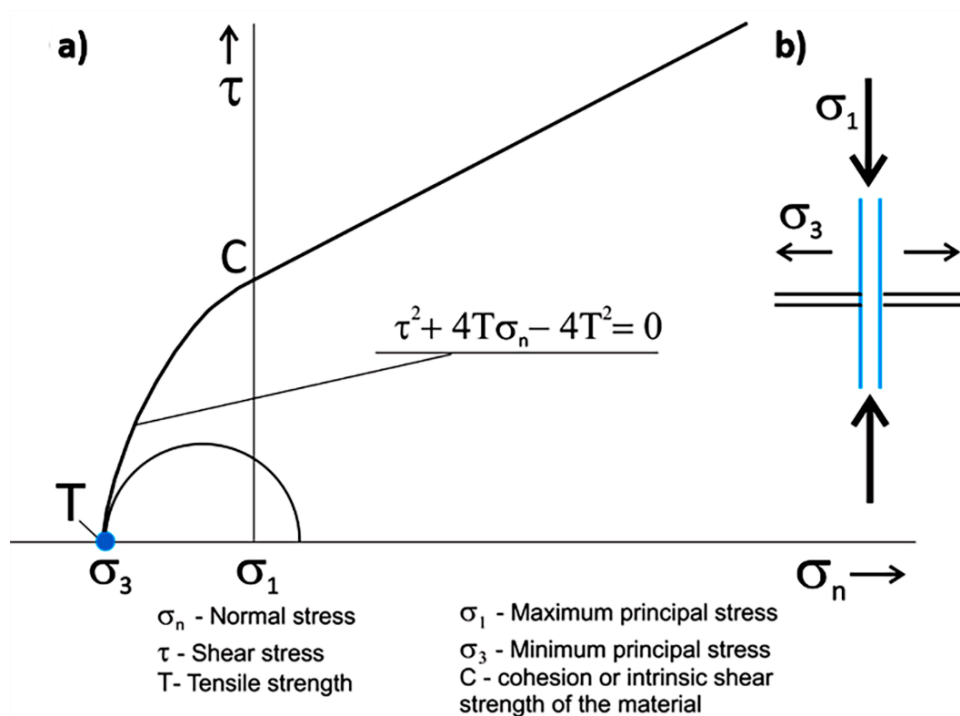
Figure 17 - Stress state associated with the formation of extension fractures (joints). a) The blue point represents the stress state at the formation of a joint; σ_3 is negative and equal to the tensile strength of the rock. b) The joint is perpendicular to σ_3 and parallel to σ_1; the opening mode is represented by the separation of the two joint faces and no shear displacement takes place (modified from Price & Cosgrove, 1990).

The conditions of joint formation require a small differential stress, and σ_1 may be positive, but of small magnitude, or even negative. Because joints are perpendicular to σ_3, they consist of a set of parallel fractures, a distinguishing feature that allows them to be recognized in rock exposures.

The stress state needed for the formation of joints (σ_3 is negative and equal to T) is expected to be more common in geological environments where the crust undergoes extension, such as regions where intraplate grabens are being formed, or at plate boundaries associated with rifting. However, joints can be abundant in several tectonic environments. The conditions for their formation can be met, for instance, by the presence of fluid overpressure, as discussed in Section 2.5.

2.4.3 Hybrid Fracture

Both hybrid and shear fractures form a pair of conjugate fractures. However, the angle between conjugate hybrid fractures is less than 45° and the propagation involves simultaneous shear and opening modes; the stress normal to the fracture (σ_n) is tensile

22

The GROUNDWATER PROJECT   © The Authors   Free download from gw-project.org

Anyone may use and share gw-project.org links. Direct distribution of the book is strictly prohibited.

(negative) as shown in Figure 18. The connection of the various points that represent the formation of hybrid fractures in the Mohr circle constitutes an envelope described by the Griffith criterion.
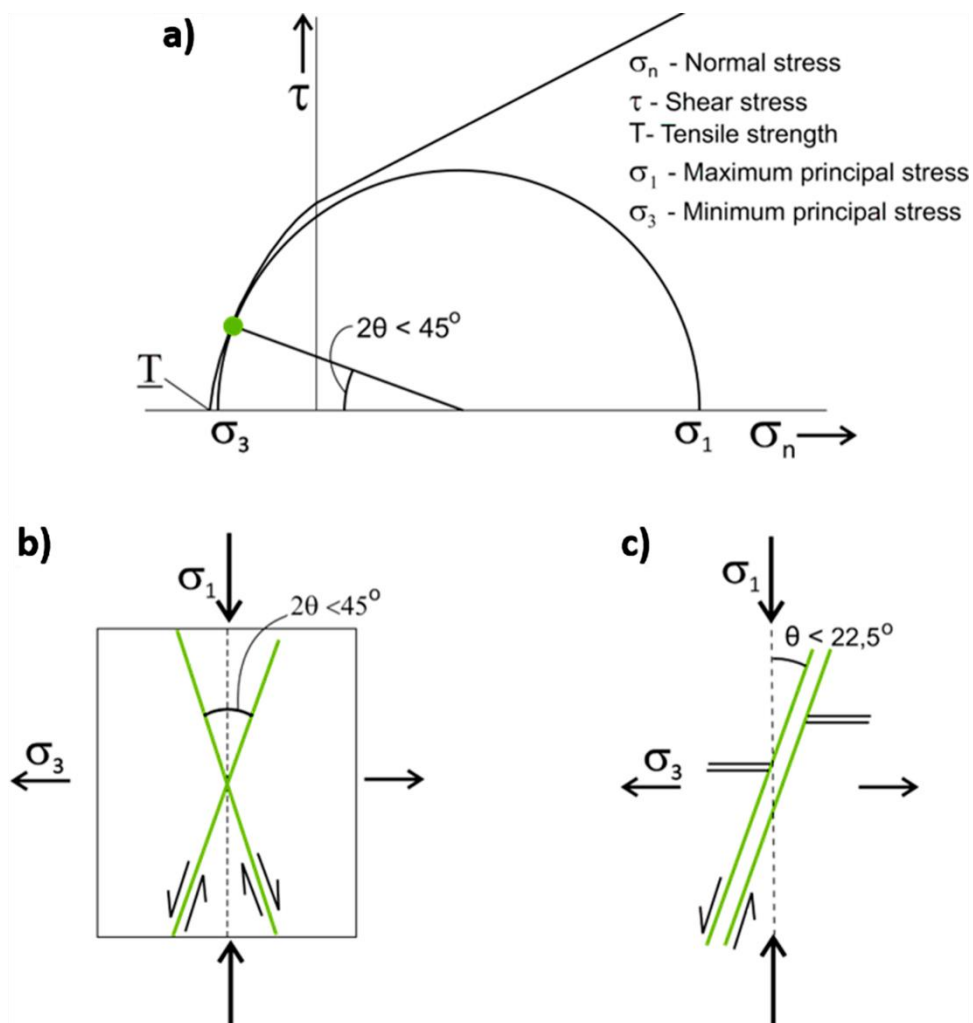
Figure 18 - Stress state associated with the formation of hybrid fractures. a) The green point on the Mohr circle represents the stress state at which the conjugate fractures (green lines) are formed. As these fractures undergo both shear and opening (with a σ_3 that is negative and close to the tensile strength T of the material), they are classified as hybrid. b) The angle between the conjugate fractures is smaller than 45°. c) The opening mode is represented by the separation of the two fracture faces and shear displacement is represented by the offset of the two close and parallel lines (modified from Price & Cosgrove, 1990).

The combined Mohr-Coulomb and Griffith criteria yield the complete failure envelopes for a variety of materials (Figure 19). Rocks such as sandstone, marble and limestone have considerably smaller values of C and T, when compared to dolomite, diabase, and granite. Moreover, the inclination of the shear envelope (friction angle φ) also varies with rock type.
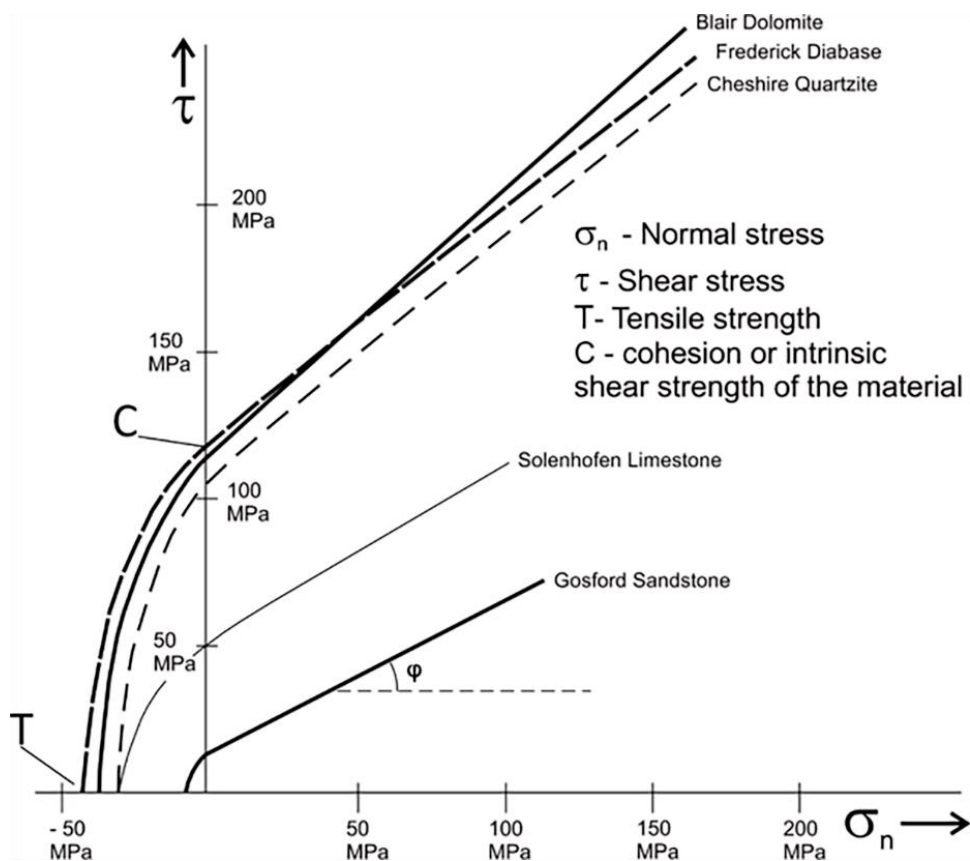
Figure 19 - Mohr-Coulomb and Griffith criteria failure envelopes for diverse materials. Rocks such as sandstone, marble and limestone have considerably smaller values of *C* and *T* when compared to dolomite, diabase, and granite. Moreover, the inclination of the shear envelope (*φ*) also varies with the rock (modified from Davis et al., 2011).

2.5 Fluid Pressure and Hydraulic Fractures

Hydraulic fracturing, a mechanism used in the field of unconventional oil and gas extraction, uses the same principles as the phenomenon of natural hydraulic fracturing. These principles are explained in this section.

Positive fluid pressure (*p*) is present in a rock when it is saturated, which is when all its pores are filled by a fluid (or fluids). This fluid can be water and/or oil, the latter formed by the degradation of organic matter. When the flow of these fluids is not impeded by any type of confinement, a hydrostatic fluid pressure is present. However, at depth, fluid is often confined and this leads to overpressure or abnormal fluid pressure (e.g., Ramsay & Hubber, 1987; Fossen, 2016). Fluid pressure is isotropic and reduces each one of the main stresses equally, resulting in the following effective stresses: $\sigma_1 - p$, $\sigma_2 - p$ and $\sigma_3 - p$. This implies that the Mohr circle, in the Mohr diagram, undergoes a shift to the left (Figure 20), and the effective normal stress on any plane is also reduced by the fluid pressure. The shift does not affect the shear stress.
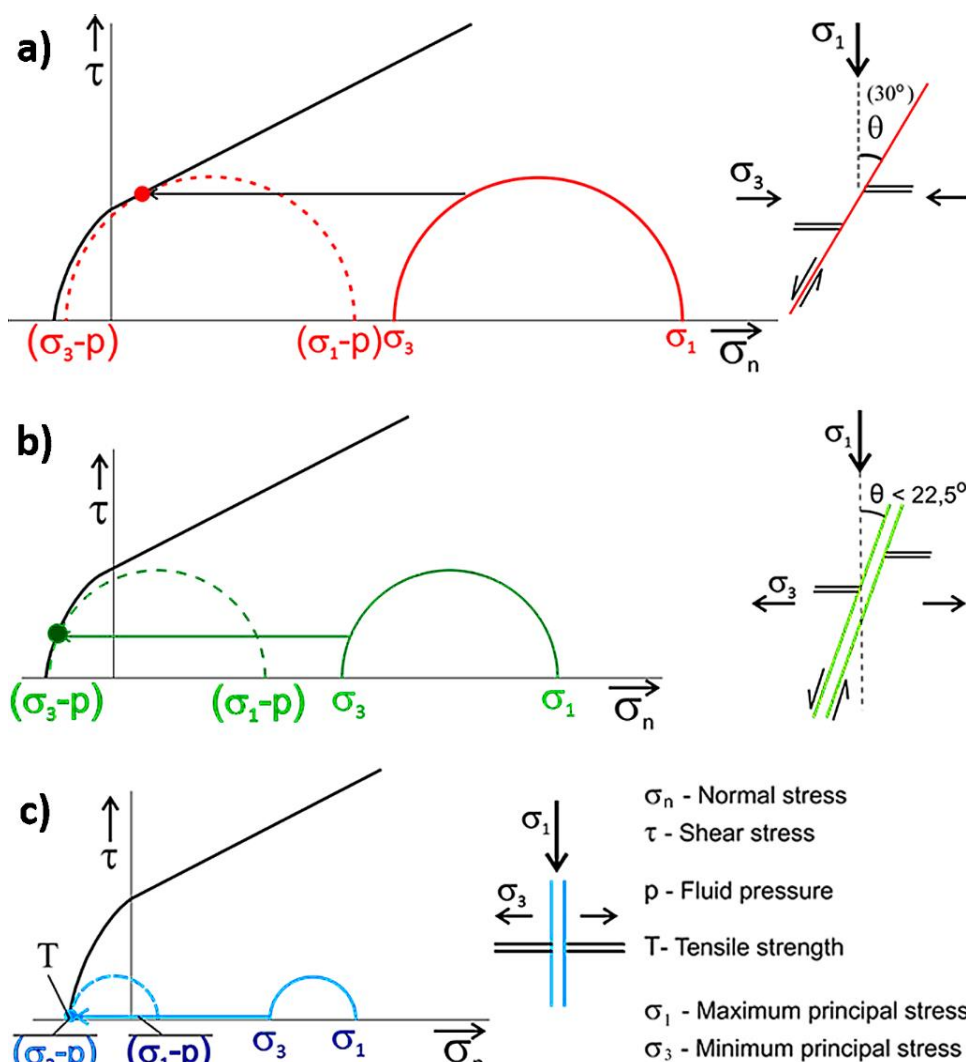
Figure 20 - Overpressure—or abnormal fluid pressure (*p*)—may generate fractures under otherwise stable conditions. Traditionally only joints are called hydraulic fractures. a) The differential stress is large and the isotropic reduction in stress, by the fluid pressure *p*, causes the displacement of the circle to the left until it touches the failure envelope (i.e., shear stress exceeds the shear failure criterion). b) The differential stress is smaller, so that with displacement to the left, the circle touches the Griffith failure envelope, and hybrid fractures are formed. c) The differential stress is even smaller and, with displacement to the left, the Mohr circle touches the Griffith envelope at point *T*, causing the generation of joints (modified from Cosgrove, 1998). The scale of the axes is constant for ease of reference when comparing the Mohr circle sizes.

The stress field in the crust tends to be compressive and, in some cases, can be lithostatic, that is, the principal stresses are derived solely from the weight of the overlying rock column at a given depth. Under lithostatic conditions, the differential stress is not great enough to cause brittle failure. However, even under these conditions, fractures can be generated when the fluid pressure is high enough. Overpressure explains the formation of joints even at great depths (5 to 10 km or even more), where the stresses are strongly compressive (Davis et al., 2011). Depending on both the magnitude of *p* and the mechanical properties of the affected rocks, the shift of the Mohr circle to the left can be large enough to cause the circle to reach either the shear envelope, generating shear fractures, or the point

25

The GROUNDWATER PROJECT   © The Authors   Free download from gw-project.org

Anyone may use and share gw-project.org links. Direct distribution of the book is strictly prohibited.

T, generating joints; it can also reach the Griffith's failure envelope generating hybrid fractures (Figure 20). Cosgrove (1998) and Cosgrove & Hudson (2016) state that all these types of fracturing are the expression of hydraulic fracturing. However, traditionally, only joints formed due to overpressure under compressive stresses are called hydraulic fractures (e.g., Engelder, 1987; Davis et al., 2011; Brenner & Gudmundsson, 2004). The <u>fracture orientation</u>↴ of the hydraulic fractures, as is the case for any fracture, depends on the tectonic regime, which is discussed in Section 3.

2.6 Expected Influence of Fracture Types on Flow

The volumetric flow rate produced by a set of parallel, persistent, and planar fractures is a function of their density (number of fractures per unit distance perpendicular to the fractures) and aperture, as expressed by the cubic law by Snow (1968) and shown in Figure 3. Snow analyzed laminar flow conditions in smooth parallel plate fractures, and reported that the flow rate is proportional to the cube of the fracture aperture and is linearly related to the fracture density. Thus, fracture aperture is more influential than fracture density in controlling the quantity of water flowing through a system of parallel fractures. However, the roughness of the fracture surfaces and the presence of contact areas between the two faces, which are expected for natural fractures, cause the flow to be more tortuous than assumed by the cubic law. Even so, this law is useful for estimating values of flow parameters, rate, and velocity.

The mode of fracture propagation has a direct influence on the fracture aperture. In principle, aperture would be larger for joints, intermediate for hybrid fractures, and smaller for shear fractures. However, aperture can be modified by reactivation during later tectonic events, as explained in Section 4.2. Infilling can significantly diminish the aperture of joints and hybrid fractures. Columnar cooling joints in basalts are an example of diminished aperture as many of them are infilled with minerals that precipitated from <u>hydrothermal fluids</u>↴ during the cooling process within basalt floods (as discussed in Section 4.1.2).

Connectivity, another key factor for fluid flow, is enhanced where conjugate fractures are present because they are frequently connected in three-dimensional space. In addition, it is expected that flow is enhanced at the linear intersections of those fractures. A single set of joints produces little connectivity because joints are generally parallel. A perfect parallelism of persistent fractures is rarely observed thus some limited connectivity among them is usually present.

2.7   Highlights on Fracture Types and Groundwater Flow with Opportunities to Exercise Knowledge Gained by Reading Sections 1 and 2

The most important implications of fracture types (i.e., extension and shear) and of structures formed at different crustal levels for groundwater flow in a fracture network are:

- Ductile structures such as foliation, formed at greater depths, do not produce porosity, however because they are commonly reactivated as fractures during brittle deformation, they influence the fracture network configuration. Thus, rocks with foliation, veins, and other previous anisotropies, will tend to have a denser fracture network and a higher transmissivity.
- The cubic law (Snow, 1968) demonstrates that fracture aperture is more influential than fracture density in controlling the quantity of water flowing in a fracture system. Thus, joints can carry more flow than shear fractures.
- Connectivity, another key factor for fluid flow, is enhanced where conjugate fractures are present because they are frequently connected in three-dimensional space. In addition, the flow can be enhanced at the linear intersections of those fractures.

Exercises 1 through 7 elucidate the constraints on the formation of joints and faults and their association in time and space. They describe plausible scenarios in terms of depth of deformation, mechanical parameters of different rock types, principal stress magnitude, tectonic regimes and fracture types that are formed. With these concrete geological scenarios, we have the opportunity to understand that different types of rock have different mechanical characteristics, such as failure envelopes, cohesion and elastic properties. These factors, together with stress magnitude, control whether extension or shear fractures (parallel or conjugate patterns) are formed, and how fracture geometry, such as spacing can vary from one rock to another. Thus, it becomes evident that stress magnitude and types of rock have influence on the fracture geometry, such as aperture, orientation, and density, and consequently on the fracture network configuration and connectivity, as well as preferential groundwater flow pathways.

Mohr diagrams synthesize the relationships between stress magnitude, mechanical properties of different rock types and types of fractures. Learning the theory underpinning a Mohr diagram, as developed in sections 2.4 and 2.5, is not a simple task. Thus, exercises 2 through 7 offer opportunities of learning and realizing the applications of the Mohr diagram on real problems.

Exercise 1↴ offers an opportunity to consider the depth and timing at which ductile and brittle structures develop and to explore their ability to carry water.

Exercises 2 through 7 address how stress magnitude and mechanical properties of rocks control the fracture types that are formed as deduced from Mohr diagram construction as well as from tectonic regimes.

Exercise 2↓ offers an opportunity to explore the ease of brittle deformation at a given depth, under non-tectonic conditions, for different rock types (dolomite and a mudstone).

Exercise 3↓ offers an opportunity to trace failure envelopes using laboratory data from compressional triaxial tests and to deduce what rock is prone to have more closely spaced fractures and a more connected fracture network.

Exercise 4↓ offers an opportunity to determine what tensile strength is necessary to form joints (fractures with larger aperture) from failure envelopes of two rock types.

Exercise 5↓ offers an opportunity to consider how fractures can be formed under non-tectonic conditions by the changes of fluid pressure. It also shows that depending on rock type the hydraulic fractures can be extension (joints) or shear types.

Exercise 6↓ offers an opportunity to consider: what fracture types will be formed under given stress states represented in the Mohr circle; what tectonic regimes would occur; and what fracture orientations would form for given orientations of the principal stresses.

Exercise 7↓ offers an opportunity to consider what would be the minimum principal stress for the formation of normal faults and the maximum principal stress for the formation of thrust faults at the same given depth. This exercise also provides field data on in-situ stress measurements and explores the types of faults that are prone to forming at shallow depths, as well as the consequences for the orientation of more transmissive fractures close to the Earth's surface.

3 Tectonic regimes, Fracture Patterns and Reactivation

This section discusses

- how the orientation of tectonic stresses near the Earth's surface, and the respective tectonic regimes, control the fracture orientation patterns;
- how joints, hybrid fractures and faults can be recognized on rock exposures; and,
- the reason why reactivation of existing weakness planes is a very common mechanism, causing the lithological types to strongly influence the configuration of the fracture system in a rock mass. Planes susceptible to being reactivated include an existing anisotropic feature, such as foliation, and discontinuities, such as veins or fractures.

3.1 Stress Orientation, Tectonic Regimes and Geometric Patterns of Faults and Joints

The main objective of fractured aquifer research is determining the magnitude and the anisotropy of fluid flow within the rock. The former mostly depends on the aperture, density, orientation, and connectivity of the fractures. Fractures are generally grouped into sets having similar orientations (strike and dip) and appearing as clusters in a stereogram (as shown in the <u>stereographic projection</u>⏎). The anisotropy of the hydraulic properties of the rock mass is mostly controlled by the orientations of the fracture sets, the variability of aperture (because it controls transmissivity) between the sets, and the configuration of fracture connections.

Fracture size and density are related to the brittleness of the rock, as well as to the intensity and duration of the deformation. The strike and dip of the fractures, in turn, are essentially a consequence of the stress orientation. Parallel to the Earth's surface, shear stresses are null, causing one of the principal stresses to be vertical and the other two to be horizontal (Anderson, 1951), as shown in Figure 13. Therefore, at shallow depths where brittle deformation takes place (generally above 10 km) at any given location one of the three tectonic regimes are dominant—namely extensional, strike-slip, and compressive—in which the vertical stresses are σ_1, σ_2 and σ_3, respectively. These are called Andersonian tectonic regimes. The names *compressive* and *extensional* are related to the type of deformation they cause in the crust. The compressive regime causes shortening and the extensional, stretching. In the strike-slip regime, neither shortening nor extension takes place. However, as discussed in this section, all the principal stresses, in each of the three regimes, can be compressive (positive) and this condition gives rise to faults. By the same token, for all of them, when σ_3 is tensile (negative), joints may be formed. Each of the three

29

regimes cause fracture direction and dip to be systematically organized. These three tectonic regimes give rise to the three classic types of faults: normal, thrust and strike-slip.

In the *extensional tectonic regime*, σ_1 is vertical and, consequently, σ_2 and σ_3 are horizontal. The resulting faults dip at about 60° and the offset is mostly vertical, thereby giving rise to slickensides↲ with striae lineation↲ parallel to the fracture dip. These are called *normal faults* (Figure 21, Figure 22, and Figure 23).

Figure 21 - Extensional tectonic regime and normal faults. a) Landscape associated with areas where normal faults of the extensional tectonic regime have been recently active or are presently active, otherwise the relief once created by the fault movement would have been suppressed by erosion. Faults and joints can be formed under the same tectonic regime because the magnitude of the principal stresses can vary over time. Conjugate shear fractures are formed under compressive (positive) σ_1 and σ_3 (red arrows). Joints, or opening mode fractures, are formed perpendicular to a tensile (negative) σ_3 (blue arrows). The joints form a set of parallel vertical fractures (the blue line is one of them). b) In the stress ellipsoid of the extensional tectonic regime, σ_1 is vertical and σ_3 is horizontal. c) The conjugate normal faults have the same strike (parallel traces on the terrain surface) and opposite dips (in this case, toward the west or toward the east) around 60°. The parallel lines on the fault surface represent the striae lineation parallel to the dip of the fault. d) Stereographic projection of north–south striking normal faults along with the orientation of the principal stresses.
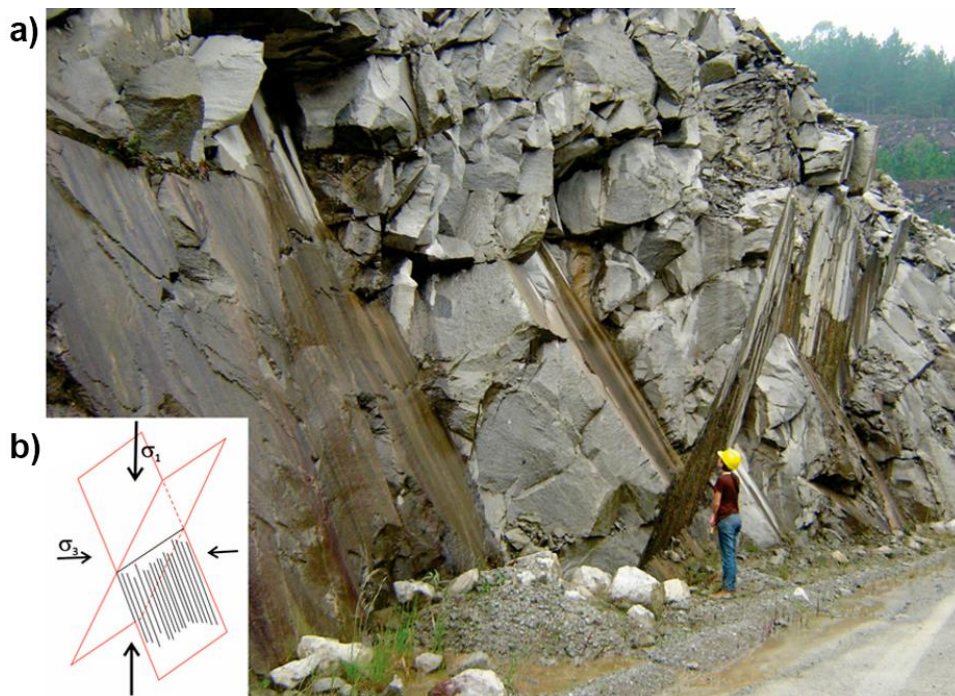
Figure 22 - Extensional tectonic regime and normal faults. a) Conjugate normal faults (Fiume, 2013) cutting through a massive granite. The outcrop is in a quarry in the São Paulo Metropolitan Region. Inset b) shows a schematic of the conjugate normal faults.

Figure 23 - Conjugate normal faults in an extensional tectonic regime (Fiume, 2013) displacing sedimentary rock beds, mostly sandstones. The shear sense is shown by the arrows. (photograph: Ricardo Hirata, nearby Tegucigalpa, Honduras).

31

In the *compressive tectonic regime*, σ_3 is vertical and, consequently, σ_1 and σ_2 are horizontal; the faults dip at around 30° and the offset is mostly vertical, thereby giving rise to slickensides with striae lineation parallel to the fault dip. These are called *thrust faults* (Figure 24, Figure 25, and Figure 26).

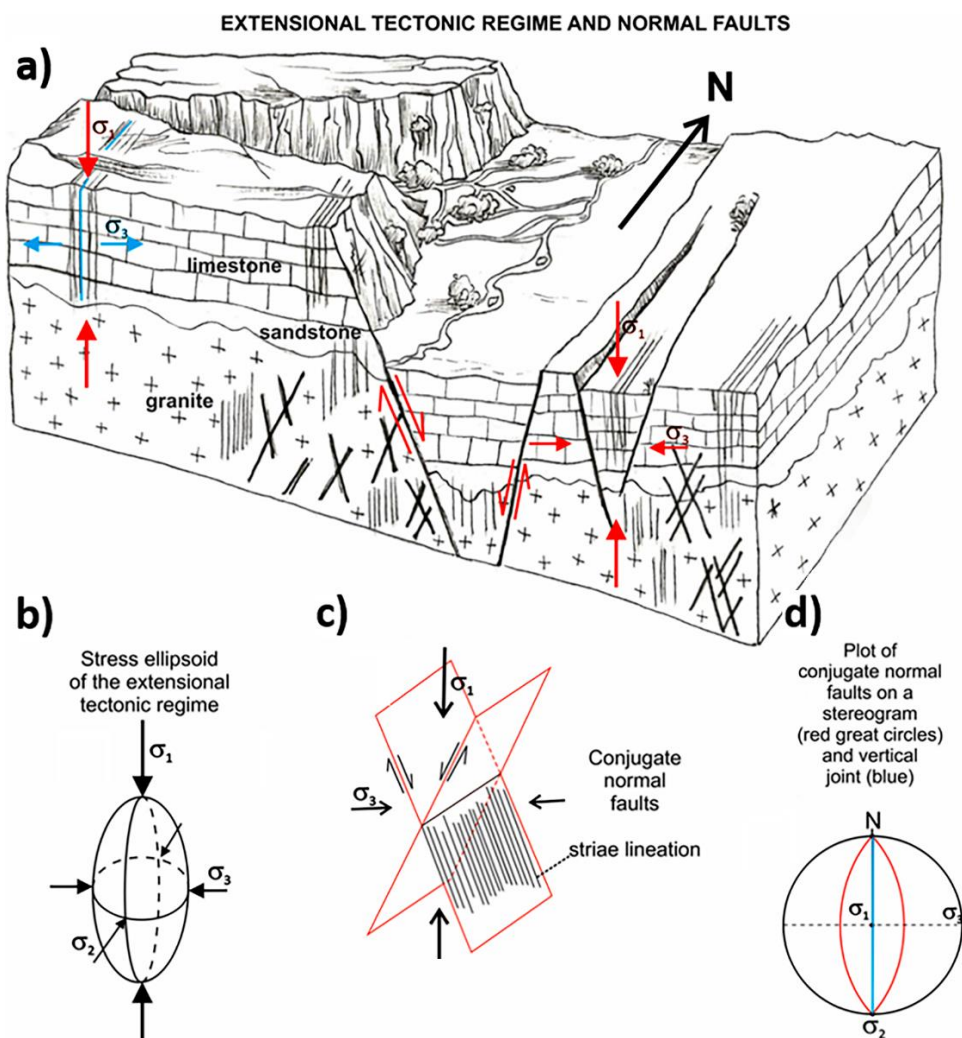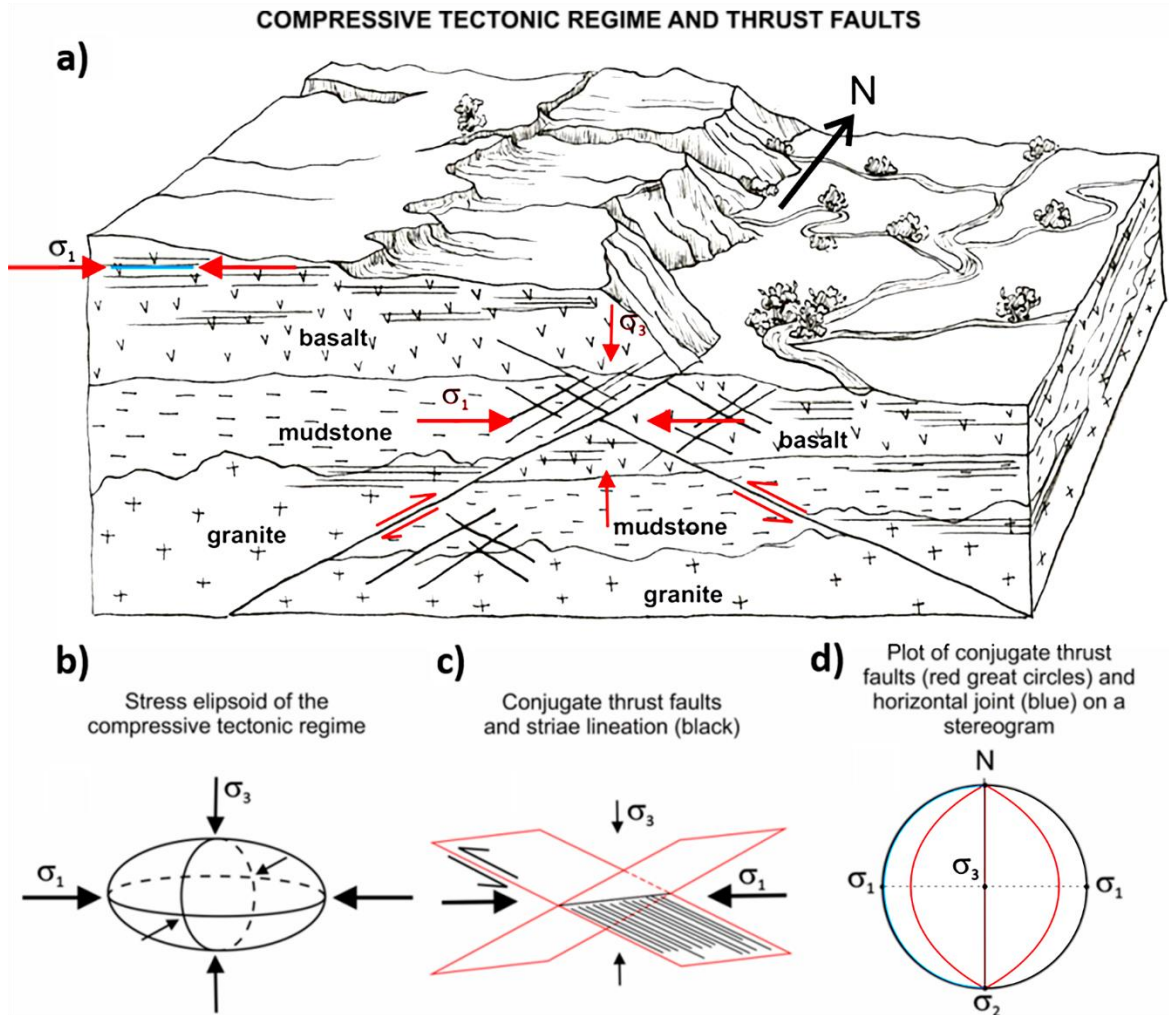**Figure 24 -** Compressive tectonic regime and thrust faults. a) Landscape associated with areas where thrust faults of the compressive tectonic regime were recently or are presently active, otherwise the relief created by the fault movement would have been smoothed by erosion. Faults and joints can be formed under the same tectonic regime because the magnitude of the principal stresses may vary over time. Conjugate shear fractures are formed under compressive (positive) σ_1 and σ_3 (red full arrows). Relative movement is indicated by red half-arrows. Joints, or opening mode fractures, are formed perpendicular to σ_3 and are horizontal (the blue line is one of them). b) In the stress ellipsoid of the compressive tectonic regime, σ_1 is horizontal and σ_3 is vertical. c) The conjugate thrust faults have the same strike (parallel traces on the terrain surface) and opposite dips (in this case, toward the west or toward the east) of around 30°; the parallel lines on the fault surface represent the striae lineation parallel to the dip of the fault. d) Stereographic projection of north-south striking normal faults, also showing the orientation of the principal stresses.
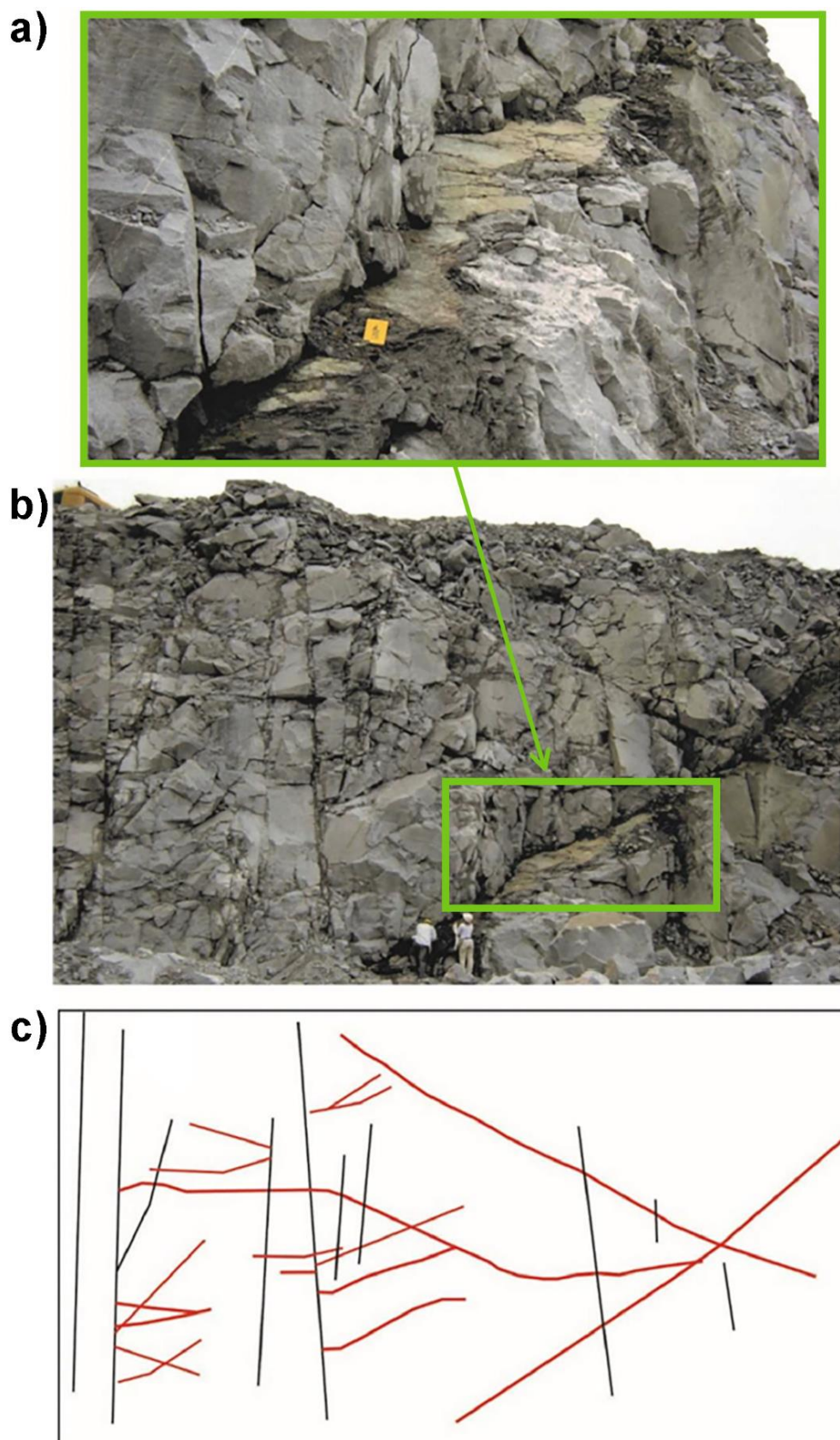
Figure 25 - Compressive tectonic regime thrust faults. a) Expanded area of green rectangular area focused on a thrust fault as shown in b). c) Schematic of (b) showing thrust faults abutting against high dip fractures (photographs: Fiume, 2013).

33

The GROUNDWATER PROJECT   © The Authors   Free download from gw-project.org

Anyone may use and share gw-project.org links. Direct distribution of the book is strictly prohibited.
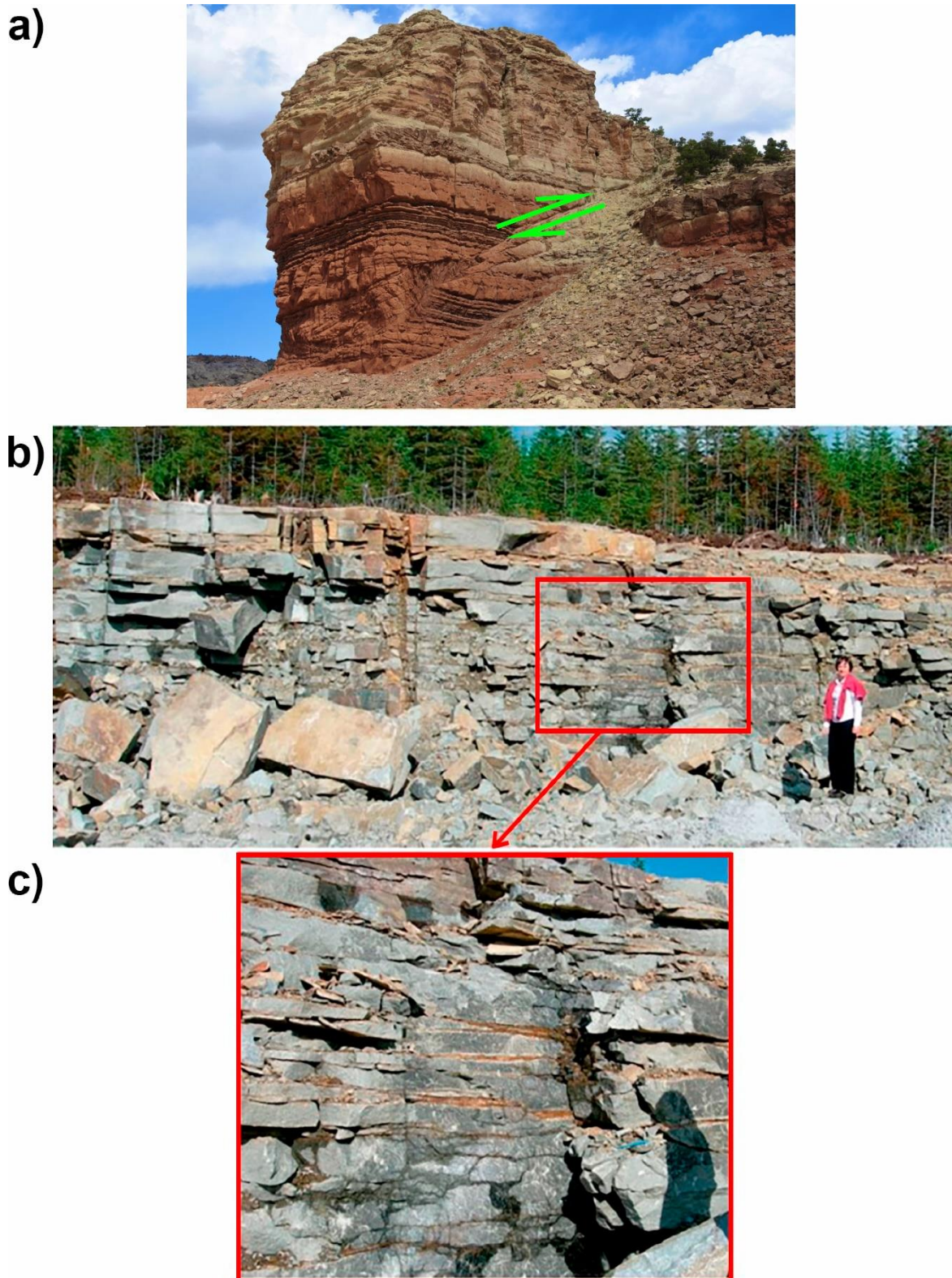
Figure 26 - Compressive tectonic regime thrust faults. a) Thrust fault (photograph: Haakon Fossen, 2016). b) Closely spaced and persistent sheeting joints that appear just below the ground surface, that are formed under a horizontal maximum principal stress (σ_1) of a compressive tectonic regime, as discussed further in Section 3.6. c) Expanded view of red area in b) showing a closeup of the sheeting joints (photographs: Alain Rouleau).

34

In the *strike-slip regime*, σ_2 is vertical and, consequently, σ_1 and σ_3 are horizontal; the faults dip close to 90° and the offset is mostly horizontal, thereby giving rise to slickensides with striae lineation parallel to the direction of the fault. These are called *strike-slip faults* (Figure 27, Figure 28, and Figure 29). The horizontal relative movement of the blocks separated by a strike-slip fault can be either sinistral or dextral. The fault is sinistral (left-handed) when the block that is to the left moves toward the observer (Figure 29a), and the fault is dextral (right-handed) when the block that is to the right moves toward the observer. In a strike-slip fault zone, the conjugate faults are called Riedel shears, R_1 and R_2 (Figure 28a). R_1 shear movement is consistent with the general sense of movement of the fault zone, and for R_2 the sense of movement is the opposite (Figure 29a). Overlapping strike-slip faults may give rise to sectors where shortening (reduction in length) and extension (increase in length) take place across the zones simultaneously with respect to the horizontal displacements (Figure 29b,c); secondary thrust or normal faults, restricted to those sectors, may develop in association with the strike-slip faults (Ramsay & Hubber, 1987; Woodcock & Schubert, 1994, among many others). These sectors may have implications for groundwater flow, as discussed in Section 3.2 where the influence of the tectonic regime on the connectivity of, and flow within, the fracture network is discussed.
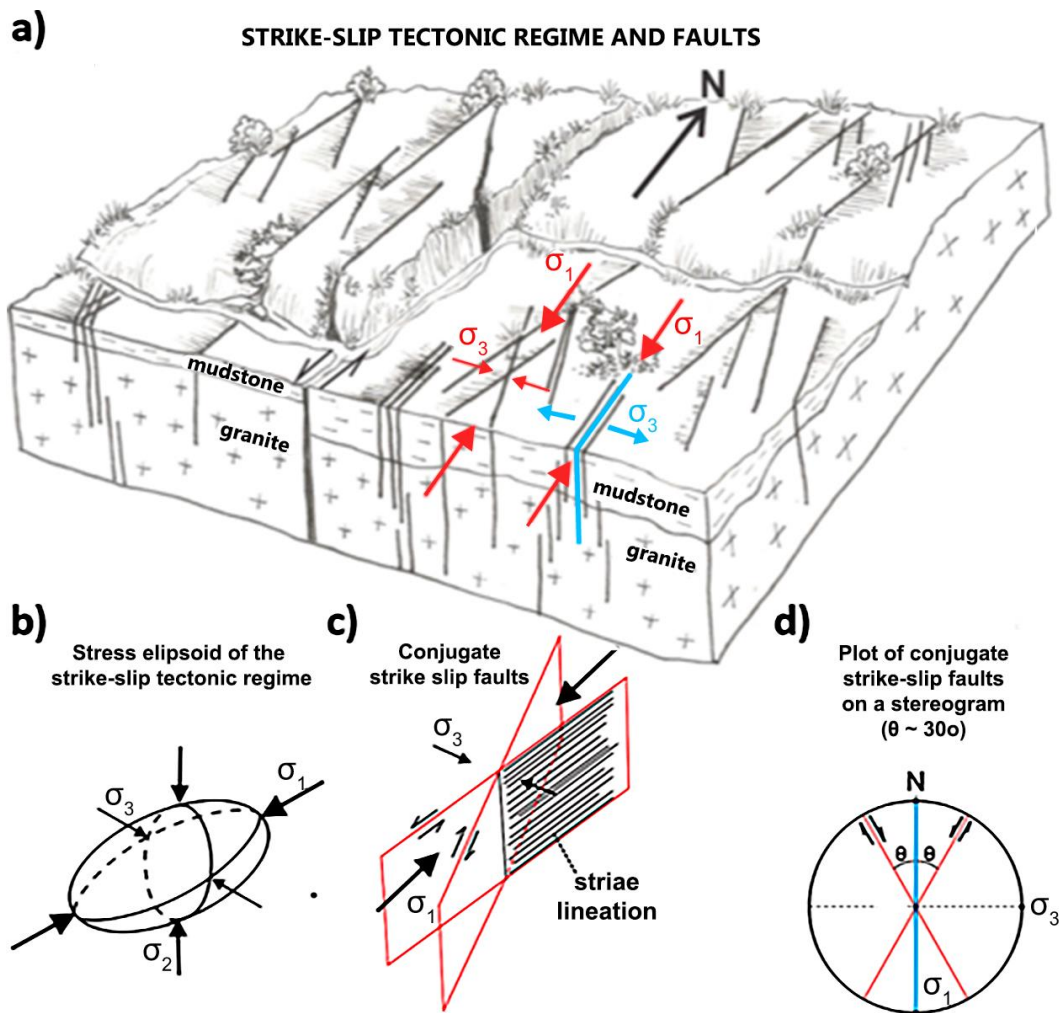
Figure 27 - Strike-slip tectonic regime and faults. a) Landscape associated with areas where strike-slip faults of the strike-slip tectonic regime were recently or are presently active, otherwise the relief created by the fault movement would have been smoothed by erosion. Faults and joints can be formed under the same tectonic regime because the magnitude of the principal stresses can vary over time. Conjugate shear fractures are formed under compressive (positive) σ_1 and σ_3 (red arrows). Joints, or opening mode fractures, are formed perpendicularly to a tensile (negative) σ_3 (blue arrows). The joints form a set of parallel vertical fractures (indicated by the blue line). b) In the stress ellipsoid of the strike-slip tectonic regime, σ_1 and σ_3 are horizontal. c) The directions of the conjugate strike-slip faults make an angle of around 60° with each other (the fault traces on the terrain surface have the same pattern) and the dips are vertical. c) The parallel lines on the fault surface represent the striae lineation parallel to the strike of the fault. d) Stereographic projection of approximately N30E- and N30W-striking conjugate faults in the strike-slip regime, and the orientation of the principal stresses.
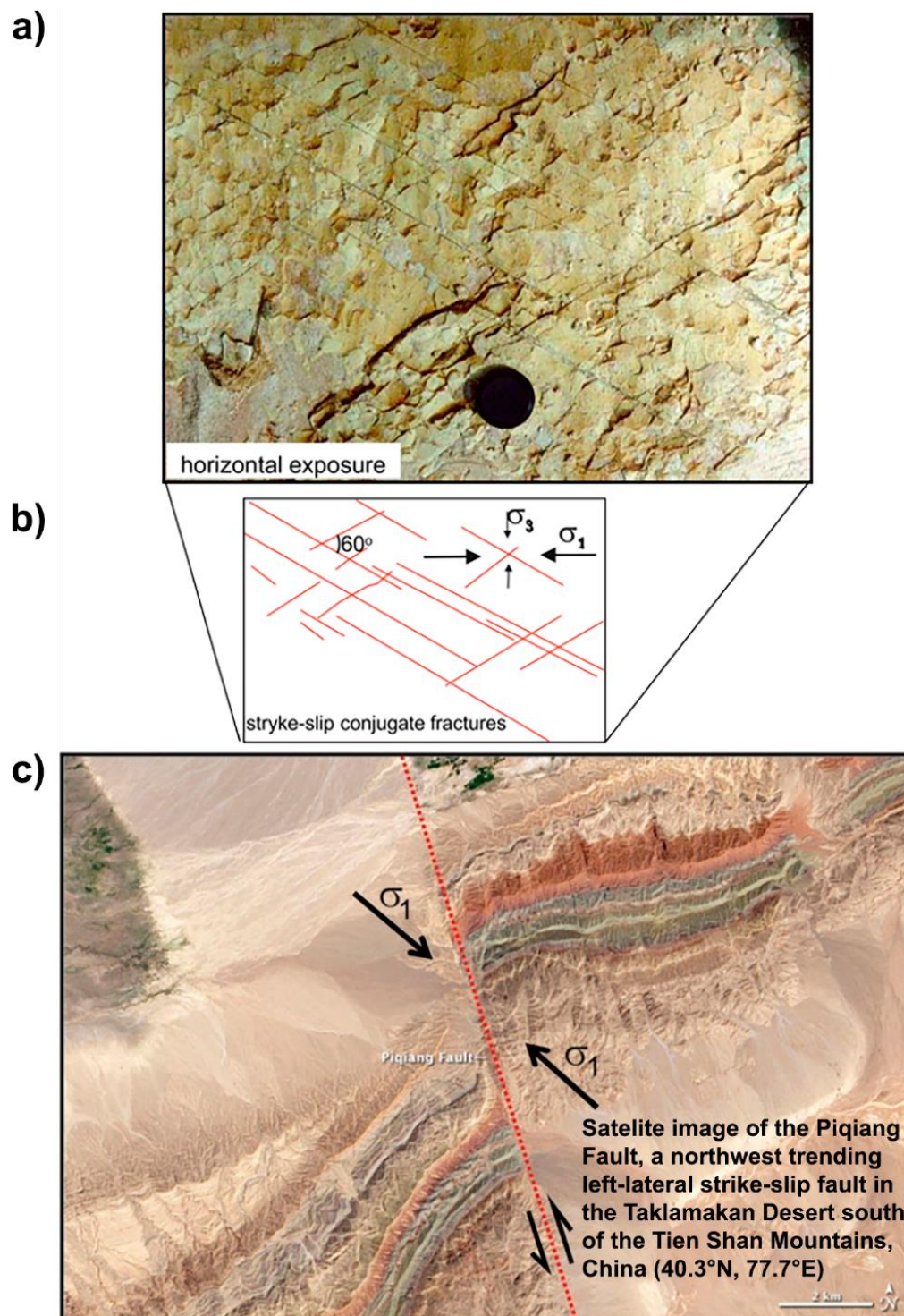
Figure 28 - Strike-slip tectonic regime shear fractures and faults. a) Horizontal exposure of a silty sandstone with fine traces of subvertical conjugate shear fractures, also called Riedel shears, as shown in the sketch b) below the photograph (Campinas, São Paulo State, Fernandes & Amaral, 2002). c) Spectacular sinistral strike-slip fault with roughly 4 km of horizontal displacement; the orientation of σ_1 is approximate (Pingyiang Fault, China, https://earthobservatory.nasa.gov/images/82853/faults-in-xinjiang↗).
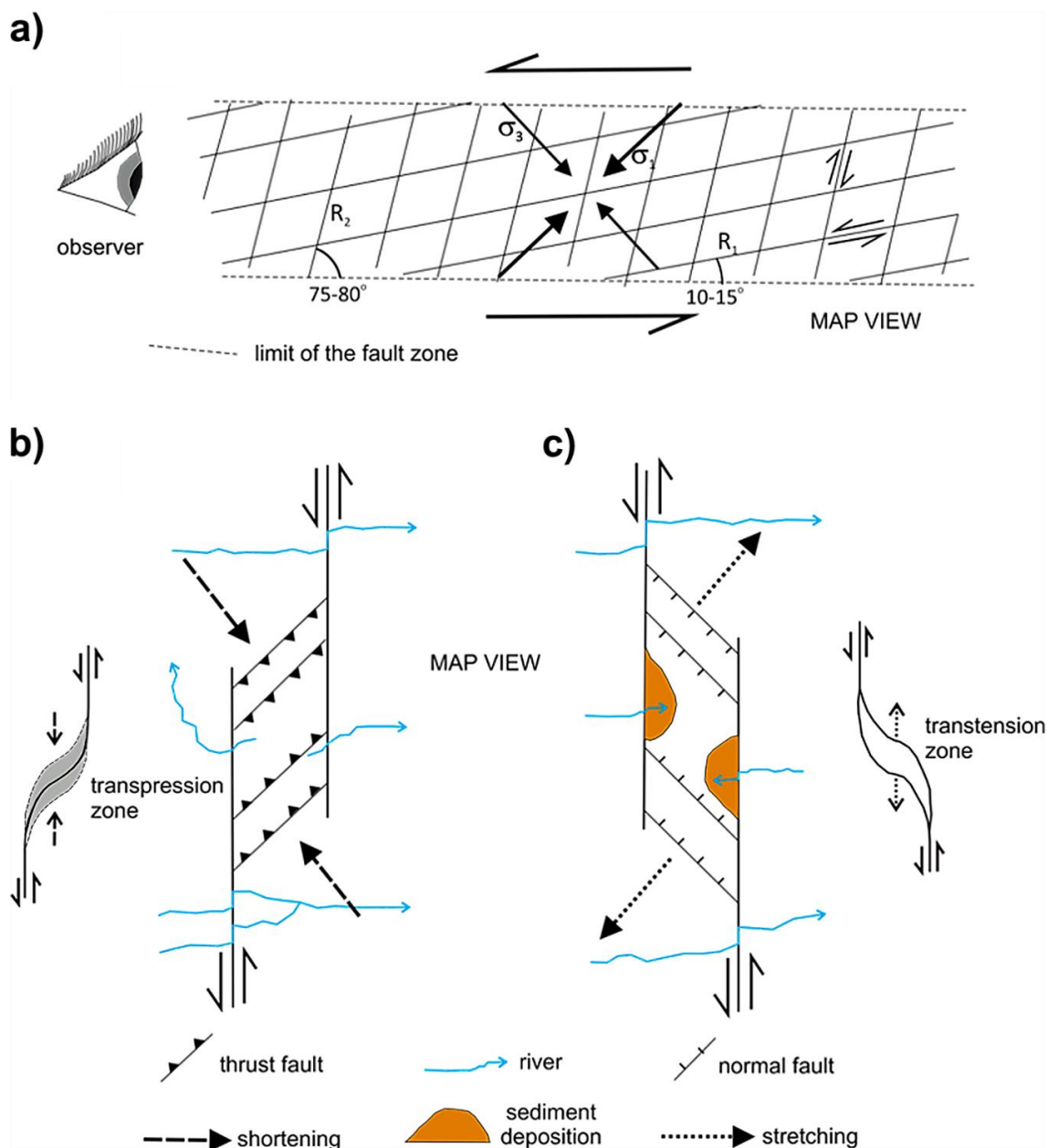
Figure 29 - Strike-slip tectonic regime faults. a) Strike-slip fault zone with a sense of left-hand movement, that is, from the observer's position (eye to the left) the portion to the left of the eye moves toward viewer. The deformation is concentrated along the fault zone where strike-slip conjugate shear fractures develop. The conjugate fractures are also called Riedel shears R_1 and R_2. R_1 represents the shear fractures that have the same sense of movement as the fault zone which is left-hand in this case. R_2 are the shear fractures with the opposite sense of movement, i.e., right-hand. Bending or overlapping strike-slip faults may give rise to zones where b) shortening (transpression) and c) extension (transtension) are present across the domain at the same time as the directional displacements are occurring. Secondary thrust faults are restricted to the transpression zones b) while normal faults are restricted to the transtension zones c). Sediment deposition is likely to take place at the depressions that may form at transtension zones. The sense of the river flow indicates the position of highlands b) and lowlands c). These structures in the zones provide a connection between the otherwise separate faults. Moreover, depending on the stress magnitude, horizontal joints may be generated in the transpression zone while vertical joints may be generated in the transtension zone and they may favor groundwater flow (modified from Ramsay & Hubber, 1987).

The rock failure criteria, expressed by the Mohr-Coulomb and Griffith envelopes, imply that faults and joints are formed under different stress conditions and, therefore, cannot propagate at the same time. However, over time, if the orientation of the stresses is constant but their magnitudes change, the tectonic regimes can generate joints, when σ_3 is tensile, and faults, when stresses are all compressive. Joints are perpendicular to σ_3 and, therefore, in the extensional and strike-slip regimes they are vertical (Figure 30). In the compressive regime, horizontal joints can be formed when the fluid pressure causes the effective vertical stress to be tensile. Stress conditions similar to the ones in the compressive tectonic regime (a compressive horizontal stress and a vertical σ_3) are thought to be associated with the generation of sheeting joints (Figure 26b,c), also called relief joints. These persistent and closely spaced joints are parallel to the topographic surface and found just below the ground surface down to depths of usually less than 100 m. These joints are observed, for example, in granites, gneisses and hard sandstones. The mechanisms for their generation are discussed in Section 3.6.

Figure 30 - Joint and fault dips formed in the three Andersonian tectonic regimes (extensional, compressive and strike-slip). The resulting deformations in the extensional and compressive regimes are horizontal stretching and shortening, respectively. In the strike-slip and extensional regimes, joints may be formed when σ_3 is negative (tensile), and faults when σ_3 is positive. The conditions required to form joints in the compressive regime are explained in the text. Although joints and faults can be formed in the same tectonic regime, they cannot be generated at the same time, as illustrated by the Mohr circle.

As the tectonic regime controls fracture orientations, it will also impose certain characteristics to the connected fracture network. This and other implications for groundwater flow, such as how depth influences the hydraulic conductivity of subhorizontal fractures and sheeting joints, are described in Section 3.2.

3.2 Influence of the Tectonic Regime on the Connected Fracture Network

Joints and faults are not generated simultaneously because the stress conditions (as expressed by the Mohr diagram) required for producing them are different. Throughout the duration of a tectonic event in which the stress orientation remains the same, the magnitude of the stresses can change. This may lead to the generation of both joints and faults at different times in the same event and may enhance connectivity and, possibly, the aperture of some fractures.

Thrust and normal conjugate faults produce horizontal intersection lines, whereas strike-slip fault intersections are vertical. Thus, depending on the tectonic regime, horizontal and vertical flow channels can potentially be formed along fault intersections. The conjugate faults generated by the compressive and extensional regimes would favor horizontal flow channels, and the strike-slip regime, vertical flow channels.

Low dip or horizontal fractures (compressive regime) are more likely to show a decrease in hydraulic conductivity (K) with depth due to the increasing overburden stress of the rock column weight (e.g., Morin & Savage, 2003). The depth from which the decrease of aperture starts to be significant may vary from place to place in response to the variation of the in-situ stress magnitudes. On the other hand, K of vertical fractures, either joints or faults, is likely less affected by depth (increasing rock column) (e.g., Morin & Savage, 2003). In general, the ratio of average horizontal stress to vertical stress of the current in-situ stresses decreases with depth as shown in Figure 31 (Hoek & Brown, 1980). This suggests that, in general, the closer to the surface, the larger the aperture of the subhorizontal fractures becomes. This is consistent with the data obtained in several regions as discussed in Section 4.1.
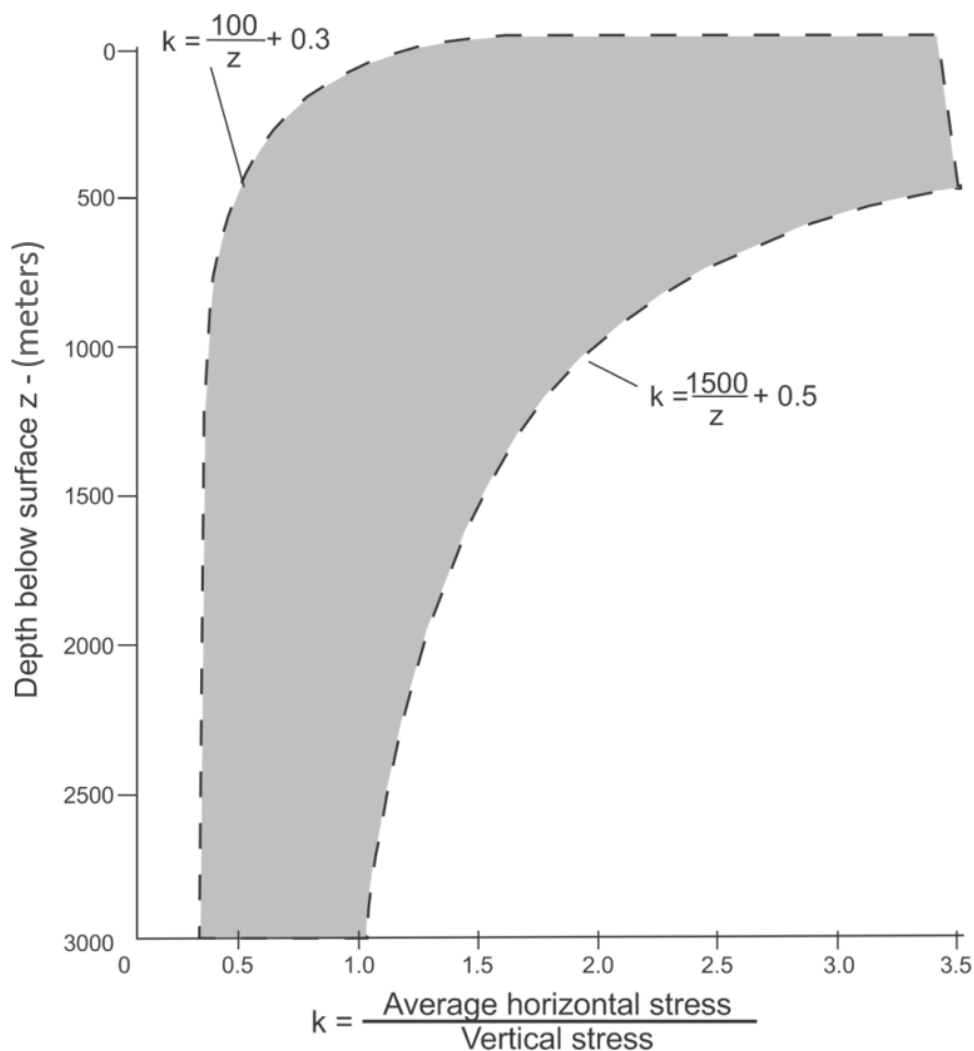
Figure 31 - In-situ stress data from several regions throughout the globe (Australia, United States, Canada, Scandinavia, southern Africa, and others). Close to the surface (above 500 m in depth), the average horizontal stress can be roughly three times larger than the vertical stress (modified from Hoek & Brown, 1980).

The persistence of sheeting joints and their large apertures favor connectivity and flow. Often, however, a significant number of them are in the unsaturated zone. The largest apertures, exceeding millimeters or centimeters, can be just below or very close to the ground surface and their permeability tends to sharply decrease with depth, as is the case for many other subhorizontal fractures.

Where strike-slip faults overlap, transpression and transtension zones can be formed (Figure 29b,c) and this induces the generation of thrust and normal faults, respectively. These structures provide connection between otherwise separate strike-slip faults. Depending on the stress magnitude, horizontal and vertical joints may be developed in the transpression and transtension zones, respectively; this process enhances not only fracture connectivity, but also groundwater flow.

41

3.3 How are Joints, Hybrid Fractures and Faults Recognized on Rock Exposures?

Because joints are perpendicular to σ_3, they typically form a set of parallel fractures (Figure 32). Their dip and direction will depend upon the tectonic regime and on the orientation of σ_3 (Figure 30). In the Andersonian tectonic regimes, joints can be either horizontal (compressive regime) or vertical (extensional and strike-slip regimes). Plumes and ribs may be present on the surface of joints, and hackle (en echelon smaller fractures with plumes on their surface) may be present at joint fringes (Figure 33 and Figure 34).
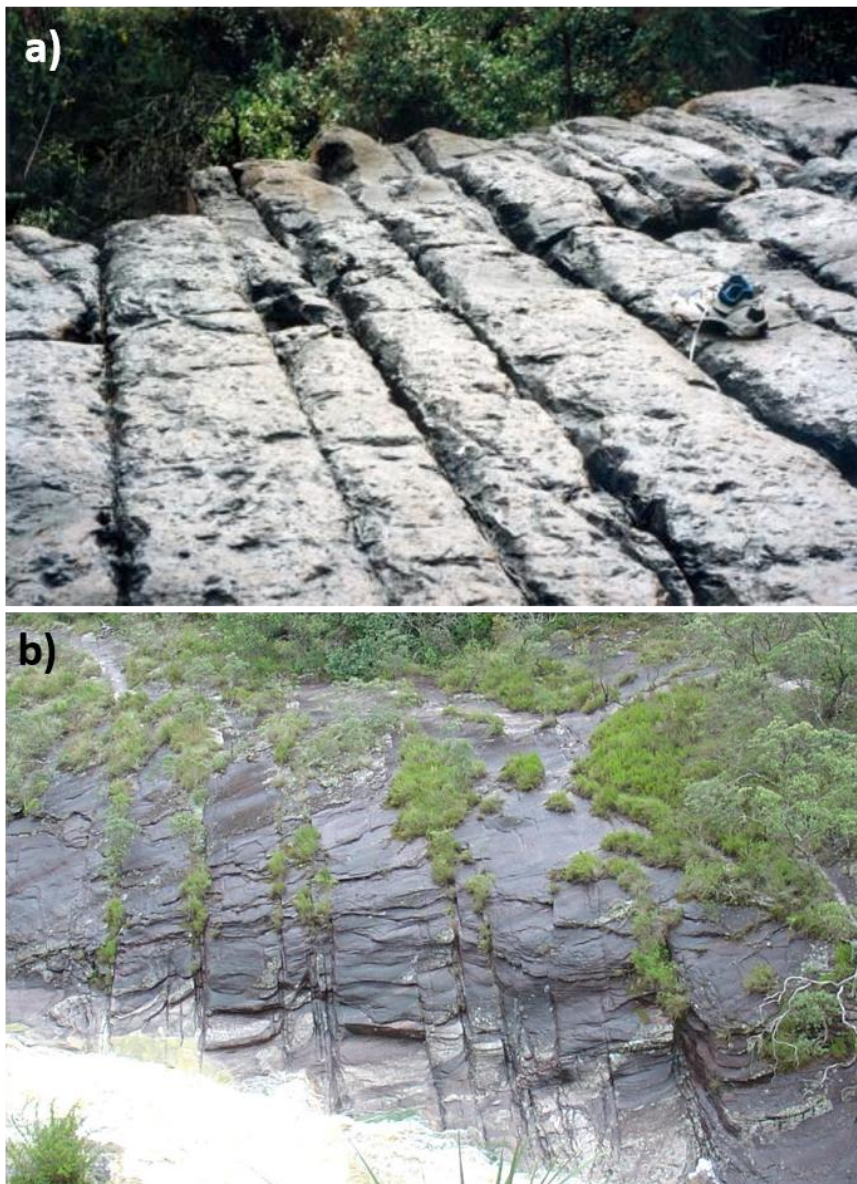
Figure 32 - The parallelism of fractures in limestone (a) and in sandstone (b) is evidence of propagation by the opening mode, so these are joint sets. Both are vertical and generated under either a strike-slip or an extensional tectonic regime (photographs: Amélia Fernandes, taken in Colombia (a) and in Brazil (b)).
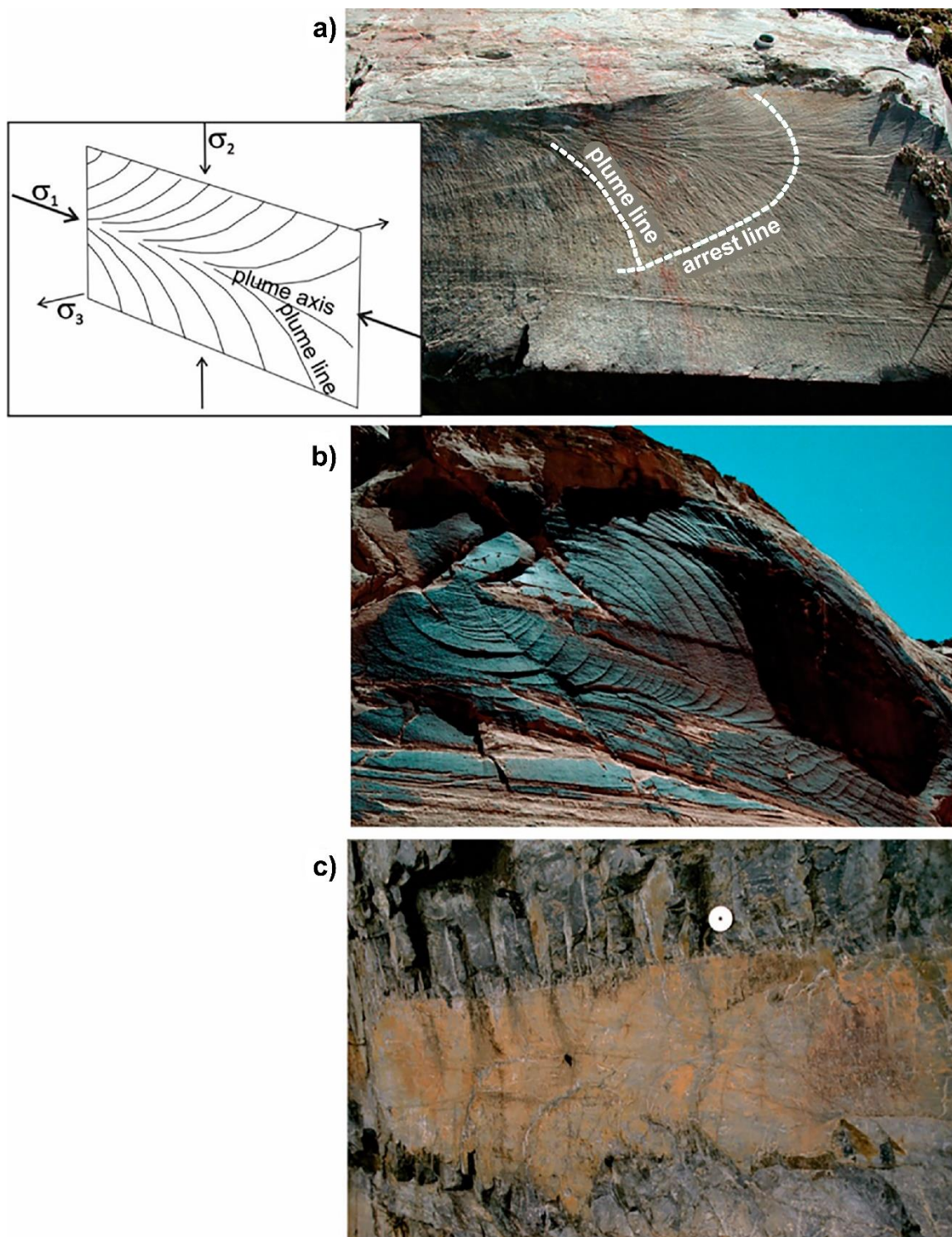
Figure 33 - Fracture surface features typical of joints (opening mode fractures) from Fossen (2016). a) Plume and arrest lines on an extensional joint in meta-graywacke. The arrest lines (red) resemble ribs and are the loci where propagation was periodically interrupted. The drawing shows the orientation of the stresses in relation to the orientation of the plume axis (based on Dunne & Hancock, 1994). b) Prominent elliptical arrest lines in sandstone. c) Joint (orange color) with hackle fringes (en echelon fractures) in meta-rhyolite. Extension fractures twist (and are arrested) as they reach an interface with a mechanically different rock layer.
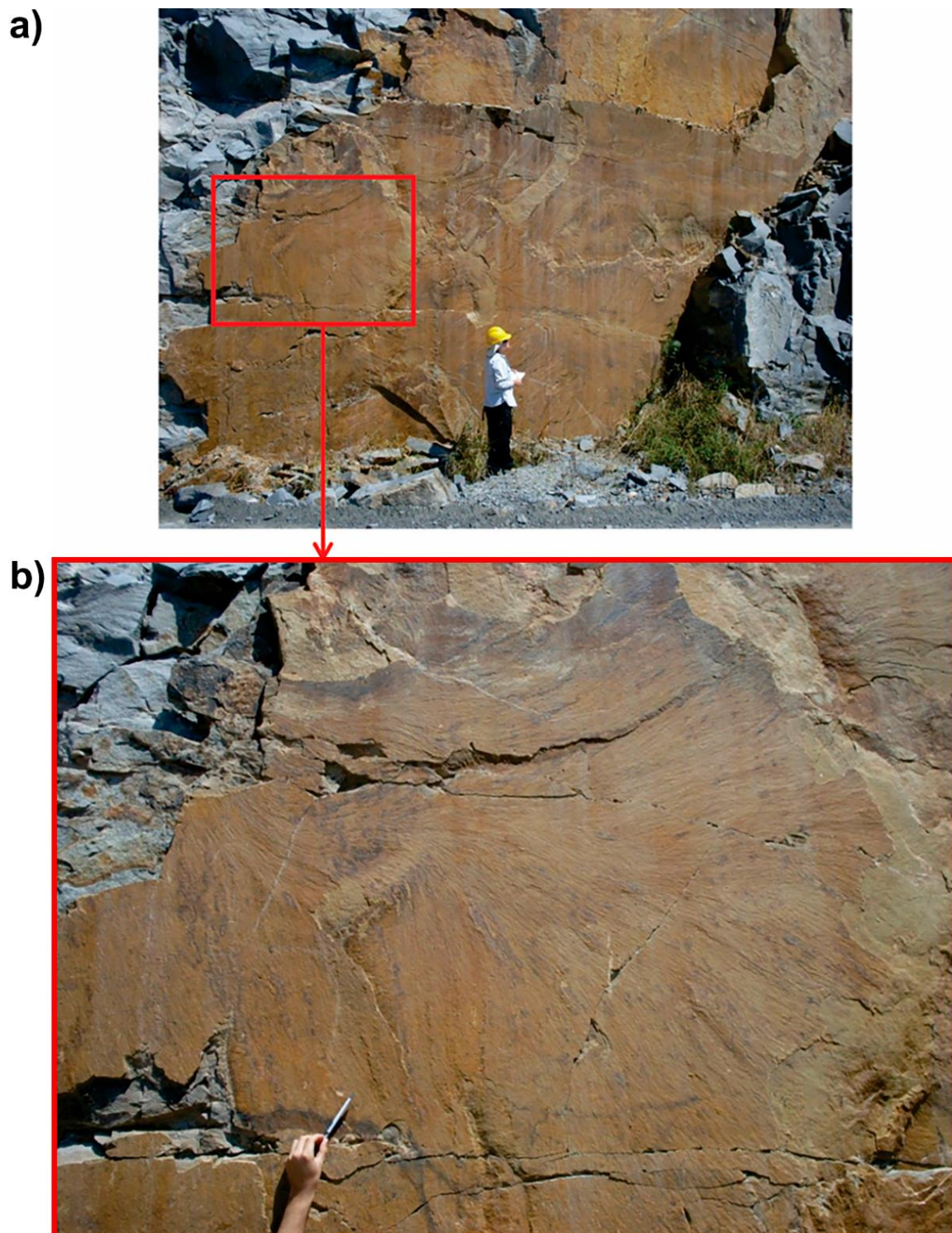
Figure 34 - Irregular plume on a joint surface in granite. The rock is un-weathered and there is an ocher coating on the joint surface from iron oxide precipitation. The approximately horizontal axis of the plume indicates that the joint was formed in a strike-slip regime (photograph: Bruna Fiume).

Shear and hybrid fractures typically form two sets of conjugate fractures (Figure 35 and Figure 36a), with an angle of approximately 60° for the former and less than 45° for the latter (Figure 16 and Figure 18). In addition, striae lineation and the respective perpendicular steps, which are used as indication of the movement sense (Petit, 1987), are frequently observed on fault and shear fracture surfaces (Figure 36b, Figure 37). Hybrid fractures may bear fainter striae lineation and plumes on the same surface. Under the Andersonian tectonic regimes, the dip of faults may be around 60° (extensional regime), 30° (compressive regime) and vertical (strike-slip regime) (Figure 30). Striae lineation is parallel to the dip in the first two cases (Figure 37a,c) and parallel to the direction in the latter (Figure 37b).
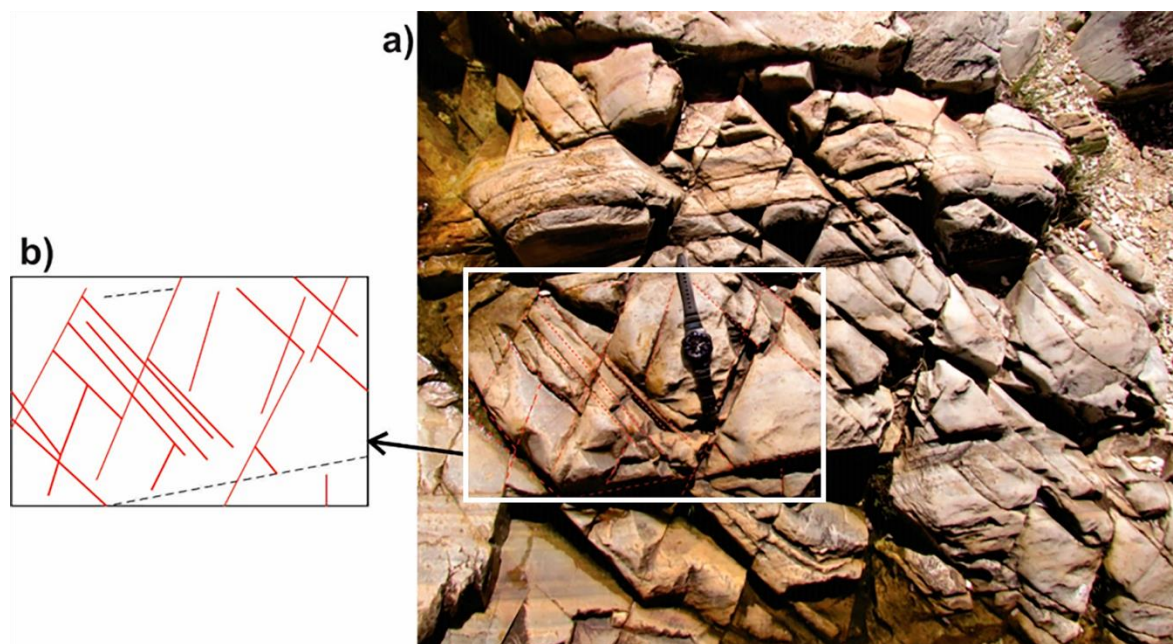
Figure 35 - Typical pattern of shear fractures. a) Conjugate fractures (red lines in the inset drawing) and bedding-parallel fractures (dashed black lines) in a low-grade-metamorphism fine sandstone. b) A detail of part a. The exposure is subhorizontal and the conjugate fractures are subvertical, and are therefore generated in the strike-slip tectonic regime. Region of Capitólio, Minas Gerais, Brazil (photograph: Amélia Fernandes).
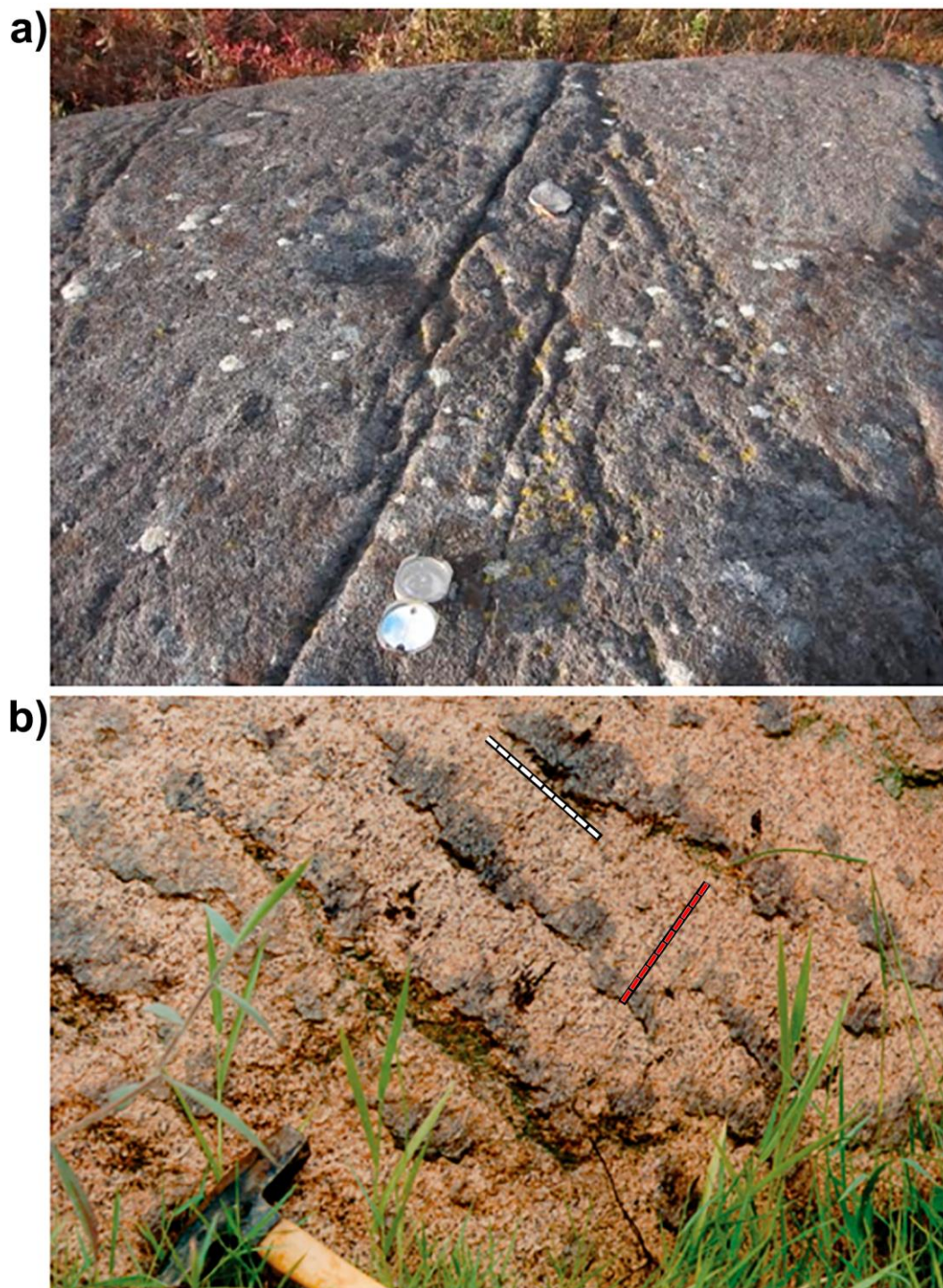
Figure 36 - Typical pattern of shear fractures. a) Pattern of hybrid conjugate fractures forming an acute angle of 45°; Abitibi region, Québec, Canada. The conjugate fractures are subvertical, therefore generated in the strike-slip tectonic regime (photographs: Amélia Fernandes). b) Surface of a subvertical fault in massive granite, in Campinas, São Paulo, Brazil (Fernandes & Amaral, 2002). The oblique striae lineation (parallel to the red dashed line) along with steps (approximately parallel to the dashed white line) on one side of the quartz infilling stripes (grey color) is a good visual indicator of the sense of movement. In this case, the movement is dextral or right-hand (the missing block moves toward the observer). The fault is subvertical, which is typical of the strike-slip tectonic regime, and the dip of the striae lineation indicates oblique movement (horizontal and vertical components).
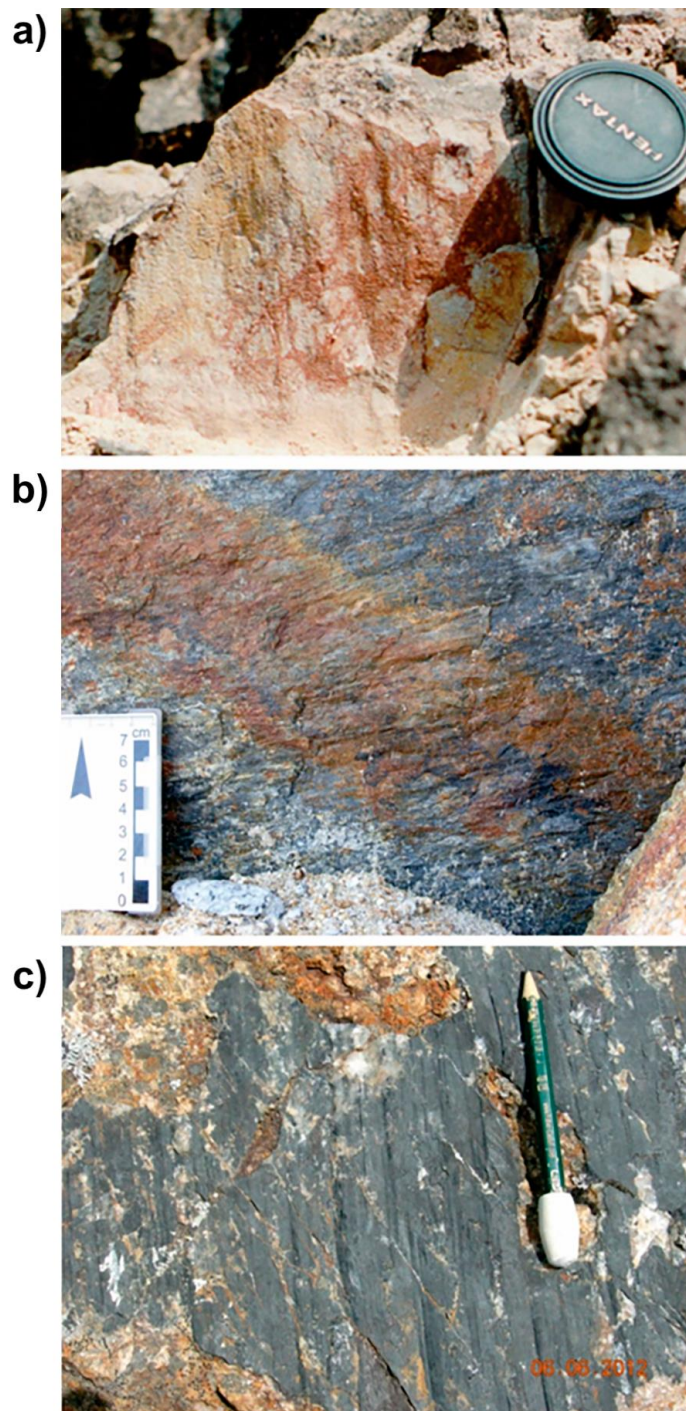
Figure 37 - Typical pattern of shear fractures. a) A small fault in Miocene mudstone, in Campinas, São Paulo, Brazil. The fault dip, around 60º, and the striae lineation, parallel to the fault dip, indicate that this is a normal fault formed under the extensional tectonic regime. b) Subvertical fault (in granite) with subhorizontal striae lineation, implying a strike-slip tectonic regime; little steps transversal to the striae lineation are used as indication of the movement sense. c) Fault in gneiss dipping around 30º, with striae lineation parallel to its dip; these characteristics are consistent with a thrust fault generated under a compressive tectonic regime (photographs: Amélia Fernandes).

The fracture type and the tectonic Andersonian regimes are deduced from data collected in the field regarding fracture patterns (parallel or conjugate), fracture dip, striae lineation orientation and features present on the fracture surfaces (plumes or striae). A flowchart showing the type of data collected from rock exposures, and the corresponding interpretation of the fracture type and tectonic regime, is given in Figure 38.
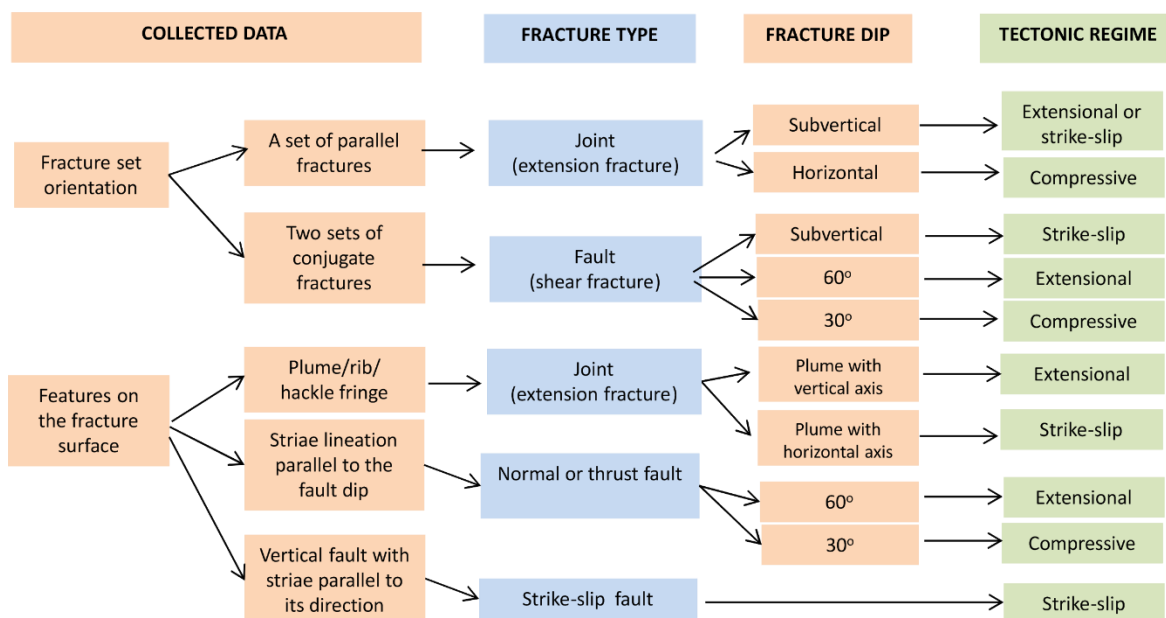
Figure 38 - The fracture type and the tectonic Andersonian regimes are deduced from the data collected from rock exposures regarding fracture patterns (parallel or conjugate), fracture dip, striae lineation orientation and features present on the fracture surfaces (plumes or striae).

3.4   Reactivation of Pre-Existing Structures

Planar features such as foliation (e.g., schistosity, gneissic banding, mylonitic orientation), sedimentary bedding, and lithological contacts can be reactivated as fractures during brittle deformation events. Likewise, fractures formed under an older tectonic event with a specific stress field may undergo displacement when subjected to a younger tectonic event. This phenomenon, called reactivation, happens when the orientation of the older fractures, with respect to the newer stress field, is favorable for opening or shear.

The Mohr diagram shows that reactivation requires smaller stresses than those needed for the generation of new fractures. This happens because the cohesion of the rock along any previous structure, such as foliation (C_f), is smaller than the one across the existing structure (C) (Figure 39). A smaller cohesion causes the failure envelope to move downward in the Mohr diagram, and the required stresses to reactivate the foliation will depend on the angle between this structure and σ_1; for specific values of differential stress, a range of foliation orientations can be reactivated by shear (Figure 39b). Fracture orientations may mimic the foliation orientation, and this is especially apparent when the foliation is folded (Manda et al., 2008; Fernandes et al., 2016b, among many others).

48

The GROUNDWATER PROJECT   © The Authors   Free download from gw-project.org

Anyone may use and share gw-project.org links. Direct distribution of the book is strictly prohibited.

Depending on the magnitude of the principal stresses and on the orientation of the foliation, reactivation can occur by shear, opening, or both.
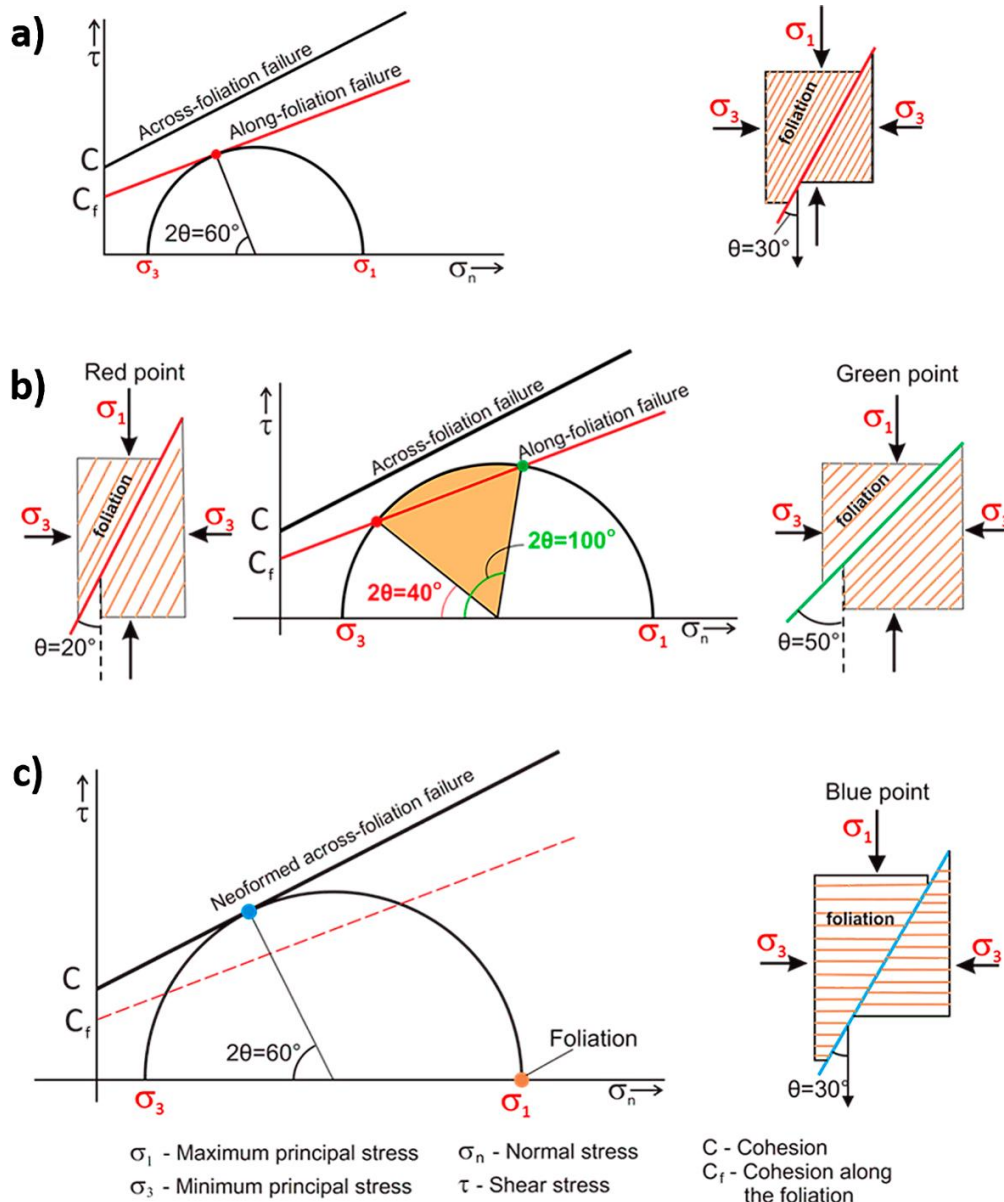
Figure 39 - Shear strength along the foliation (C_i) is smaller than that across foliation (C). Thus, fractures formed by reactivation along foliation (brown traces) require smaller stresses than fractures that cut across foliation. a) The foliation is approximately 30° ($2\theta = 60°$) from σ_1; this is the most favorable angle for reactivation because the required values of σ_1 and σ_3 are smallest at this angle. b) The angle between the foliation and σ_1 ranges from 20° ($2\theta = 40°$ red point) up to 50° ($2\theta = 100°$ green point); in this latter case the stresses, σ_1 and σ_3, required to reactivate the foliation as a fracture are larger. c) The foliation is perpendicular to σ_1; in this case, only across-foliation fractures will be formed. The scale of the axes is the same in each diagram for ease of reference to compare the Mohr circle sizes (based on Fossen, 2016).

The reactivation of pre-existing fractures occurs more easily than reactivation along foliation because there is no cohesion (C) along fracture surfaces (Figure 40). The most

readily reactivated fractures are those that make an angle θ close to 30° with σ_1 (Figure 40a). However, under larger differential stresses, a range of pre-existing fracture orientations will be reactivated by shear (Figure 40b). When the existing structures make a near-normal angle with a tensile σ_3, the reactivation can occur by opening.
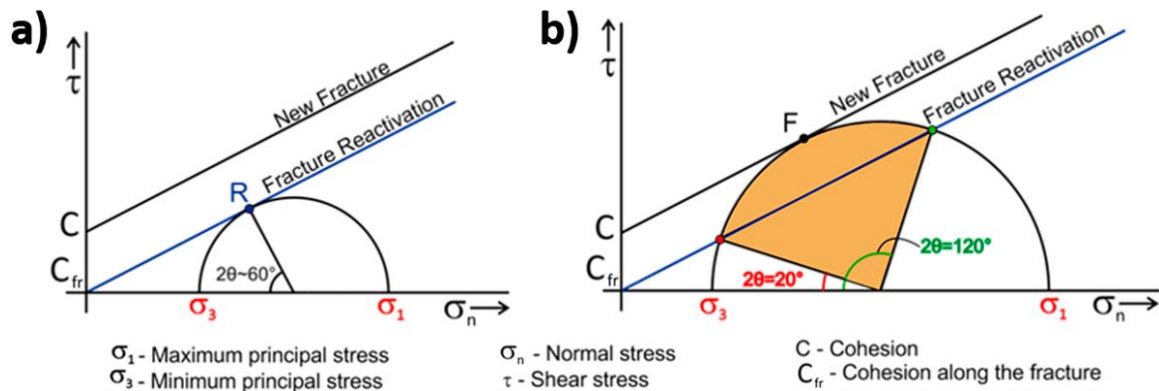
Figure 40 - Conditions required for reactivation of previous fracture surfaces. a) As the cohesion along an existing fracture (C_{fr}) approaches zero, reactivation of existing fractures requires smaller differential stress. b) When the differential stress is larger, a wide range of existing fractures making a variety of angles with σ_1 (2θ ranges from 20° to 120° in the example) will be reactivated. In this example, the differential stress is also large enough to form new fractures (point F in the Mohr circle). The scale of the axes is the same in each diagram for ease of reference to compare the Mohr circle sizes (based on Fossen, 2016).

The reactivation of pre-existing structures is a common phenomenon, mainly in rock terrains that have undergone a long geological evolution. Even small shear displacements caused by reactivation may increase fracture <u>transmissivity</u>⤸ and influence the flow of groundwater. The implications of reactivation on flow are explained below in Section 3.5.

3.5   Expected Influence of Reactivation on Flow

Many fractured rock terrains have undergone a long geological evolution during which a succession of tectonic events occurred, each with specific tectonic regimes and stress magnitudes. When compared to the formation of new fractures, smaller stresses are required for reactivating previously existing planar structures (e.g., foliation and older fractures); thus, reactivation through shear or opening is a common phenomenon. Even when the shear displacement caused by reactivation is on the order of only a few millimeters, it can cause a fracture transmissivity increase of up to three orders of magnitude, as determined through a laboratory experiment carried out by Lamontagne (2001). This takes place because natural fracture surfaces have a certain degree of roughness due to asperities on the fracture surface, and reactivation by shear causes mismatch of the irregularities that lead to an increase in the fracture openings; this is called shear dilation. The experiment demonstrated that, under a normal stress of 3 MPa (corresponding to a depth of roughly 110 m), the increase in transmissivity is as much as three orders of

magnitude, no matter the orientation of shear with respect to the irregularities on the fracture plane (Figure 41). With a larger normal stress, such as 9 MPa (depth of approximately 330 m), the transmissivity increase appears to vary with the shear orientation (Figure 41). The normal stress acting on horizontal fractures is approximately equal to the weight of the rock column, and it gradually decreases toward the ground surface. Therefore, it is expected that the transmissivity increase due to reactivation is larger at shallower depths. Details of the experiment conducted by Lamontagne (2001) can be found in Box 1↴ *Effects of Shear Displacement on the Transmissivity of a Rock Fracture*.
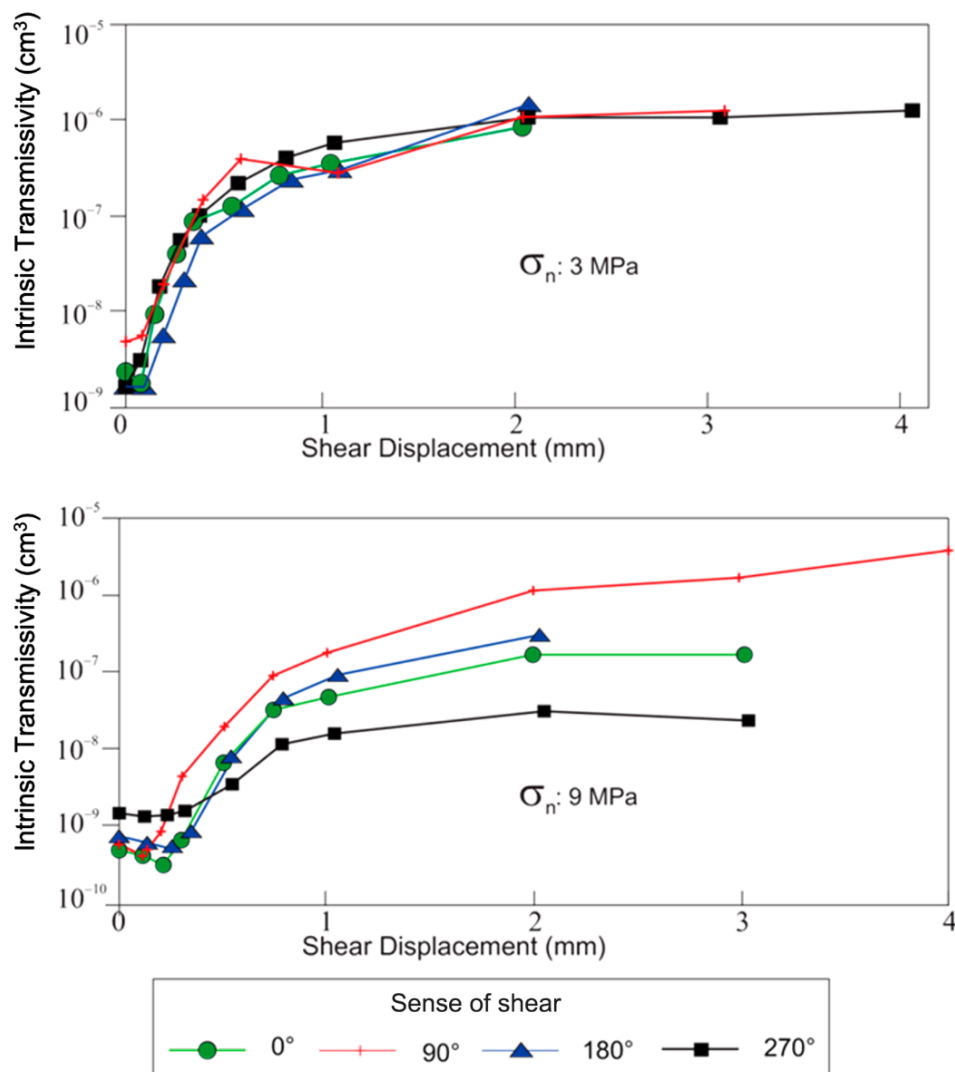
Figure 41 - Laboratory tests were conducted on many replicas of the same rock fracture. Results indicate a net increase of intrinsic transmissivity with increased shear displacement along the fracture plane. Intrinsic transmissivity is defined in Box 1. In the experiment the fracture is subjected to shear under different normal stress (σ_n) values. Under 3 MPa normal stress, a shear displacement of only 2 mm is enough to cause a general increase of three orders magnitude in the transmissivity. Under 9 MPa normal stress, the increase depends on the sense of shear along the fracture plane 0°, 90°, 180° and 270°. Sense of shear is explained in Box 1, specifically in Figures Box1-1 and Box 1-7. Modified from Lamontagne (2001).

An overall conclusion is that fractures reactivated under current tectonic stresses will likely have an increased aperture; this is also discussed in Section 4.2 and Section 4.3. Another important implication of reactivation is that rocks showing anisotropy (e.g., foliation) and pre-existing discontinuities (e.g., bedding surfaces and frequent intercalation of different lithologies) will tend to have a denser and more connected fracture network. These characteristics increase the potential for transmitting water when compared to massive, less-fractured rocks such as granites. This is corroborated by studies conducted throughout many regions, as described in Section 4.1.

3.6   Further Theories and Readings

Sections 2 and 3 describe basic concepts that focus on explaining fracture orientation and patterns; those concepts provide information on the magnitude of stress and other criteria required for generation of different fracture types and propagation modes. However, other fracture characteristics are important in relation to their role in hydrogeology. These characteristics include, for example, spacing and persistence, also referred to as intensity and size, respectively. These characteristics are relevant as they directly influence the fracture network connectivity and, therefore, the groundwater flow. To improve the understanding of such characteristics, it is important to consider the mechanical description of processes leading to initiation and propagation of fractures in rocks. Theories have been proposed on this topic such as linear elastic fracture mechanics (LEFM), initially developed to explain processes leading to fracture propagation in metals. More recently, LEFM has been applied to understand fracture propagation processes in rocks. Basic knowledge and applications of LEFM to structural geology problems are currently described in structural geology textbooks and articles such as Gudmundsson (2011), Fossen (2016) and Pollard and Martel (2020). Although the theory is perhaps too advanced for beginners, it is relevant and informative and readers may find the mentioned references useful.

Understanding mechanisms that explain the generation of sheeting joints, or relief joints, is also relevant for hydrogeology as these fractures may affect groundwater flow near the ground surface. They parallel the ground surface which implies that the minimum principal stress (σ_3) is generally vertical. The scientific community generally accepts that the most probable mechanism causing the formation of sheeting joints is axial splitting associated with in-situ compressive horizontal stresses and unloading due to erosion, (e.g., Holzhausen, 1989; Hencher, 2011). Higher horizontal stresses, in relation to the vertical stresses, may appear during erosion processes, and this condition near the ground surface approaches an unconfined state of stress. Using a uniaxial laboratory test as an analogy, Griffith´s theory (Jaeger & Cook, 1979) predicts the creation of sheeting joints as the result of axial (parallel to σ_1) propagation of critically oriented microcracks. These fissures are

normally seen in thin sections of hard rocks and their overall propagation results in sheeting joints that are parallel to σ_1. As confining stresses increase with depth microcracks tend to close, thereby preventing axial splitting from taking place. As proposed by Martel (2017), the large extensions that are often observed for sheeting joints could be explained by gentle, large-amplitude curvatures of the ground surface.

3.7 Highlights on Tectonic Regimes and Groundwater Flow with Opportunities to Exercise Knowledge Gained by Reading Sections 1, 2 and 3

The most important implications of the tectonic regimes and fracture patterns (i.e., parallel and conjugate) for groundwater flow in a fracture network are:

- Connectivity and, possibly, the aperture of some fractures, can be enhanced by the generation of faults and joints not simultaneously but in the same tectonic event.
- Flow channels can potentially be formed along fault intersections, being horizontal for thrust and normal conjugate faults, and vertical for strike-slip conjugate faults.
- Hydraulic conductivity (K) of low dip or horizontal fractures, generated in the compressive tectonic regime, is more likely to show a decrease with depth due to the increasing overburden stress of the rock column weight. Thus, the closer to the surface, the more transmissive horizontal or low-dip fractures tend to be. On the other hand, K of vertical fractures, either joints or faults, is likely less affected by depth.
- The structures formed where strike-slip faults overlap (i.e., transpression and transtension zones) provide connection between otherwise non-intersecting faults. At these overlaps groundwater flow may be enhanced by either horizontal or vertical joints in the transpression and transtension zones, respectively.

Thus, understanding how tectonic regimes are related to stress orientation and fracture types is important for a better assessment of groundwater flow paths and the connectivity in fractured media. In order to learn these implications in practical terms, Exercises 8 through 14 provide ways of identifying fracture type based on field data. Additionally, they investigate the relationships between fracture type, tectonic regimes, and fracture orientation.

The information collected in the field and provided by exercises 8 through 14 are: fracture orientation (strike and dip), features observed on fracture faces, fracture patterns (parallel or conjugate), groundwater flow evidence along fracture traces, as well as sketches and photographs of outcrops. These exercises explore a number of topics, such as what

evidence of groundwater flow along fractures can be observed in the field; the role of sheeting joints in groundwater flow; the implications of fracture patterns and persistence for the connectivity of the fracture network.

Links to the exercises are provided here: Exercise 8↳; Exercise 9↳; Exercise 10↳, Exercise 11↳; Exercise 12↳; Exercise 13↳; and Exercise 14↳.

4 Conceptual Fracture Network Models

The geological setting, i.e., the association of lithological types and their intrinsic structures, as well as the brittle deformation history of a given region significantly influence the fracture network configuration of a rock mass. These components of a region and the possible effect of the contemporary tectonic stress field on fracture aperture and transmissivity⏎ are discussed in this section and illustrated by several case studies.

4.1   Geological Settings

Anisotropy and existing discontinuities, inherent to the various types of rock, have a strong influence on the fracture network (Figure 42). For example, bedding planes can lead to the existence of fractures limited by strata (stratabound model) with spacing and length related to thickness of the layers (Gross, 1993). On the other hand, the non-stratabound model applies to massive rocks in which there are no lithological layers confining the fractures. In this case, fractures show a wide range of sizes (distribution of their sizes are often lognormal or exponential). These fractures are vertically persistent and spatially grouped (clustered), forming fracture zones⏎ (Odling et al., 1999).

a) Stratabound fracture network: fractures abut against lithological contacts (dashed lines)

b) Non-stratabound fracture network: length and spacing are not controlled by bedding or other previous structures

c) Hierarchical fracture network: part of the fractures abut against bedding and part cut across it.

d) Top-bounded fracture network: fractures are short and contained in the sedimentary beds.

Figure 42 - Fracture network idealized models: a) stratabound, b) non-stratabound, c) hierarchical, and d) top-bounded (modified from Odling et al., 1999; Gross & Eyal, 2007; Laubach et al, 2009, in Hooker et al., 2013).

Considering the general conceptual models of the fracture networks associated with specific lithologies, rocks are herein grouped into the following geological settings: sedimentary rocks, volcanic rocks, metamorphic and igneous rocks, and fault zones.

4.1.1 Sedimentary Rocks

In the fracture systems of sedimentary rocks, the bedding-plane partings (fractures parallel to and along bedding) generally form a subhorizontal fracture set. These bedding-plane partings are frequent and usually relevant to flow (Morin et al., 1997; Michalski & Britton, 1997; Lemieux et al., 2006; Gross & Eyal, 2007; Chesnaux et al., 2009).

Intercalated lithological beds, especially when their composition and/or texture are contrasting, can control the fracturing as shown in Figure 43 (Gross, 1993; Underwood et al., 2003; Cooke et al., 2006). In those settings a large number of fractures are bed-confined, resulting in stratabound fracture networks (Odling et al., 1999). Older and persistent fractures can also control the propagation of younger fractures, and this may give rise to a pattern of older systematic joints and younger cross joints (Figure 43b, Figure 44). Cross joints may also be called non-systematic joints. Multilayer (throughgoing) fracture zones may occur in the form of large fracture corridors and are more widely spaced than the more contained and bed-confined fractures, as shown in Figure 44 (Gross & Eyal, 2007). In summary, variations, and combinations between stratabound and non-stratabound fractures are observed in sedimentary rocks, with the possibility of interchanging from one to the other (Odling et al., 1999).
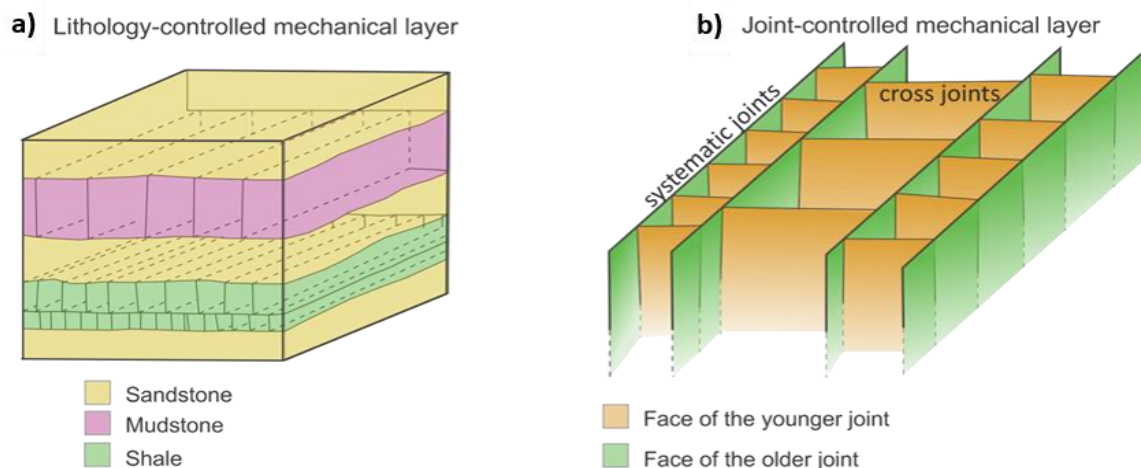
Figure 43 - Controls on fracturing in sedimentary rocks. a) Spacing and length of joints are controlled by bedding. b) Older and persistent fractures control the propagation of younger fractures, giving rise to a pattern of systematic and cross joints (modified from Gross, 1993).
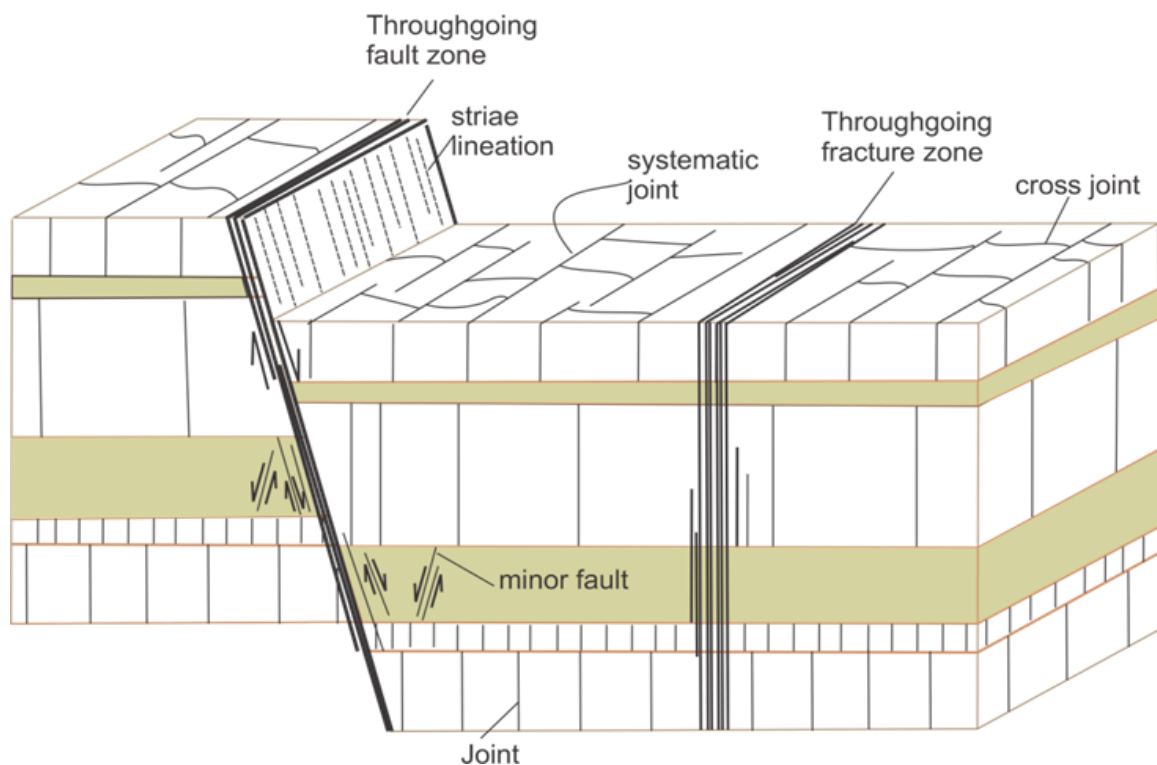
Figure 44 - Schematic of fracture hierarchy observed in layered sedimentary rocks with different bed thicknesses. Throughgoing faults and fracture zones (large-scale fracture corridors) are more widely spaced than the contained fractures that are mid-scale and bed-confined (modified from Gross & Eyal, 2007).

Bedded rocks, such as sedimentary and the very low-grade metasedimentary rocks, may be affected by curvatures and gentle folds formed at shallower crustal levels, a condition that allows the concomitant formation of fractures. These can be shear conjugates and joints organized in a predictable way with regard to the fold elements. The formed patterns vary with regard to the limbs of the fold, especially when it is asymmetric, and to its outer and inner portions particularly in thick layers. These fractures are described in textbooks such as Price & Cosgrove (1990, pages 378–379) and Ramsay & Huber (1987, page 458).

Transmissive bedding-plane fractures, usually present at shallow depths, are considered to be the major groundwater flow paths in sedimentary rocks. This and other flow characteristics of this geological setting are presented in Section 5.1 which describes conceptual groundwater flow models in sedimentary rocks developed in case studies.

4.1.2 Continental Flood Basalts

For discussion of volcanic rocks in this book we chose to deal with continental flood basalts. These represent the most remarkable examples of volcanic activity on the Earth's surface (Bondre et al., 2004; Jerram & Widdowson, 2005). Their mean thickness ranges from 500 to 1,000 m and their volume can be of the order of 300,000 to 450,000 km^3 (Tolan et al., 1989; Frank et al., 2009). The most studied continental flood basalt provinces include the Columbia River Basalt Group (age ranging from 17.5 to 6 Ma; Hooper, 1997) in the

57

northwestern United States, and the Deccan Traps (70 to 60 Ma; Baksi, 1987) in west-central India. These continental floods mainly comprise very extensive basalt sheet-like lobes. A sheet flow is a body of very fluid basaltic lava in which new lava is continuously injected in the central portion of the flow, a phenomenon called inflation that is typical of pahoehoe flows. Emplacement on flat and low dip surfaces favors the production of sheet-like lobes with lateral extension that can reach more than 1,000 km (Self et al., 1998; Self et al., 2008).

Each solidified basalt flow bears two horizontal vesicular layers, one at the base (typically about 1 m thick) and another at the top (generally a few meters to a few tens of meters thick). Between the vesicular zones lies the central layer, from several meters to tens of meters thick, that consists of compact basalt (Figure 45) usually characterized by a dense fracture network formed from the shrinkage of the rock during the lava cooling. This network contains both horizontal and vertical joints. The latter are the most prominent as they frequently form tall vertical columns, usually several decimeters in diameter, typical of the so-called columnar basalts that form <u>colonnade layers</u>⤵. The upper portions of some basalt flows are characterized by very dense joints that may be either chaotic or form thin irregular columns usually up to 10 or 20 centimeters in diameter; these features are typical of <u>entablature</u>⤵ basalt. One would expect that the primary porosity of these rocks (vesicles and spaces between cooling joints) would provide a significant permeability, and this is often the case for younger basalts. However, in older basalts, this porosity can be substantially reduced due to mineral infilling of the shrinkage cracks (Jalludin & Razack, 1994; Gannett et al., 2007). In basalts that have an entablature layer, subhorizontal and persistent transmissive fractures may be present at the contact between the entablature and colonnade layers, or at the lower contact of the basalt flood; these are described by Fernandes and others (2016a) in the Serra Geral basalts, Paraná Basin in Brazil (Figure 45, Figure 46, Figure 47, Figure 48, Figure 49). The authors report that these persistent fractures were generated by hydraulic fracturing due to the trapping of residual fluids caused by the rapid cooling, typical of the entablature layer. Thus, they conclude that it is useful to record the presence of an entablature when prospecting for water supply. Sediments, usually occurring as thin and discontinuous layers between successive basalt flows, are quite common and may bear significant groundwater flow. The interaction of the lava with water-saturated sediments produces peperites that usually look like breccia and consist of fragments of vesicular basalt contained in a sandstone matrix.
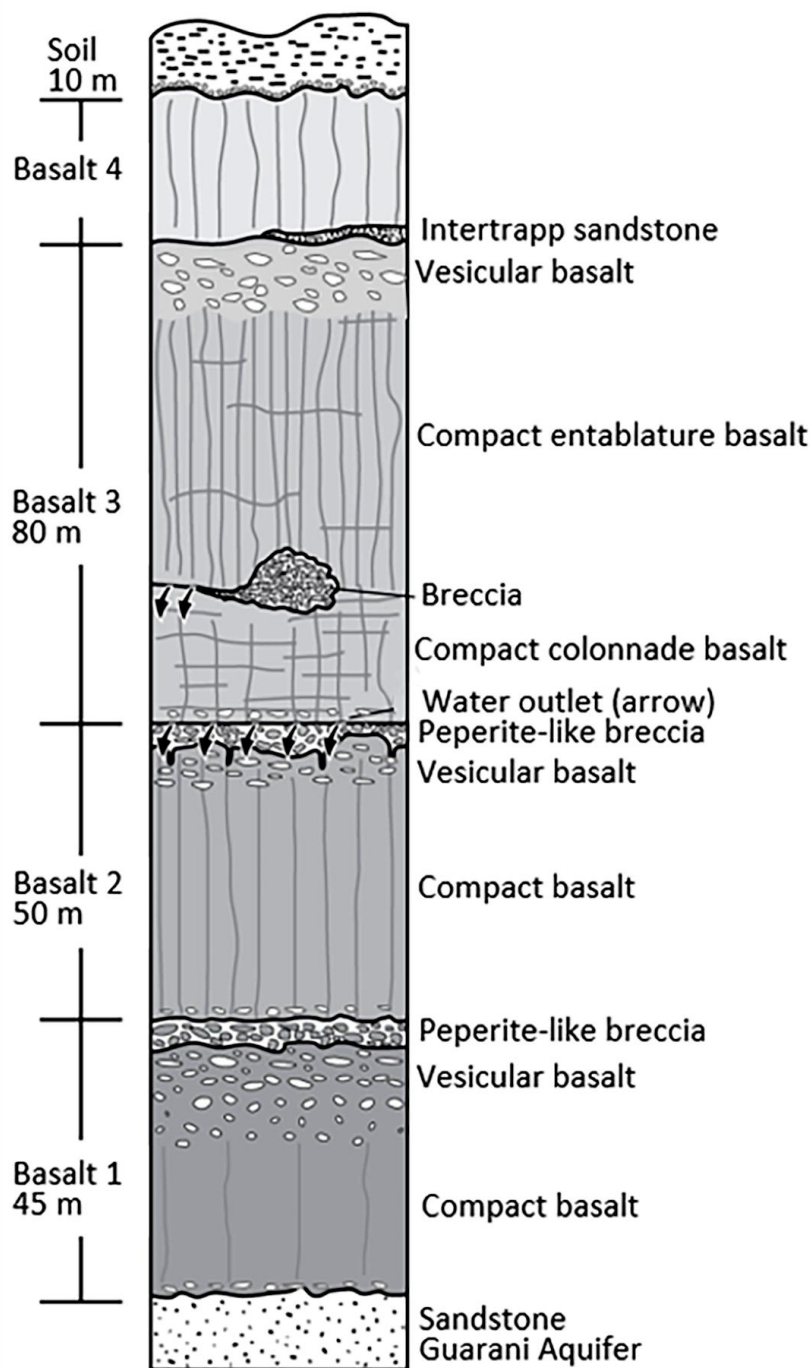
Figure 45 - Vertical sequence of sheet-like lobe basalt flows with a minimum lateral extent ranging from 100 to 200 km (Fernandes et al., 2018). Basalts 1, 2 and 3 bear the typical internal zones of a solidified flow: a thin vesicular layer at the bottom, compact and usually densely fractured (cooling joints) basalt in the middle portion, and a thicker vesicular layer at the top. Thin and laterally discontinuous intertrapp sandstones and breccias (usually at the bottom of the flow) are also common features. Peperite-like breccias are formed by the interaction between the sandstone intertrapp layers with the basaltic lava. The most transmissive fractures (water outlets shown as black arrows) in this basalt sequence are associated with hydraulic fracturing in Basalt 3 at the bottom of the colonnade layer or between the colonnade and entablature layers (modified from Fernandes and others, 2010).

59
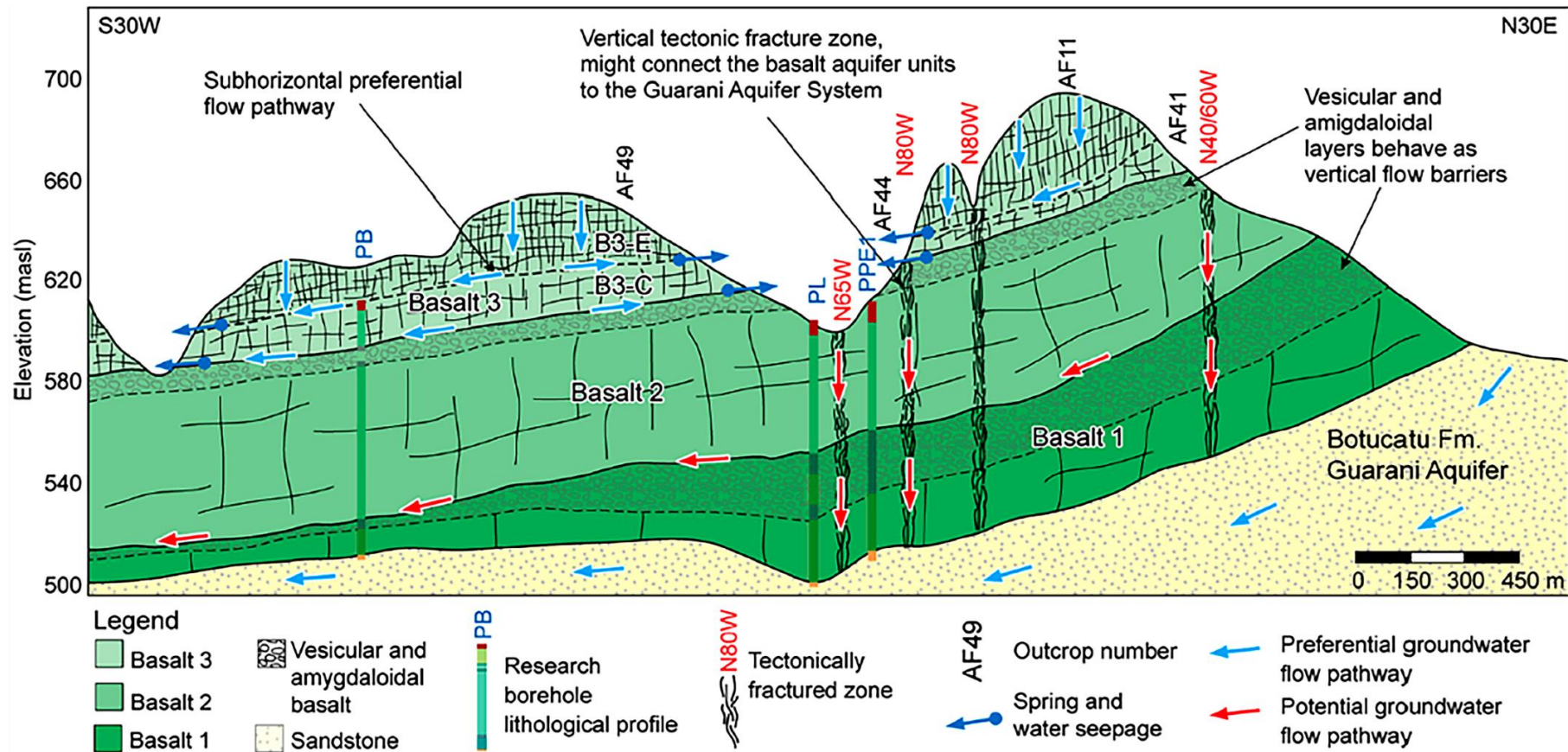
Figure 46 - Groundwater flow conceptual model of the fractured Serra Geral Aquifer System in Ribeirão Preto area, São Paulo, Brazil. The aquifer system consists of basalts of the Paraná Magmatic Province. Blue arrows show preferential flow pathways, which were identified in outcrops and boreholes (Wahnfried, 2010), as well as the flow in the underlying Botucatu Formation (Fm.) of the Guarani Aquifer System. Red arrows indicate potential groundwater flow paths along the contact between Basalt 1 vesicular layer and Basalt 2 as well as along possible subvertical fracture zones. Whether and, if so, where subvertical fracture zones cross the vesicular layers is unknown. Basalt 3 is constituted of colonnade (B3-C) and entablature (B3-E) layers. In the vesicular layers, both vertical and horizontal fractures are very sparse and discontinuous, thereby causing them to typically act as regional hydraulic barriers, i.e., aquitards (Fernandes et al., 2016a).
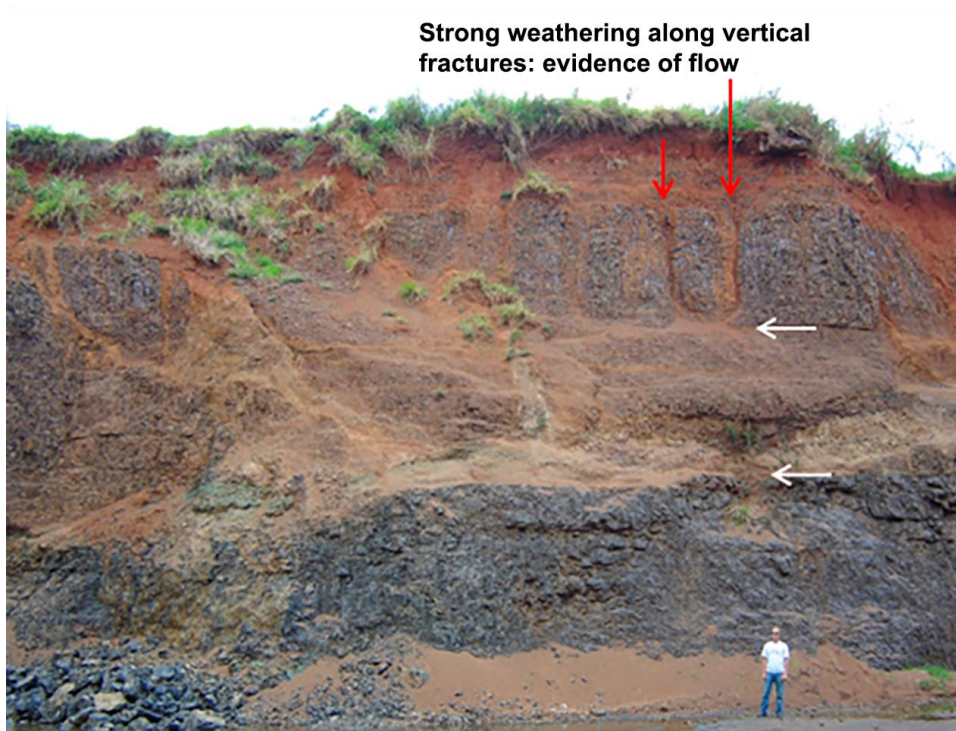
Figure 47 - Close to the surface, both vertical (red arrow) and horizontal (white arrow) fractures show intense weathering that is evidence of groundwater flow. Deeper, flow through vertical fractures becomes less and less common as flow is primarily carried to the horizontal fractures (Fernandes et al., 2011 and 2016a).

Figure 48 - Vertical tectonic fractures are deeply weathered (ocher colors) at depths of more than 40 m (the lower limit is not visible), indicating the presence of flow. The red arrows point to one persistent subvertical fracture (Fernandes et al., 2011 and 2016a).

61
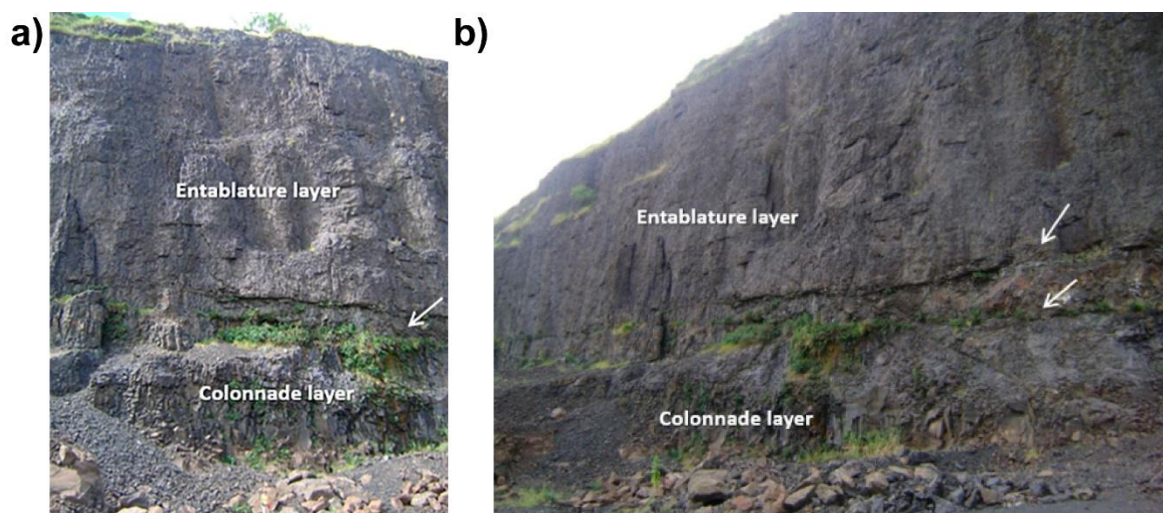
Figure 49 - In the Serra Geral Aquifer (São Paulo, Brazil), the most important groundwater flow pathways in basalt are persistent subhorizontal fractures, which usually occur at the colonnade and entablature contact, as shown in a) and b). Vegetation and water seepage along the fractures are evidence of water flow (Fernandes et al., 2011 and 2016a).

Preferential pathways for groundwater flow in basalts associated with the typical basalt layering and fracture patterns are presented in Section 5.2 which describes conceptual groundwater flow models of layered flood basalts developed from case studies. Section 5.2 also discusses the numerous dolerite dikes associated with flood basalts. The dikes act as both carriers of and barriers to groundwater flow.

4.1.3   Metamorphic and Intrusive Igneous Rocks

The fracture system configurations of massive intrusive rocks such as granite, and of metamorphic rocks, have some typical characteristics that constrain their conceptual groundwater flow models, as explained in Section 5.3 based on case studies. Due to the usual reactivation of foliation, for example, the metamorphic rocks will have a denser and more connected fracture network compared to that of massive granites, implying a usually larger amount of groundwater flow. Persistent high dip fractures and fracture zones, which increase the vertical flow and connectivity, are much more common in these hard rocks than in the sedimentary ones. Massive and foliated granites may have fracture sets that are regionally identified in other granites and metamorphic rocks. However, it is not uncommon to find unique fracture systems in granites. Therefore, defining the extent of the domain of a conceptual fracture network model requires that structural surveys be conducted in a larger number of rock exposures. In this section we briefly describe the results of some case studies that illustrate the characteristics typical of metamorphic and intrusive rocks.

Fractures parallel to and along foliation surfaces and along other types of structures, such as veins, are abundant in metamorphic and intrusive rocks (Boutt et al., 2010; Manda et al., 2008; DesRoches et al., 2014; Fernandes et al., 2016b). This is because the reactivation

process requires lower stresses (as described in Section 3.4) compared to the formation of fractures transverse to existing structures. Throughgoing fractures are much more common in metamorphic rocks than in sedimentary rocks. Even low-grade metasedimentary rocks, which preserve strong stratification, can bear significant throughgoing fractures; this is the case of the meta-sandstones of the Canastra Group in Minas Gerais, Brazil (Figure 50).
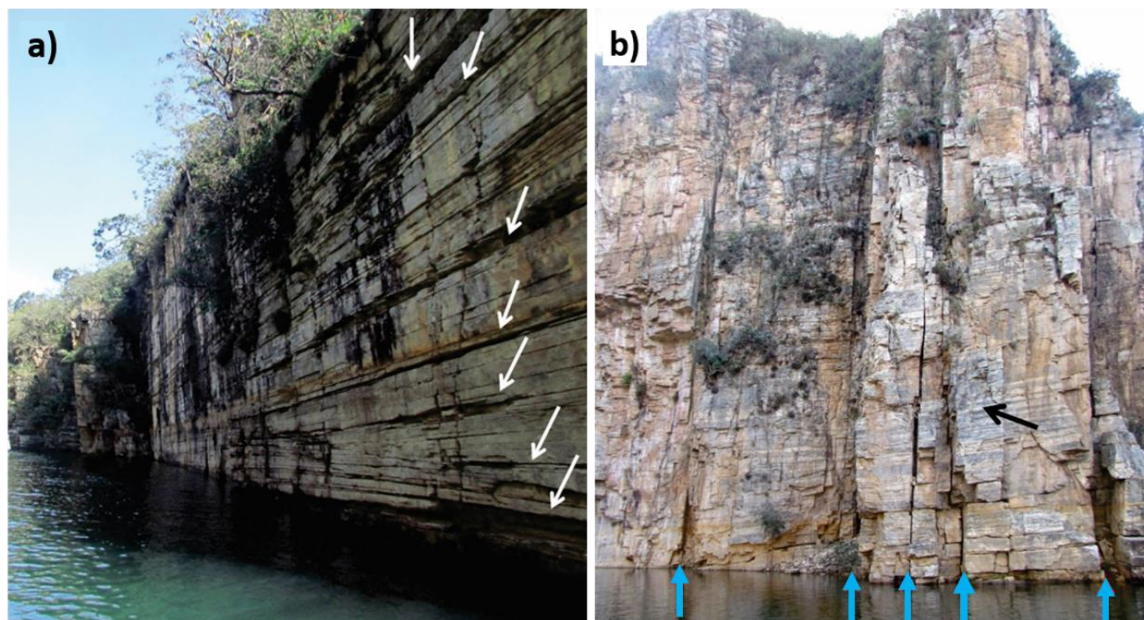
Figure 50 - Meta-sandstones of the Canastra Group, Capitólio Canyons, in Minas Gerais, Brazil. a) The outcrop vertical face is itself a throughgoing subvertical fracture that is laterally very continuous. This fracture cuts across the bedding of low-grade metamorphic sandstones. Horizontal fractures parallel to and along the bedding (white arrows) are conspicuous (photograph: Amélia Fernandes). b) Throughgoing subvertical fractures (blue arrows) cut across the bedding of low-grade metamorphic sandstones. Another subvertical fracture set (whitish faces, black arrow) is parallel to the frontal wall of the rock exposure (photograph: Amélia Fernandes).

Two high-angle throughgoing fracture sets, striking NNE and WNW, that form a well-developed non-stratabound network in folded bedrock (Figure 51a) composed of fine-grained turbidites in northwestern New Brunswick, Canada, were described by DesRoches and others (2014). The integration of borehole televiewer logging, outcrop mapping and hydraulic packer tests revealed enhanced hydraulic conductivity associated with a subset of fractures dominated by bedding-plane and high-angle fractures striking NNE, both with directions near-parallel to the current direction of the maximum principal stress. Figure 51b shows a roadcut outcrop in the Appalachian terrain of southern Québec, Canada, where fractures are parallel and along folded foliation in schist, even at the fold hinges. Foliation parallel fractures may be significant for groundwater flow, as shown in Figure 51c; this is more thoroughly discussed below.

63
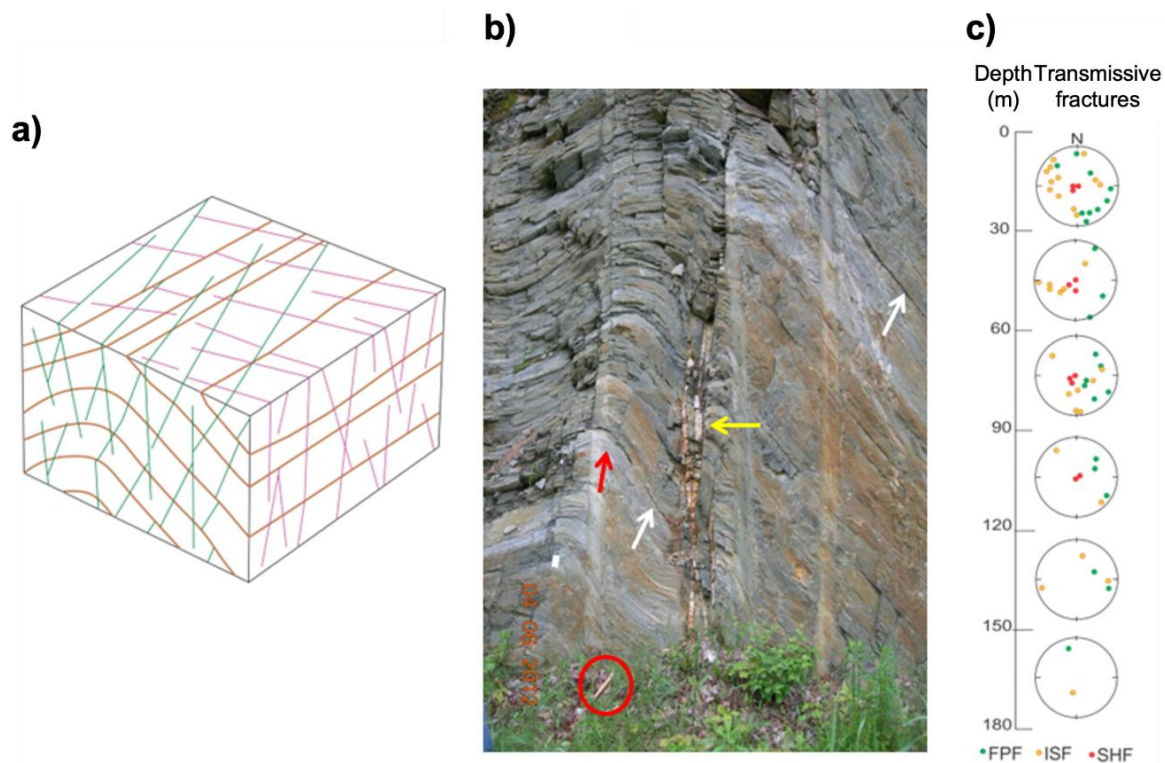
Figure 51 - Non-stratabound fracture networks in metamorphic rocks. a) Bedding parallel fracture set (brown) and two transverse high-angle throughgoing fracture sets (green and pink) forming a well-developed non-stratabound network in folded bedrock (modified from DesRoches et al., 2014). Both high-angle fracture sets seem to form conjugate shear fractures of the tectonic extensional regime. b) Example of fractures parallel and along folded schistosity (white arrows) and high dip veins (yellow arrow), which transect the foliation in the southern Québec Appalachians, Canada. The fractures accompany the foliation of schist even at the fold hinges (red arrow). For scale, the red circle highlights the position of a rock hammer (photograph: Alain Rouleau). c) The number of transmissive fractures in foliated crystalline rock decreases with depth (modified from Boutt et al., 2010). FPF = foliation parallel fracture. ISF = intermediate to high dip fracture. SHF = subhorizontal fracture.

In a crystalline basement quarry located in the São Paulo Metropolitan Region, Brazil rock weathering along and adjacent to fractures parallel to low dip foliation in granitic gneiss provided evidence of significant groundwater flow along the fractures (Fernandes et al., 2016b; Fiume et al., 2020). Flowmeter measurements in vertical wells, drilled through gneisses, granites, and schists, also indicate that foliation parallel fractures are the ones that mostly contribute to the production of the wells. At the studied locations, foliation is gently folded and this imposes an orientation variation on the fractures that are parallel to the foliation. Although the orientation variation observed in the data might lead a person to think that the fractures intersect to form a connected network, this is not the case because the foliation surfaces are parallel. High dip fractures can be either throughgoing or abut against part of the foliation parallel fractures, leading either to a non-stratabound or to a hierarchical fracture network in different sectors of the same rock mass (**Figure 52**).
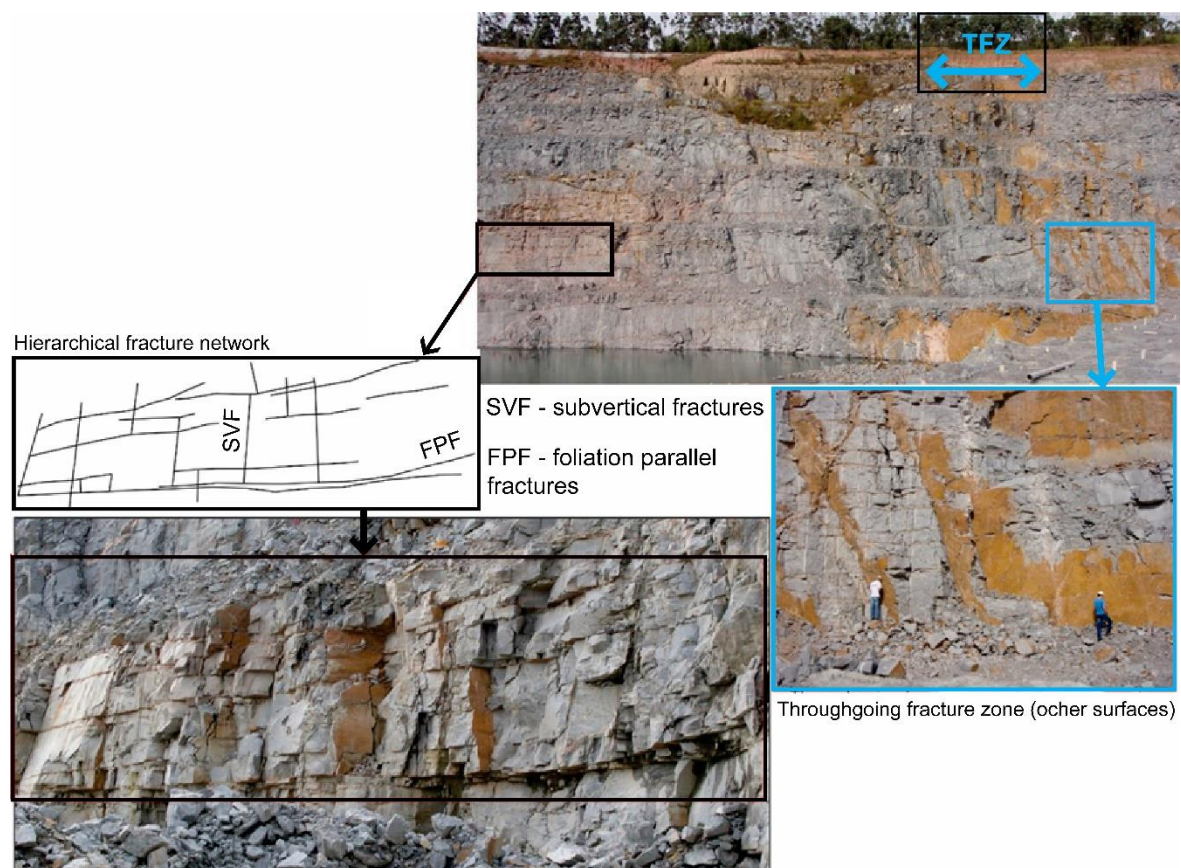
Figure 52 - The same granitic gneiss exposure shows two types of fracture networks. In the black box on the left subhorizontal fractures parallel to the gneiss foliation (FPF in the sketch) are persistent, while the subvertical fractures (SVF) are discontinuous and partially abut against the subhorizontal fractures. This gives rise to a hierarchical fracture network. On the other hand, a throughgoing vertical fracture zone (TFZ, ocher surfaces) is present in the right portion of the upper photograph; a detail of this TFZ is shown in the blue box on the right (modified from Fernandes et al., 2016b).

Igneous and metamorphic rocks of Nashoba and Avalon terranes, located in eastern Massachusetts, ranging from massive, non-foliated intrusive rocks to foliated high-grade metamorphism rocks were investigated by Manda and others (2008) and Boutt and others (2010). These authors surveyed and analyzed fracture attributes (i.e., trace-length, spacing, termination, and orientation) to assess the influence of lithology and fabric on fracture distribution and type. The orientation of two major regional steep fractures is independent of rock type, whereas foliation-parallel fractures (FPFs) are subparallel to the axis of the terrane. Subhorizontal fractures (i.e., fractures with dip less than 25°) were described as sheeting joints and are also pervasive in the area. Trace-length and spacing distributions for steep fractures and FPFs are best described by lognormal distributions. The median trace lengths for FPFs vary as a function of the degree of foliation development, and the median fracture spacing for all FPFs is half that of all steep fractures. The wide variation of median spacings for FPFs in specific rock groups is explained by the presence of multiple units with varying degrees of penetrative fabric development. Generally metamorphic rocks have smaller fracture spacing than igneous rocks.

65

Analysis of groundwater flow in the three main fracture types (FPF and high and low dip fractures) was undertaken in the boreholes drilled in the Nashoba and Avalon terranes (Boutt et al., 2010). FPFs comprise approximately 39 percent of the total fractures in the terrane. Regional high dip tectonic fractures comprise 51 percent of the total fractures measured. Subhorizontal joints (dip < 25°) comprise the remaining 10 percent and play the largest role in conducting water in the shallow subsurface. Steeply dipping fractures, including the FPFs, act as the major connection for vertical flow. Only 2.7 percent of the fractures are hydraulically active and, of these, 32 percent are classified as FPF, 17 percent are subhorizontal and the remaining 51 percent are steep fractures. Most hydraulically active fractures (more than 70 percent) are in the upper 100 m, with a large percentage of those being even shallower (Figure 51c). The number of hydraulically active fractures is large in the upper 30 m with fracture sets of several orientations contributing to the flow. The hydraulically active subhorizontal joints disappear below 100 m. Fractures with dips greater than 40° appear to be supporting flow at greater depths.

Detailed fracture surveys in granitic intrusions (around 550 Ma in age), in moderate- to low-grade metamorphic rocks, were conducted in eight large quarries spread throughout the Metropolitan Region of São Paulo (Fiume, 2013; Fernandes et al., 2016b; Christofolletti, 2020). The integrated analysis of their results indicates the existence of three types of fracture patterns in the granites, as summarized below.

- In five quarries comprised of massive granite, subvertical fracture sets generated under the strike-slip tectonic regime are dominant and correlated to regional fracture sets that affect the host metamorphic rocks. Medium dip (around 60°) and low dip (around 30°) fracture sets were generated in the Andersonian extensional and compressive regimes, respectively. The subvertical fracture set spacings are irregular (from decimeters to decameters) and the trace lengths vary from around a meter to much more than 70 m (Figure 53) with the latter being typical of very persistent fracture zones.

66

The GROUNDWATER PROJECT   © The Authors   Free download from gw-project.org

Anyone may use and share gw-project.org links. Direct distribution of the book is strictly prohibited.

Figure 53 - Persistent (more than 70 m tall) subvertical fracture zone (blue arrows) in massive granite. The fracture zone partially abuts against medium dip fractures (white arrow) (photograph: Bruna Fiume).

● In two quarries located approximately 40 km apart, a distinct fracture network pattern exists. It consists of two sets of orthogonal fractures with the same strike but dipping in opposite senses; the dip varies from 30° to 60° and does not fit any of the Andersonian tectonic regimes. One of the sets is the product of the reactivation of quartz-feldspar veins (Figure 54). One or two regional fracture sets are also present but are less prominent. In one quarry, the granite is foliated and the quartz-feldspar veins are more abundant and parallel to the foliation. Boutt and others (2010) emphasize that foliated granites may provide the most consistent orthogonal networks of interconnected fractures. However, Wise (2005) proposed that this orthogonal pattern (called rift and grain) could be controlled by closely spaced microscopic fracture planes in quartz. These microfractures could have been produced by stresses generated during

67

differential thermal contraction. Thermally induced grain-scale stresses, possibly augmented by weak regional stress fields, could lead to the production of systematic regional patterns during uplift (Wise, 2005).
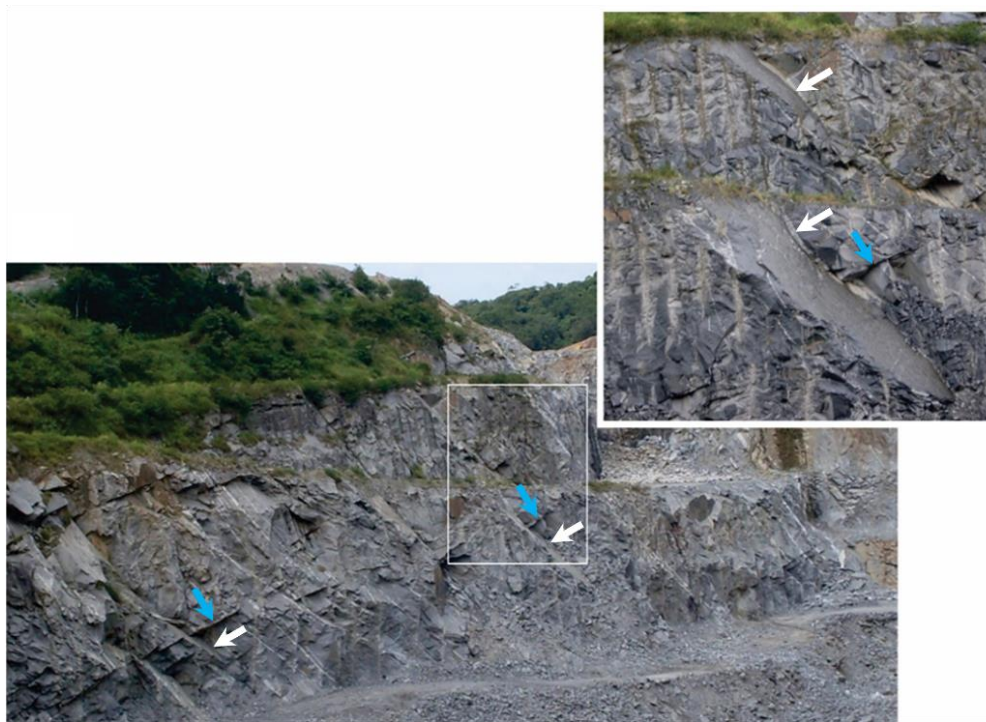
Figure 54 - Two sets of almost orthogonal fractures with the same strike while dipping in opposite senses. One set is the product of the reactivation of quartz-feldspar veins (white arrow) and the other set (blue arrows) is perpendicular to and abuts against the first one (red arrows) (photograph: Bruna Fiume).

- The remaining surveyed granite is less than 1 km away from a large-scale east-west (EW)-trending mylonitic shear zone. This is a massive granite in which, by far, the most prominent fracture set is parallel to thin EW mylonitic shear zones and hydrothermal veins. These structures have high to medium dip and are correlated to the deformation caused by the EW-trending shear zone. This pattern again demonstrates the significance of reactivation for producing specific fracture patterns.

4.1.4 Fault Zones and Fluid Flow

Fault zones have an important impact on local and regional groundwater flow in the shallow crust (< 1 km) and, at depth, they significantly contribute to hydrocarbon migration and hydrothermal fluid circulation (Bense et al., 2013). Although these zones can constitute hydraulic conduits, the core of a fault often acts as a barrier to flow. To understand this behavior, the fault architecture, which is the focus of this section, must be characterized.

A comprehensive synthesis of permeability distribution in fault zones and flow experiments characterizing flow in four idealized types of fault architectures (Figure 55) were conducted Caine & Forster (1999). The idealized fault architectures were developed from the results of three-dimensional stochastic modeling of faults using outcrop-scale data. The data were from Stillwater Normal Fault in Dixie Valley, Nevada, USA (Caine & Forster, 1999), and a series of normal fault zones in east Greenland (Caine et al., 1996). The distribution of fault core and damage zone components in non-deforming (during tectonic quiescence) fault zones can be placed in one of four types of fault zone architectures (Figure 55). Each type has a related idealized permeability structure, that is, localized conduits (Single Fracture Fault model), distributed conduits (Distributed Conduits model), localized barriers (Localized Deformation model) and combined conduit-barriers (Combined Conduit-Barriers model). The idealized architectures represent one moment in time and space *(Caine et al., 1996)* and a range of styles should be expected along any single fault zone. When not actively deforming, a fault core commonly acts as a localized barrier that restricts fluid flow across the fault zone because of its reduced permeability as illustrated in Figure 55b *(Caine et al., 1996; Evans et al., 1997; Gudmundsson et al., 2003).*
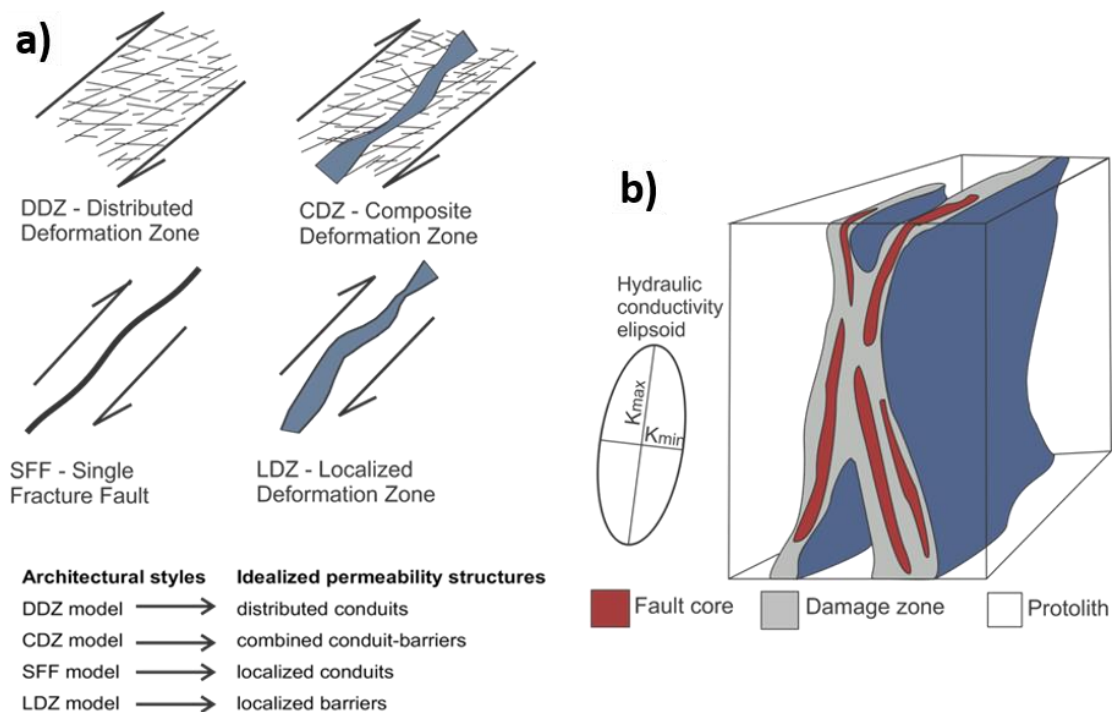
Figure 55 - Fault zone architecture styles and associated distribution of permeability. a) Idealized strike-slip faults viewed on horizontal exposures. The DDZ (distributed deformation zone) and LDZ (localized deformation zone) represent two idealized members. In SFF (single fracture fault) the deformation is accommodated along a single fault. The CDZ (composite deformation zone) is a hybrid between the DDZ and LDZ. DDZ contains networks of both open and closed macroscopic fractures that act as distributed conduits (modified from Caine et al., 1996, and Caine & Forster, 1999). b) Sketch of the distribution of fault core materials and damage zones and how the distribution relates to the overall hydraulic conductivity anisotropy (modified from Caine et al., 1996).

69

Rock in the fault core undergoes progressive grain-size reduction, dissolution, reaction, and mineral precipitation. This evolution typically causes the core to have reduced permeability relative to that of the adjacent damage zone and the unaffected host rock, i.e., the <u>protolith</u>⤵. The host rock type has a strong influence on the structure and composition of fault cores and their permeability structure. For example, in granitic rocks the presence of feldspars may result in a fault core rich in clay minerals, and this may significantly lower permeability. Rocks with high primary permeability, such as sandstones, usually develop <u>deformation bands</u>⤵. Detrital granular sequences can develop core sectors and damage zones similar to the composite deformation zone in faults that reactivated existing joints in sandstone (Aydin et al., 2006). However, the fault zone has reduced permeability compared to the primary granular permeability of the sandstone.

Damage zones adjacent to fault core components bear a network of structures such as small faults, veins, joints, and pressure solution seams. They result from the growth and linkage of fracture networks that accompany episodic deformation of the fault zone. Together these structures produce a heterogeneous and anisotropic permeability; however, the bulk damage zone permeability is greater relative to both the fault core and the protolith (Caine et al., 1996; Evans et al., 1997). Measured hydraulic conductivity (*K*) of fault components indicate values of *K* in the damage zone that are three orders of magnitude larger than that of the fault core (Evans et al., 1997). The specific characteristics of each component's permeability depends on the in-situ stress state, rock heterogeneity, fracture interconnectivity, and the extent of fracture infilling by mineral precipitation.

In addition to the references cited in this section, we recommend reading of Bense and others (2013). It is a comprehensive paper that evaluates geological deformation mechanisms, hydrogeologic observations and conceptual models of faults in diverse rock types. We strongly recommend that structural geologists and hydrogeologists work closely together to gain a more integrated, comprehensive understanding of fault zone hydrogeology.

4.2   Past Deformation and Present Stress-Field Effects on Fracture System Properties

Lithological types have a strong influence on the configuration of the fracture network in two ways.

1. Layers of contrasting mechanical behavior control the propagation of fractures, giving rise to bed-confined fractures with spacing that is usually related to the thickness of the layer.

2. Lithologies with pre-existing anisotropy and discontinuities (which is inherent to some lithologies) are frequently reactivated during brittle deformation

resulting in a large number of fractures along pre-existing structural features such as bedding planes, foliation and veins.

Furthermore, the configuration of the fracture network strongly depends on the brittle deformation history, that is, on the deformation intensity and the orientation of the stress fields of the tectonic events that have affected a region. The brittle deformation, especially in older crystalline basement and volcano-sedimentary basins, which usually occupy vast areas on all continents, has probably taken place over a large time span; thus, the superposition of several brittle tectonic events is common. For example, the Precambrian crystalline rocks that crop out in large regions of Brazil began to intensively deform in a brittle manner at least in the Early Cretaceous, with important deforming events in the Cenozoic including the Quaternary period.

These long deformation histories usually produce several fracture sets under different tectonic regimes, and the interaction of the fractures thus formed influence the configuration of the fracture network. Four types of interactions can be deduced from the observation of fracture traces on outcrops (Figure 56 and Figure 57):

- an older joint trace offset by a younger fault;
- a younger joint trace abutting against an older joint trace;
- short traces of older sealed joints cut by the long trace of younger joint; and,
- crossing traces of joints.

Younger fractures abut against older fractures, likely because of voids along the latter. This is shown in the second image of Figure 56 and occurs in the orthogonal pattern that contains systematic (older) and cross (younger) joints, and also in the gridlock pattern (Figure 58a,b). However, in the latter (Figure 58b), the mutual abutting relationships between the two orthogonal sets indicate that they were formed under tectonic conditions characterized by the alternation of σ_2 and σ_3 orientations (Dunne & Hancock, 1994). Specific "conditions of internal tensions during the final stages of joint development" is another possible explanation for the gridlock pattern development (Rives et al., 1994).
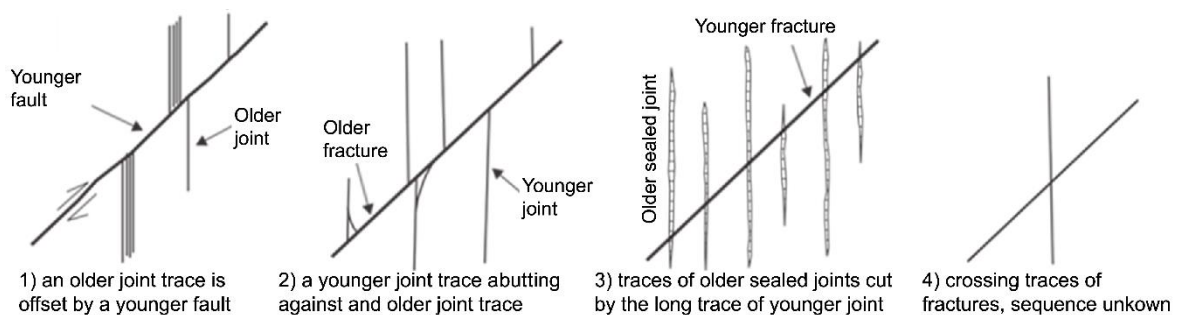
Figure 56 - Fracture interactions and interpretation of the relative ages (modified from Dunne & Hancock, 1994).
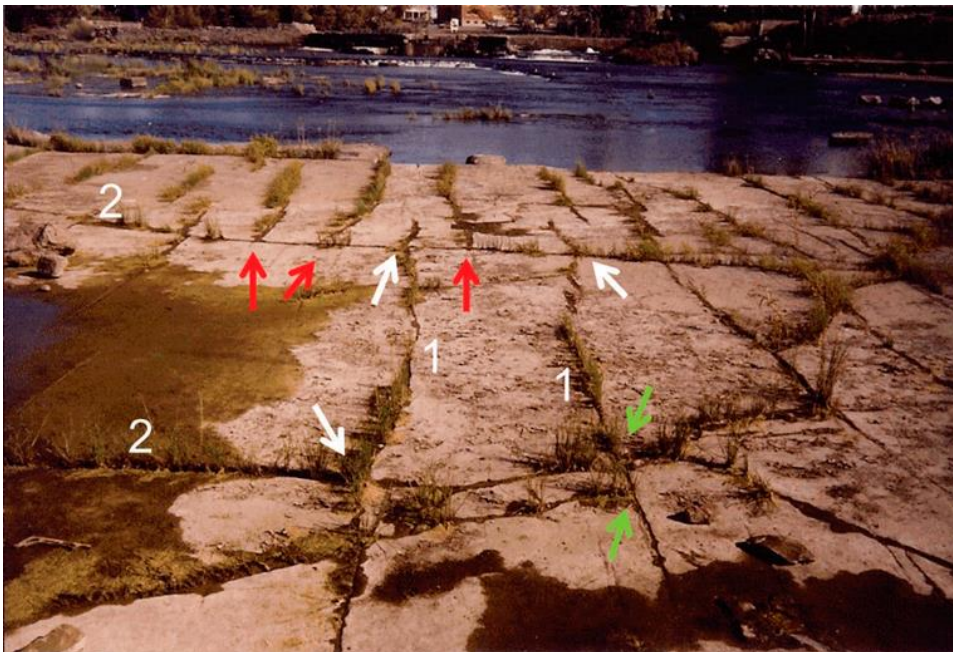
Figure 57 - Horizontal outcrop of quartzite of the Theresa Formation in the St. Lawrence Lowlands, southern Québec, Canada, showing two well-defined vertical fracture sets; set 1 abuts against set 2 at 90° (red arrows), implying that set 2 is older than set 1. Set 1 can also cut across set 2 at some location (white arrows). Other fractures (green arrows) are more irregular and seem to abut against set 1 (photograph: Alain Rouleau).
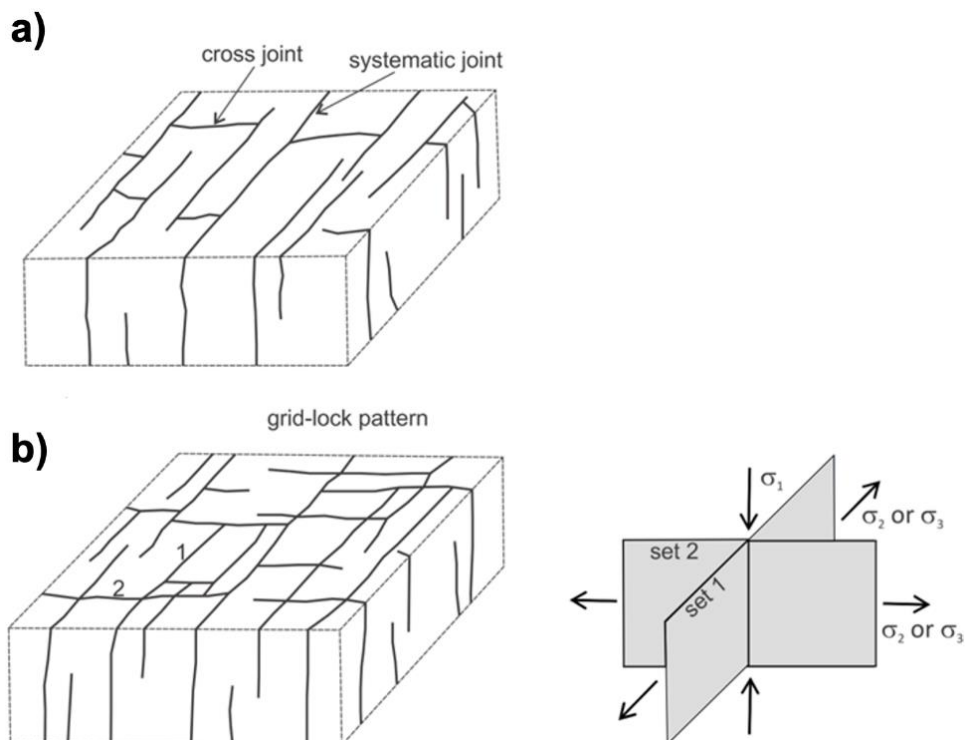
Figure 58 - The abutting relationships of two orthogonal joint sets unveil different deformation histories. a) The systematic and cross joint pattern indicates older and younger ages, respectively. b) Sets 1 and 2 form a gridlock pattern characterized by mutual abutting relationships; a possible explanation is that they were formed in a tectonic setting in which σ_2 and σ_3 alternated orientation over time (modified from Dunne & Hancock, 1994).

72

Figure 59 illustrates how the termination of type 2 shown in Figure 56 (a younger joint trace abutting against an older joint trace) can be used for identifying the age relationships of three fracture sets. For interested readers, an instructional exercise on how to identify the relative age of fractures is presented by Price & Cosgrove (1990, pages 49–51).
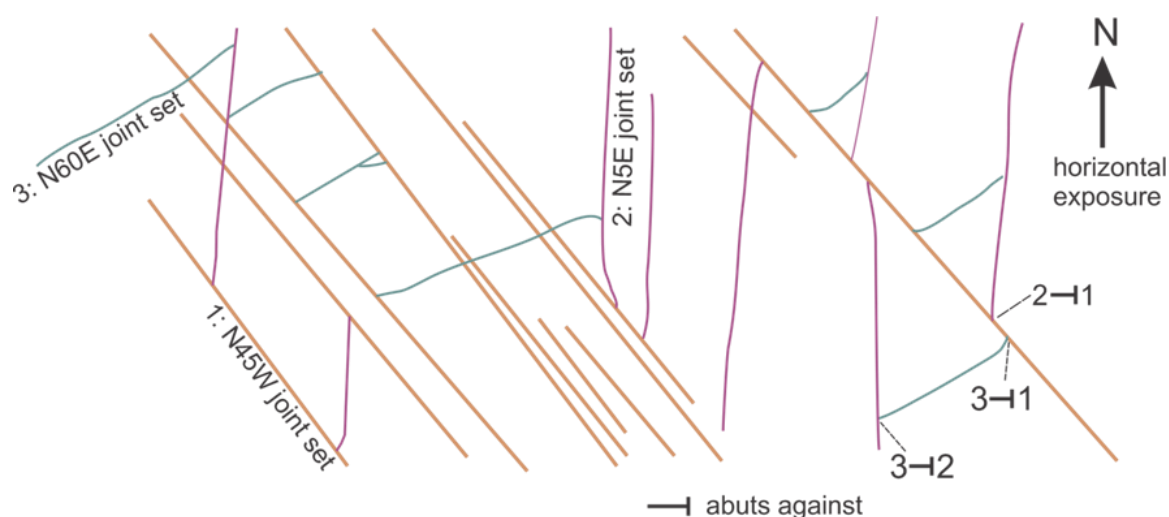
Figure 59 - Idealized sketch of a horizontal rock exposure with three sets of joints with type 2 terminations as shown in Figure 56. Set 3 (N60E direction) abuts against set 1 (N45W) and set 2 (N5E), while set 2 abuts against set 1. These interactions provide evidence that set 1, the more persistent, is the oldest and that set 3 is the youngest. By the time a younger fracture set propagates, the stress field is perturbed by the presence of older fractures. This is why the traces of the younger set may bend as they approach the traces of the older fracture set.

The architecture of the fracture network that arises from cross-cuttings and abutments (Figure 56) has significant consequences on groundwater flow pathways. Considering the fracture configuration in Figure 59, if set 1 contains the most transmissive fractures, flow pathways will be long in the NW direction. However, if set 3 is the most transmissive and set 1 generally impermeable, then the flow paths will be short, along the NE direction, and mostly interrupted by set 1. Thus, the succession of brittle deformation events over time is an important topic of investigation for construction of conceptual models.

The effect of the current stress field on the fracture network is another important topic of investigation because it can influence the variability of transmissivity of fracture sets. A review of the current tectonic stress fields worldwide is presented by Zoback and others (1989). These are expressed in terms of orientation of the <u>maximum horizontal stress</u>↴, S_{Hmax}, at each location and the corresponding tectonic regime. Data on the orientation of contemporary principal stresses are obtained mostly from seismicity, wellbore breakouts (elliptical sections of wells) and geological data. As described in Section 2.3, tectonic stresses in the crust are driven by global scale (i.e., tectonic plate movement and interaction) and regional scale (i.e., bending due to surface loadings) forces.

73

Contemporary tectonic stresses can reach regional significance even at shallow depths, which is the domain of most fractured aquifers. One example is the roughly EW direction of S_{Hmax} in the South American plate interior obtained from Holocene fault data and seismicity as shown in Figure 60. This EW direction of S_{Hmax} is in agreement with the stress models for the South American plate (Riccomini & Assumpção, 1999). Some observed discrepancies regarding the orientation of S_{Hmax} for different areas have been attributed to the interaction of regional and local tectonic stresses. Besides the active tectonic stresses due to present-day straining of the Earth's crust, remnant stresses related to paleotectonic events (e.g., Zang & Stephansson, 2009) may affect specific rocks of a region and impose variability on the orientation and magnitude of the current stress field. The effect of other factors, such as topography in mountainous regions, may cause abrupt variations of the in-situ stresses (Zang & Stephansson, 2009). However, Morin and others (2006) concluded that the topography effect is primarily felt near (within 100 m) steep slopes.

Case studies have demonstrated that the aperture of fractures can be influenced by the current in-situ tectonic stresses (Banks et al., 1994; Barton et al., 1995; Ferril et al., 1999; Morin & Savage, 2003; Morin et al., 2006; DesRoches et al., 2014). The results of some of the case studies are briefly described in Section 4.3. Furthermore, the relationship between reactivation by shear and increased fracture transmissivity is illustrated by a laboratory experiment described in Box 1↴ *Effects of Shear Displacement on the Transmissivity of a Rock Fracture*.

74
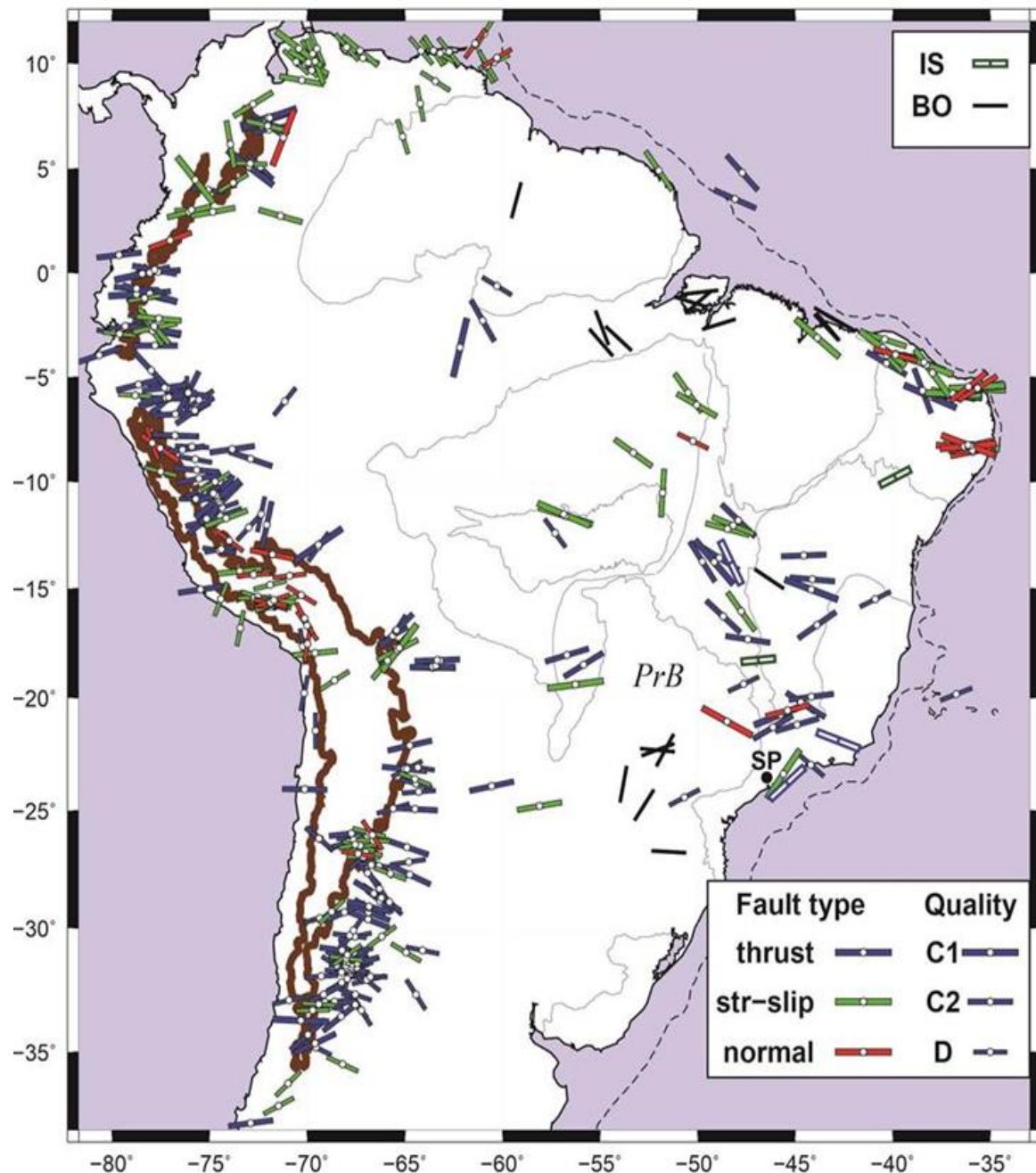
Figure 60 - S_{Hmax} estimates in South America based on focal mechanisms (seismic data from faults) as well as in-situ (IS) and borehole (BO) breakout measurements (from Assumpção et al., 2016; updated by Marcelo Assumpção in 2020). C1, C2 and D, as well as the size of the respective bars, express the quality and reliability of data, from the most to the least reliable.

4.3 Brittle Deformation History and Current Fracture Network Flow Properties

The architecture of the connected network and its flow properties (e.g., anisotropy, transmissivity) depend on the geometric characteristics of the fractures, namely orientation, aperture, size (or persistence), spacing, and fracture interactions. These, in turn, are determined by the characteristics of the affected rock and by its brittle deformation history,

75

i.e., the number of tectonic events as well as their duration, stress magnitude and orientation.

The influence of <u>fracture persistence</u>⤵ on variation of hydraulic conductivity (*K*) of a fractured aquifer over physical dimensions ranging from meters to kilometers was studied by Shapiro and others (2007). Single-hole hydraulic tests conducted at a scale of a few meters showed a range of *K* from 10^{-10} to 10^{-4} m/s. Cross-borehole hydraulic tests at distances ranging from 10 to 100 m showed the presence of highly transmissive fractures with a *K* of approximately 10^{-4} m/s. However, for distances over 100 m, the bulk *K* was approximately 10^{-7} m/s because it was controlled by the less conductive fractures. The same values were found up to distances of kilometers. The authors attributed this behavior to the poor connectivity of the fracture network which was imparted by the short trace lengths of the fractures that rarely exceeded 10 m, as was observed on the surveyed road cuts.

The current stress field may control the final stage of the brittle deformation history and can influence the aperture and transmissivity of fractures (Banks et al., 1994; Barton et al., 1995; Ferril et al., 1999; Morin & Savage, 2003; Morin et al., 2006; DesRoches et al., 2014). Barton and others (1995) demonstrated that there is a relationship between in-situ stress and fluid flow. The analysis of data obtained from three boreholes indicated that, in the highly fractured crystalline rocks they studied, the critically stressed faults appear to be the most important hydraulic conduits. These faults are either parallel to or at an acute angle (up to 30° to 40°) with the orientation of S_{Hmax} at a specific site. This means that they are optimally oriented for reactivation by opening or by shear in the current stress field. Similarly, Ferril and others (1999) proposed that "faults with favorable orientations for slip or dilation are potential fluid flow pathways" and demonstrated that it is consistent with "anisotropic transmissivity controlled by faults and fractures active in the present-day in-situ stress field." The transmissivity values were obtained from data derived from a long-term aquifer pumping test.

In terms of the effect of topography on the in-situ stress, Morin and others (2006) demonstrated that it can locally influence the transmissivity of fractures and concluded that high dip fractures, parallel and close to a steep topographic slope, were more transmissive due to the influence of the laterally free slope face on the in-situ stress. This topography effect is quite local, being present within only 100 m of the slope face. Morin & Savage (2003) considered the effects of regional and local stresses to better understand the hydrologic system of a fractured-rock aquifer. Gravity and tectonic stresses vary with depth and with the specific location of a site. For example, along a slope fracture connectivity systematically increases with depth, whereas it increases only moderately with depth below a valley floor.

Flow evidence along fractures observed in outcrops and wells shows that the orientation of more transmissive fractures can vary substantially over tens of kilometers (e.g., Fernandes et al., 2016b), or abruptly at the same location (Talbot & Sirrat, 2001). Thus, the simple extrapolation of results from one region to another is not recommended; on the contrary, local data should always be collected. For example, Fernandes & Rudolph (2001) show that wells on NW lineaments are more productive in certain structural domains, whereas wells in NNE lineaments are more productive in other domains. The authors concluded that such domains are related to two Quaternary tectonic events having different stress orientations. Lineament interpretation has been used in hydrogeological studies as an auxiliary method for structural characterization (e.g., Mabee et al., 1994; Gleeson & Novakowski, 2009). Considerations regarding the limitations, reach, and scope of lineament studies are provided in Box 2⏎.

4.4   Systematic Collection of Data for Fracture Network Modeling

The geometric characteristics of each fracture set in a fracture network usually have a significant degree of variability that need to be quantitatively characterized in order to build conceptual and numerical models. Consequently, these geometric characteristics of fractures should be systematically collected over large outcrops, either along scanlines with variable orientations or using a window sampling procedure. Fracture data collection along vertical boreholes is desirable; however, this should be complemented by surveys along inclined holes with different orientations and, if possible, on rock exposures. This is necessary for the following reasons.

- Vertical boreholes do not provide sufficient sampling of high dip fractures.
- Natural fractures are not smooth parallel plates thus it is difficult to assign a representative flow descriptor to a fracture by inspection of small well images (Morin et al., 1997).
- Fractures, locally identified as permeable, are not always connected to the larger-scale flow systems and this cannot be observed in the small exposures provided by individual borehole walls (Paillet, 1991; Long et al., 1982).
- Larger-scale flow direction may be controlled by fracture zones rather than by the orientation of specific fractures intercepted by boreholes (Paillet et al., 1987). Consequently, the integration of information from boreholes and large rock exposures is needed to both formulate hypotheses and interpret hydraulic properties of the fractured rock over increasingly large physical dimensions (Shapiro et al., 2007; Fernandes et al., 2016b; and Fiume et al., 2020).

It is important to systematically collect data on fracture orientation, spacing, length, and interactions, as well as evidence of groundwater flow along fractures. Evidence of flow is generally manifested by weathering of the rock near the fracture or on its surface, as well

77

The GROUNDWATER PROJECT   © The Authors   Free download from gw-project.org

Anyone may use and share gw-project.org links. Direct distribution of the book is strictly prohibited.

as by the presence of vegetation and water leakage along the fracture (Figure 61, Figure 62, Figure 63). This systematic method of collection and interpretation of fracture data provides results that can be integrated to construct realistic conceptual and numerical models of fracture network connectivity and preferential flow pathways (Figure 64).

Figure 61 - Intense weathering along a subvertical fracture in massive granite is evidence of groundwater flow indicating that this fracture is significantly transmissive, Votorantim quarry, Metropolitan Region of São Paulo, Brazil (Fiume, 2013).
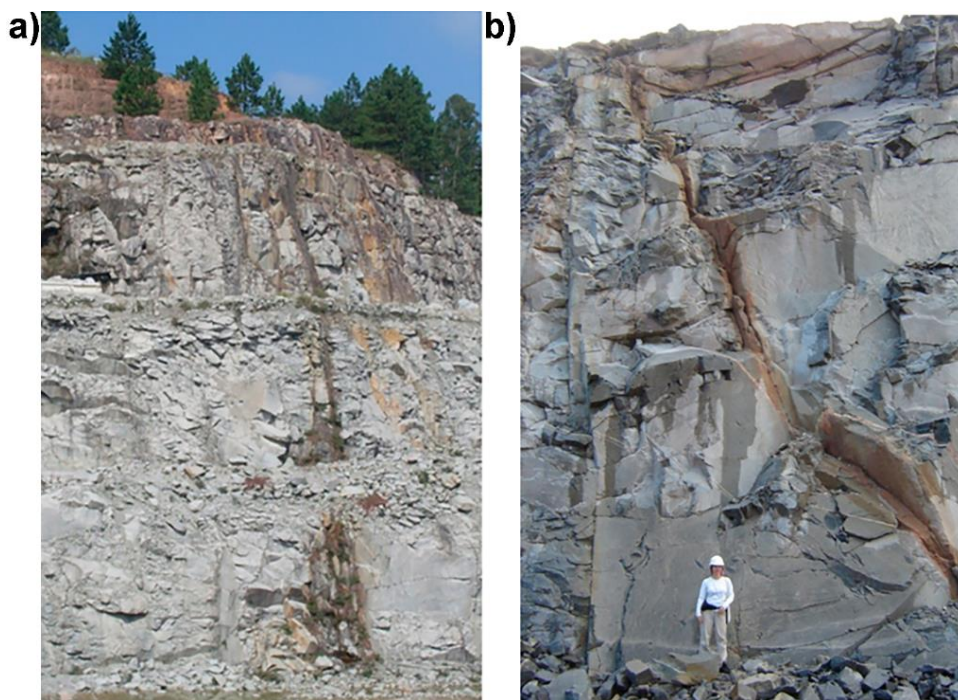
Figure 62 - Intense weathering along subvertical fractures in massive granite (Votorantim quarry, Metropolitan Region of São Paulo) that is otherwise fresh; the weathered fracture in (a) is more than 70 m long (Fiume, 2013).

78
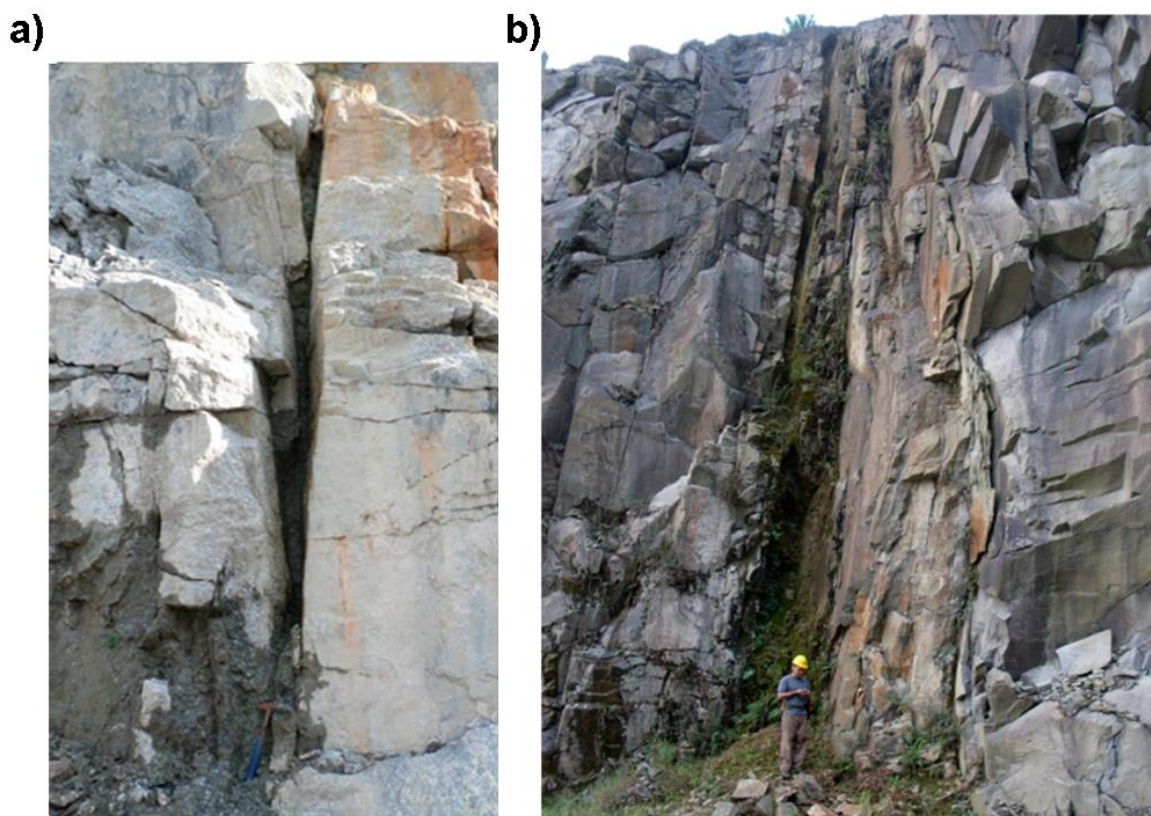
Figure 63 - Weathered fracture zones. a) A massive granite was deeply weathered at the fracture zone and the resulting loose material was eroded away forming a depression (Itapeti granite, Metropolitan Region of São Paulo) (photograph: Amélia Fernandes). b) Fresh massive granite with a deeply weathered subvertical fracture zone that sustains vegetation and was partially eroded away (Votorantim quarry, Metropolitan Region of São Paulo; photograph: Fiume, 2013).
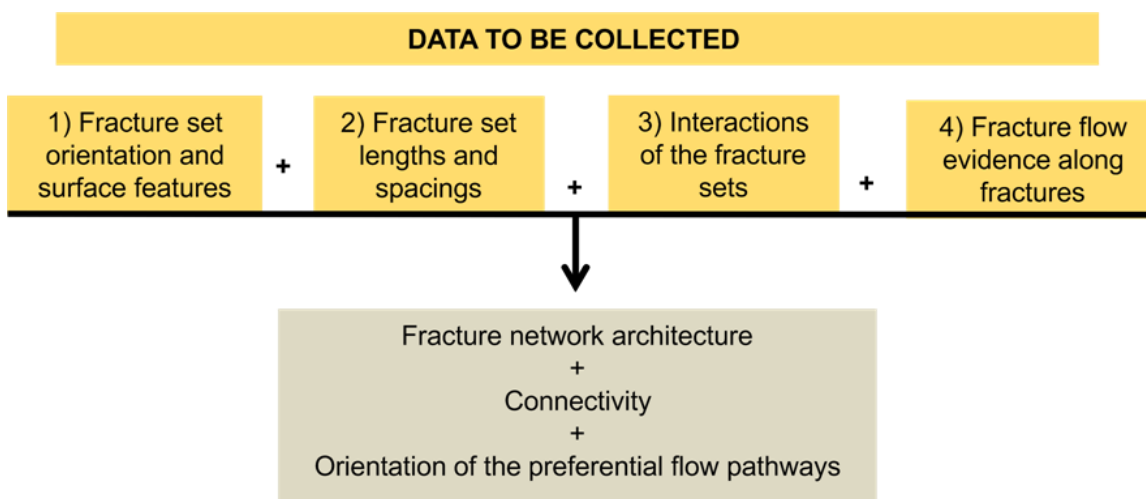
Figure 64 - Flowchart indicating the steps and the type of data (numbers 1–4) that have to be systematically collected in field surveys. The analysis of the data results in knowledge on the fracture network architecture and connectivity, as well as on the orientation of the preferential groundwater flow pathways. A detailed chart on interpretations that arise from data collected in step 1 is given in Figure 38.

Figure 38 presents a flowchart that synthesizes an interpretation procedure of fracture orientation and patterns. The combination the flow chart of Figure 38 with the flowchart of Figure 64 defines a strategic approach for the characterization of the fracture network configuration, as well as the indication of potential connectivity and preferential flow pathways. This scheme was deployed by the authors of this book (Fernandes et al., 2011; Pino et al., 2011; Fernandes et al., 2012, 2016a, 2016b) in the context of continental flood basalts and Precambrian crystalline aquifers. A similar strategy can be found in Peacock and Sanderson (2018); these authors state that vital inputs into modeling of fluid flow are provided by structural surveys and analyses that involve appropriate methods and terminology.

4.5 Highlights on Groundwater Flow along Fracture Networks with Opportunities to Exercise Knowledge Gained by Reading Sections 1 through 4

Highlights on groundwater flow along fracture networks dealt with in sections 3.5 and 4.3 can be summarized as follows.

- Reactivation of previously existing planar structures (e.g., foliation and older fractures) through shear or opening can increase fracture transmissivity. This is a common phenomenon because fractured rock masses usually have several fracture sets, some of them with orientations that facilitate reactivation during later tectonic events. Fractures that are reactivated will likely have an increased aperture, particularly if this occurs under the current tectonic stress field.

- Because of reactivation, rocks showing anisotropy (e.g., foliation in gneisses) and pre-existing discontinuities (e.g., bedding surfaces and frequent intercalation of different lithologies) will tend to have a denser and more connected fracture network when compared to a massive and homogeneous rock body. These characteristics increase the potential for transmitting water.

- Fracture persistence⤵ is key for the connectivity of a fracture network having important implications for flow over larger distances, i.e., hundreds of meters or kilometers.

- The current stress field may control the final stage of the brittle deformation history and can influence the aperture and transmissivity anisotropy of a fracture network. This occurs because the critically stressed fractures, i.e., the ones parallel to or at an angle smaller than 30° with the current maximum principal stress have favorable orientations for slip or dilation. Consequently, they are potential groundwater flow pathways.

- High dip fractures, parallel and close to a steep topographic slope can be more transmissive due to the influence of the laterally free slope face on the in-situ stress.

This is called effect of topography and locally influences the in-situ stress field within distances of about a 100 m from steep slope faces.

- Orientation of the more transmissive fractures can vary substantially over tens of kilometers, thus, the simple extrapolation of results from one region to another is not recommended. Local data should always be collected and lineament interpretation can be an auxiliary method for the identification of the main directions of high-dip fractures.

- Fracture interactions, along with transmissivity values of fracture sets, bear a strong influence on the configuration of the fracture network and its flow anisotropy. These interactions, such as crosscuttings and abutments, are to a great extent controlled by the brittle deformation history. Thus, a better characterization of the succession of tectonic events is important for constructing conceptual models as well as for finding out similarities between different regions.

Exercises 15 through 17 offer opportunities to learn more on some of the aspects listed above by analyzing data collected in field work (as did Exercise 12 that was provided in Section 3.7). The exercises provide photographs, stereograms, drawings of outcrop walls and scanlines, as well as information on: orientation of fractures belonging to different sets; features present on fracture faces; fracture persistence and patterns (parallel or conjugate); evidence of groundwater flow along specific fractures; interaction between fracture sets. The solutions of the exercises explore the analysis and determination of preferential groundwater pathways, brittle deformation history, connectivity, and flow anisotropy. Links to the exercises 15 through 17 are provided here: Exercise 15⤓; Exercise 16⤓; and Exercise 17⤓.

5 Insights on Conceptual Models and Geological Settings from Case Studies

Geological settings and brittle deformation history have a strong influence on the fracture architecture and flow paths; this relationship is validated by case studies, as shown in Sections 5.1 through 5.3.

5.1 Fracture Network and Conceptual Flow Models in Sedimentary Rocks

In the stratabound fracture networks typical of sedimentary rocks, horizontal permeability parallel to bedding-plane fractures can be much greater than the transversal permeability, because the latter depends on fractures that are generally discontinuous and frequently limited to individual layers. For example, in the Passaic Formation, Newark Basin, Michalski & Britton (1997) concluded that the bedding-plane partings tend to provide principal groundwater flow pathways, and a few of these fractures can constitute discrete units of a multiunit aquifer system formed by a sequence of mudstones and shales. The distribution of transmissive zones can be restricted to a few bedding-plane fractures that may vary with the sedimentary rock type as demonstrated by Morin and others (2007). Transmissive zones are more numerous in hard sandstones than in soft ones because soft sandstones generally have the smaller permeability perpendicular to bedding (Figure 65). Lithology often controls the permeability perpendicular to bedding, which depends on the flow paths winding along joints and bedding-plane fractures (Morin et al., 2007). Close to the surface, the transmissivity of the bedding-plane partings is large but significantly decreases from 10 to 25 m in depth (Morin et al., 1997; Morin & Savage, 2003). A high-angle fracture set is also part of the system, being approximately orthogonal to the bedding fractures. Its transmissivity (about half of the bedding fractures) showed no apparent dependence upon depth (Morin et al., 1997). However, this behavior depends on the orientation of the present tectonic stresses (Morin & Savage 2003).

Figure 65 - Photograph of a sandstone covered by basalt. Orthogonal fractures (striking ~N20E and ~N70W) occur only in the upper portion of the sandstone layer that was indurated by cementation caused by the percolation of fluids derived from the basalt lava. The soft sandstone (lower part of the layer) is devoid of fractures, illustrating that hard sandstones are more likely to have a denser fracture network than soft ones. The contact between the two types of sandstones is sharp. (photograph: Francisco Negri, near Botucatu city, São Paulo State, Brazil).

For a well-bedded, flat-lying Ordovician dolostone observed in a quarry approximately 60 m deep large-extent, bedding-plane fractures with high hydraulic conductivity (*K*) represent major groundwater flow paths (Lemieux et al., 2006). Two high-permeability bedding planes occur at depths of 13 m and 24 m. Four sets of vertical fractures of lower *K* provide vertical connections. In general, these terminate at the bedding planes forming a stratabound/hierarchical network as shown in Figure 42 (Hooker et al., 2013). Parker and others (2018) also assign the high bulk *K* of a dolostone aquifer to the combination of fractures along and parallel to the bedding planes, stylolites (serrated surfaces within a rock mass where mineral material has been removed by pressure dissolution), and high-angle fractures. These dolostone conceptual models are consistent in that both rely on highly permeable shallow horizontal openings connected by vertical fractures.

The conceptual model shown in Figure 66 summarizes relevant characteristics of an aquifer formed by fractured sedimentary rock, as described in Morin and others (1997), Morin & Savage (2003) and Lemieux and others (2006).
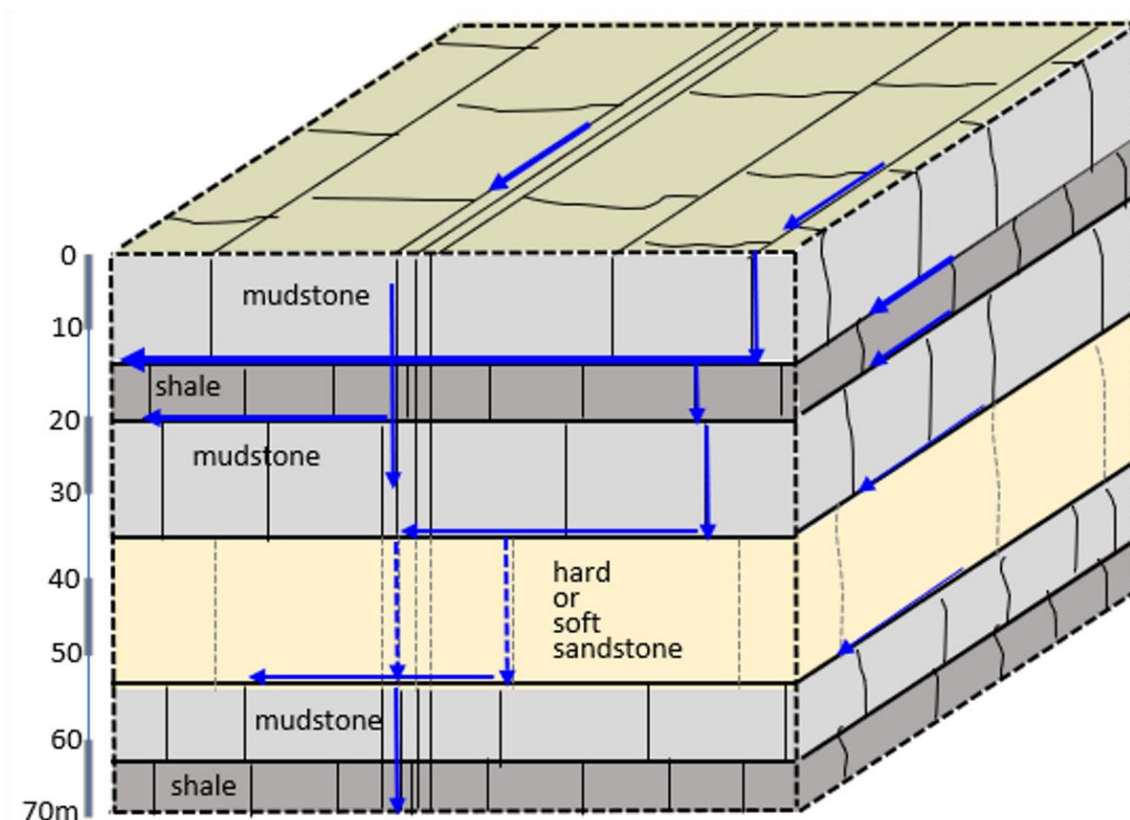
Figure 66 - Conceptual model of a stratabound/hierarchical fracture network (Figure 42) in a sedimentary aquifer formed by mudstone, shale, and sandstone layers. The following aspects are common in nearly all of these systems: 1) bed partings (fractures along the layer contacts) may form aquifer units; 2) close to the surface, the permeability (proportional to the thickness of the blue arrows) of these partings is larger than that of the vertical fractures and decreases with depth; 3) transmissive throughgoing vertical fracture zones are important for flow and are sparser than the bed-confined fractures; 4) in the sandstone layer the number of fractures (dashed lines) will depend on the toughness of the rock and tends to be larger in harder sandstones than in softer sandstones; 5) vertical flow winds its way along horizontal and vertical fractures. The illustrated depths of the more transmissive horizontal fractures are based on data from Morin and others (1997), Morin & Savage (2003) and Lemieux and others (2006).

The systematic and cross joint pattern (Figure 43b and Figure 44) forms a well-connected fracture network and the flow configuration may be strongly affected by the aperture range of each set. If the systematic fractures bear a higher hydraulic connectivity than the cross joints, the flow will take place over large horizontal distances along the systematic fractures; the opposite aperture relationship will interrupt horizonal flow. The vertical extension of flow greatly depends on how far the fractures propagate across the existing sedimentary layers.

Surrette and others (2008) define hydrostructural domains in order to characterize permeability at a regional scale, where fracture distributions are heterogeneous. The domains are partly lithology-dependent and reflect changes in fracture intensity within the rock mass. For the southern Gulf Islands, British Columbia, Canada, they defined three domains in decreasing order of potential permeability:

84

The GROUNDWATER PROJECT   © The Authors   Free download from gw-project.org

Anyone may use and share gw-project.org links. Direct distribution of the book is strictly prohibited.

- fault and fracture zone domain;
- highly fractured interbedded mudstone and sandstone domain; and,
- less fractured sandstone domain.

It was concluded that the relative potential transmissivity values, derived from models based on the domains, show good spatial agreement with transmissivity values obtained from pumping tests at selected sites.

5.2   Fracture Network Conceptual Models of Flood Basalts

The preferential flow paths in continental flood basalts may comprise a variety of components:

- laterally discontinuous, blocky (very fractured) and partially weathered vesicular basalt (Versey & Singh, 1982);
- sheet-jointed vesicular layers (Kulkarni et al., 1997; Pakhmode et al., 2003);
- highly fractured vesicular interflow zones between successive flow units (Johnson et al., 2002a; Douglas et al., 2007; Larson et al., 2000);
- fractures at the contacts between superior vesicular layers and compact basalt (Kulkarni et al., 1997);
- heavily fractured flow contacts (Johnson et al., 2002a);
- vesicular and scoriaceous interflow zones (McGrail et al., 2006);
- subhorizontal fractures interconnected by subvertical fractures of lower transmissivity (Tressoldi & Kitahara, 1991); and,
- long subhorizontal fractures at interflow contacts or at entablature and colonnade contacts (Fernandes et al., 2016a).

Most of the preferential groundwater flow paths in continental flood basalts are subhorizontal structures or layers, and this characteristic generally imparts a stratabound fracture network model. Despite the prominence of the cooling joints in both entablature and colonnade layers, the compact basalt is not the most conductive portion of the basalt flow. Fernandes and others (2016a) concluded that flow along vertical cooling joints is precluded or greatly reduced due to the presence of mineral infillings, the same as those found in vesicles. Larson and others (2000) point out that vertical flow is impeded by the entablature and colonnade flow interiors despite the presence of columnar cooling joints. The vesicular layers, even with a significant amount of vesicle voids, may work as regional hydraulic barriers to vertical flow because the vesicular voids are not connected, and vertical or horizontal fractures in those layers are scarce and discontinuous (Fernandes et al., 2016a).

Due to the generally minimal vertical connectivity of these horizontal aquifer levels, even when contained within one single basalt flood they are often modeled as multiple aquifer/aquitard systems (Douglas et al., 2007; Wanhfried, 2010). This approach is

supported by studies based on the difference in hydrogeochemistry and isotope content of waters in the permeable zones (Versey & Singh, 1982; Larson et al., 2000; McGrail et al., 2006). In the eastern portion of the Columbia River Basalt Group, continuous water level declines in deeper aquifers have been observed in response to pumping from municipal water supply and private wells. This strongly indicates that the groundwater in the deep aquifers is being mined (Douglas et al., 2007). Larson and others (2000) report that water in the deep aquifers is old and has not been recharged under current climate conditions. Thus, it was concluded that the aquifer recharge rates to the deep basalt aquifer are substantially lower than previously estimated.

Structural data collected at several rock exposures, produced by excavations for the construction of dams in the southern states of Brazil, indicate that the basalt layers of the Serra Geral Formation can be divided in two prominent regions, each having distinct fracture network models. In the southernmost states of Rio Grande do Sul, Santa Catarina, and Paraná, subvertical, throughgoing, tectonic fracture zones cut across the basalt layers, including the vesicular zones, and probably cause the connection of the multiple aquifer levels. In contrast, the stratabound model can be regionally applied to the vast region of São Paulo State. In this area connection of subhorizontal flow paths by subvertical tectonic fracture zones occur only locally in the Serra Geral basalts as illustrated in Figure 45 (Fernandes et al., 2016a).

Flood basalt regions exhibit a great number of dikes and sills intruding sedimentary rocks. It is important to investigate their occurrence because they influence the groundwater flow. It has also been observed that boreholes in dolerite intrusion–host rock contact zones have significantly greater probability of yielding high quantity of groundwater (Sami, 1996). The dolerites that intrude the sedimentary rocks (sandstones and mudstones) of the Karoo Sequence in southern Africa act as both carriers of and barriers to groundwater flow (Gustafsson, 1994; Senger et al., 2015). A quantitative fracture analysis on outcrops in and around the dolerite intrusions (Senger et al., 2015) concluded that:

- fluid flow will most likely be focused along the intrusion–host rock contact zones (Figure 67); and,
- the central portion of the dolerite acts mostly as a barrier to flow because its fractures are generally mineralized and sealed.
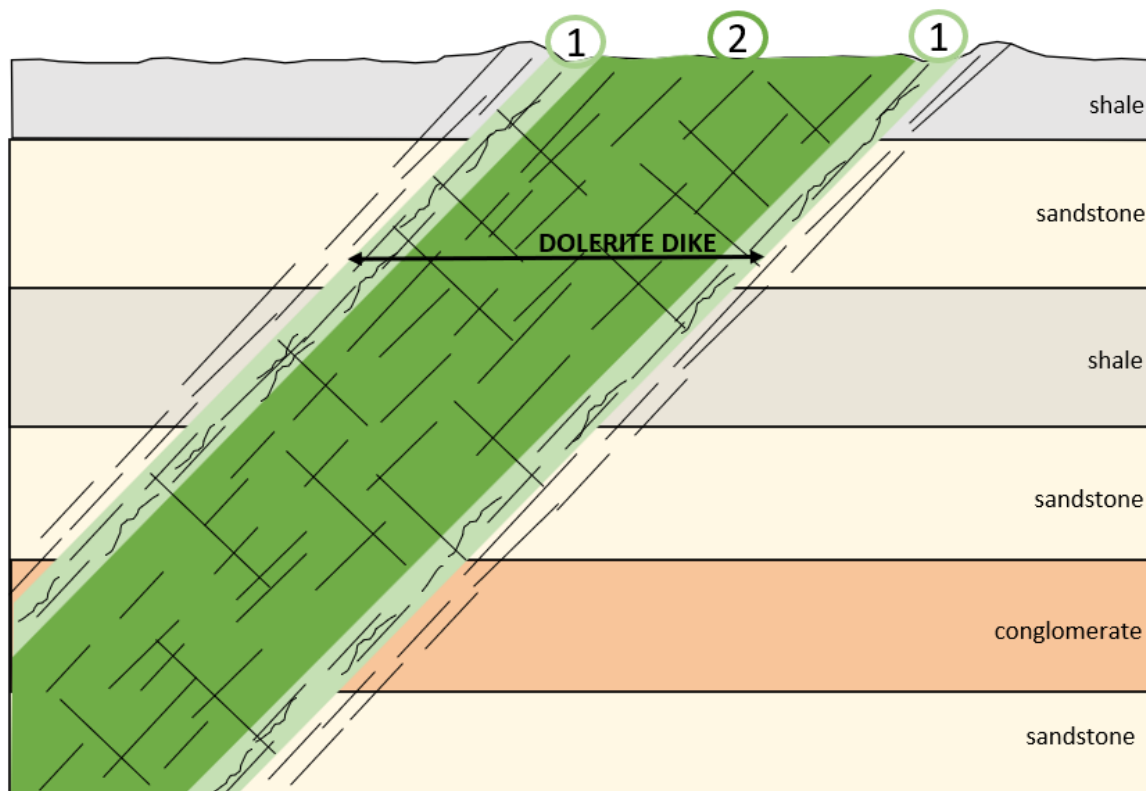
(1) The two lighter green stripes represent the chilled margin of the dolerite dike. These zones, with increased fracturing, are usually flow carriers. Wells tapping these zones are more productive.

(2) The central portion (darker green) of the dolerite dike tends to be a flow barrier, because the fractures in this zone tend to be sealed by mineralization.

Figure 67 - Dolerite dikes intrude the sedimentary rocks of the Karoo Sequence in southern Africa and act as both carriers and barriers to groundwater flow. Senger and others (2015) concluded that fluid flow will most likely be focused along the intrusion–host rock contact zones, and that the permeability of the fractures decreases with depth. The intrusion process generated one joint set that is perpendicular to dike walls and another that is parallel (modified from Senger et al., 2015).

5.3 Fracture Network Conceptual Models for Metamorphic and Intrusive Igneous Rocks

In general, the non-stratabound fracture network model is applicable for intrusive and metamorphic rocks. These rocks have highly variable fracture (and fracture zone) spacings. Fracture lengths are also very variable and with lognormal distributions (e.g., Rouleau & Gale, 1985). In metamorphic rocks, the hierarchical model can also be present because part of the fractures may abut against FPFs (foliation parallel fractures), and these generally comprise a prominent fracture set. This pattern and the throughgoing fractures may form a dense and connected fracture network. Zones of persistent and closely spaced fractures are common in metamorphic and igneous intrusive rocks and can impart high fracture connectivity and transmissivity (Paillet et al., 1987). Fractures that result from reactivation of foliation, veins and other previously existing structures can contribute significantly to groundwater flow. The importance of subhorizontal fractures for flow at

87

The GROUNDWATER PROJECT   © The Authors   Free download from gw-project.org

Anyone may use and share gw-project.org links. Direct distribution of the book is strictly prohibited.

shallow depths (i.e., a few tens of meters) has been described in several regions (Manda et al., 2008; Boutt et al., 2010; Fiume, 2013; Fernandes et al., 2016b). Reactivation of subhorizontal pre-existing structures at small normal stresses, as described in Section 3.5, is a likely explanation for this phenomenon. The subhorizontal sets become hydraulically non-active at depth, and fractures with dips greater than 40° support flow at greater depths (Boutt et al., 2010). Numerical modeling experiments conducted by Manda and others (2008) show that FPFs account for increases of 20 to 30 percent of flow in fracture networks. However, in the numerical simulations, the same aperture was assigned for all fracture sets and types, and the authors report that this was done because fracture apertures are subject to local variations in stress fields and rock properties. We suggest that a systematic field survey of features that indicate flow could be used to assign different apertures and different percentages of open fractures to each fracture set. Such a survey can be conducted along scanlines in large outcrops, as suggested by Fernandes and others (2016b) and Fiume and others (2020), as well as in well image records (Section 4.4). Wells in metamorphic rocks, when compared to those in massive rocks such as non-foliated granites, tend to present higher specific capacity values; this is likely due to the positive influence of FPFs in these aquifers (Fernandes et al., 2016b).

Granites may bear the same regional fracture sets that are present in metamorphic rocks. However, different fracture patterns, probably related to thermal contraction and tectonic stresses during uplift, are to be expected in these rocks. The practical implication is that the regional fracture sets observed in the host metamorphic rocks cannot be assumed to be present in the intrusive rocks, and vice versa.

Both plutonic and metamorphic rocks may fracture in sheet or exfoliation joints that form parallel to the Earth's surface at depths generally less than 100 m. They are typically subhorizontal but may have dips depending on the variability of surface topography. Near-surface joints are often most significant for water storage and movement.

88

The GROUNDWATER PROJECT   © The Authors   Free download from gw-project.org

Anyone may use and share gw-project.org links. Direct distribution of the book is strictly prohibited.

6 Wrap-up

Fractured aquifers occupy large areas of all continents and, although they are relevant or essential for water supply and other applications, there are many areas of study still to be developed and challenges to be overcome, as presented in this section.

Fractured aquifers pose scientific and methodological challenges because fracture porosity is heterogeneously distributed, and its characterization requires detailed studies. To understand the factors that control fracture heterogeneity, theoretical fundamentals of rock mechanics and structural geology must be applied so that the data collected in the field can be properly organized, allowing the mechanisms controlling the heterogeneity to be revealed.

There has been a significant increase in the application of structural geology studies to the investigation of fractured aquifers. Nevertheless, detailed structural surveys need to be carried out more frequently to build an increasingly sound knowledge about these aquifers. For this to be accomplished, the training of professionals and/or the migration of structural geologists to this area of study is needed.

Another fundamental issue is that geologists and hydrogeologists must interact and carry out a better coordination of their respective work, which will provide a mutual advancement of both specializations. This will certainly help to overcome some of the major difficulties in structural and hydrogeological characterization of fractured media.

Fracture surveys need to be carried out on large outcrops to obtain a representative description of field conditions. Quarries present good opportunities for study because they provide long horizontal scanlines with different orientations, as well as vertical scanlines. The development of technologies for data collection in places of difficult access, such as high vertical exposures with risk of collapse, is progressing. The use of drones will allow for more representative surveys, as they offer the possibility to observe otherwise inaccessible exposures. This facilitates the gathering of more complete data including fracture trace length (i.e., persistence) which is a parameter that faces a restrictive limitation in most traditional surveys due to the usually limited height of vertical exposures that can be directly and safely accessed. Fracture trace length is one of the fundamental geometric parameters used for defining the fracture network configuration, especially connectivity. This, together with the fracture aperture, determines the potential for flow in these media.

The difficulty in estimating the aperture of fractures imposes a significant limitation to the development of mathematical models. For this reason, a single value of aperture is assigned to all fractures in a model. This limitation can lead to unrealistic results, particularly when considering that flow is proportional to the cube of the fracture aperture. As emphasized in Section 4.4, the systematic collection of evidence indicating flow along fractures may lead to a ranking of fracture sets with regard to aperture. Determination of

89

in-situ stresses is another relevant research topic because such stresses affect fracture aperture. It is important to conduct studies that assess how the in-situ stresses vary from place to place and with depth, and to what extent they affect the variation of aperture. This tool could prove to be useful for inferring the orientation of the main flow paths in areas where structural data are scarce such as, for instance, places with wells but without rock exposures.

The extrapolation of fractured aquifer characterization to locations beyond the area where fracture and hydraulic data were collected, is an imposing challenge; to address this issue, it is necessary to make a distinction between the terms "surveying" and "mapping." Mapping assumes that the mapped elements are in fact where they are represented on the map. Lithological units and some fault zones are large enough to be mapped. On the other hand, a fracture survey is the systematic collection of fracture data but it does not result in a fracture map, as this would demand an exorbitant amount of work due to the required map scale. In addition, such a survey would be applicable only to the area where the data were collected.

Thus, the only way to extrapolate the fracture network characteristics from one place to another is to use statistical analyses, although this approach is often insufficient for some types of applications such as the migration of a contamination plume. Plume migration is a local phenomenon and, therefore, in some cases the accurate location of the fracture or fracture zone along which contaminants are transported needs to be known. Geological contacts and fault zones represented in detailed geological maps need to be considered in the extrapolations because they constrain specific properties of the fracture networks (Sections 3.4 and 4). Fault zones may be addressed in a deterministic manner because many of them can be mapped. Thus, an effort needs to be made to produce detailed geological maps in regions where only regional-scale maps are available. This is the case for nearly all of Brazil and for many other regions throughout the world.

We conclude that, although much has already been done, much remains to be accomplished. Thus, we wrote this book to motivate students and professionals to dedicate themselves to the study of fractured aquifers.

7 Glossary

Colonnade Layer↥

Layer of compact (without vesicles) columnar basalt in which the column sections are decimeters in diameter. This layer is usually located at the base of the basalt flood. Due to the cooling front, columns are usually roughly perpendicular to the basalt contacts, resulting in the existence of either vertical or inclined columns.

Deformation Band↥

Narrow zone of deformation that typically occurs in highly porous granular media, notably porous sandstones. There are several types of deformation bands in which shear, dilation and compaction bands are the end-members.

Ductile Deformation↥

Deformation in which the rock "flows" and originally continuous structures (e.g., rock contacts and veins) remain continuous after the deformation. Foliation is a typical result of ductile deformation and consists of a planar structure formed by mineral orientation.

Entablature↥

Layer of compact fractured basalt in which the closely spaced cooling joints either are chaotic or form irregular and small diameter (a maximum of 10 to 20 cm) vertical columns. The entablature layer is usually located above a colonnade layer in a basalt flood. In the colonnade layer the cooling joints form regular and larger diameter (several tens of centimeters) vertical columns.

Failure Envelope↥

The line that is obtained through the connection of points, representing specific combinations of shear and normal stresses that cause fractures to be generated. It is determined through laboratory experiments and describes the stress conditions at failure for a given rock.

Fault Zone↥

A series of closely spaced and subparallel faults that clearly form a cluster in a given rock mass. The width of the zone ranges from centimeters or meters, as observed at the scale of rock exposures in the field, to a kilometer or more for large-scale faults such as the San Andreas Fault.

Fracture Orientation↥

The full description of a fracture orientation, also called fracture attitude, includes the compass directions of its strike and dip direction, as well the angle of dip. The angle

91

that a horizontal line within the fracture plane makes with north is the strike direction. The angle between the horizontal plane and the line defining the maximum dip of the fracture plane is the dip value; it is measured down from horizontal. The following image is a stereographic projection that illustrates these items among others.
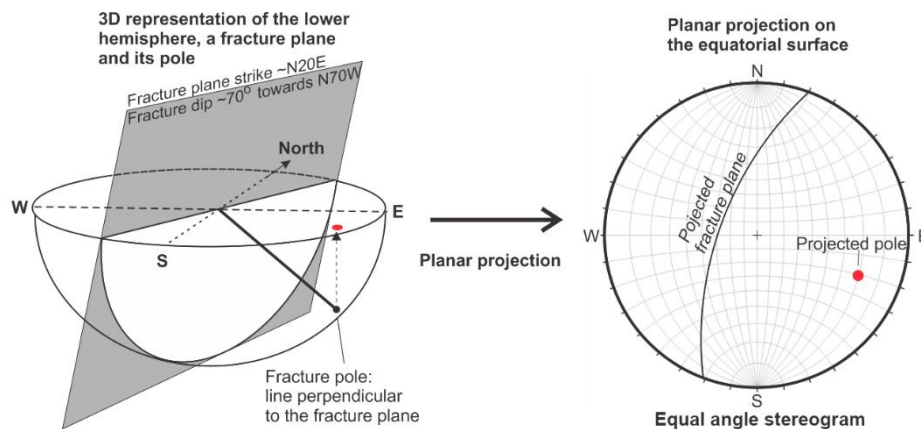
The stereographic projection is a planar plot of the intersections of planes and lines with the outer limit of the lower hemisphere on the equator surface of the same sphere (based on Johnson et al., 2002b).

fracture persistence⬆

A fracture is said to be persistent, or continuous, when its trace length on a surface exposure of rock is long, usually tens of meters or more.

Fracture Set⬆

Fractures that have a similar orientation, appearing as clusters in a stereogram (defined in this glossary under stereographic projection). The limit of a fracture set on a stereogram usually corresponds to a sharp decrease in the number of poles of that given set. In the stereogram shown here, each color represents a different fracture set.
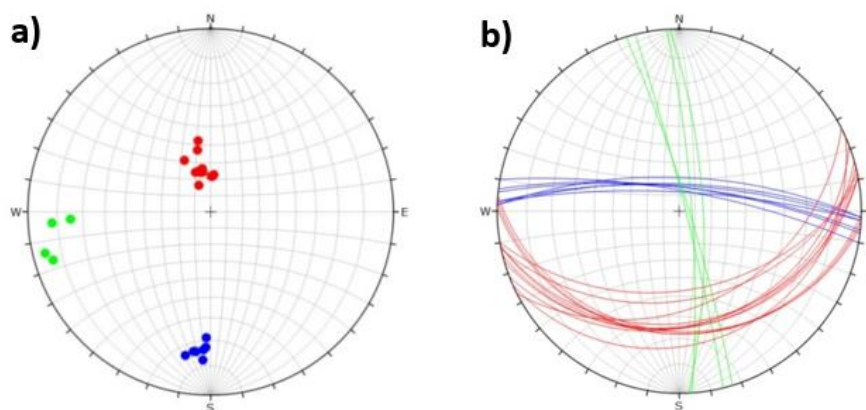
Three fracture sets, represented by different colors, appearing as clusters in a stereogram. A) Stereogram – fracture poles. Each dot is the projection of a line perpendicular to the fracture plane. B) Stereogram – fracture great circles. Each arc (great circle) is the projection of a fracture plane.

92

The GROUNDWATER PROJECT   © The Authors   Free download from gw-project.org

Anyone may use and share gw-project.org links. Direct distribution of the book is strictly prohibited.

Fracture Zone⤴

A series of subparallel fractures (belonging to the same fracture set) that are close enough to each other to define a zone. The fracture spacing in the zone is distinctly smaller than the spacing of the same set outside the zone.

hydrothermal fluids⤴

Fluid that remains after rock crystallization, from which they originated, and that percolate through the same rock, eventually forming veins and/or causing hydrothermal alteration.

Isostatic Compensation⤴

The adjustment of the lithosphere of the Earth to maintain equilibrium among units of varying mass and density; excess mass above sea level (e.g., large mountain ranges) is balanced by a deficit of density below sea level, and vice versa (Mindat, 2022). The isostatic compensation gives rise to some areas that are experiencing uplift and others that are undergoing subsidence.

Maximum Horizontal Stress – S_{Hmax}⤴

The maximum horizontal stress acting on a region, whose direction is usually deduced from seismicity data and borehole breakouts. For the compressive and strike-slip tectonic regimes, S_{Hmax} represents σ_1 and for the extensional regime, it represents σ_2.

Mohr circle⤴

Circle in the Mohr diagram that depicts the normal and shear stresses acting on planes having all possible orientations in a rock body. These orientations are represented by points in the circle.

Mohr Diagram⤴

Diagram where the horizontal and vertical axes represent the normal (σ_n) and shear (τ) stresses that act on planes in a rock mass.

Mylonite⤴

Rock displaying a distinctive foliation and grain size reduction that was formed by intense ductile deformation in shear zones. In the progression of mylonitic rock development, grain size reduction may be accompanied by some degree of recrystallization.

Primary Permeability⤴

Permeability that is provided by pores that are formed along with the processes that form the rock itself, for example the voids between the granular clasts of sedimentary rocks.

Protolith⬆

The host rock, with its structures and textures, prior to the deformation being considered.

Shear zone⬆

Tabular zone typically dominated by shear and ductile deformation.

Slickensides⬆

Finely polished fault surfaces formed by grain crushing during the sliding/shearing movement of a fault.

Stereographic Projection⬆

Planar plot of the intersections of planes and lines with the outer limit of a lower hemisphere on the equator surface of the same sphere. Planes (e.g., fracture, foliation) will appear as arcs, called great circles. Besides the great circles, planes can also be represented by their poles, which are normal (perpendicular) to the planes and appear as points. The result is a stereogram that is used to analyze the spatial distribution of geological structures. This is shown in the following three-dimensional image and stereogram, which in this case illustrates a fracture plane with a strike of N20E and dip of 70° toward the NW.
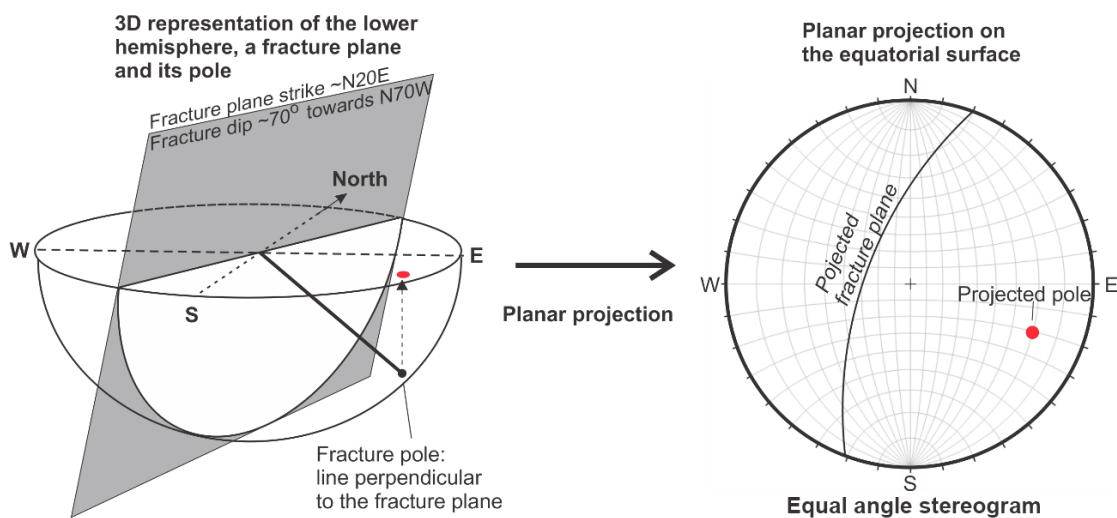
A stereographic projection is a planar plot of the intersection of planes and lines with the outer limit of the lower hemisphere on the equator surface of the same sphere (based on Johnson et al., 2002b).

Striae Lineation⬆

Parallel lines on the fault surfaces expressed by scratches and grooves. They are produced by the friction of small, hard particles sliding over the fault surfaces. Small steps, approximately perpendicular to the striae lineation, are often observed and are used for deducing the relative movement of the fault surfaces.

Tectonic Event (Deformation Phase) ⬆

A time period during which structures form continuously within an area or region in response to a specific stress orientation and tectonic regime that remains relatively unchanged.

Transmissivity ⬆

A measure of the potential of an aquifer to produce water based on the hydraulic conductivity and the thickness of the aquifer. In fractured aquifers, transmissivity is measured through a hydraulic test that isolates a certain depth interval of the rock mass containing one or more fractures. Transmissivity has dimensions of (L^2/T) and is commonly expressed in units of m^2/s.

8 Exercises

8.1 Exercises on Constraints on Fracture Formation and Implications for Fracture Network Properties

Exercise 1 considers deformation history and crustal level, while Exercises 2 through 7 address stress states and fracture formation as deduced from Mohr circle data as well as from tectonic regimes.

Exercise 1

The image below shows a massive granite deformed by structures of different types. Examine the relationships (interactions) between the structures represented in the figure and describe the deformation history of the massive granite. Explain the mechanism that enabled all these structures to occur side by side today. Indicate which structures are likely to carry significant water and which are not, and explain your response.
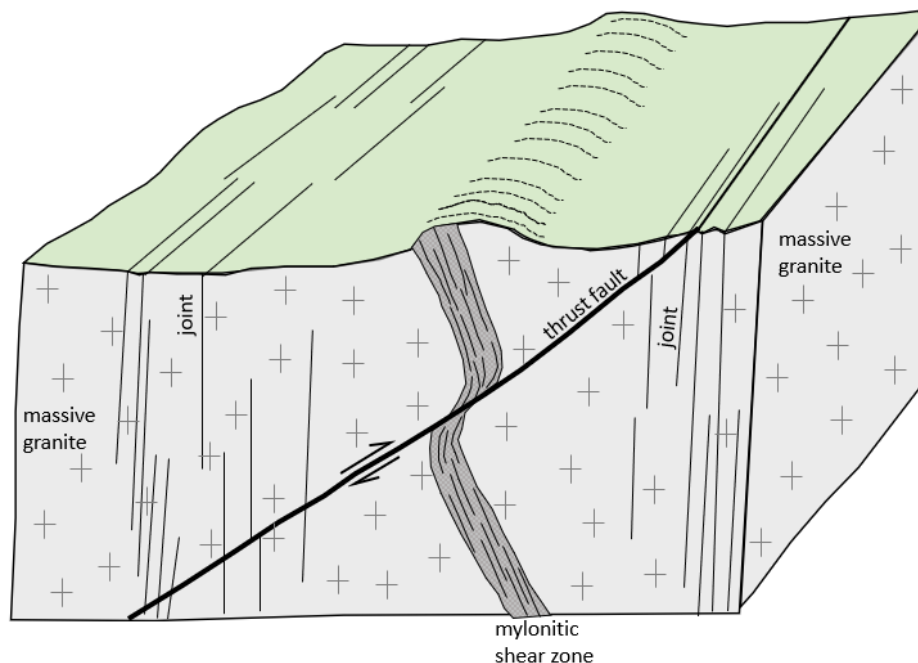
Click to return to where text linked to Exercise 1↳

Click for Solution to Exercise 1↴

Exercise 2

Two different rock layers are represented in the block diagram below: dolomite (orange layer) and mudstone (green layer). Points D (dolomite) and M (mudstone) are both 3 km deep, and the average rock density above each one is the same. This rock mass is under lithostatic conditions, which means tectonic stresses are not present, i.e., the vertical and horizontal stresses are derived solely from the weight of the overlying rock column.
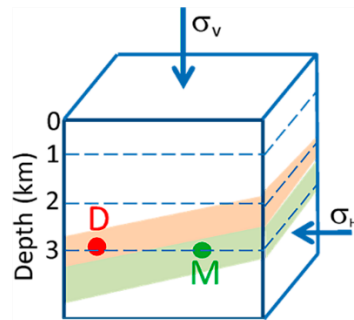
a) Calculate the vertical stress (σ_v) at points D and M in MegaPascals (MPa) using the following equation.

$$\sigma_v = \rho\, g\, h$$

where:

   ρ = 2,500 kg/m^3 (average rock density)
   g = 10 m/s^2 (gravitational acceleration)
   h = 3 km (depth)

b) Calculate the horizontal stress (σ_h) in MegaPascals (MPa) which, under lithostatic conditions, is a fraction of σ_v and depends on the elastic properties[1] of each rock as follows.

$$\sigma_{h\,dol} = \sigma_v/(m_{dol} - 1)$$
$$\sigma_{h\,mud} = \sigma_v/(m_{mud} - 1)$$

where:

   $\sigma_{h\,dol}$ = dolostone horizontal stress
   $\sigma_{h\,mud}$ = mudstone horizontal stress
   m_{dol} = 5 (dolomite Poisson number)
   m_{mud} = 4 (mudstone Poisson number)

c) Draw a Mohr diagram for each rock representing the stresses and the failure envelopes given the following equations
   Failure envelope of the dolostone: τ = 75 MPa + 0.7 σ_n
   Failure envelope of the mudstone: τ = 15 MPa + 0.53 σ_n

---

[1] Explanation of elastic properties is given as supplemental information for exercise 2.

97

The GROUNDWATER PROJECT   © The Authors   Free download from gw-project.org

Anyone may use and share gw-project.org links. Direct distribution of the book is strictly prohibited.

where:

MPa = Megapascal = 10^6 pascal

MPa = 1 N/m^2

Pa = 1 N/m^2

N = 1 (kg m)/s^2

$$\text{Pa} = \frac{1\frac{\text{kg m}}{\text{s}^2}}{\text{m}^2} = 1\frac{\text{kg}}{\text{m s}^2}$$

d) Under this stress state, will the rocks undergo failure?

e) Which rock has the greater cohesion?

f) Which of the two rocks will fracture by shear mode under smaller differential stresses, that is, under milder tectonic conditions?

Supplemental information - Elastic Properties Explanation

The diagram below (based on Price & Cosgrove, 1990) depicts an elemental cube (stippled) in the Earth's crust. The weight of rock column above the cube produces the vertical stress (σ_v) that causes an infinitesimal vertical compression (e_v). If the cube were not confined laterally, as illustrated by the gray areas, the vertical stress would cause the cube to expand (red arrows) by a certain amount (represented by the red dashed lines). However, the rock beside the cube is also under the effect of the same vertical stress and tends to laterally expand by the same amount (green dashed lines), but in the opposite direction (green arrow). This situation prevents the expansion and simultaneously creates a horizontal stress that is a fraction of the vertical stress; the magnitude of this horizontal stress varies with the rock type. In the lithostatic condition, where all the stresses are derived from the rock column weight, the horizontal stress for stiffer rocks (when compared to softer rocks) is a smaller fraction of the vertical stress. This happens because the lateral expansion of stiffer rocks is smaller.

ground surface

σ_v = vertical stress
ρ = rock density
g = gravity acceleration
h = depth

h $\sigma_v = \rho \, g \, h$
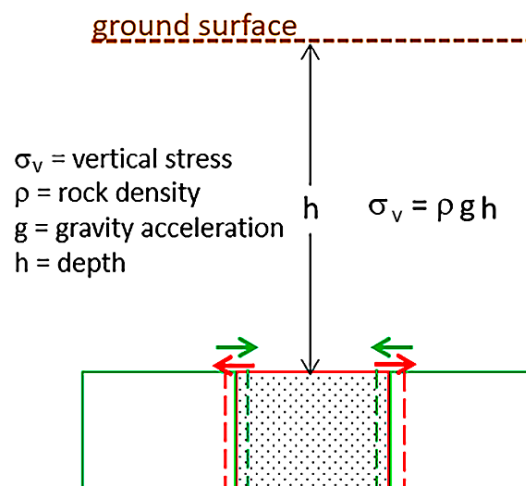
The elastic properties of the materials shown in the image below control horizontal stress in a lithostatic condition: a) the stress-strain relationship is linear; b) the elastic strains (e_v, e_h) are infinitesimal; and, S_z = vertical stress (Price & Cosgrove, 1990).
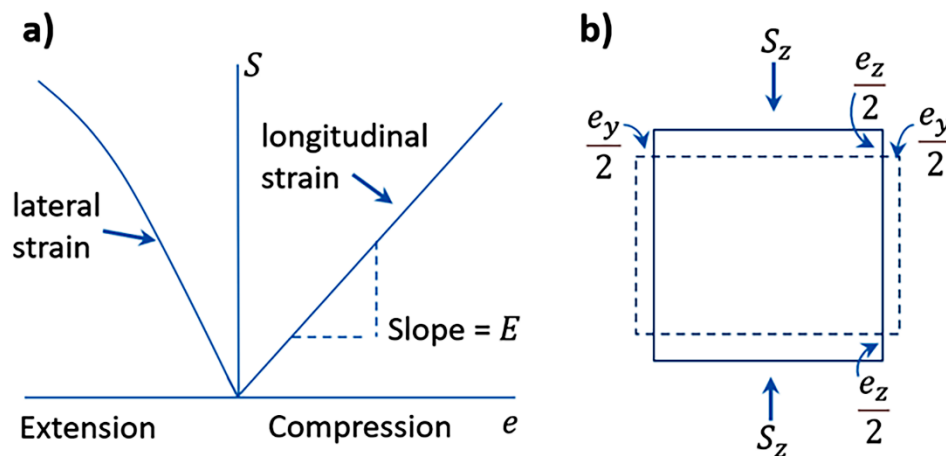
The simplifying premises of the elasticity theory are:

- The material is homogeneous.
- The material is isotropic (its properties do not vary with the direction).
- The elastic strains (deformations) are infinitesimal (limit ~3 percent).
- The stress–strain relationship is linear and expressed by the ratio $S/e = E$,

where:

$$E \;=\; \text{Young's modulus (material constant)}$$
$$e_h/e_v \;=\; \nu, \text{Poisson's ratio}$$
$$1/\nu \;=\; m, \text{Poisson's number}$$

and S_z is vertical stress (based on Price & Cosgrove, 1990, pages 18-20).

Supplemental information - Stress State Explanation

The following Mohr diagrams (Fossen, 2016) represent a) stable and b) unstable conditions.
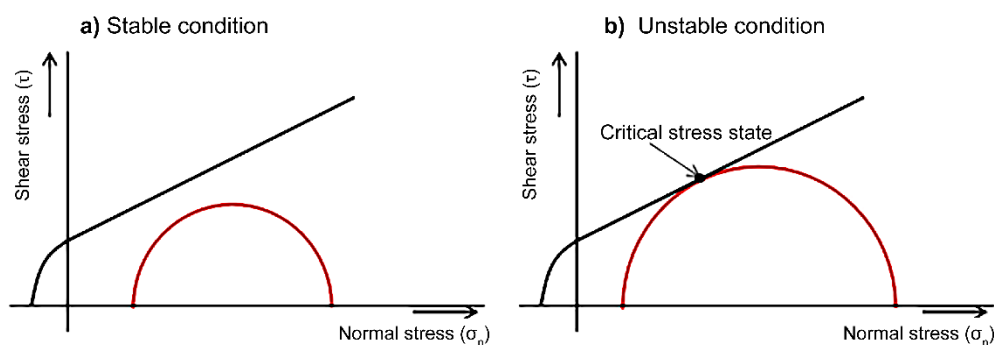
In diagram a, the Mohr circle does not intersect the failure envelope because the principal stresses are not large enough. This is a stable situation in which no fractures are formed. In diagram b, the principal stresses are such that the Mohr circle intercepts the failure envelope at one point (critical stress state) at which shear conjugate fractures are generated. Because fractures are formed, this is called "unstable condition."

Exercise 3

Sandstone and limestone samples subjected to laboratory compression triaxial tests (Tests 1 through 4 in the tables below) undergo shear fracturing. The fractures are generated under the following critical stress states:

Sandstone

Test #	Principal stresses (MPa)	σ_n (MPa)	τ (MPa)
1	$\sigma_3 = 27.5$, $\sigma_1 = 116.25$		
2	$\sigma_3 = 68.75$, $\sigma_1 = 217.5$		

Limestone

| Test #	Principal stresses (MPa)	σ_n (MPa)	τ (MPa)
3	$\sigma_3 = 7.5$, $\sigma_1 = 192.5$		
4	$\sigma_3 = 41.25$, $\sigma_1 = 308.75$		

a) Construct the Mohr diagram for the sandstone and plot the principal stresses for tests 1 and 2; draw the Mohr circles and determine the failure envelope equation of the sandstone. In a separate diagram, follow the same procedure for the limestone, plotting the principal stresses of tests 3 and 4.

b) What is the value of the slope (φ, friction angle) of the sandstone failure envelope? What is the value of φ for the limestone failure envelope?

c) For each rock, what is the angle between the shear conjugate fractures (2θ)? What is the angle between σ_1 and the shear fractures (θ)?

d) Determine the critical normal stress (σ_n) and shear stress (τ) at which the shear fractures were generated in each test and enter their values in columns σ_n and τ in the two tables.

e) Compare the critical Mohr circles and the failure envelopes of the two rocks. Which rock has the greater cohesion (C)? Which rock would undergo brittle deformation under lower stresses?

f) In the case where both rocks are present in the same geological context and are subjected to the same stress fields (same tectonic events), should we expect one of them to have a denser fracture network? Explain your answer. What should you expect regarding the connected fracture network in each rock?

101

The GROUNDWATER PROJECT   © The Authors   Free download from gw-project.org

Anyone may use and share gw-project.org links. Direct distribution of the book is strictly prohibited.

Exercise 4

The Mohr diagrams below show the complete failure envelopes of the sandstone and limestone of the Exercise 3. What should be the value of σ_3 in order for joints to be formed in the limestone? And in the sandstone? Explain your answers.
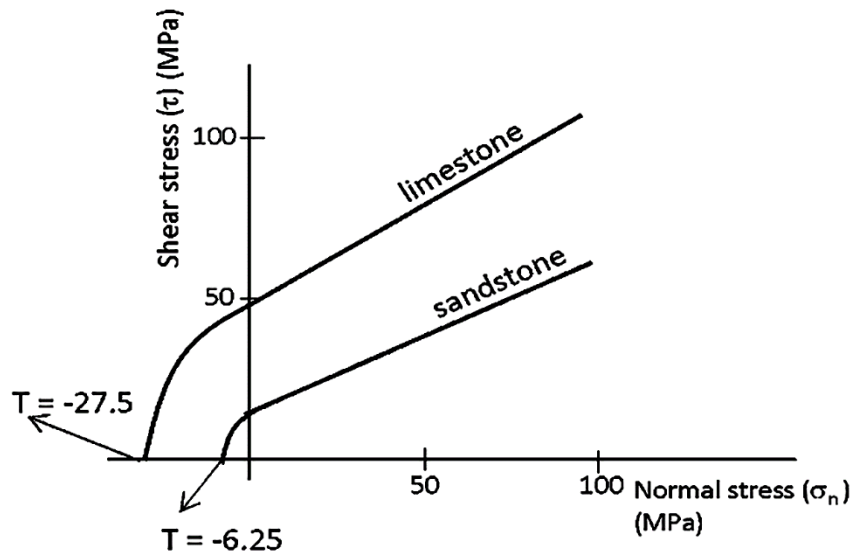
Exercise 5

In Exercise 2 we saw that the lithostatic stress state does not, by itself, generate fractures. With this in mind, use the Mohr diagrams of the Solution for Exercise 2 (failure envelopes and the Mohr circles that represent the lithostatic stress state for the dolostone and mudstone) to answer the questions below.

a) In the case that fluid pressure (p) is present, what would happen to the Mohr circles?

b) If this fluid pressure is high enough to make the Mohr circles intercept the failure envelopes, what type of fractures would be formed in the dolostone? And in the mudstone? Explain your answers.

c) Is it possible that fractures propagated by the opening mode and by the shear modes be formed in the same rock at a given location, at the same time? Explain.
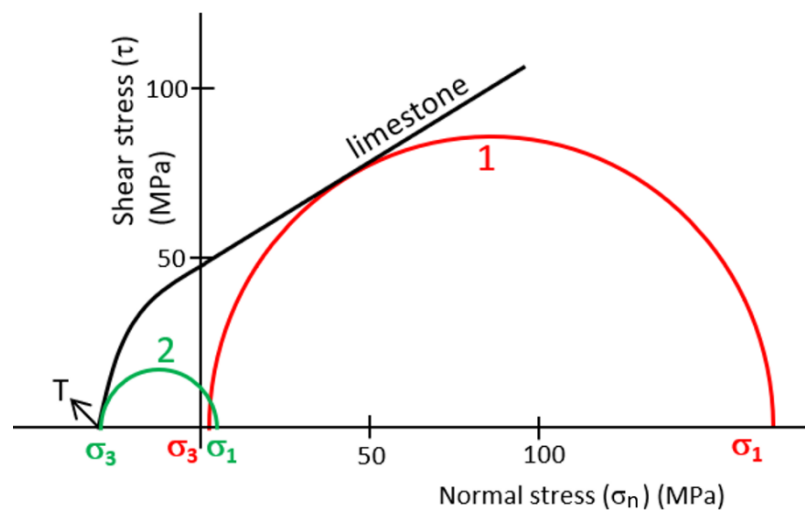
Exercise 6

Based on the limestone Mohr diagram below that was taken from the solution of Exercise 3, answer the following questions.

a) What type of fractures will be formed under the stress conditions represented by the Mohr circle number 1? What will be the tectonic regime and the orientation of the fractures for the following three situations:

- when σ_1 is vertical and σ_3 is horizontal and strikes EW;

- when σ_1 and σ_3 are horizontal and strike NS and EW, respectively; and,

- when σ_3 is vertical and σ_1 strikes EW?

Enter your answers in the table below and make drawings representing the stresses and the resulting fractures in each case.

Stress orientation	Tectonic regime	Fracture strike	Fracture dip
σ_1 is vertical σ_3 is horizontal and strikes EW			
σ_1 is horizontal and strikes NS σ_3 is horizontal and strikes EW			
σ_3 is vertical σ_1 is horizontal and strikes EW			

b) What type of fractures will be formed under the stress conditions represented by Mohr circle number 2? What will be the tectonic regime and the orientation of the fractures for the following three situations:

- when σ_1 is vertical and σ_3 is horizontal and strikes EW;
- when σ_1 and σ_3 are horizontal and strike NS and EW, respectively; and,
- when σ_3 is vertical and σ_1 strikes EW?

Answer this question using the table below and make drawings representing the stresses and the resulting fractures in each case.

| Stress orientation	Tectonic regime	Fracture strike	Fracture dip
σ_1 is vertical σ_3 is horizontal and strikes EW			
σ_1 is horizontal and strikes NS σ_3 is horizontal and strikes EW			
σ_3 is vertical σ_1 is horizontal and strikes EW			

105

Exercise 7

A mudstone at 3,000 m depth is under a stress state represented by the Mohr circle shown below, in which the vertical ($\sigma_v°$) and horizontal ($\sigma_h°$) stresses correspond to σ_1 and σ_3, respectively. At this stress state no faults are formed because the circle does not intersect the failure envelope of the mudstone. Given the state of stress at the depth of 3,000 m in the mudstone, where $\sigma_v = 75$ MPa, $\sigma_h = 30$ MPa, $C = 15$ MPa and $\varphi = 28°$, develop the following:

a) Represent the Mohr circles that correspond to the formation of normal and thrust faults in the mudstone at the given depth.

b) Determine the dip of each type of fault.
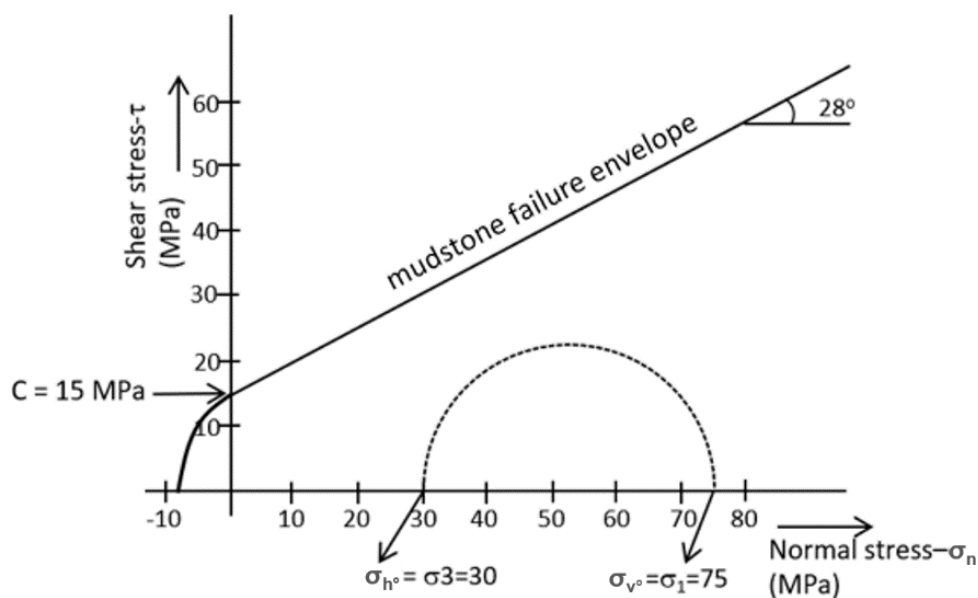
c) The graph below (modified from Hoek & Brown, 1980) shows in-situ stress from several regions throughout the globe. Close to the surface (above 500 m in depth), the average horizontal stress can be on the order of three times larger than the vertical stress. Analyze the graph and explain at what depths the thrust faults tend to be formed and what consequences this may have for the flow. Information required to complete (a) and (b) of the exercise is given below (Supplemental Information).

$$k = \frac{100}{z} + 0.3$$

$$k = \frac{1500}{z} + 0.5$$

$$k = \frac{\text{Average horizontal stress}}{\text{Vertical stress}}$$
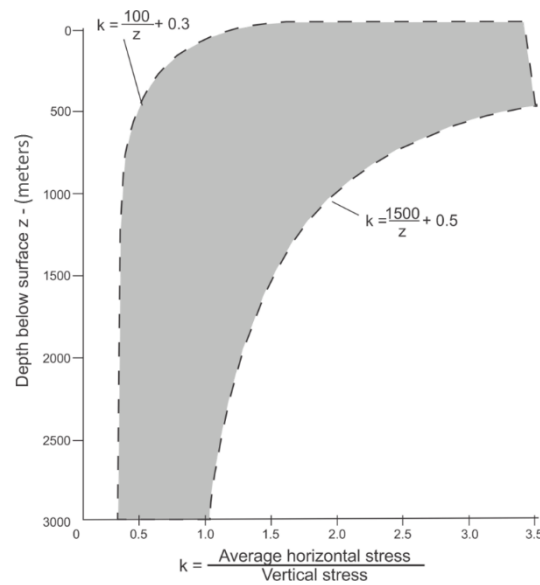
Supplemental information - Determination of Stress State Acting on a Plane

On the left side of the image below, line AA′ represents a plane that makes an angle with the main stresses (20 and 40 MPa). The stress state acting on this plane is determined by drawing a line on the Mohr diagram with the same slope and passing through its pole (OP); the stress state on the plane AA′ is given by point M. The determination of a plane pole is explained below.
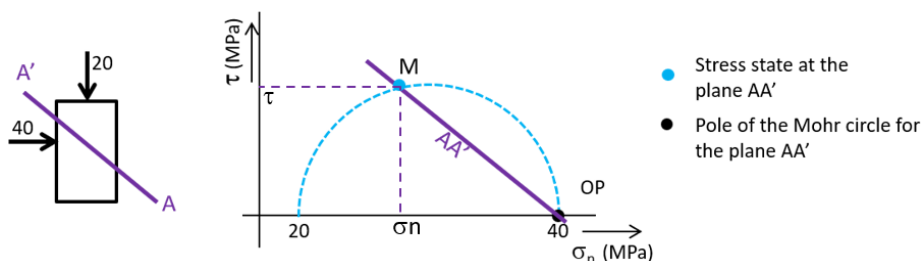
Supplemental information - Determination of the Pole of a Plane

Start with a plane having a known stress state, e.g., a horizontal plane as shown by the red line in the image below, for which the values of σ_1 (40 MPa) and σ_3 (20 MPa) are known. Next draw the Mohr circle in the Mohr diagram. Draw a horizontal line (BB′) on the Mohr diagram that starts at its state of stress (20,0; blue point) and continues until it intersects the Mohr circle again; this second point of intersection is the pole (OP).

107
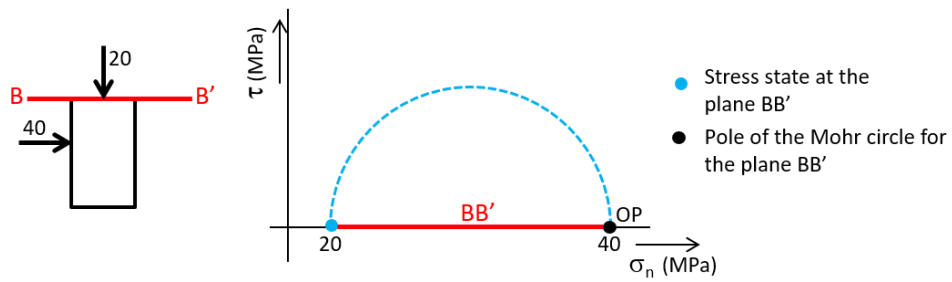
[Click to return to where text linked to Exercise 7](#)⤴

[Click for solution to Exercise 7](#)⤵

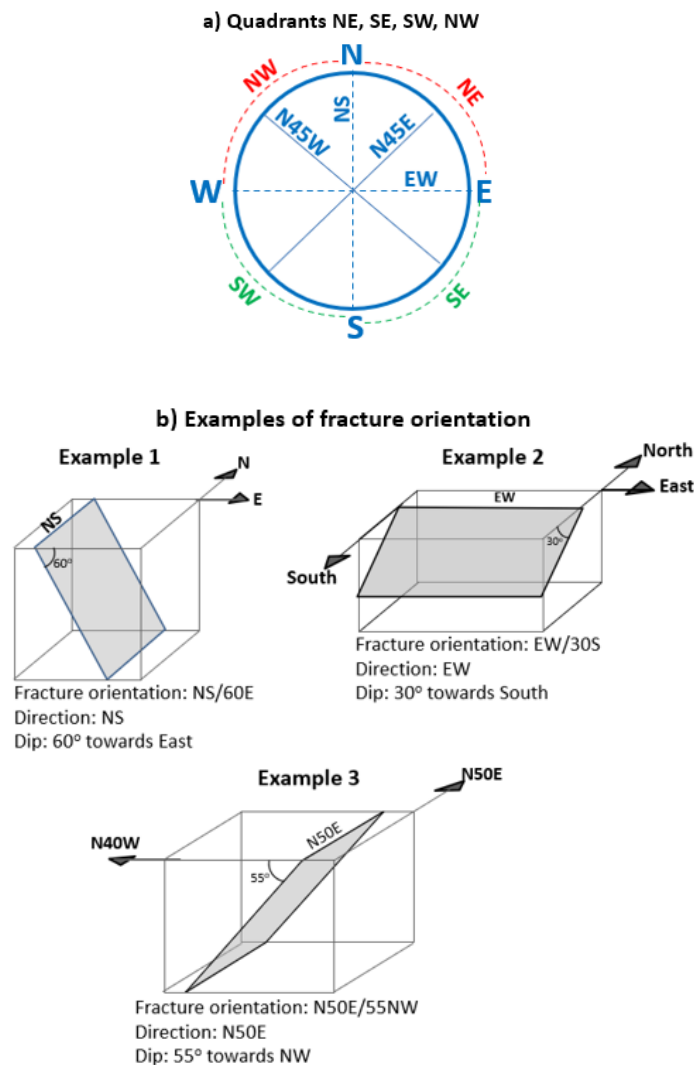## 8.2 Exercises on the Interpretation of Fracture Data Collected in the Field and their Consequences for Groundwater Flow

The following exercises (8 through 17) concern fracture formation (fracture types), tectonic regimes and orientation of the principal stresses that can be inferred from data, such as fracture orientation, collected by the authors during academic-related field work or informal excursions. The orientation (or attitude) of fractures displayed in photographs and sketches follows the quadrant notation because this is more readily understandable, even though books and articles generally use the dip-direction and right-hand-rule notations. Illustrations that explain the quadrant notation, along with three examples of fracture orientations, are shown in the images below. Part (a) of the image shows quadrants NE, NW, SW, and SE. Part (b) of the image provides examples of fracture orientation. Directions are expressed either as NS and EW or in terms of NW and NE quadrants. The dip direction is referred either to N, S, E and W or to one of the four quadrants. For instance, for an NS fracture, the dip is either to W or to E.

a) Quadrants NE, SE, SW, NW

b) Examples of fracture orientation

Example 1

Fracture orientation: NS/60E
Direction: NS
Dip: 60° towards East

Example 2

Fracture orientation: EW/30S
Direction: EW
Dip: 30° towards South

Example 3

Fracture orientation: N50E/55NW
Direction: N50E
Dip: 55° towards NW

109

Exercise 8

Photographs of three rock exposures are presented below. In each of them, the fracture face displays striae lineation that is assumed to be formed at the same time as the fracture, i.e., the striae lineation was not formed by reactivation.

a) In the following photograph, the fracture orientation is N40E/60SE and striae lineation on the surface is parallel to the dip of the fracture. What type of fracture is this? In which tectonic regime was it generated? What was the orientation of the principal stresses?
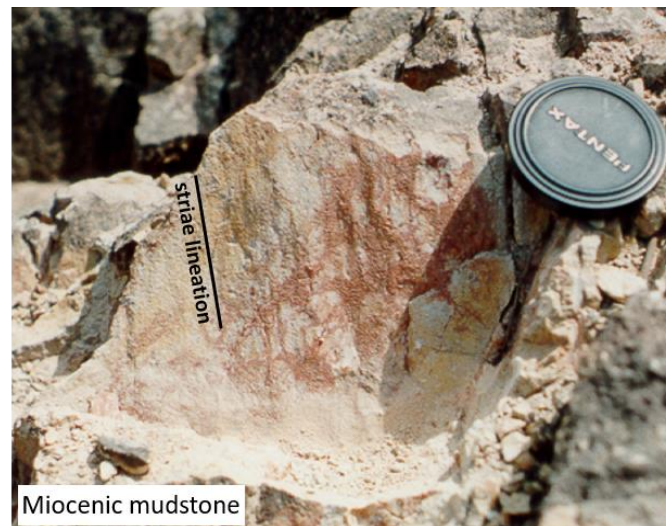
Photograph from Campinas, São Paulo, Brazil, by Amélia Fernandes

b) In the following photograph, the fracture orientation is N80E/88NW and striae lineation is subhorizontal. What fracture type is this? In which tectonic regime was it generated? What was the orientation of the principal stresses?

Photograph from Campinas, São Paulo, Brazil, by Amélia Fernandes

110
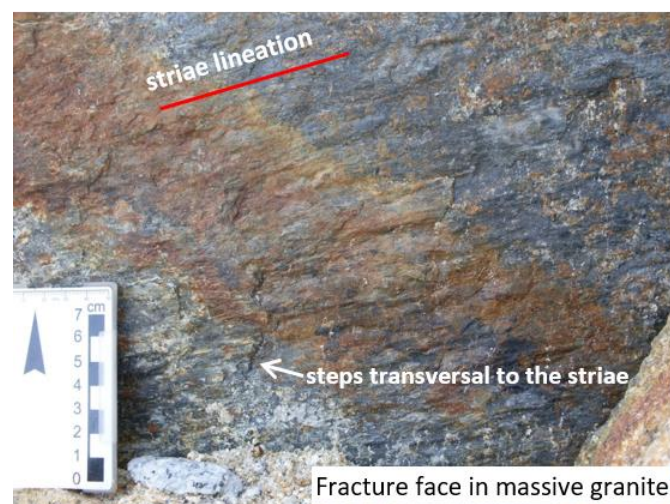
c) In the following photograph, the fracture orientation is EW/30S and striae lineation is parallel to the dip of the fracture. What fracture type is this? In which tectonic regime was it generated? What was the orientation of the principal stresses?

Photograph from Abitibi-Québec, Canada, by Alain Rouleau

Click to return to where text linked to Exercise 8↱

Click for solution to Exercise 8↳

Exercise 9

The photograph below shows two fracture faces. One is vertical (N30W/90) and bears a plume, and the other has an intermediate dip (N76W/42SW).

Given this image, answer the following questions.

a) What type of fracture is the vertical fracture? What is the orientation of the principal stresses and the tectonic regime that produced it?

b) What is the mode of formation of the N76W/42SW fracture? What is the orientation of the principal stresses and the tectonic regime that generated it?

c) Is it possible that both fractures could have been formed in the same tectonic event (same stress field)? Explain your answer.

Photograph from Itapecerica da Serra, São Paulo, Brazil, by Amélia Fernandes

Click to return to where text linked to Exercise 9⇡

Click for solution to Exercise 9⇣

Exercise 10

The photograph below shows a N62E/74SE-oriented fracture cutting a massive granite. The fracture bears a plume with a vertical axis; two of the plume traces are shown in white. What type of fracture is this? What is the orientation of the principal stresses and the tectonic regime that gave rise to this fracture?

Photograph from São Paulo, São Paulo, Brazil, by Amélia Fernandes

Click to return to where text linked to Exercise 10⤴

Click for solution to Exercise 10⤵

Exercise 11

Consider the fractures in the photograph below and the corresponding sketch. The fractures belong to two sets with the same strike but with opposite dips: one set dips toward NW and the other toward SE. Answer the following questions:

a) What type of pattern do the fractures form and under what tectonic regime were they generated?

b) What was the orientation of the main stresses and what type are these fractures?

c) What does this fracture pattern imply for the connected network and flow?

N45W

Vertical rock exposure of massive granite, São Paulo, Brazil
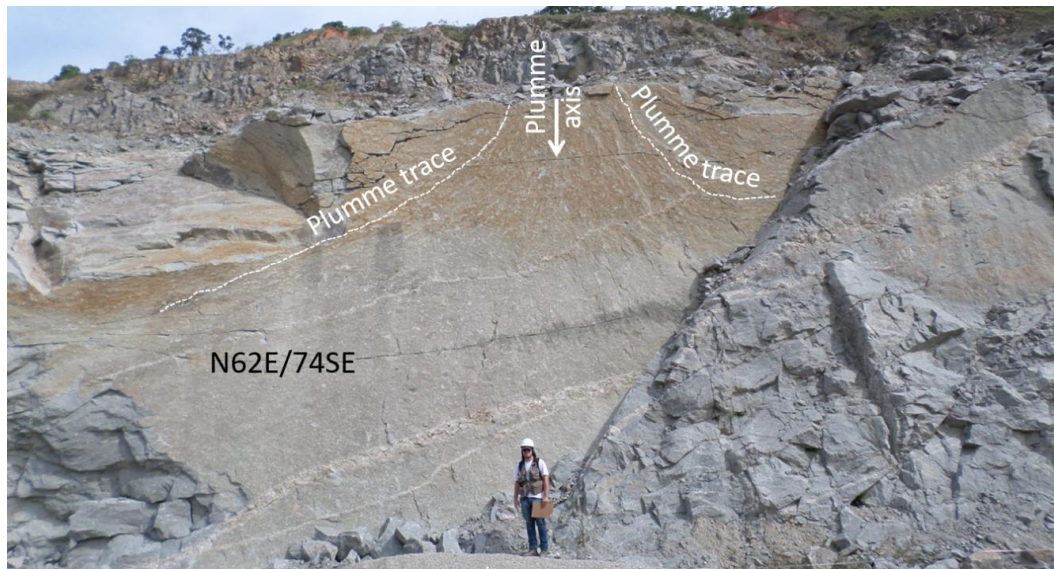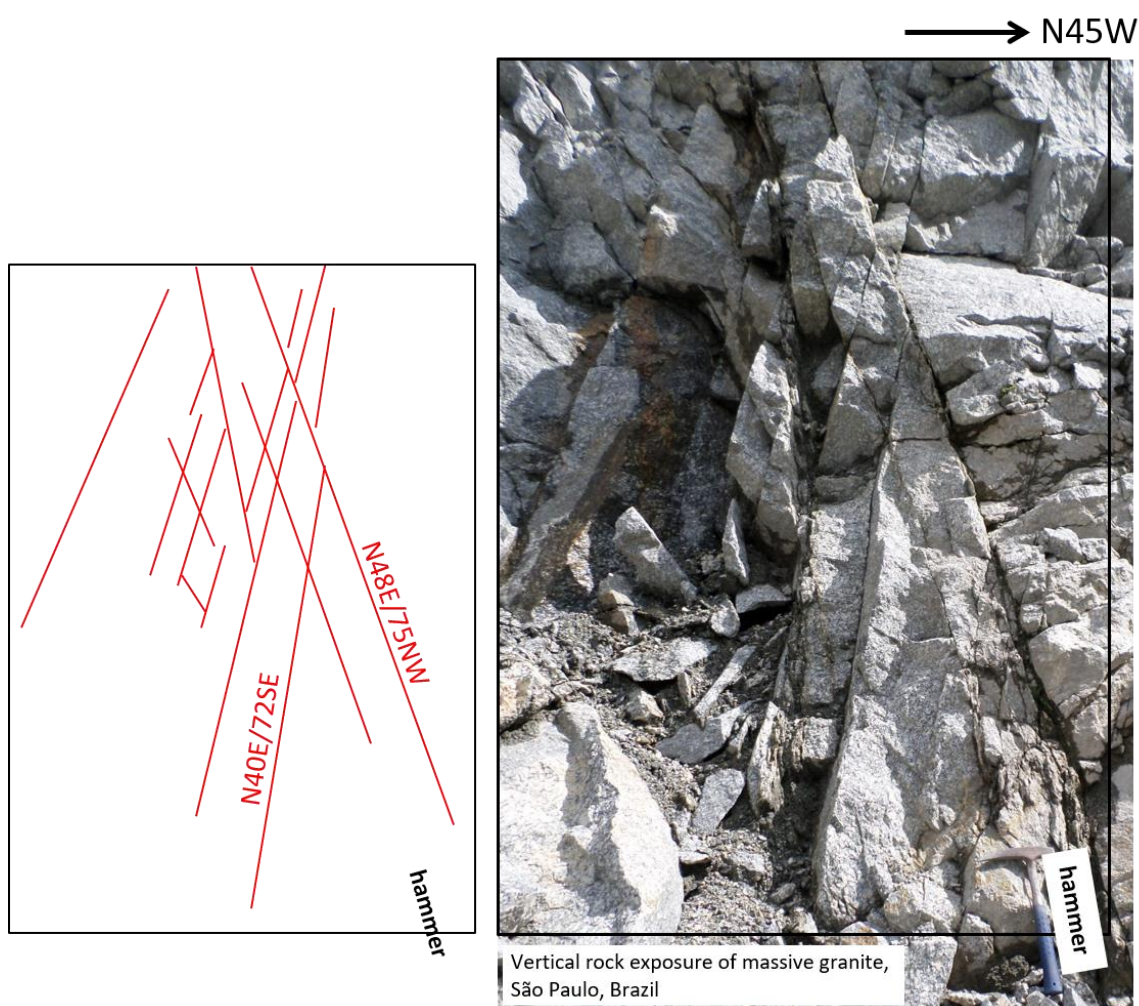
Photograph from Suzano, São Paulo, Brazil, by Amélia Fernandes

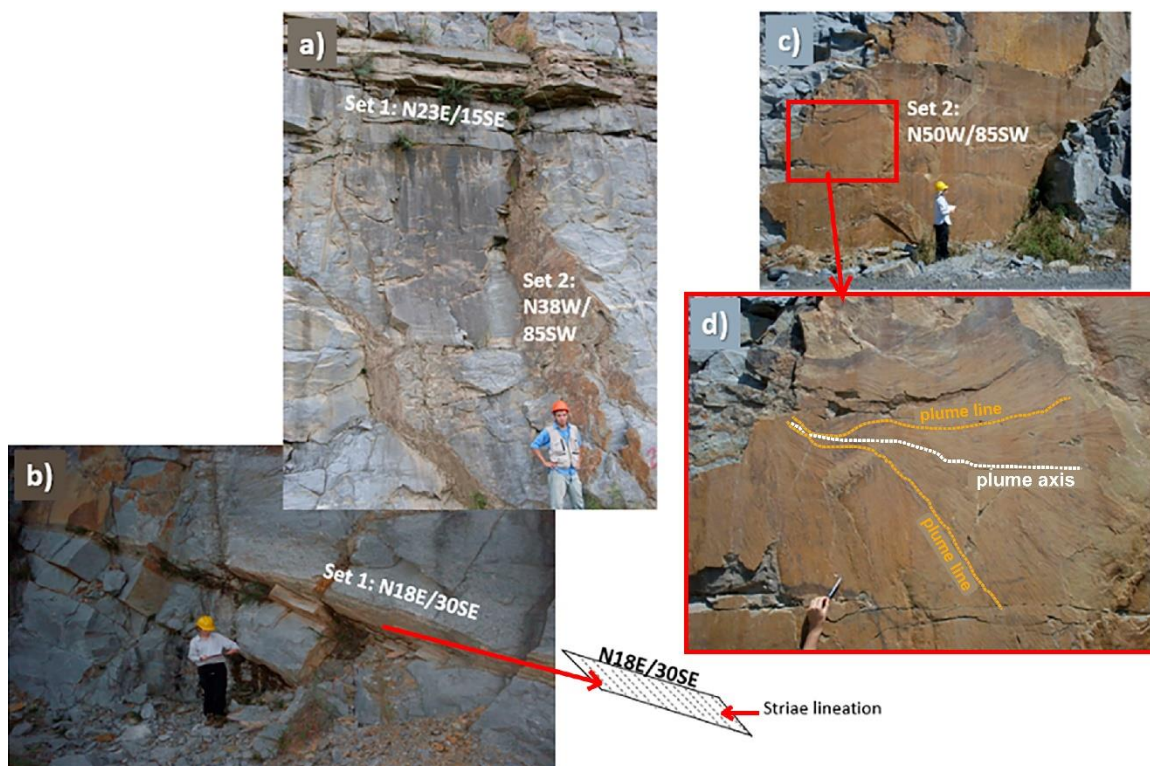**Click to return to where text linked to Exercise 11**

Click for solution to Exercise 11

Exercise 12

Fractures belonging to two different sets are shown in the photographs below. Set 1 strikes at around N20E and dips between 15° and 30° toward SE (photographs a and b); set 2 strikes at roughly N45W and has subvertical dips around 85° toward SW (photographs a, c and d). The fracture surfaces of set 1 bear striae lineation parallel to the dip of the fractures, as shown in the sketch to the left of photograph b. Besides the presence of vegetation and oxidation, the rock is weathered to some extent along set 1. A fracture of set 2 bears a plume feature on its oxidized surface (photographs c and d).

a) What are the fracture types, the tectonic regimes, and the orientation of the principal stresses that gave rise to each fracture set?

b) Is there indication of flow along any of the fractures? Explain your answer.

c) Describe and explain the potential flow paths, as well as the characteristics of the connected network, based on the photographs and the presented data.

Photographs from Embu das Artes, São Paulo, Brazil, by Bruna Fiume

Click to return to where text linked to Exercise 12

Click for solution to Exercise 12

Exercise 13

Two quartz-feldspar veins cutting across schist foliation are displayed on the right side of the photograph below and barren fractures occur on the left. The two quartz-feldspar veins have the same strike, roughly N70E, but they have high dips in opposite senses and crosscut each other. There are also fractures that mimic the schist foliation, even at the fold hinge. What type of fractures are the infilled ones (i.e., the veins)? What are the tectonic regime and the principal stresses orientation? Present the evidence that justifies your answers.

Schist, Quebec Province, Canada
(picture taken by Alain Rouleau)

116

Exercise 14

The horizontal fractures depicted in the photographs below can be interpreted as sheeting joints because they are parallel to the ground surface, shallow, persistent, and closely spaced. A possible mechanism for their formation is axial splitting under a horizontal compressive σ_1 and a vertical σ_3 (Section 3.6).

In this case the rock is a massive granite and the sheeting joints are connected through relatively sparse vertical fractures (left side of the larger photograph). The weathering (brown color) accompanying the sheeting joints may indicate a present day or recent existence of flow along them. Would you expect this flow to be present at depths greater than, say, 100 m?

Photograph from Québec City-Saguenay highway, Canada, by Alain Rouleau

Click to return to where text linked to Exercise 14⬆

Click for solution to Exercise 14⬇

117

Exercise 15

The granite that forms a small peninsula (Google Earth image at the top-left of the image below) on the coast of São Paulo State, Brazil, faces the Atlantic Ocean. The granite bears three subvertical fracture sets, two of the fracture sets strike approximately N15E and N75E as shown in photograph (a) which was taken looking NE. The third fracture set strikes N45E as shown in photograph (b) which was taken by looking SW. The third set is subparallel to the elongation of the peninsula. Answer the following questions.

a) What typical patterns do you observe in photograph a and in photograph b? What fracture types do they imply?

b) What is the orientation of the principal stresses and the tectonic regime?

c) What fractures seem to be more persistent?

d) Does this observation have implications for flow?

e) What can you say about the fracture connectivity?
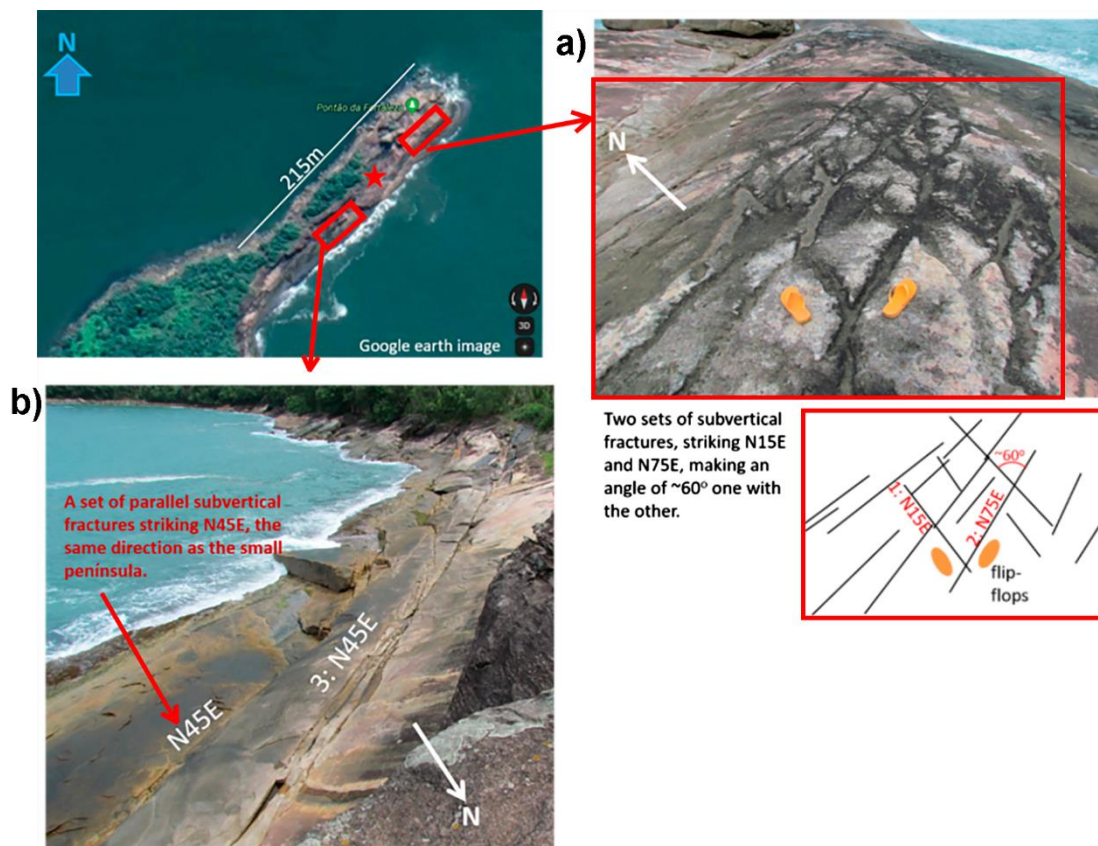
The photographs (a) and (b) were taken from the red star looking toward NE and SW, respectively. Photographs from Ubatuba, São Paulo, Brazil, by Amélia Fernandes

Click to return to where text linked to Exercise 15

Click for solution to Exercise 15

118

Exercise 16

The two rock exposures in the photographs below are in the same quarry and show three fracture sets; their respective great circles and poles are represented in the stereograms. In photograph (a), the subvertical fracture zone (white arrow) belongs to fracture set 1 and consists of vertical, persistent (>80 m long) parallel fractures (N30–35W). They are occasionally infilled by narrow dikes (a few decimeters thick) of alkaline rocks (darker color depressions indicated by red arrows). Fracture zones that belong to set 1 can be tens of meters apart.
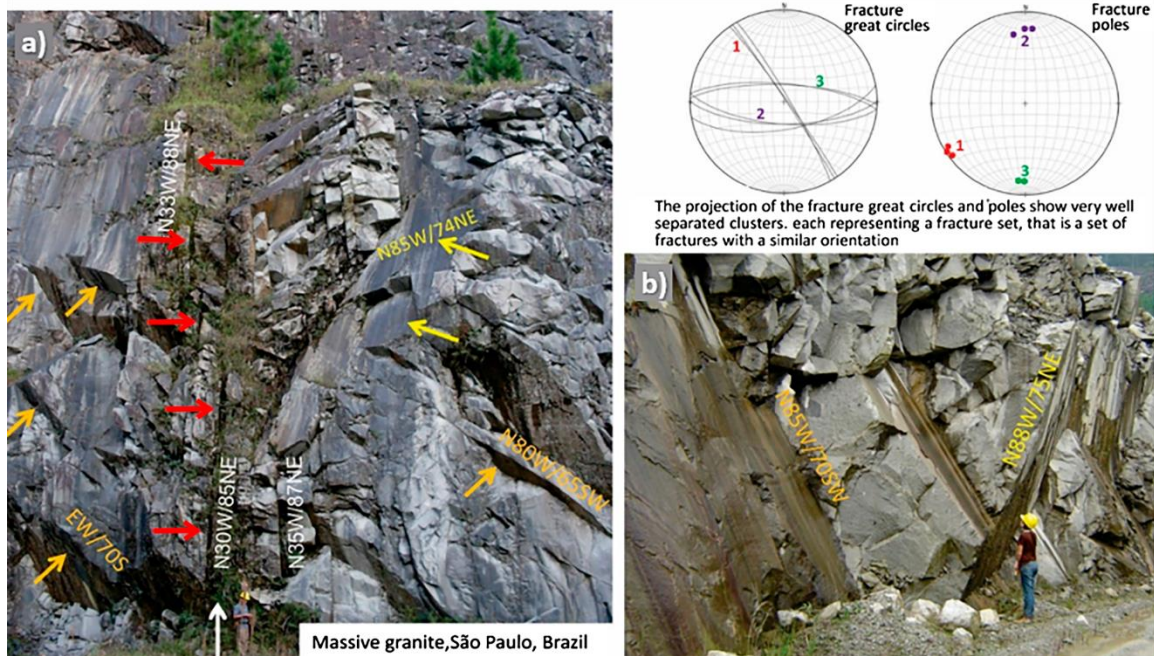
Photographs from Itapecerica da Serra, São Paulo, Brazil, by Bruna Fiume

a) What type of fractures do these characteristics, by themselves, indicate?
b) In which tectonic regime may they have been formed?
c) What was the possible orientation of the principal stresses at the time set 1 was generated?

Orange and yellow arrows in photographs (a) and (b) identify fracture sets 2 and 3, respectively. Both strike EW and dip around 60° to 70° with set 2 dipping to the south and set 3 to the north.

d) What type of fractures and tectonic regime do these characteristics indicate?
e) What is the orientation of the principal stresses? The dikes that infill fracture set 1 are intensely weathered, which explains the depressions indicated by the red arrows in photograph (a); conversely, the fracture surfaces of sets 2 and 3 are fresh.

f) Considering the fracture type of each set, the connectivity outlined by the orientations and persistence of the fractures, and the presence or absence of weathering, what would be expected with regard to the connected network and the groundwater flow anisotropy?

Exercise 17

A fracture survey along a total of 11 scanlines was conducted on subvertical exposures in a massive granite quarry. The image from Google Earth at the top left of the image below shows the location of two scanlines, line 1 and line 2, whose directions are N70W and N70E, respectively. The drawings of line 1 and 2 show the fractures observed on the respective quarry walls. The two photographs show details of the walls.
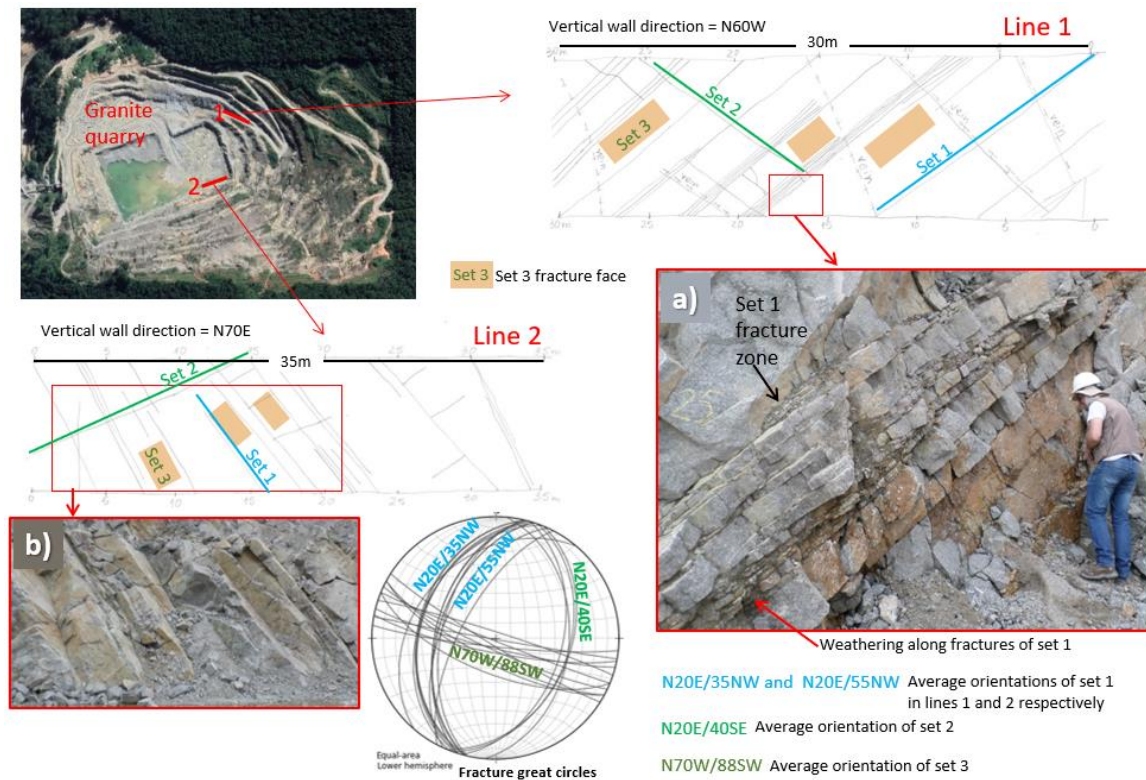
Photographs from Suzano, São Paulo, Brazil, by Amélia Fernandes

Fractures along these scanlines belong to sets 1, 2 and 3, as shown in the scanline sketches, photographs, and stereogram below.

Fracture set 1 average strike is N20E, dipping around 35° to 40° in line 1, or 50–55° in line 2, toward NW. A distinctive characteristic of this set is that it frequently forms zones of parallel fractures as shown in photograph (a).

Fracture set 2 average strike is the same as set 1, N20E, but it dips around 40° toward SE. Therefore, fracture sets 1 and 2 form an angle of around 80° to 90° with each other. Fracture set 2 frequently abuts against set 1 and the opposite also takes place.

Whereas sets 1 and 2 are planar, set 3 (average orientation is N70W/88SW) is wavy and includes narrow gouge zones, and its faces show subhorizontal striae lineation. Fracture sets 1 and 2 cut through set 3 and are not disturbed by it.

a) What are the types of displacements, the tectonic regimes and stress orientation that generated each of the sets? Explain your answer.

b) What can we deduce about the deformation history of the granite?

c) What are the implications of the fracture set characteristics for groundwater flow?

Click to return to where text linked to Exercise 17⬏

Click for solution to Exercise 17⬎

9 References

Anderson, E.M., 1951, The Dynamics of Faulting and Dyke Formation with Application to Britain. Edinburgh, Oliver and Boyd, second edition, 206 pages.

Assumpção, M., F.L. Dias, I. Zevallos, & J.B. Naliboff, 2016, Intraplate stress field in South America from earthquake focal mechanisms. Journal of South American Earth Sciences, volume 71, pages 278-295, doi: 10.1016/j.jsames.2016.07.005↗.

Aydin, A., R.I. Borja, & P. Eichhubl, 2006, Geological and mathematical framework for failure, modes in granular rock. Journal of Structural Geology, volume 28, issue 1, pages 83-98, doi: 10.1016/j.jsg.2005.07.008↗.

Baksi, A.K., 1987, Critical evaluation of the age of the Deccan Traps, India: implications for flood-basalt volcanism and faunal extinctions. Geology, volume 15, issue 2, pages 147-150, doi: 10.1130/0091-7613(1987)15%3C147:CEOTAO%3E2.0.CO;2↗.

Banks, D., E. Rhor-Torp, & H. Skarphagen, 1994, Groundwater resources in hard rock: experiences from the Hvaler study, Southeastern Norway. Applied Hydrogeology, volume 2, issue 2, pages 33-42, doi: 10.1007/s100400050040↗.

Barton, C.A., M.D. Zoback, & D. Moos, 1995, Fluid flow along potentially active faults in crystalline rock. Geology, volume 23, issue 8, pages 683-686, doi: 10.1130/0091-7613(1995)023%3C0683:FFAPAF%3E2.3.CO;2↗.

Bense, V.F., T. Gleeson, S.E. Loveless, O. Bour, & J. Scibek, 2013, Fault zone hydrogeology. Earth-Science Reviews, volume 127, pages 171-192, doi: 10.1016/j.earscirev.2013.09.008↗.

Bondre, N.R., R.A. Duraiswami, & G. Dole, 2004, A brief comparison of lava flows from the Deccan Volcanic Province and the Columbia-Oregon Plateau flood basalts: implications for models of flood basalt emplacement. Journal of Earth System Science, volume 113, pages 809-817, doi: 10.1007/BF02704039↗.

Boutt, D.F., P. Diggins, & S. Mabee, 2010, A field study (Massachusetts, USA) of the factors controlling the depth of groundwater flow systems in crystalline fractured-rock terrain. Hydrogeology Journal, volume 18, issue 8, pages 1839-1854, doi: 10.1007/s10040-010-0640-y↗.

Brenner, S.L. & A. Gudmundsson, 2004, Arrest and aperture variation of hydrofractures in layered reservoirs. Geological Society, Special Publications, London, United Kingdom, volume 231, issue 1, pages 117-128, doi: 10.1144/GSL.SP.2004.231.01.08↗.

Caine, J.S., J.P. Evans, & C.B. Forster, 1996, Fault zone architecture and permeability structure. Geology, volume 24, issue 11, pages 1025-1028, doi: 10.1130/0091-7613(1996)024%3C1025:FZAAPS%3E2.3.CO;2↗.

Caine, J.S. & C.B. Forster, 1999, Fault zone architecture and fluid flow: insights from field data and numerical modeling *in* Faults and Subsurface Fluid Flow in the Shallow Crust, Geophysical Monograph Series, editors, W.C. Haneberg, Mozley, Moore, and

Goodwin, American Geophysical Union, volume 113, pages 101-128, doi: 10.1029/GM113p0101↗.

Chesnaux, R., D.M. Allen, & S. Jenni, 2009, Regional fracture network permeability using outcrop scale measurements. Engineering Geology, volume 108, issues 3-4, pages 259-271, doi: 10.1016/j.enggeo.2009.06.024↗.

Christofolletti, C., 2020, Assessment of the Potential of Crystalline Aquifers in the Metropolitan Region of São Paulo Based on Regional and Detailed Scale Methods. Doctor of Philosophy Dissertation, Geosciences Institute, University of São Paulo, São Paulo, Brazil, 241 pages, doi: 10.11606/T.44.2020.tde-03082020-103908↗.

Cooke, M.L., J.A. Simo, C.A. Underwood, & P. Rijken, 2006, Mechanical stratigraphic controls on fracture patterns within carbonates and implications for groundwater flow. Sedimentary Geology, volume 184, issues 3-4, pages 225-239, doi: 10.1016/j.sedgeo.2005.11.004↗.

Cosgrove, J., 1998, The role of structural geology in reservoir characterization *in* Structural Geology in Reservoir Characterization, editors, M.P. Coward, Daltaban, and Johnson. Geological Society, Special Publication, London, United Kingdom, volume 127, pages 1-13, https://sp.lyellcollection.org/content/127/1/1↗.

Cosgrove, J.W. & J.A. Hudson, 2016, Structural Geology and Rock Engineering. World Scientific Publishing Company, 352 pages, doi: 10.1142/p1084↗.

Davis, G.H., S.J. Reynolds, & C.F. Kluth, 2011, Structural Geology of Rocks and Regions. John Wiley and Sons, New York, USA, 864 pages.

DesRoches, A., S. Danielescu, & K. Butler, 2014, Structural controls on groundwater flow in a fractured bedrock aquifer underlying an agricultural region of northwestern New Brunswick, Canada. Hydrogeology Journal, volume 22, issue 5, pages 1067-1086, doi: 10.1007/s10040-014-1134-0↗.

Domenico, P.A. & F.W. Schwartz, 1990, Physical and Chemical Hydrogeology. John Wiley and Sons, New York, USA, 528 pages.

Douglas, A.A., J.L. Osiensky, & C.K. Keller, 2007, Carbon-14 dating of ground water in the Palouse Basin of the Columbia River basalts. Journal of Hydrology, volume 334, issues 3-4, pages 502-512, doi: 10.1016/j.jhydrol.2006.10.028↗.

Dunne, W.M & P.L. Hancock, 1994, Palaeostress analysis of small-scale brittle structures *in* Continental Deformation, editor, P.L. Hancock, Pergamon Press, United Kingdom, pages 101-120.

Engelder, T., 1987, Joints and shear fractures in rock *in* Fracture Mechanics of Rock, editor, B.K. Atkinson, Academic Press, pages 27-69, doi: 10.1016/B978-0-12-066266-1.50007-7↗.

Evans, J.P., C.B. Forster, & J.V. Goddard, 1997, Permeability of fault-related rocks, and implications for hydraulic structure of fault zones. Journal of Structural Geology, volume 19, issue 11, pages 1393-1404, doi: 10.1016/S0191-8141(97)00057-6↗.

Fernandes, A.J. & D. Rudolph, 2001, The influence of Cenozoic Tectonics on the groundwater-production capacity of fractured zones: a case study in São Paulo, Brazil. Hydrogeology Journal, volume 9, pages 151-167, doi: 10.1007/s100400000103↗.

Fernandes, A.J. & G. Amaral, 2002, Cenozoic tectonic events at the border of the Paraná Basin, São Paulo, Brazil. Journal of South American Earth Sciences, volume 14, issue 8, pages 911-931, doi: 10.1016/S0895-9811(01)00078-5↗.

Fernandes, A.J., C.H. Maldaner, J.M. Sobrinho, M.M.N. Pressinotti, & I. Wahnfried, 2010, Stratigraphy of the basalt flows of the Formação Serra Geral (Ribeirão Preto – SP) based on physical geology, petrography and geochemistry. Geologia USP, Série Científica, volume 10, number 2, pages 73-99, doi.org/10.5327/Z1519-874X2010000200006↗.

Fernandes, A.J., C.H. Maldaner, & A. Rouleau, 2011, Fracture analysis of the Ribeirão Preto basalts, SP: application for developing a conceptual hydrogeological model. Geologia USP, Série Científica, volume 11, issue 3, pages 43-64, doi: 10.5327/Z1519-874X2011000300003↗.

Fernandes, A.J., F.A. Negri, J.M. Azevedo Sobrinho, & C. Varnier, 2012, Analysis of basalt fractures of the Serra Geral aquifer and the regional recharge potential of the Guarani aquifer system. Boletín Geológico y Minero, volume 123, issue 3, pages 325-339, https://www.igme.es/Boletin/2012/123_3/13_ARTICULO%209.pdf↗.

Fernandes, A.J., C.H. Maldaner, F. Negri, A. Rouleau, & I.D. Wahnfried, 2016a, Aspects of a conceptual groundwater flow model of the Serra Geral basalt aquifer (São Paulo, Brazil) from physical and structural geology data. Hydrogeology Journal, volume 24, issue 5, pages 1199-1212, doi: 10.1007/s10040-016-1370-6↗.

Fernandes, A.J., B. Fiume, R. Bertolo, & R.C.A. Hirata, 2016b, Geometric fracture model and analysis of brittle tectonics applied to the study of crystalline aquifer flow, São Paulo (SP). Geologia USP, Série Científica, volume 16, issue 3, pages 71-88, doi: 10.5327/Z1519-874X2011000300003↗.

Fernandes, A.J., F.D.A Negri, J.M. Azevedo Sobrinho, & V.D.A. Janasi, 2018, Local geological sections and regional stratigraphy based on physical geology and chemical stratigraphy of the Serra Geral Group from Araraquara to Avaré, SP. Brazilian Journal of Geology, volume 48, issue 2, pages 243-261, doi: 10.1590/2317-4889201720180093↗.

Ferril, D.A., J. Winterle, G. Wittmeier, D. Sims, S. Colton, A. Armstrong, & A.P. Morris, 1999, Stressed rock strains groundwater at Yucca Mountain, Nevada. Geological Society of America, GSA Today, volume 9, issue 5, pages 1-8, https://www.semanticscholar.org/paper/Stressed-Rock-Strains-Groundwater-at-Yucca-Nevada-Ferrill-Winterle/6713b04e8801b1bbaf069214548b83624ebec40a↗.

Fiume, B., 2013, Detailed structural geology for the elaboration of a conceptual model of groundwater circulation: a case study in Jurubatuba, SP. Master of ScienceThesis,

Geosciences Institute, University of São Paulo, São Paulo, Brazil, 165 pages, doi: 10.11606/D.44.2014.tde-25092014-150022↗.

Fiume, B., A.J. Fernandes, M.B. Barbosa, R. Hirata, & R.A. Bertolo, 2020, Integrated application of geophysical loggings and fracture survey on rock exposures for identifying transmissive fractures in crystalline aquifer: case study in the city of São Paulo. Brazilian Journal of Geology, volume 50, issue 1, doi: 10.1590/2317-4889202020190034↗.

Fossen, H., 2016, Structural Geology. Cambridge University Press, second edition, 15 pages, https://assets.cambridge.org/97811070/57647/frontmatter/9781107057647_frontmatter.pdf↗.

Frank, H.T., M.E.B. Gomes, & M.L.L. Formoso, 2009, Review of the areal extent and the volume of the Serra Geral Formation, Paraná Basin, South America. Pesquisas em Geociências, volume 36, issue 1, pages 49-57, doi: 10.22456/1807-9806.17874↗.

Freeze, R.A. & J.A. Cherry, 1979, Groundwater. The Groundwater Project, Guelph, Canada, 604 pages, https://gw-project.org/books/groundwater/↗.

Gannett, M.W., K.E. Lite, J.L. La Marche, B.J. Fisher, & D.J. Polette, 2007, Groundwater hydrology of the upper Klamath basin, Oregon and California. United States Geological Survey, 85 pages, doi: 10.3133/sir20075050↗.

Gleeson, T. & K. Novakowski, K., 2009, Identifying watershed-scale barriers to groundwater flow: lineaments in the Canadian shield. Geological Society of America Bulletin, volume 121, issue 3-4, pages 333-347, doi: 10.1130/B26241.1↗.

Goodman, R.E., 1989, Introduction to Rock Mechanics. Wiley, second edition, 576 pages.

Gross, M.R., 1993, The origin and spacing of cross joints: examples from the Monterey Formation, Santa Barbara Coastline, California. Journal of Structural Geology, volume 15, issue 6, pages 737-751, doi: 10.1016/0191-8141(93)90059-J↗.

Gross, M.R. & Y. Eyal, 2007, Throughgoing fractures in layered carbonate rocks. Geological Society of America Bulletin, volume 119, issues 11-12, pages 1387-1404, doi: 10.1130/0016-7606(2007)119[1387:TFILCR]2.0.CO;2↗.

Gudmundsson, A., O. Gjesdal, S.L. Brenner, & I. Fjeldskaar, 2003, Effects of linking up of discontinuities on fracture growth. Hydrogeology Journal, volume 11, issue 1, pages 84-99, doi: 10.1007/s10040-002-0238-0↗.

Gudmundsson, A., 2011, Rock Fractures in Geological Processes, Cambridge University Press, 578 pages, doi: 10.1017/CBO9780511975684↗.

Gustafsson, P., 1994, Spot satellite data for exploration of fractured aquifers in a semi-arid area in southeastern Botswana. Applied Hydrogeology, volume 2, issue 2, pages 9-18, doi: 10.1007/s100400050246↗.

Heidbach, O., J. Reinecker, M. Tingay, B. Müller, B. Sperner, K. Fuchs, & F. Wenzel, 2007, Plate boundary forces are not enough: second-and third-order stress patterns

126

The GROUNDWATER PROJECT   © The Authors   Free download from gw-project.org

Anyone may use and share gw-project.org links. Direct distribution of the book is strictly prohibited.

highlighted in the World Stress Map database. Tectonics, volume 26, issue 6, doi: 10.1029/2007TC002133↗.

Hencher, S., 2011, Sheeting joints: characterization, shear strength and engineering. Rock Mechanics and Rock Engineering, volume 44, pages 1-22, doi: 10.1007/s00603-010-0100-y↗.

Hoek, E. & E.T. Brown, 1980, Empirical strength criterion for rock masses. Journal of Geotechnical and Geoenvironmental Engineering, Report ASCE 15715, volume 106, issue GT9, 23 pages, https://www.rocscience.com/assets/resources/learning/hoek/Empirical-Strength-Cruiterion-for-Rock-Masses-1980.PDF↗.

Holzhausen, G., 1989, Origin of sheet structure, 1. Morphology and boundary conditions. Engineering Geology, volume 27, issues 1-4, pages 225-278, doi: 10.1016/0013-7952(89)90035-5↗.

Hooker, J.N., S.E. Laubach, & R. Marrett, 2013, Fracture-aperture size – frequency, spatial distribution, and growth processes in strata-bounded and non-strata-bounded fractures, Cambrian Mesón Group, NW Argentina. Journal of Structural Geology, volume 54, pages 54-71, doi: 10.1016/j.jsg.2013.06.011↗.

Hooper, P.R., 1997, The Columbia River flood basalt province: current status *in* Large Igneous Provinces: Continental, Oceanic, and Planetary Flood Volcanism, editors, J.J. Mahoney and Coffin, American Geophysical Union, Washington, D.C., volume 100, 27 pages, doi: 10.1029/GM100p0001↗.

Hudson, J.A. & J.P. Harrison, 1997, Engineering Rock Mechanics, Elsevier Science, 456 pages.

Jaeger, J.C. & N.G.W. Cook, 1979, Fundamentals of Rock Mechanics, Science Paperbacks, 475 pages.

Jalludin, M. & M. Razack, 1994, Analysis of pumping tests, with regard to tectonics, hydrothermal effects and weathering, for fractured Dalha and stratiform basalts, Republic of Djibouti. Journal of Hydrology, volume 155, issues 1-2, pages 237-250, doi: 10.1016/0022-1694(94)90167-8↗.

Jerram, D.A. & M. Widdowson, 2005, The anatomy of Continental Flood Basalt Provinces: geological constraints on the processes and products of flood volcanism. Lithos, volume 79, issue 3, pages 385-405, doi: 10.1016/j.lithos.2004.09.009↗.

Johnson, G.S., D.B. Frederick, & D.M. Cosgrove, 2002a, Evaluation of a pumping test of the Snake River Plain aquifer using axial-flow numerical modeling. Hydrogeology Journal, volume 10, issue 3, pages 428-437, doi: 10.1007/s10040-002-0201-0↗.

Johnson, C.D., F.P. Haeni, J.W. Lane, & E.A. White, 2002b, Borehole-geophysical investigation of the University of Connecticut landfill, Storrs, Connecticut. US Department of the Interior, US Geological Survey, number 1, 50 pages, https://water.usgs.gov/ogw/bgas/publications/wri014033/wri014033.pdf↗.

Kulkarni H., A. Lalwani, & S.B. Deolankar, 1997, Selection of appropriate pumping systems for bore wells in the Deccan basalt of India. Hydrogeology Journal, volume 5, issue 3, pages 75-81, doi: 10.1007/s100400050258↗.

Lamontagne, E., 2001, Hydromechanical Study of a Shear Fracture under Constant Normal Stress. Doctor of Philosophy Dissertation in Mineral Resources, University of Québec at Chicoutimi, Canada, 530 pages, doi: 10.1522/12336870↗.

Larson, K.R., C.K. Keller, P.B. Larson, & R.M. Allen-King, 2000, Water resource implications of 18O and 2H distributions in a basalt aquifer system. Groundwater, volume 38, pages 947-953, doi: 10.1111/j.1745-6584.2000.tb00695.x↗.

Laubach, S.E., J.E. Olson, & M.R. Gross, 2009, Mechanical and fracture stratigraphy. American Association of Petroleum Geologists Bulletin, volume 93, issue 11, pages 1413-1426, doi: 10.1306/07270909094↗.

Lemieux, J.M., R. Therrien, & D. Kirkwood, 2006, Small scale study of groundwater flow in a fractured carbonate-rock aquifer at the St-Eustache quarry, Québec, Canada. Hydrogeology Journal, volume 14, issue 4, pages 603-612, doi: 10.1007/s10040-005-0457-2↗.

Long, J.C.S., J.S. Remer, C.R. Wilson, & P.A. Witherspoon, 1982, Porous media equivalents for networks of discontinuous fractures. Water Resources Research, volume 18, issue 3, pages 645-658, doi: 10.1029/WR018i003p00645↗.

Mabee, S.B., K.C. Hardcastle, & D.U. Wise, 1994, A method of collecting and analyzing lineaments for regional-scale fractured-bedrock aquifer studies. Groundwater, volume 32, issue 6, pages 884-895, doi: 10.1111/j.1745-6584.1994.tb00928.x↗.

Manda, A.K., S.B. Mabee, & D.U. Wise, 2008, Influence of rock fabric on fracture attribute distribution and implications for groundwater flow in the Nashoba Terrane, eastern Massachusetts. Journal of Structural Geology, volume 30, issue 4, pages 464-477, doi: 10.1016/j.jsg.2007.12.006↗.

Martel, S.J., 2017, Progress in understanding sheeting joints over the past two centuries. Journal of Structural Geology, volume 94, issue 68-86, doi: 10.1016/j.jsg.2016.11.003↗.

McGrail, B.P., H.T. Schaef, A.M. Ho, Y.J. Chien, J.J. Dooley, & C.L. Davidson, 2006, Potential for carbon dioxide sequestration in flood basalts. Journal of Geophysical Research, volume 111, doi: 10.1029/2005JB004169↗.

Michalski, A. & R. Britton, 1997, The role of bedding fractures in the hydrogeology of sedimentary bedrock – evidence from the Newark Basin, New Jersey. Groundwater, volume 35, issue 2, pages 318-327, doi: 10.1111/j.1745-6584.1997.tb00089.x↗.

Mindat, 2022, Definition of isostatic compensation, https://www.mindat.org/glossary/isostatic_compensation↗.

Morin, R.H., G.B. Carleton, & S. Poirier, 1997, Fractured-aquifer hydrogeology from geophysical logs, the Passaic Formation, New Jersey. Groundwater, volume 35, issue 2, pages 328-338, doi: 10.1111/j.1745-6584.1997.tb00090.x↗.

Morin, R.H. & W.Z. Savage, 2003, Effects of crustal stresses on fluid transport in fractured rock: case studies from northeastern and southwestern USA. Hydrogeology Journal, volume 11, issue 1, pages 100-112, doi: 10.1007/s10040-002-0235-3↗.

Morin, R., W. Savage, & C. Rivard, 2006, Hydrologic consequences of gravity-induced stresses along a ridge: example from Annapolis Valley, Nova Scotia *in* Golden Rocks 2006, The 41st United States Symposium on Rock Mechanics (USRMS), American Rock Mechanics Association, https://onepetro.org/ARMAUSRMS/proceedings-abstract/ARMA06/All-ARMA06/ARMA-06-1054/115954↗.

Morin, R., R. Godin, M. Nastev, & A. Rouleau, 2007, Hydrogeologic controls imposed by mechanical stratigraphy in layered rocks of the Châteauguay River Basin, a U.S.-Canada transborder aquifer. Journal of Geophysical Research: Solid Earth, volume 112, issue B4, doi: 10.1029/2006JB004485↗.

Odling, N.E., P. Gillespie, B. Bourgine, C. Castaing, J.P. Chiles, N.P. Christensen, & R. Trice, 1999, Variations in fracture system geometry and their implications for fluid flow in fractures hydrocarbon reservoirs. Petroleum Geoscience, volume 5, issue 4, pages 373-384, doi: 10.1144/petgeo.5.4.373↗.

Paillet, F.L., A.E. Hess, C.H. Cheng, & E. Hardin, 1987, Characterization of fracture permeability with high-resolution vertical flow measurements during borehole pumping. Groundwater, volume 25, issue 1, pages 28-40, doi: 10.1111/j.1745-6584.1987.tb02113.x↗.

Paillet, F.L., 1991, Use of geophysical well logs in evaluating crystalline rocks for siting of radioactive waste repositories. The Log Analyst, volume 32, issue 2, pages 85-107.

Pakhmode, V., H. Kulkarni, & S.B. Deolankar, 2003, Hydrological-drainage analysis in watershed-programme planning: a case from the Deccan basalt, India. Hydrogeology Journal, volume 11, issue 5, pages 595-604, doi: 10.1007/s10040-003-0279-z↗.

Parker, B.L., K. Bairos, C.H. Maldaner, S.W. Chapman, C.M. Turner, L.S. Burns, & J.A. Cherry, 2018, Metolachlor dense non-aqueous phase liquid source conditions and plume attenuation in a dolostone water supply aquifer. Geological Society, Special Publications, London, United Kingdom, volume 479, issue 1, pages 207-236, doi: 10.1144/SP479.9↗.

Peacock, D.C.P. & D.J. Sanderson, 2018, Structural analyses and fracture network characterization: seven pillars of wisdom. Earth-Science Reviews, volume 184, pages 13-28, doi: 10.1016/j.earscirev.2018.06.006↗.

Petit, J.P., 1987, Criteria for the sense of movement on fault surfaces in brittle rocks. Journal of Structural Geology, volume 9, issue 5, pages 597-608, doi: 10.1016/0191-8141(87)90145-3↗.

Pino, D.S., A. Rouleau, D.W. Roy, & R. Daigneault, 2011, Analysis of the joint system in the Kenogami uplands bedrock aquifer: methodology and preliminary results.

129

The GROUNDWATER PROJECT   © The Authors   Free download from gw-project.org

Anyone may use and share gw-project.org links. Direct distribution of the book is strictly prohibited.

GeoHydro 2011, Joint Meeting of Canadian Quaternary Association (CANQUA) and Canadian Chapter of the International Association of Hydrogeologists (IAH-CNC), Québec City, August 28–31, 2011, 7 pages.

Pollard, D. & S. Martel, 2020, Structural Geology: A Quantitative Introduction, Cambridge University Press, 450 pages.

Price, N.J. & J.W. Cosgrove, 1990, Analysis of Geological Structures, Cambridge University Press, 502 pages.

Ramsay, J.G. & M.I. Huber, 1987, The Techniques of Modern Structural Geology – Volume 2: Folds and Fractures, Academic Press, 391 pages.

Riccomini, C. & A. Coimbra, 1992, Geology of the sedimentary basin *in* Soils of the City of São Paulo, editors, A. Negro Jr., Ferreira, Alonso, & Luz, ABMS/ABEF, São Paulo, Brazil, pages 37-94.

Riccomini, C. & M. Assumpção, 1999, Quaternary tectonics in Brazil. Episodes, volume 22, issue 3, pages 221-225, doi: 10.18814/epiiugs/1999/v22i3/010.

Rives, T., K.D. Rawnsley, & J.P. Petit, 1994, Analogue simulation of natural orthogonal joint set formation in brittle varnish. Journal of Structural Geology, volume 16, issue 3, pages 419-429, doi: 10.1016/0191-8141(94)90045-0.

Rouleau, A. & J.E. Gale, 1985, Statistical characterization of the fracture system in the Stripa granite, Sweden. International Journal of Rock Mechanics and Mining Sciences and Geomechanics Abstracts, volume 22, issue 6, pages 353-367, doi: 10.1016/0148-9062(85)90001-4.

Rouleau, A., C. Denis, P. Cousineau, & P. Lapcevic, 1996, The estimation of hydraulic parameters of a fractured orthoquartzite formation at the laboratory and field scales *in* Rock Mechanics Tools and Techniques, editors, M. Aubertin, Hassani and Mitri, Proceedings of Second North American Rock Mechanics Symposium, Montreal, Québec, Canada, June 1996, pages 1359-1366, https://onepetro.org/ARMANARMS/proceedings-abstract/NARMS96/All-NARMS96/ARMA-96-1359/130827.

Sami, K., 1996, Evaluation of the variations in borehole yield from a fractured Karoo Aquifer, South Africa. Groundwater, volume 34, issue 1, pages 114-120, doi: 10.1111/j.1745-6584.1996.tb01871.x.

Sanderson, D.J. & C.W. Nixon, 2015, Topology, connectivity and percolation in fracture networks. Journal of Structural Geology, volume 115, pages 167-177, doi: 10.1016/j.jsg.2018.07.011.

Self, S., A.E. Jay, M. Widdowson, & L.P. Keszthelyi, 2008, Correlation of Deccan and Rajahmundry trap lavas: Are these the longest and largest lava flows on Earth? Journal of Volcanology and Geothermal Research, volume 172, issues 1-2, pages 3-19, doi: org/10.1016/j.jvolgeores.2006.11.012.

Self, S., L. Keszthelyi, & T. Thordarson, 1998, The importance of pahoehoe. Annual Review of Earth and Planetary Sciences, volume 26, pages 81-110, doi: org/10.1146/annurev.earth.26.1.81↗.

Senger, K., S.J. Buckley, L. Chevallier, Å. Fagereng, O. Galland, T.H. Kurz, & J. Tveranger, 2015, Fracturing of doleritic intrusions and associated contact zones: implications for fluid flow in volcanic basins. Journal of African Earth Sciences, volume 102, pages 70-85, doi: 10.1016/j.jafrearsci.2014.10.019↗.

Shapiro, A.M., P.A. Hsieh, W.C. Burton, & G.J. Walsh, 2007, Integrated multi-scale characterization of ground-water flow and chemical transport in fractured crystalline rock at the Mirror Lake Site, New Hampshire *in* Subsurface Hydrology: Data Integration for Properties and Processes, editors, D.W. Hyndman, Day-Lewis, and Singha, American Geophysical Union, 25 pages, doi: 10.1029/171GM15↗.

Sibson, R.H., 1977, Fault rocks and fault mechanisms. Journal of the Geological Society, volume 133, issue 3, pages 191-213, doi: 10.1144/gsjgs.133.3.0191↗.

Singhal, B.B.S. & R.P. Gupta, 2010, Applied Hydrogeology of Fractured Rocks. Springer Science and Business Media.

Snow, D.T., 1968, Rock fracture spacings, openings, and porosities. Journal of Soil Mechanics and Foundations Division, volume 94, issue 1, doi: 10.1061/JSFEAQ.0001097↗.

Surrette, M., D.M. Allen, & M. Journeay, 2008, Regional evaluation of hydraulic properties in variably fractured rock using a hydrostructural domain approach. Hydrogeology Journal, volume 16, issue 1, pages 11-30, doi: 10.1007/s10040-007-0206-9↗.

Talbot, C.J. & M. Sirat, 2001, Stress control of hydraulic conductivity in fracture-saturated Swedish bedrock. Engineering Geology, volume 61, issue 2, pages 145-153, doi: 10.1016/S0013-7952(01)00047-3↗.

Tolan, T.L., S.P. Reidel, M.H. Beeson, J.L. Anderson, K.R. Fetch, & D.A. Swanson, 1989, Revisions to the estimates of the areal extent and volume of the Columbia River basalt group. Geological Society of America, Special Papers, volume 239, pages 1-20, doi: 10.1130/SPE239-p1↗.

Tressoldi, M. & S. Kitahara, 1991, Three-dimensional hydrogeotechnical tests and scale effects on fractured basalts. Seventh ISRM Congress, September 16–20, Aachen, Germany, https://onepetro.org/isrmcongress/proceedings-abstract/CONGRESS91/All-CONGRESS91/ISRM-7CONGRESS-1991-126/167635↗.

Underwood, C.A., M.L. Cooke, J.A. Simo, & M.A. Muldoon, 2003, Stratigraphic controls on vertical fracture patterns in Silurian dolomite, northeastern Wisconsin. American Association of Petroleum Geologists Bulletin, volume 87, issue 1, pages 121-142, doi: org/10.1306/072902870121↗.

Van Golf Racht, T.D., 1982, Fundamentals of Fractured Reservoir Engineering. Elsevier, New York, USA.

Versey, H.R. & B.K. Singh, 1982, Groundwater in Deccan basalts of the Betwa Basin, India. Journal of Hydrology, volume 58, issues 3-4, pages 279-306, doi: 10.1016/0022-1694(82)90040-3↗.

Wahnfried, I.D., 2010, Conceptual Model of Flow of Serra Geral Aquitard and Guarani Aquifer System in Ribeirão Preto Region, São Paulo. Unpublished Doctor of Philosophy Dissertation, University of São Paulo, Brazil, 135 pages, doi: 10.11606/T.44.2010.tde-07072010-163245↗.

Wanner, P., B.L. Parker, & D. Hunkeler, 2018, Assessing the effect of chlorinated hydrocarbon degradation in aquitards on plume persistence due to back-diffusion. Science of The Total Environment, volume 633, pages 1602-1612, doi: 10.1016/j.scitotenv.2018.03.192↗.

Wise, D.U., 2005, Rift and grain in basement: thermally triggered snapshots of stress fields during erosional unroofing of the Rocky Mountains of Montana and Wyoming. Rocky Mountain Geology, volume 40, issue 2, pages 193-209, doi: 10.2113/40.2.193↗.

Woodcock, N.H. & C. Schubert, 1994, Continental strike-slip tectonics *in* Continental Deformation, editor P.L. Hancock, Pergamon Press, pages 251-263.

Zang, A. & O. Stephansson, 2009, Stress field of the Earth's crust. Springer Science and Business Media.

Zektser, I.S. & L.G. Everett, 2004, Groundwater Resources of the World and Their Use, IHP-VI, Series on Groundwater, number 6, UNESCO (United Nations Educational, Scientific and Cultural Organization), https://unesdoc.unesco.org/ark:/48223/pf0000134433↗.

Zoback, M.L., M.D. Zoback, J. Adams, M. Assumpção, S. Bell, E.A. Bergman, P. Blümling, N.R. Brereton, D. Denham, J. Ding, K. Fuchs, N. Gay, S. Gregersen, H.K. Gupta, A. Gvishiani, K. Jacob, R. Klein, P. Knoll, M. Magee, J.L. Mercier, B.C. Müller, C. Paquin, K. Rajendran, O. Stephansson, G. Suarez, M. Suter, A. Udias, Z.H. Xu, & M. Zhizhin, 1989, Global patterns of tectonic stress. Nature, volume 341, issue 6240, pages 291-298, doi: 10.1038/341291a0↗.

10　Boxes

Box 1 Effects of Shear Displacement on the Transmissivity of a Rock Fracture

Authors: Alain Rouleau, Éric Lamontagne, Amélia João Fernandes

Shear displacement between the two faces of a rock fracture can have important impact on the flow properties of the fracture, particularly its transmissivity. This box summarizes the procedure and selected results of laboratory experiments, conducted by Lamontagne (2001), on the effects of shear on flow properties of a fracture under constant normal stress conditions. These experiments used many replicas of the same natural rock fracture.

A number of laboratory experiments have been reported in the literature over the last few decades on the effects of shear displacement on hydraulic properties of rock fractures subjected to various shear and normal stress loading conditions. The *Complementary Bibliography on Shear-Flow Coupling Experiments (1990-2019)* at the end of this note presents sources of information on the various laboratory equipment and methods that have been used in the experiments, the different types of specimens that have been tested, as well as the results obtained and the interpretation made by the researchers.

Box 1.1 Fabricating Replicas of a Natural Fracture

The original sample was a natural extension fracture in a granitic rock from France. The rock core containing the fracture had been collected with a 120 mm core barrel in a hole drilled perpendicular to the average fracture plane (Gentier, 1987; Flamand, 2000). A silicone negative mold was fabricated of both faces of the rock fracture. Fracture face replicas were fabricated by pouring mortar into the negative mold and letting it cure for at least 30 days. Each fracture replica was obtained by superposing the concrete-fabricated replica of both fracture faces, taking proper care to reproduce the exact relative orientation of the faces. The mechanical and hydraulic properties (hydraulic conductivity, K, of 5.1×10^{-13} m/s) of the replica material were considered adequate to simulate the original granitic rock. The mechanical properties of many fracture replicas have been characterized by careful testing systematically conducted under a wide variety of normal and shear stress conditions (Flamand et al., 1994; Flamand, 2000); the fabricated fractures have shown mechanical characteristics similar to those of a natural fracture in granite.

The morphology of the fracture was almost identical from one replica to the other. The upper and bottom surfaces of the same fracture replica shown in Figure Box1-1 illustrate how the two faces formed a well-imbricated fracture surface. An orientation

marker was placed at the same location on both faces of every replica (Figure Box1-1) to determine the sense of shear to be applied in the testing machine.
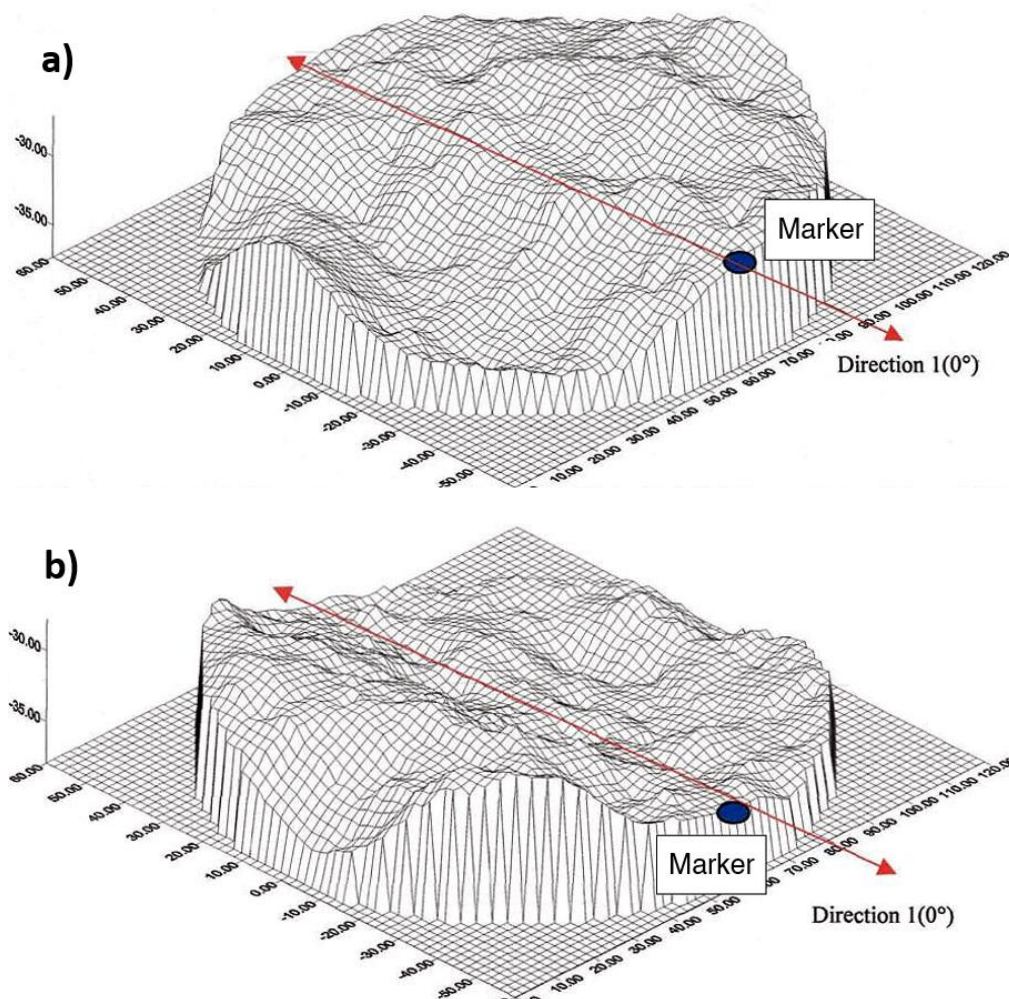
Figure Box1-1 - Replicated fracture. a) Reconstructed upper wall and b) bottom wall of a fracture replica before testing, showing the position the orientation marker; vertical exaggeration 10x (Lamontagne, 2001).

Box 1.2 Test Equipment and Procedure

For the replicas to be subjected to hydromechanical tests, a 6 mm diameter hole was drilled in the center of the bottom wall to be used for water injection during testing. Each fracture replica was constructed by superposing the concrete-fabricated walls of both fracture faces, each one in its own stainless-steel case placed one on top of the other (Figure Box1-2), thereby ensuring the exact relative orientation of the original fracture faces. The space separating the two cases permitted the installation of a water collecting system over the entire periphery of the tested fracture, the outflow being controlled by a thick sealing latex coat and a total of 16 drain tubes. The flexibility of the water collection system allowed a shear displacement of up to 5 mm along the fracture plane without significant

134

The GROUNDWATER PROJECT   © The Authors   Free download from gw-project.org

Anyone may use and share gw-project.org links. Direct distribution of the book is strictly prohibited.

water leakage outside of the controlled drainage system. The outflow was collected in eight receptacles distributed around the tested fracture, each one fed by two of the draining tubes (Figure Box1-3) and resting on an individual weighing apparatus. This design allowed a continuous measurement of flow rate in each one of eight pie-shaped sectors constituting the entire fracture surface.
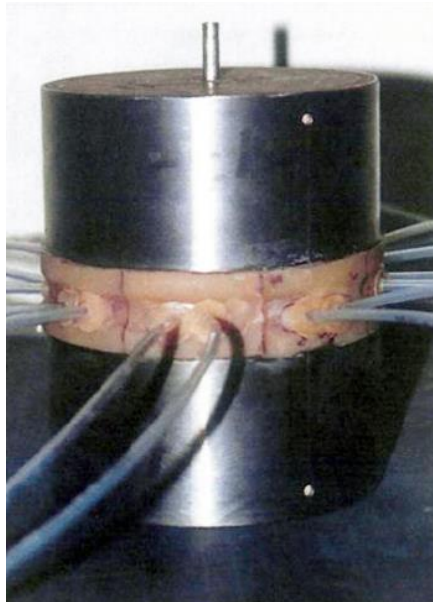
Figure Box1-2 - A fracture replica in its two steel casings, ready for installation in the shear test machine (Lamontagne, 2001).
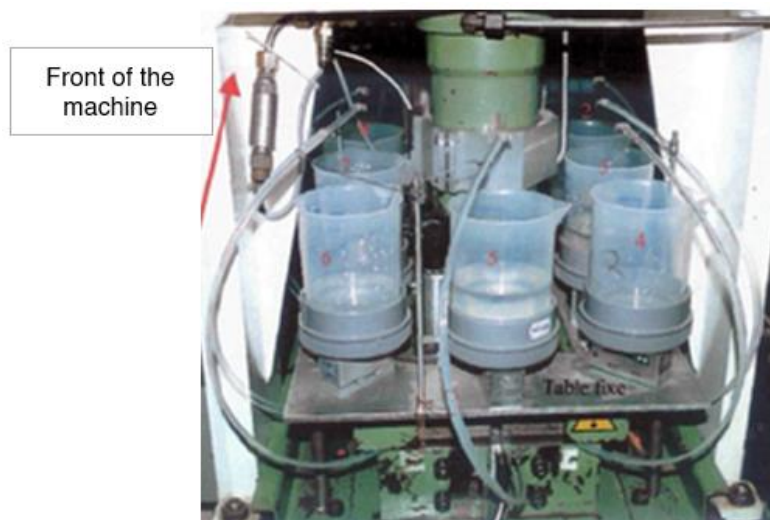
Figure Box1-3 - The system of eight collection receptacles around the testing cell (Lamontagne, 2001).

The fracture replica and its two rock walls, the hanging wall, and the footwall, each one in a steel casing, were placed in the shear testing machine (Figure Box1-4). This is

135

The GROUNDWATER PROJECT   © The Authors   Free download from gw-project.org

Anyone may use and share gw-project.org links. Direct distribution of the book is strictly prohibited.

shown on the extreme right of the photograph of the laboratory setup for hydromechanical testing (Figure Box1-5).

1. Horizontal actuator
2. Vertical actuator
3. Mobile rudder
4. Horizontal L.V.D.T. (0-20 mm)
5. Vertical L.V.D.T.
6. Horizontal L.V.D.T. (0-60 mm)
7. Upper-half shear case
8. Lower-half shear case
9. Fracture hanging wall
10. Fracture footwall
11. Roller bearin
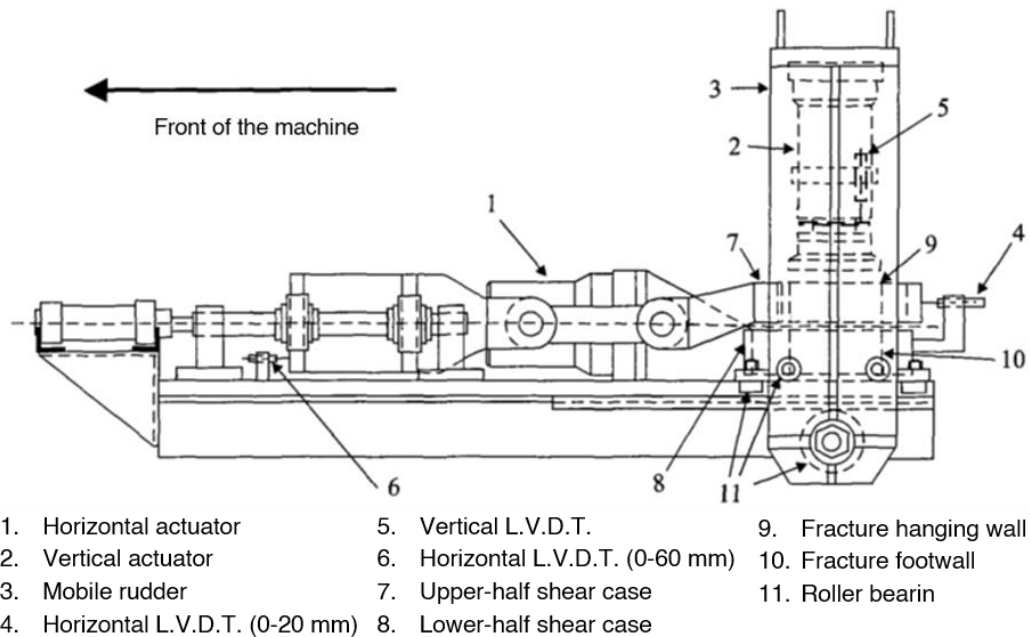
Figure Box1-4 - Shear machine.

Figure Box1-5 - Laboratory setup for hydromechanical shear testing (Lamontagne, 2001).

Each fracture replica was subjected to a single test with a constant value of normal stress and to shear displacement in one of four directions (0º, 90º, 180º and 270º). The value of normal stress and the shear direction varied from one fracture replica to the other. Water was injected at a constant flow rate through the central hole, producing diverging flow in

136

the fracture plane. The normal stress values that were applied were 3, 5, 7 and 9 MPa. During each test, the same value of shear strain rate, 0.5 mm/min, was applied. At a number (between 4 and 13) of predetermined values of shear displacement (between 0.1 to 5.0 mm), shearing was stopped. Water was then injected at constant flow rates, between 2 and 6 different values, through the central hole in the fracture plane. The quantity of water collected in the eight receptacles, combined with the measured water pressure, was used to estimate the fracture transmissivity T and to assess the potential anisotropy of flow in the fracture plane.

Box 1.3 Selected Results

Figure Box1-6 presents the variation of the intrinsic transmissivity t_f (cm^3) as a function of the shear displacement based on the results of 16 tests using as many fracture replicas as possible and grouped by the value of applied normal stress (σ_n), which ranged from 3 to 9 MPa.
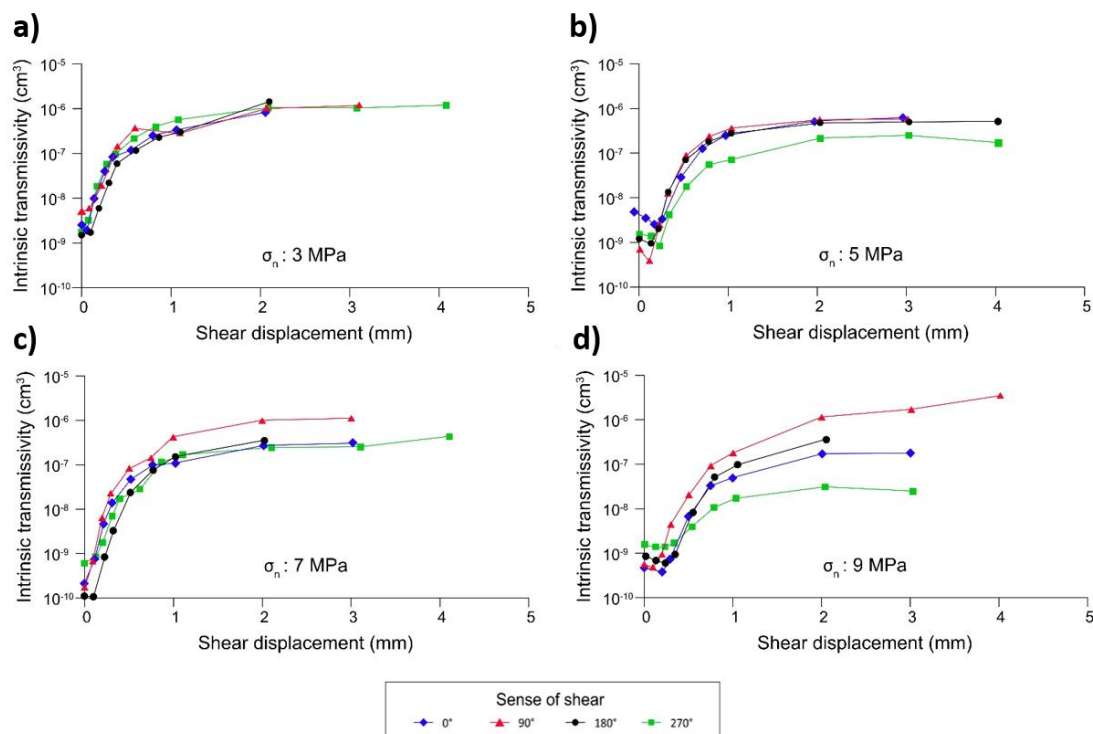
Figure Box1-6 - Intrinsic transmissivity variation with shear displacement grouped by normal stress value: a) 3 MPa, b) 5 MPa, c) 7 MPa and d) 9 MPa (Lamontagne, 2001). Some of the graphs, particularly (b) and (d), indicate a small decrease in transmissivity (t_f) for short displacements, up to about 0.5 mm, but all of the graphs show a considerable increase thereafter. Shear failure corresponding to the peak shear strength (not shown here) occurred at displacement values varying between 0.3 and 0.7 mm from one test to the other. A significant increase in t_f occurred before failure. Overall, the value of t_f increased by at least one, and up to more than three, orders of magnitude for all values of normal stress considered in these experiments.

The parameter t_f is derived from the Navier–Stokes equation describing the flow of a viscous fluid in an open conduit. In this case, the assumed conduit is an open fracture formed by two smooth parallel walls. Let us make a comparison with Darcy's law in a porous medium, as shown in Equation Box1-1.

$$v = -K\Delta h \qquad [\text{LT}^{-1}] \tag{Box1-1}$$

where:

v = Darcy flux

K = hydraulic conductivity of the medium [LT⁻¹]

Δh = hydraulic head gradient (dimensionless)

Similarly, the hydraulic conductivity of a fracture with smooth, parallel walls is expressed as shown in Equation Box1-2.

$$K_f = \frac{\rho g\, e^2}{12\mu} \tag{Box1-2}$$

where:

K_f = fracture hydraulic conductivity [LT⁻¹]

e = fracture aperture [L]

ρ = fluid density [ML⁻³]

μ = fluid viscosity [ML⁻¹T⁻¹]

g = gravitational acceleration [LT⁻²]

The transmissivity of a porous aquifer of thickness B is defined as $T = KB$ [L²/T]. Similarly, for a fracture with an aperture of e, the thickness $B=e$, so its transmissivity is shown in Equation Box1-3 (Gentier, 1987).

$$T_f = K_f\, e = \frac{\rho g\, e^2}{12\,\mu}\, e = \frac{\rho g\, e^3}{12\,\mu} \qquad [\text{L}^2/\text{T}] \tag{Box1-3}$$

Intrinsic parameters are also defined for a fracture as they are for a porous medium. The intrinsic parameters are independent of the fluid properties, such as its density and viscosity, and they are valid for any flowing fluid either a gas or a liquid. We know that the intrinsic permeability of a porous medium (k) is defined by $k = K(\mu/\rho g)$. Then, from Equation Box1-2 we can write Equation Box1-4.

$$k_f = K_f\, \frac{\mu}{\rho g} = \frac{e^2}{12} \qquad [\text{L}^2] \tag{Box1-4}$$

The intrinsic transmissivity of a fracture is then defined by Equation Box1-5.

$$t_f = k_f\, e = \frac{e^2}{12}\, e = \frac{e^3}{12} \quad [\text{L}^3] \tag{Box1-5}$$

Another result of these tests concerns the preferential flow direction and its variation during shear (Gentier et al., 1997). Figure Box1-7 indicates that flow tends to be

138

higher in the direction perpendicular to shear and that this flow anisotropy generally becomes more pronounced with increasing flow rate.
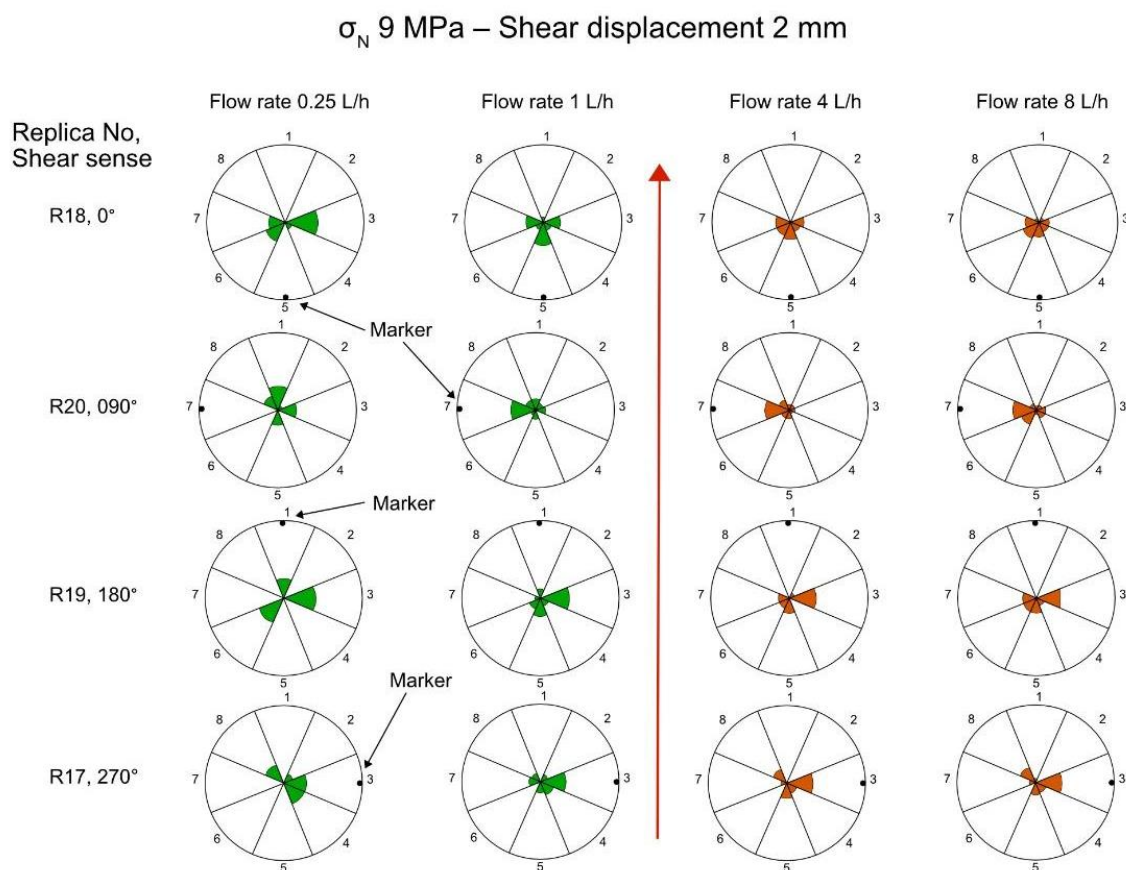
Figure Box1-7 - Volume percentage of water collected from each of the eight sectors of the fracture plane for the four tests conducted at $\sigma_n = 9$ MPa on four different fracture replicas, R17 to R20. At a shear displacement of 2 mm, four water injection tests were conducted at 0.25, 1.0, 4.0 and 8.0 L/h. The red arrow indicates the sense of displacement of the upper fracture face, the lower face being immobile. The scale varies from 0 to 100% on each radius. The location of the orientation marker shows the fracture plane orientation in the shear testing machine, which varied by 90° from one test to the other. The results show that flow tends to be higher in the direction perpendicular to shear and that this anisotropy generally becomes more pronounced with increasing flow rate (Lamontagne, 2001).

Box 1.4 Applications to Field Conditions

The experiments described thus far in this section are called shear-flow coupling tests. Interpretations of the results of these tests are summarized in this section. Further information about shear-flow coupling experiments conducted by other researchers is summarized in the references cited in Section Box 1.7 *Complementary Bibliography on Shear-Flow Coupling Experiments (1990-2019)*.

Any fracture in rock bears asperities that are more or less matching between its two faces. When a fracture is subjected to shear stress, shear displacement takes place not only along the general fracture plane, but also along asperity surfaces that are oriented at some

139

angle (angle *i* in Figure Box1-8a) with respect to the general fracture plane. Sliding along the slope of asperities induces a displacement component that is normal to the fracture plane, commonly called "shear dilation" (Figure Box1-8b). The resulting fracture opening significantly increases the fluid flow properties of the fracture.

Figure Box1-8 - Effects of shear displacement on fracture aperture. a) The asperities on fracture faces are relatively well matched before shear displacement, with little void space for water flow. b) Shear stress (τ) is applied under low normal stress (σ_n) conditions; the resulting shear displacement includes a component normal to the fracture plane (shear dilation) due to local shear along asperity slopes oriented at an angle *i* with respect to the fracture 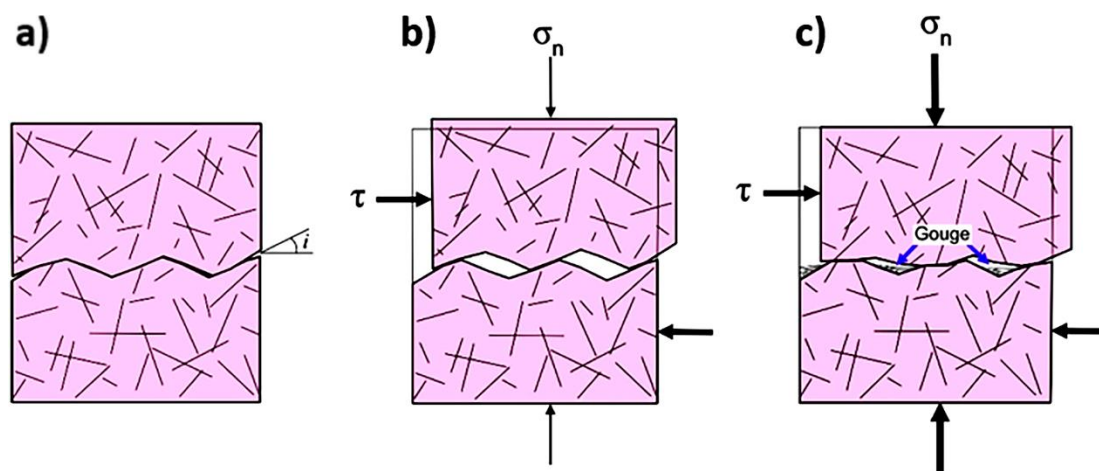plane. c) At higher normal stress the shear dilation is constrained and the asperities tend to be crushed by the displacement parallel to the fracture plane, generating fine-grained material (gouge) that partly fills the void space (after T. Doe, personal communication, 2020).

Many experiments have demonstrated that this shear dilation decreases with increasing normal stress applied to a fracture during the shear test. This decrease in dilation is considered to be the result of a higher proportion of asperities being crushed during the test at higher normal stress (Figure Box1-8c). Moreover, asperity crushing generates fine grained material (gouge) that fills parts of the voids and may hamper fluid flow along the fracture plane. The process of shear dilation increases fracture transmissivity; conversely, the processes of asperity crushing and infilling of voids by gouge material tend to decrease transmissivity. All of these processes are likely to take place in all fractures subjected to shear, and their relative importance varies depending on a number of factors, including the normal stress, rock type and amount of shear displacement. A detailed field study describing the generated features at a specific site will help to determine the effects of shear on transmissivity of that site.

The depth range relevant to many fractured aquifer applications extends to around 350 m, and most of the laboratory experiments indicate that shear dilation is the predominant process taking place at those depths. In the depth range between 100 to approximately 350 m, the vertical stress values vary from 3 MPa up to 9 MPa, estimated using the relationship $\sigma_v = \rho g z$, where ρ is the average rock density, g is the gravitational acceleration and *z* is depth. Considering a horizontal fracture, the normal stress is equal to

140

The GROUNDWATER PROJECT   © The Authors   Free download from gw-project.org

Anyone may use and share gw-project.org links. Direct distribution of the book is strictly prohibited.

the vertical stress. At normal stresses of 3 MPa to 9 MPa, the laboratory tests in general show an increase in the fracture transmissivity due to shear displacement (Figure Box1-6).

These results are applicable to the flow properties of fractured rock at a wide variety of scales. Field observations at a regional scale have been reported where higher transmissivity values are obtained for fractures that are critically oriented for shear displacement due to in-situ stress conditions (Barton et al., 1995; Ferril et al., 1999). Sedimentary rock units often experience some shear, particularly for fractures along bedding planes, even under minimal gentle folding. These conditions are commonly observed in sedimentary rock basins; an example is described by Morin and others (2007) in the St. Lawrence Lowlands in southern Québec, Canada.

At a local scale, shear along fracture planes is likely induced in existing fracture systems around underground excavations such as tunnels and mining stopes. Indeed, the presence of an excavation results in variations in the in-situ stress tensor, both in magnitude and in orientation, in the host rock mass. These variations are significant up to a radial distance of about twice the diameter of the excavation. Figure Box1-9a shows the orientation of the major (σ_1) and the minor (σ_3) principal stresses, as well as the increase in magnitude of σ_1 ($\sigma_1' - \sigma_1$) due to the presence of the excavation. These stress tensor variations are translated into changes in normal stress (σ_n) and shear stress (τ) conditions along every fracture plane that is present in the disturbed zone (Figure Box1-9b). The variation in shear stress along a fracture plane is likely inducing displacement along that plane, which, in turn, could result in a significant increase in the transmissivity of the fracture, at least locally. Considering this effect could be useful in gaining a more accurate estimation of groundwater flow into an underground excavation.
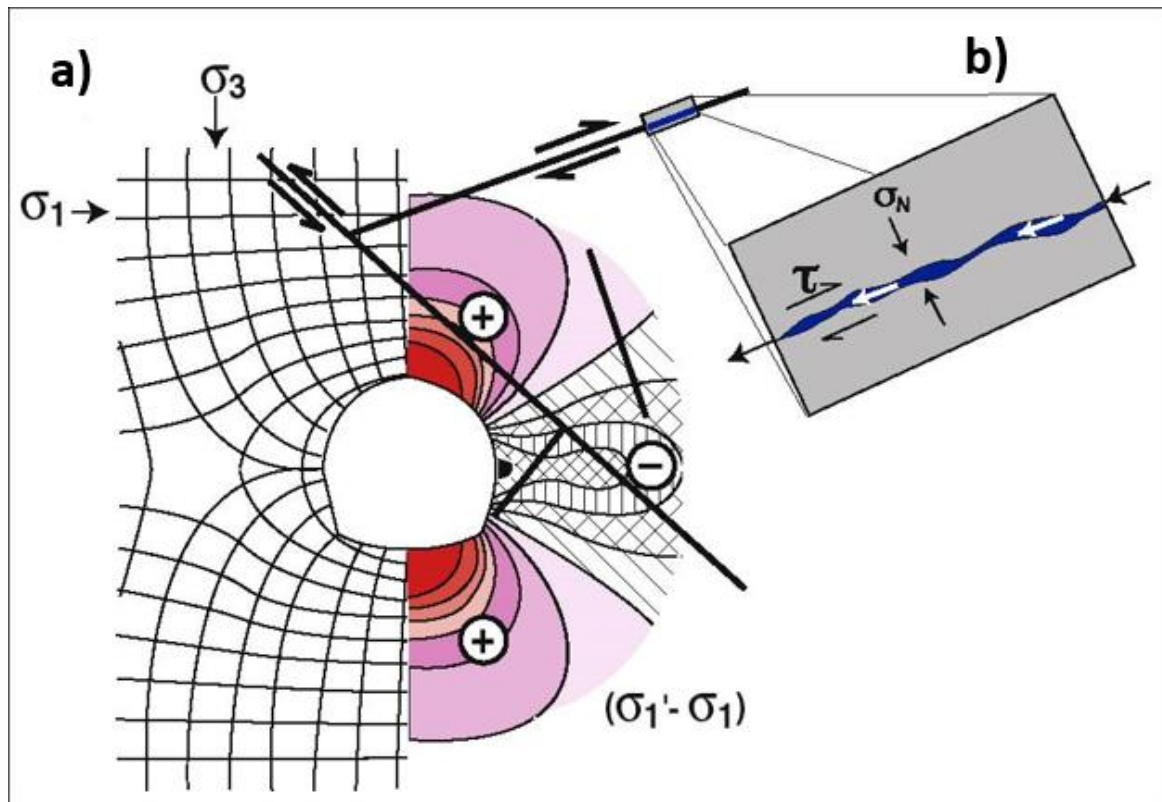
141

The GROUNDWATER PROJECT   © The Authors   Free download from gw-project.org

Anyone may use and share gw-project.org links. Direct distribution of the book is strictly prohibited.

Figure Box1-9 - a) Schematic illustration of stress around an excavation in a homogeneous elastic medium; σ_1 and σ_3 are initial conditions of the major (horizontal) and minor principal stresses; $\sigma_1/\sigma_3=2$; $\sigma_{1'}$ is the major principal stress in the presence of the excavation. The stress field is symmetric so the right side of the image is used to illustrate $\sigma_{1'}-\sigma_1$ which is the change in stress caused by the excavation. There is an important increase in the major principal stress at the ceiling and at the floor of the excavation, and a substantial decrease at the wall (modified after Hoek & Brown, 1980b, page 492). b) Normal stress (σ_n) and shear stress (τ) on a fracture plane.

Let us now consider the scale of a borehole in hard rock. A borehole is a small diameter vertical tunnel that introduces a stress disturbance which changes stress components in existing fracture planes extending to a radial distance corresponding to a few times the hole diameter. The resulting shear displacement along fracture planes around the borehole could affect the transmissivity of the fractures. This effect may impact the capacity of a borehole to yield water from a fractured aquifer.

Box 1.5 Wrap-up

Shear is an essential component in the formation and propagation of both shear and hybrid fractures. The results of laboratory experiments presented in this section show that shear along an existing fracture plane may considerably increase the transmissivity of a fracture. These conclusions underscore the importance of conducting careful structural geologic surveys in the hydrogeological characterization of fractured aquifers. Evidence of shear displacement in the reactivation of a fracture plane, mainly under the current stress field, may constitute a sound indication that a fracture has hydrogeological importance.

Indeed, the possible or even likely tendency for the shear to increase transmissivity may have also caused a flow anisotropy within the fracture plane. Furthermore, knowledge about the present in-situ stress magnitude and orientation, combined with data regarding the fracture system, can permit identification of fractures that are critically oriented for a possible reactivation by shear under the present conditions. That reactivation by shear may also produce further fracture propagation thus greater spatial extent of fractures, possibly resulting in a more connected fracture network.

Box 1.6 References

Barton, C.A., M.D. Zoback, & D. Moos, 1995, Fluid flow along potentially active faults in crystalline rock. Geology, volume 23, issue 8, pages 683-686, doi: org/10.1130/0091-7613(1995)023%3C0683:FFAPAF%3E2.3.CO;2 .

Ferrill, D.A., J. Winterle, G. Wittmeyer, D. Sims, S. Colton, A. Armstrong, & A.P. Morris, 1999, Stressed rock strains groundwater at Yucca Mountain, Nevada. GSA Today, Geological Society of America, volume 9, issue 5, pages 1-8, https://www.geosociety.org/gsatoday/archive/9/5/ .

Flamand, R., 2000, Validation of a mechanical behavior model for rock shear fractures. Doctor of Philosophy Dissertation, University of Québec at Chicoutimi, Canada, 379 pages, https://constellation.uqac.ca/966/ (in French).

Flamand, R., G. Archambault, S. Gentier, J. Riss, & A. Rouleau, 1994, An experimental study of the shear behavior of irregular joints based on angularities and progressive degradation of the surfaces. 47th Canadian Geotechnical Conference, Halifax, Nova Scotia, Canada, pages 253-263.

Gentier, S., 1987, Morphology and hydromechanical behavior of a fracture in a granite under normal stress: experimental and theoretical study. Bureau of Geological and Mining Research, Orléans, France, number 134, 597 pages, http://www.sudoc.fr/04355797X (in French).

Gentier, S., E. Lamontagne, G. Archambault, & J. Riss, 1997, Anisotropy of flow in a fracture undergoing shear and its relationship to the direction of shearing and injection pressure. International Journal of Rock Mechanics and Mining Sciences, volume 34, issues 3-4, 12 pages, doi: org/10.1016/S1365-1609(97)00085-3 .

Hoek, E. & E.T. Brown, 1980b, Underground Excavations in Rock. The Institution of Mining and Metallurgy, London, United Kingdom, 527 pages.

Lamontagne, E., 2001, Hydromechanical study of a shear fracture under constant normal stress. Doctor of Philosophy Dissertation, University of Québec at Chicoutimi, Canada, 484 pages, https://constellation.uqac.ca/903/ (in French).

Morin, R., R. Godin, M. Nastev, & A. Rouleau, 2007, Hydrogeologic controls imposed by mechanical stratigraphy in layered rocks of the Chateauguay River Basin, a U.S.-

Canada transborder aquifer. Journal of Geophysical Research, volume 112, issue B4, doi: org/10.1029/2006JB004485↗.

Box 1.7 Complementary Bibliography on Shear-Flow Coupling Experiments (1990-2019)

Auradou, H., G. Drazer, J.P. Hulin, & J. Koplik, 2005, Permeability anisotropy induced by the shear displacement of rough fracture walls. Water Resources Research, volume 41, issue 9, doi: org/10.1029/2005WR003938↗.

Esaki, T., S. Du, Y. Mitani, K. Ikusada, & L. Jing, 1999, Development of a shear-flow test apparatus and determination of coupled properties for a single rock joint. International Journal of Rock Mechanics and Mining Sciences and Geomechanics Abstracts, volume 36, issue 5, pages 641-650.

Gale, J.E., R. MacLeod, & P. LeMessurier, 1990, Site characterization and validation— measurement of flowrate, solute velocities and aperture-variation in natural fractures as a function of normal and shear stress, stage 3. Stripa Project Technical Report, volume 90, issue 11, 96 pages, https://inis.iaea.org/collection/NCLCollectionStore/_Public/22/037/22037162.pdf↗.

Hans, J. & M. Boulon, 2003, A new device for investigating the hydro-mechanical properties of rock joints. International Journal for Numerical Analytical Methods in Geomechanics, volume 27, issue 6, pages 513-548, doi: org/10.1002/nag.285↗.

Javadi, M., M. Sharifzadeh, K. Shahriar, & Y. Mitani, 2014, Critical Reynolds number for nonlinear flow through rough-walled fractures: the role of shear processes. Water Resources Research, volume 50, issue 2, pages 1789-1804, doi: org/10.1002/2013WR014610↗.

Lee, H.S. & T.F. Cho, 2002, Hydraulic characteristics of rough fractures in linear flow under normal and shear load. Rock Mechanics Rock Engineering, volume 35, issue 4, pages 299-318, doi: org/10.1007/s00603-002-0028-y↗.

Li, B., Y. Jiang, T. Koyama, L. Jing, & Y. Tanabashi, 2008, Experimental study on hydromechanical behavior of rock joints by using parallel-plates model containing contact area and artificial fractures. International Journal of Rock Mechanics and Mining Sciences, volume 45, issue 3, pages 362-375, doi.org/10.1016/j.ijrmms.2007.06.004↗.

Matsuki, K., Y. Kimura, K. Sakaguchi, A. Kizaki, & A.A. Giwelli, 2010, Effect of shear displacement on the hydraulic conductivity of a fracture. International Journal of Rock Mechanics and Mining Sciences, volume 47, issue 3, pages 436-449, doi.org/10.1016/j.ijrmms.2009.10.002↗.

144

Olsson, R. & N. Barton, 2001, An improved model for hydromechanical coupling during shearing of rock joints. International Journal of Rock Mechanics and Mining Sciences, volume 38, issue 3, pages 317-329, doi: org/10.1016/S1365-1609(00)00079-4↗.

Olsson, W.A. & S.R. Brown, 1993, Hydromechanical response of a fracture undergoing compression and shear. International Journal of Rock Mechanics and Mining Sciences & Geomechanics Abstracts, volume 30, issue 7, pages 845-851, doi: org/10.1016/S1365-1609(00)00079-4↗.

Rong, G., J. Yang, L. Cheng, & C.B. Zhou, 2016, Laboratory investigation of nonlinear flow characteristics in rough fractures during shear process. Journal of Hydrology, volume 541, part B, pages 1385-1394, doi: org/10.1016/S1365-1609(00)00079-4↗.

Wang, C., Y. Jiang, H. Luan, J. Liu, & S. Sugimoto, 2019, Experimental study on the shear-flow coupled behavior of tension fractures under constant normal stiffness boundary conditions. Processes, volume 7, issue 2, 57 pages, doi: org/10.3390/pr7020057↗.

Xiong, X.B., B. Li, Y.J. Jiang, T. Koyama, & C.H. Zhang, 2011, Experimental and numerical study of the geometrical and hydraulic characteristics of a single rock fracture during shear. International Journal of Rock Mechanics and Mining Sciences, volume 48, issue 8, pages 1292-1302, doi: org/10.1016/j.ijrmms.2011.09.009↗.

Yeo, I.W., M.H. de Freitas, & R.W. Zimmerman, 1998, Effect of shear displacement on the aperture and permeability of a rock fracture. International Journal of Rock Mechanics and Mining Sciences, volume 35, issue 8, pages 1051-1070, doi: org/10.1016/S0148-9062(98)00165-X↗.

Yin, Q., G.W. Ma, H.W. Jing, H. Su, Y. Wang, & R.C. Liu, 2017, Hydraulic properties of 3D rough-walled fractures during shearing: an experimental study. Journal of Hydrology, volume 555, pages 169-184, doi: org/10.1016/j.jhydrol.2017.10.019↗.

145

The GROUNDWATER PROJECT   © The Authors   Free download from gw-project.org

Anyone may use and share gw-project.org links. Direct distribution of the book is strictly prohibited.

Box 2 Lineament Extraction for Hydrogeologic Applications

The method of lineament interpretation has been used for a long time as a tool to select places for well drilling in fractured media. The criterion used is to drill the well as close as possible to at least one lineament. This is justified because a positive correlation between well production and lineaments has been identified in several places and by several authors (e.g., Parizek & Gold, 1993; Fernandes & Rudolph, 2001; Akinluyi et al., 2018). The premise of this application is based on the following: the circulation of water in fractured aquifers is linked to secondary porosity (fractures) and lineaments are often the surface expression of fracture zones (Figure Box2-1). Therefore, drilling wells along or close to these features should increase the chance of obtaining larger water production.

The most accepted definition of a lineament is provided by O'Leary and others (1976), who consider that lineaments are geomorphological linear features on the terrain surface, which are mappable and presumably reflect subsurface geological structure that is expressed as straight segments on the ground surface. The linear features do not necessarily correspond to fractures and this limitation should be taken under consideration.

A second possible application of lineament extraction is to identify the structural trends dominant in a region, aiming to identify their spatial variability from one area to another and thus the limits of structural domains. This application can be key to the study of the fracture network configuration and the establishment of conceptual flow models in fractured aquifers.
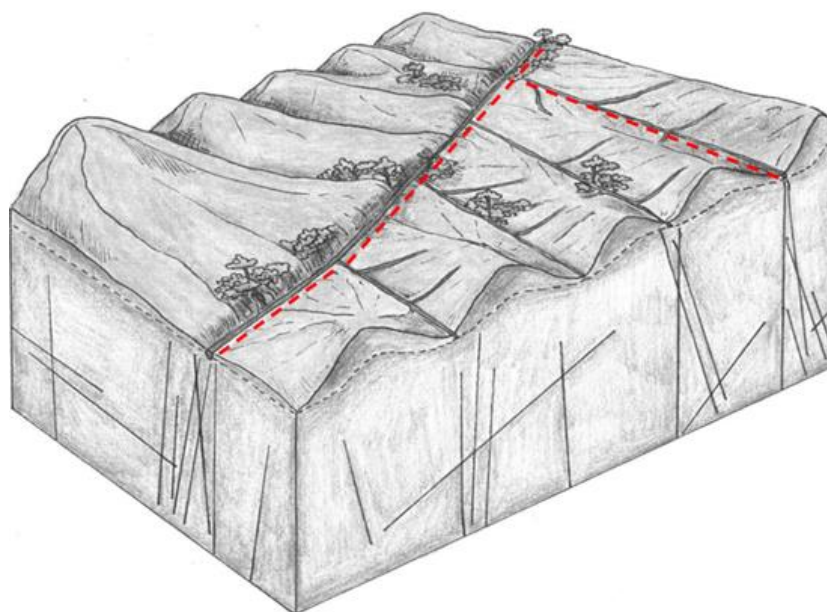

Figure Box2-1 - A lineament is a geomorphological linear feature on the terrain surface that presumably reflects subsurface geological structures. Lineaments are associated with straight stretches of rivers (some are highlighted by red dashed lines) and are the expression of fracture zones.

Box 2.1 Constraints on Lineament Interpretation

In order to take the most advantage of lineament interpretation, it is necessary to keep the following in mind:

- rectilinear morphological features can represent structures that often are not permeable;
- the geometric properties of fractures (aperture, density, dip) manifested as lineaments are highly variable;
- the scale of lineament extraction must be compatible with the purpose of the analysis;
- a large amount of subjectivity is involved in the task of identifying lineaments and procedures must be adopted to reduce this subjectivity;
- factors such as relief and thickness of the soil can significantly influence the extent and success of the application of lineament analysis; and,
- the representativeness and usefulness of a lineament map for evaluating fracture networks depends on the configuration of the fracture network.

These issues are briefly discussed in this box.

Box 2.2 Rectilinear Morphological Features

Lineaments can represent several types of planar structures that do not contain voids or support groundwater flow. These structures can be mylonitic shear zones, contacts between different lithologies, foliations, dikes, layers or veins of more resistant materials (e.g., quartzites). Gleeson & Novakowski (2009), for example, demonstrated that, in a specific crystalline rock setting of the Canadian Shield, the bedrock underlying lineaments is composed of poorly connected zones due to the presence of reduced permeability materials produced by fault processes. These authors suggest that the lineaments are mainly the expression of barriers to recharge and flow. Thus, in order to perform an adequate lineament interpretation, it is necessary to have a prior knowledge of the components that comprise the structural framework of a region. This knowledge must preferably come from detailed geological maps, which will enable a more realistic and reliable categorization of lineaments. The categorization is useful, for example, to make a distinction between lineaments associated with ridges and the ones associated with valleys. The former are frequently linked with rocks more resistant to erosion, such as dikes, veins, and mylonites, which by themselves do not carry groundwater and may represent barriers to flow.

Box 2.3 Geometric Properties of the Fractures

Brittle structures manifested as lineaments have variable geometric properties. Connectivity, persistence (Figure Box2-2), thickness and fracture density, either of a joint zone or a fault zone, are all variable and, as a consequence, one well located close to a lineament may intercept a variety of fractures with variable transmissivities. In general, a small percentage of fractures provide most of the groundwater flow. Another important geometric characteristic is the dip of a fracture zone; whenever possible it should be known in order to successfully intersect it when locating a well (Figure Box2-3).
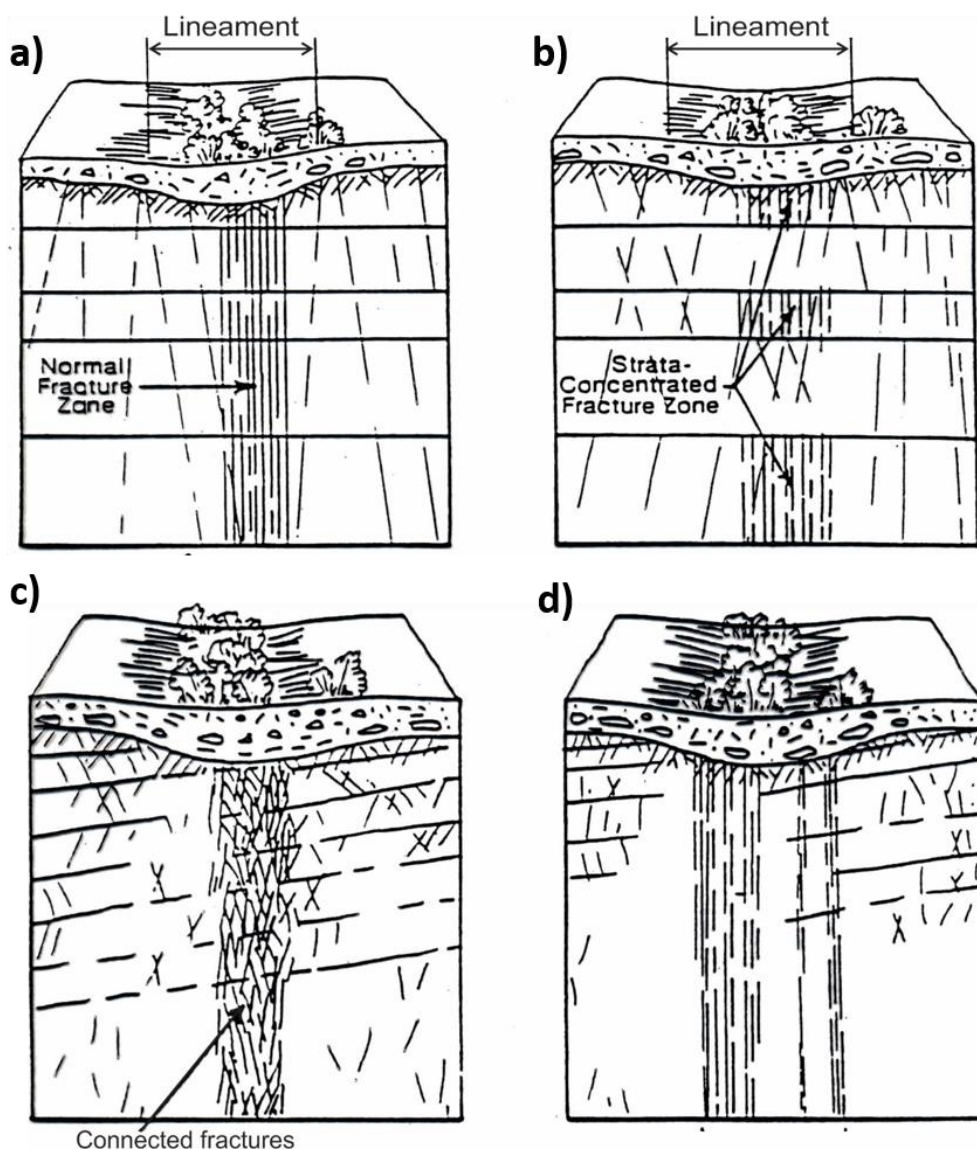
Figure Box2-2 - Lineaments are frequently expressed by straight stretches of rivers, brooks or ephemeral water streams. They can be related to several types of fracture zones as depicted in these sketches. (Parizek & Gold 1993). a) Single fracture zone of vertical, non-connected, and some throughgoing fractures. b) Discontinuous fracture zone of mostly bed-confined fractures. c) Fracture zone of relatively short but well-connected fractures. d) A few fracture zones formed by parallel non-connected fractures.
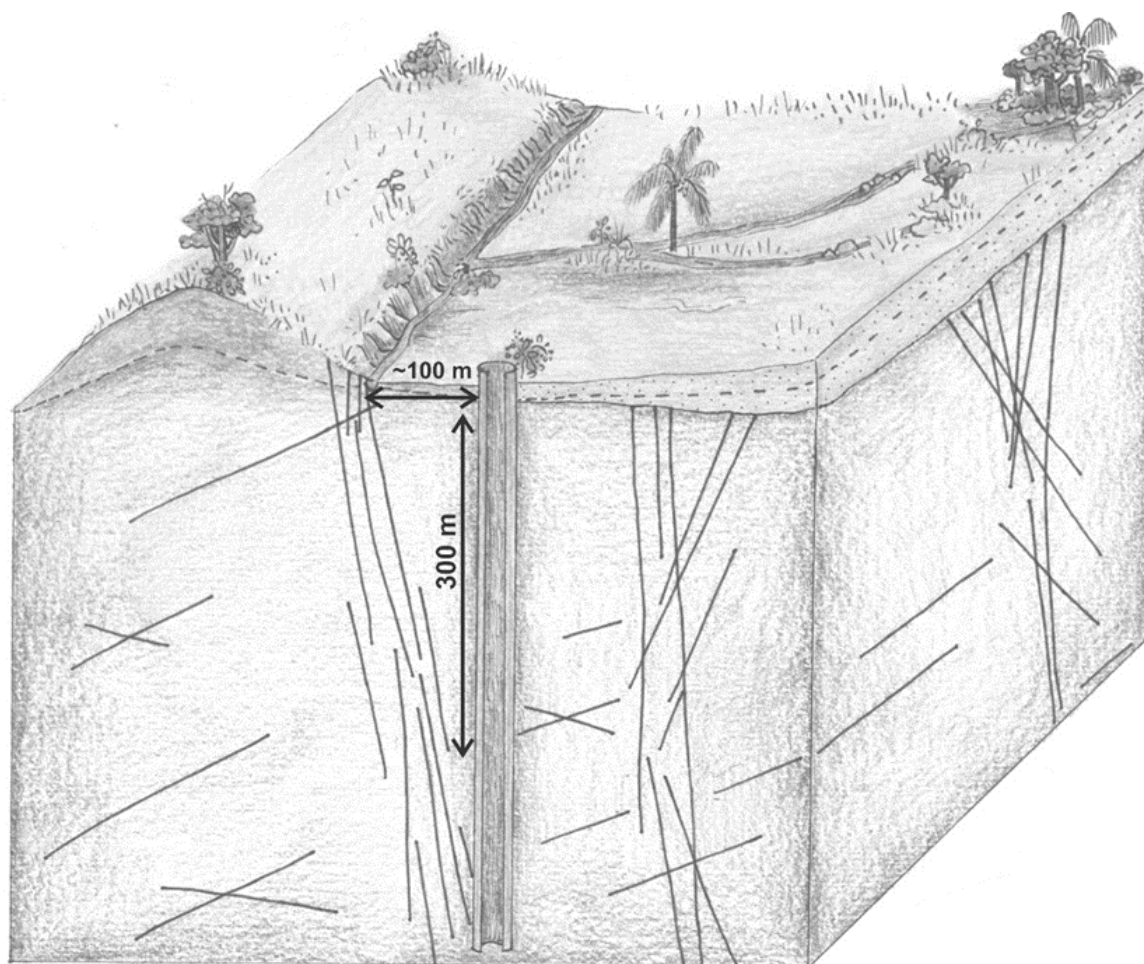
Figure Box2-3 - For a fracture zone that dips around 75° and a borehole that is 300 m deep, the maximum distance at which this zone will be intercepted by the well is around 100 m. At the scale of 1:25,000, 100 m corresponds to 4 mm on the terrain image or map. So, when it comes to selecting a place to drill a well, it is recommended that scales of around 1:25,000, or with a higher resolution, be used in order to precisely select the well location with regard to a lineament. On the right side of the image, the sedimentary cover, even though quite thin, precludes the expression of bedrock fracture zones as lineaments.

Box 2.4 Scale of Lineament Extraction

The scale of lineament extraction allowed by the type and resolution of the source material (i.e., satellite image, aerial photograph, or digital elevation model) is a key factor in the value of lineament analysis for a given application. When it comes to selecting locations to drill wells, it is necessary to have an accuracy of a few tens of meters in order to ensure that the well is drilled close to the lineament. Thus, scales greater than 1:25,000 (1 cm = 250 m) are recommended. Figure Box2-3 and Figure Box2-4 illustrate this issue. Figure Box2-3 also shows the importance of knowing the dip of the fracture zone so that the drilled well intersects it along its subsurface trajectory.

Figure Box2-4 - The lines shown in the two sketches are actual fracture traces (or lineaments) extracted from photographs taken at heights of 35 m and 80 m above the terrain surface in Norway (Odling, 1997). In this area there is no soil or sediment cover, and the bedrock is directly visible. The different h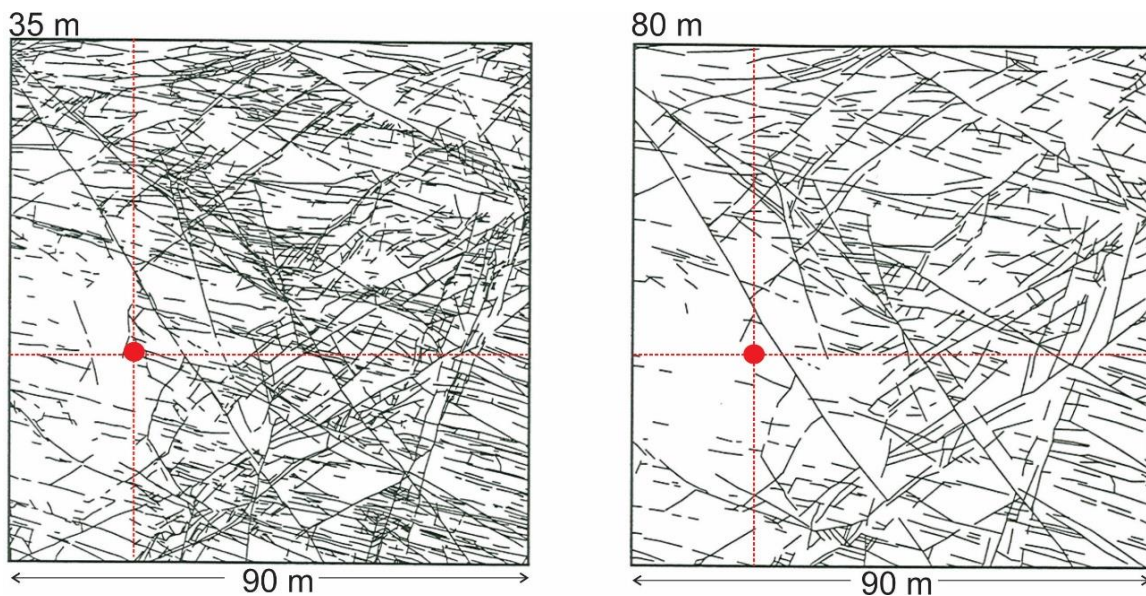eights at which the photographs were taken render different resolutions, and this strongly influences the number of lines that are identified. The red dot represents a well that has the same location on both maps. In the sketch of higher resolution (height = 35 m), the well is at the intersection of fracture traces. However, in the smaller resolution sketch (height = 80 m), no trace is seen at the well location.

Box 2.5 Subjectivity of Lineament Interpretation

Lineament extraction involves a great deal of subjectivity; this has already been recognized by everyone who dedicated themselves to this endeavor. A way of overcoming this drawback is for the data extraction to be separately conducted by two or three people and, afterwards, for a consolidation of the results to be carried out. Mabee and others (1994) showed that this procedure yields more reliable results. Some authors recommend automatic extraction, but this faces the great difficulty that features such as roads and rural property limits end up being falsely traced as lineaments. So, no matter how good the automatic outcome is, a non-automatic screening of the extracted lineaments will always be required. When it comes to locating wells, the target areas are usually quite small, and it is likely that manual extraction performed by a few people provides the best cost-benefit relationship.

Box 2.6 Rugged Topography

Rugged topography has a significant influence on the surface expression of joint and fault zones. This is because the more intense erosion, that takes place in rugged terrains, favor the appearance of geological structures in the form of linear features on the ground surface. On the other hand, the presence of sediments covering fractured rock masses may hinder the appearance of lineaments (Figure Box2-3). Thus, lineament maps tend to be more

150

The GROUNDWATER PROJECT © The Authors Free download from gw-project.org

Anyone may use and share gw-project.org links. Direct distribution of the book is strictly prohibited.

representative of the fracture trends in areas that are devoid of sediment cover and that experience more intense erosive processes.

Box 2.7 Lineament Map Representativeness

The extraction of lineaments carries an intrinsic sampling bias because they are, in general, the surface expression of steeply dipping fractures. Depending on the relief ruggedness, shallower dipping fractures, say less than 60°, will tend not to appear as lineaments on the surface and, therefore, a map of lineaments will not be representative of the entire fracture network. In addition, production wells are vertical thus mostly intercept fractures of low dip. A side consequence of wells being vertical is that their profiles do not provide representative estimates of the density of the high dip fractures. Thus, the assessment of the scope and reach of the lineament tracing method in a region must be based on the knowledge of the fracture network configuration, and this is achieved through rock exposure surveys.

The fracture configuration depends, to a large extent, on the rock types that constitute a given region (as described in Section 4.1). For example, in a region of flood basalts Fernandes and others (2007) concluded that the lack of correlation between the production rate of wells and lineaments was caused by the fact that the preferential groundwater flow paths in the basalts were subhorizontal fractures and these did not appear as lineaments on the terrain surface. Thus, even if some vertical fractures influence the production of the wells, this effect can be easily obscured by the greater influence of the subhorizontal fractures. Other authors (e.g., Parizek & Gold, 1993; Fernandes & Rudolph, 2001; Akinluyi et al., 2018) reported a positive correlation between the production of wells and lineaments in crystalline rocks, such as granite, gneiss, and schist, thereby reinforcing the idea that high dip fractures likely have a positive influence in those geological settings as illustrated in Figure Box2-5. However, Mabee (1999) points out that a set of factors, including proximity to lineaments, that explain the production of wells in one region are not necessarily relevant in another.
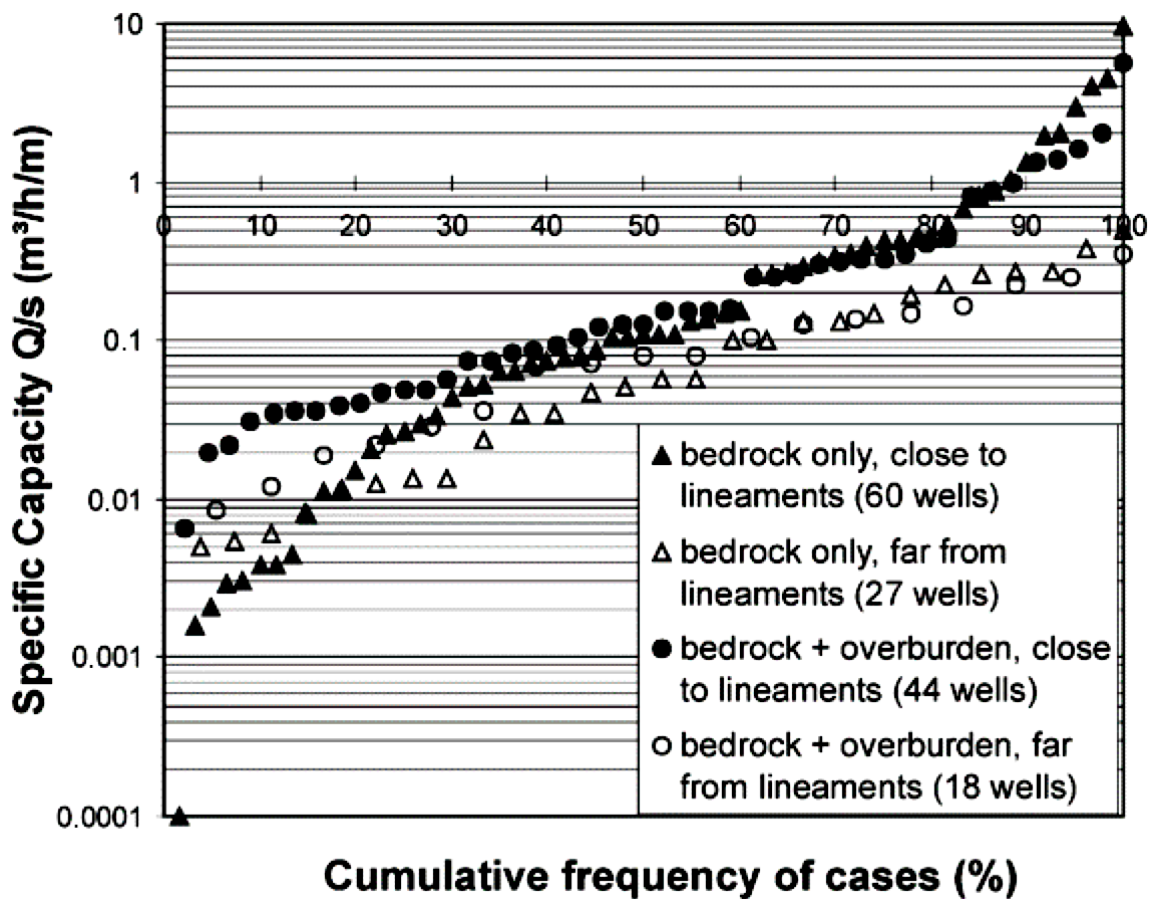
Figure Box2-5 - In a granitic-gneissic bedrock, the specific capacity is larger for wells located close to lineaments (solid circles and triangles). The median specific capacity of wells near lineaments exceeds 0.1 m³/h/m. Above the cumulative frequency of 60 percent, the difference between productivity of wells near to (solid markers) and far from lineaments (open markers) increases. The presence of overburden (both open and solid circles) influences only the wells with smaller specific capacities, as shown by the difference in productivity indicated by solid versus open circles and the difference between solid and open triangles on the left side of the graph (Fernandes & Rudolph, 2001).

Box 2.8 Recommendations

Given the above considerations, it is evident that although lineament analysis may be helpful, information on the configuration of the fracture network gleaned from bibliographic and/or field data is essential for evaluating the effectiveness of the method.

Although there are significant limitations, as mentioned above, this technique is inexpensive and may be of benefit to increase the chances of drilling higher-yield wells. This is especially important to communities that are threatened by water shortages and that do not have the resources to use more sophisticated methods.

Vulnerable regions, such as the ones in Africa, India, and northeastern Brazil, are largely made up of crystalline fractured aquifers. In addition, many of these regions have a drier climate, in which case analyzing the relationship between vegetation and lineaments may be a good strategy. For example, Gustafsson (1994) showed that the lineaments that maintain green vegetation at the end of the dry season could indicate the location of

152

fractures that are good groundwater conduits. Lineaments holding vegetation during the dry season were also reported by Corgne and others (2010).

The location of wells close to at least one lineament is considered a good criterion for increasing the chance of obtaining significant yields (e.g., Parizek & Gold, 1993). This is justified because intercepting fractures of different orientations increases the chance of crosscutting more permeable fractures.

The reduction of subjectivity involved in the method and the selection of sources that provide a proper scale are key aspects to successful application of lineament analysis. Unlike a few decades ago, when only aerial photographs and small-scale satellite images (e.g., 1:100,000) were available, there is now a wide range of available materials and digital elevation models are among the best (Figure Box2-6 and Figure Box2-7).
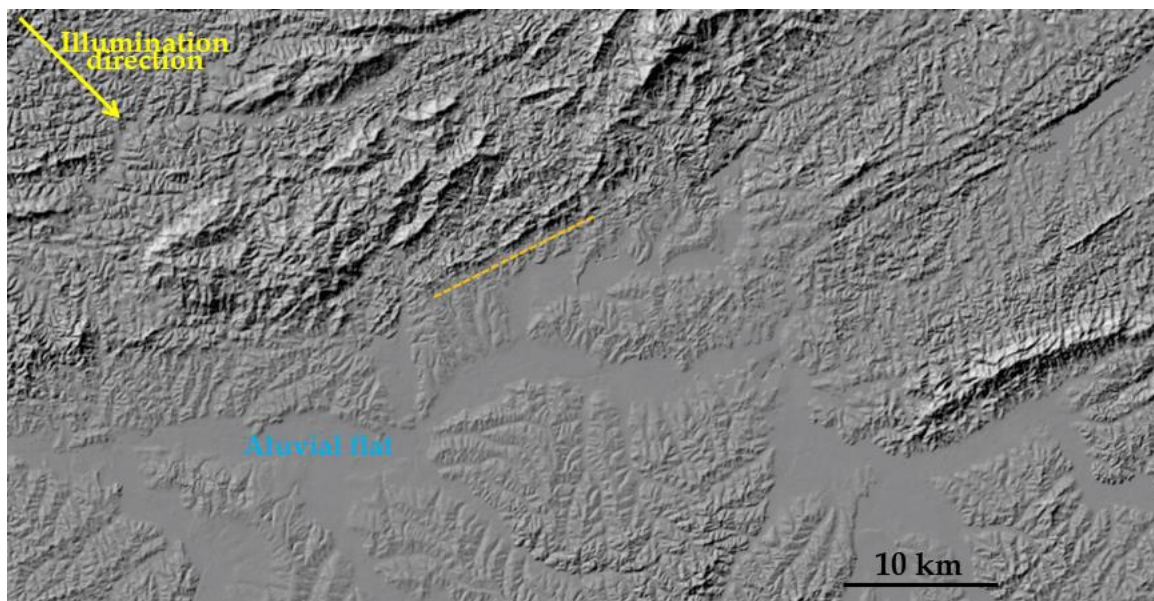
Figure Box2-6 - Shaded relief image from a digital surface model (DSM) (Zhou, 2016) showing a portion of the Metropolitan Region of São Paulo (Brazil) consisting of crystalline Precambrian rocks, covered in the central area by Tertiary and alluvial sediments (flat areas). This is a regional scale DSM (EMPLASA, 2010; Datageo, 2021) with a resolution compatible with the scale of ~1:60,000. In this image, the illumination comes from Northwest (N45W), so that the darkest shadows mostly highlight the NE lineaments (dashed orange line is an example). This DSM could be used to identify regional structural trends; however, it does not allow the estimation of the proximity of wells to lineaments.

153
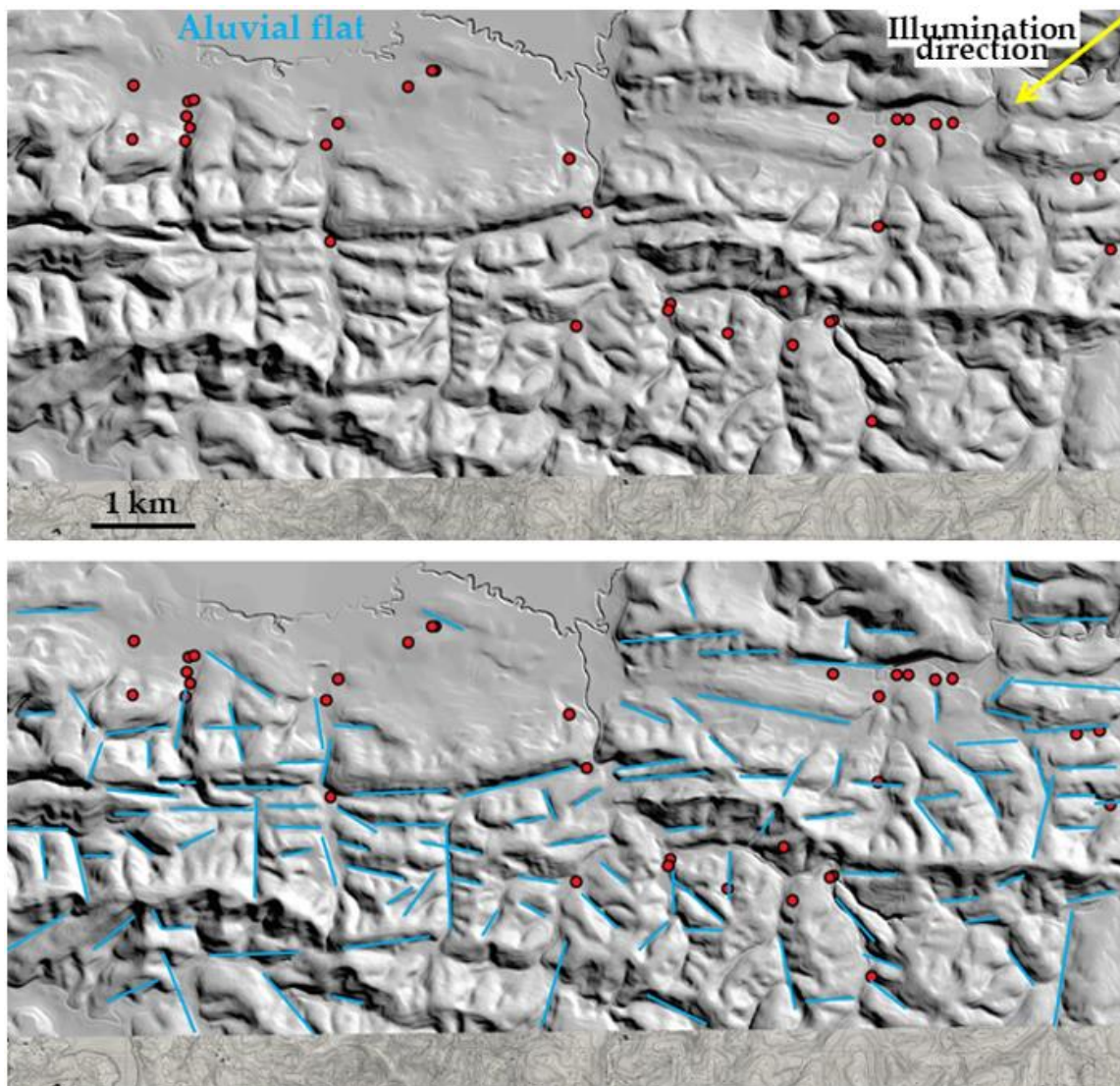
Figure Box2-7 - Shaded relief image from a digital elevation model (DEM) produced from a 1:10,000 topographic map (the bottom has altitude contours). This renders a resolution compatible with a scale between 1:10,000 and 1:25,000. Small drainages and water divides (top of rolling hills) are shown. The illumination comes from northeast (N45E). Lineaments (blue lines) are shown on the bottom image; noticeable ~EW-trending lineaments indicate that structures in this direction are very important in this area. The red dots show the location of existing wells. The DEM resolution is large enough to allow the estimation of the proximity of the wells to lineaments; this can be used to investigate, for example, the influence of proximity and direction of lineaments on well production. The definition and sources of DSM and DEM data can be found in, for example, Mukherjee and others (2013) and Zhou (2016).

For the successful application of the lineament method, it is essential to gather and build specific knowledge not only on the structural elements of a particular region, but also of the rock types and soil thickness.

The method of tracing lineaments has at least three types of applications:

a) selection of locations for drilling wells;

b) study of the relationships between hydraulic properties and brittle structures (e.g., Gleeson & Novakowski, 2009); and,

154

c) identification of the main structural trends as a first approach for delimiting hydrostructural domains.

In the first two cases, it is essential to make a very detailed and precise lineament extraction using materials that have an appropriate resolution. For the third case, the definition of the appropriate scale required to identify fracture trends and structural domains depends on the size of the domain being studied.

In the case of delimiting hydrostructural domains, exhaustive lineament extraction is not mandatory, the resulting lineament map only needs to be representative of the structural trends. The use of lineament extraction for mapping the limits of structural domains has been explored to some extent by Fernandes & Rudolph (2001). The authors showed that in areas with a certain pattern of lineament trends, wells near NW lineaments were more productive, whereas in areas with another pattern, wells in NNE lineaments were more productive. Furthermore, Fiume and others (2020) compared regional and local lineament patterns to evaluate whether fracture data from outcrops could be extrapolated to a site where no outcrops were available; at this site the survey of fracture data was conducted through scanlines along well optical televiewer (OPTV) images. The authors concluded that most of the fracture sets from both outcrop and well data were similar. The regional and local lineaments extracted from small- and large-scale sources, respectively, also showed similar trends.

The overall conclusion is that, if appropriate scales are used and care is taken to reduce the intrinsic subjectivities of this method, lineament extraction can and should be used as a preliminary structural characterization tool for various applications in hydrogeology. However, it is essential to recognize its inherent limitations such as the sampling bias related to the non-detection of low dip fractures, the type of relief and the presence of sediment cover.

Box 2.9 References

Akinluyi, F.O., M.O. Olorunfemi, & O.G. Bayowa, 2018, Investigation of the influence of lineaments, lineament intersections and geology on groundwater yield in the basement complex terrain of Ondo State, Southwestern Nigeria. Applied Water Science, volume 8, issue 49, pages 1-13, https://doi.org/10.1007/s13201-018-0686-x↗.

Corgne, S., R. Magagi, M. Yergeau, & D. Sylla, 2010, An integrated approach to hydrogeological lineament mapping of a semi-arid region of West Africa using Radarsat-1 and GIS. Remote Sensing of Environment, volume 114, issue 9, pages 1863-1875, https://doi.org/10.1016/j.rse.2010.03.004↗.

DATAGEO, 2021, Environmental Spatial Data Infrastructure of the State of São Paulo, Digital Surface Model of the State of São Paulo, datageo.ambiente.sp.gov.br (in Portuguese).

155

EMPLASA, 2010, São Paulo Metropolitan Planning Company, Digital Surface Model of the State of São Paulo, Mapeia São Paulo Project, São Paulo, Brazil, http://catalogo.governoaberto.sp.gov.br/dataset/http-www-mapeiasp-sp-gov-br↗ (in Portuguese).

Fernandes, A.J., M.M. Perrotta, E.D. Salvador, S.G. Azevedo, A. Gimenez Filho, & N. Paulon, 2007, Potential of fractured aquifers in the state of São Paulo: geological constraints. Ground Waters, volume 21, issue 1, pages 65-84, http://dx.doi.org/10.14295/ras.v21i1.16168↗ (in Portuguese).

Fernandes, A.J. & D. Rudolph, 2001, The influence of Cenozoic tectonics on the groundwater-production capacity of fractured zones: a case study in São Paulo, Brazil. Hydrogeology Journal, volume 9, issue 2, pages 151-167, http://dx.doi.org/10.1007/s100400000103↗.

Fiume, B., A.J. Fernandes, M.B. Barbosa, R. Hirata, & R.A. Bertolo, 2020, Integrated application of geophysical loggings and fracture survey on rock exposures for identifying transmissive fractures in crystalline aquifer: case study in the city of São Paulo. Brazilian Journal of Geology, volume 50, issue 1, 17 pages, https://doi.org/10.1590/2317-4889202020190034↗.

Gleeson, T. and K. Novakowski, 2009, Identifying watershed-scale barriers to groundwater flow: lineaments in the Canadian Shield. Geological Society of America Bulletin, volume 121, issues 3-4, pages 333-347, http://dx.doi.org/10.1130/B26241.1↗.

Gustafsson, P., 1994, Spot satellite data for exploration of fractured aquifers in a semi-arid area in Southeastern Botswana. Applied Hydrogeology, volume 2, issue 2, pages 9-18, https://doi.org/10.1007/s100400050246↗.

Mabee, S.B., 1999, Factors influencing well productivity in glaciated metamorphic rocks. Groundwater, volume 37, issue 1, pages 88-97, https://doi.org/10.1111/j.1745-6584.1999.tb00961.x↗.

Mabee, S.B; C.H. Hardcastle, & D.U. Wise, 1994, A method of collecting and analyzing lineaments for regional scale fractured-bedrock aquifer studies. Groundwater, volume 32, issue 6, pages 884-894, https://doi.org/10.1111/j.1745-6584.1994.tb00928.x↗.

Mukherjee, S., P.K. Joshi, S. Mukherjee, A. Ghosh, R.D. Garg, & A. Mukhopadhyay, 2013, Evaluation of vertical accuracy of open-source Digital Elevation Model (DEM). International Journal of Applied Earth Observation and Geoinformation, volume 21, pages 205-217, https://doi.org/10.1016/j.jag.2012.09.004↗.

Odling, N. E., 1997, Scaling and connectivity of joint systems in sandstones from western Norway. Journal of Structural Geology, volume 19, issue 10, pages 1257-1271, https://doi.org/10.1016/S0191-8141(97)00041-2↗.

O'Leary, D.W., J.D. Friedman, & H.A. Pohn, 1976, Lineament, linear, lineation: some proposed new standards for old terms. Geological Society American Bulletin,

156

The GROUNDWATER PROJECT   © The Authors   Free download from gw-project.org

Anyone may use and share gw-project.org links. Direct distribution of the book is strictly prohibited.

volume 87, issue 10, pages 1463-1469, https://doi.org/10.1130/0016-7606(1976)87%3C1463:LLLSPN%3E2.0.CO;2↗.

Parizek, R. & D. Gold, 1993, Fracture trace and lineament analysis. Pennsylvania State University, Course Notes, 91 pages.

Zhou, Q., 2016, Digital elevation model and digital surface model *in* International Encyclopedia of Geography: People, the Earth, Environment and Technology, pages 1-17, https://doi.org/10.1002/9781118786352.wbieg0768↗.

Return to where text linked to Box 2↱

11 Exercise Solutions

Solution Exercise 1

The block diagram below shows three types of structures: a mylonitic shear zone, a thrust fault, and a set of vertical joints. The shear zone is older than the thrust fault because the former is offset by the latter (termination of type "1" in Figure 56, Section 4.2). The joints are the youngest structures because some of them abut against the thrust fault at several locations (red circles in the figure below), implying that the fault existed when the joints were formed (termination of type "2" in Figure 56). One could argue that the joints could have been displaced by the fault. However, this is not the case because the presumed movement indicated by the joint traces (red circles) is not consistent with the fault offset.
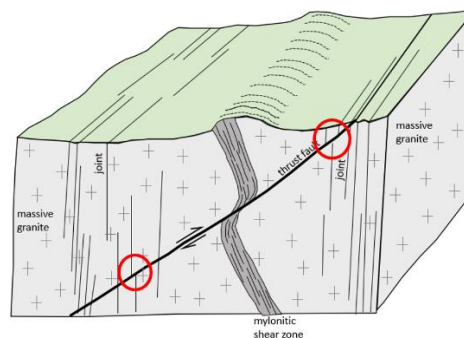
With increasing depth, brittle structures give way to ductile structures as illustrated by this modified image from Ramsay & Huber (1987).
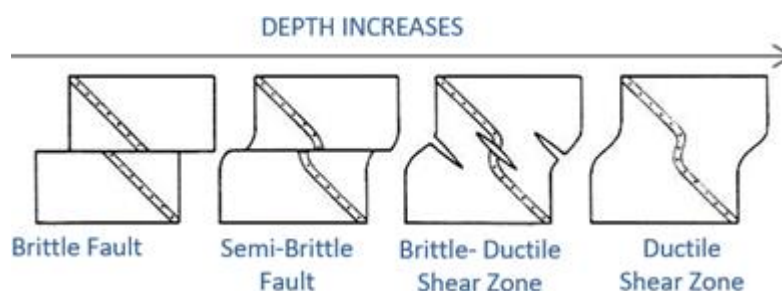
Shear zones comprised of mylonitic rocks are ductile structures, so they were formed at greater temperature and depth, or at a deeper crustal level. The joints are typical of shallower depths where brittle deformation occurs under lower temperatures. The thrust fault was formed under intermediate depths and semi-brittle conditions because it simultaneously offsets and causes the folding of the shear zone mylonitic rocks. These structures are currently side by side because uplift took place, causing the rock mass to pass from great to intermediate and finally to shallow depth, at which point the shear zone, thrust fault and joints were formed, respectively.

At the terrain surface, there is a long ridge accompanying the mylonitic shear zone. This indicates the rocks at the shear zone are more resistant to erosion than the host rock.

In this rock mass, the joints are the structures that, by themselves, are likely to be the most transmissive structures. Depending on the stress fields that affected the region after the formation of the joints, reactivation of the thrust fault surface and of the mylonitic foliation of the shear zone could have formed transmissive fractures along one or both.

Solution Exercise 2

Parameter values for use in this exercise are listed below. At the end of this solution, a section titled *Supplemental information for Exercise 2 - Elastic Properties Explanation* describes elastic properties.

$$\sigma_v \quad = \quad \text{vertical stress}$$

$$\rho \quad = \quad 2{,}500 \text{ kg/m}^3 \text{ (average rock density)}$$

$$g \quad = \quad 10 \text{ m/s}^2 \text{ (gravity acceleration)}$$

$$h \quad = \quad 3{,}000 \text{ m (depth)}$$

$$m_{dol} \quad = \quad 5 \text{ (dolomite Poisson number)}$$

$$m_{mud} \quad = \quad 4 \text{ (mudstone Poisson number)}$$

a) Vertical stress for the dolostone and mudstone

$$\sigma_v = \rho \; g \; h$$

$$\sigma_v = \frac{2500 \text{ kg}}{\text{m}^3} \frac{10 \text{ m}}{\text{s}^2} 3000 \; m = \frac{75{,}000{,}000 \text{ kg}}{m \text{ s}^2} \frac{1 \text{ Pa}}{\frac{1 \text{ kg}}{m \text{ s}^2}} \frac{1 \; MPa}{1x10^6 \; Pa} = 75 \text{ Mpa}$$

$$\sigma_v = 75 \text{ Mpa}$$

b) Horizontal stress for the dolostone

$$\sigma_{h \, dol} = \sigma_v / (m_{dol}-1) = 75 \text{ MPa} / (5 - 1) = 19 \text{ MPa}$$

Horizontal stress for the mudstone

$$\sigma_{h \, mud} = \sigma_v / (m_{mud}-1) = 75 \text{ MPa} / (4 - 1) = 25 \text{ MPa}$$

c) σ_v and σ_h are the larger and smaller stresses, respectively, so they correspond to the principal stresses σ_1 and σ_3, respectively. With the values of σ_v and σ_h known for each rock, the Mohr circles can be plotted in the Mohr diagram as shown below. Using the given equations, the mudstone and dolostone failure envelopes are plotted by calculating the shear stress τ at two points, for example, when σ_n is zero and 10 MPa (blue and brown dots, respectively). With these two points the failure envelopes can be drawn on the Mohr diagram.
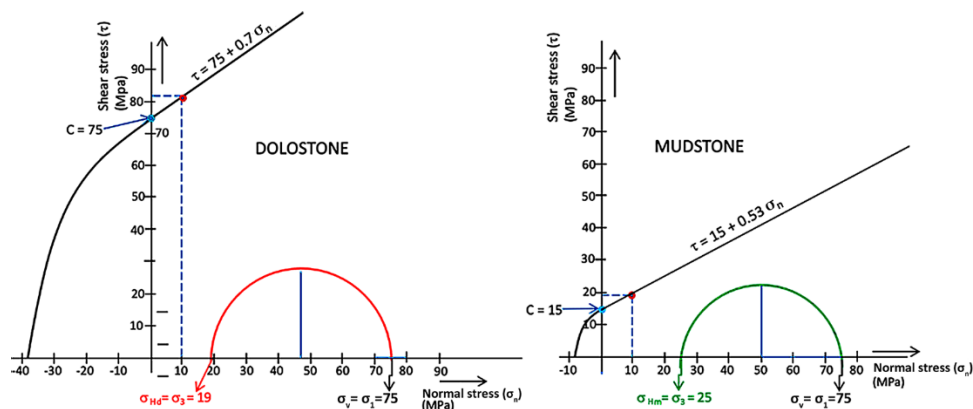
At the end of Section *Exercise 2*, a subsection titled *Supplemental information for Exercise 2 - Stress State Explanation* provides information that is useful to the developing the following answers.

d) Under the represented stress state, neither rock will undergo fracturing because neither Mohr circle intersects the shear failure envelope.

e) The cohesion (*C*) is determined where the failure envelope intersects the shear stress axis, so it is 75 MPa for the dolostone and 15 MPa for the mudstone.

f) *C* is much smaller for the mudstone, so it will undergo shear fracturing under smaller tectonic stresses than the dolostone.

Solution Exercise 3

a) The first Mohr diagram below shows the Mohr circles of tests 1 and 2 (sandstone tests) and a straight line drawn to intercept each circle at a single point. The same procedure is repeated on the second Mohr diagram for tests 3 and 4 (limestone tests). These lines are the failure envelopes for the sandstone and limestone, and the points represent the critical stresses at which shear fractures were formed.

Sandstone
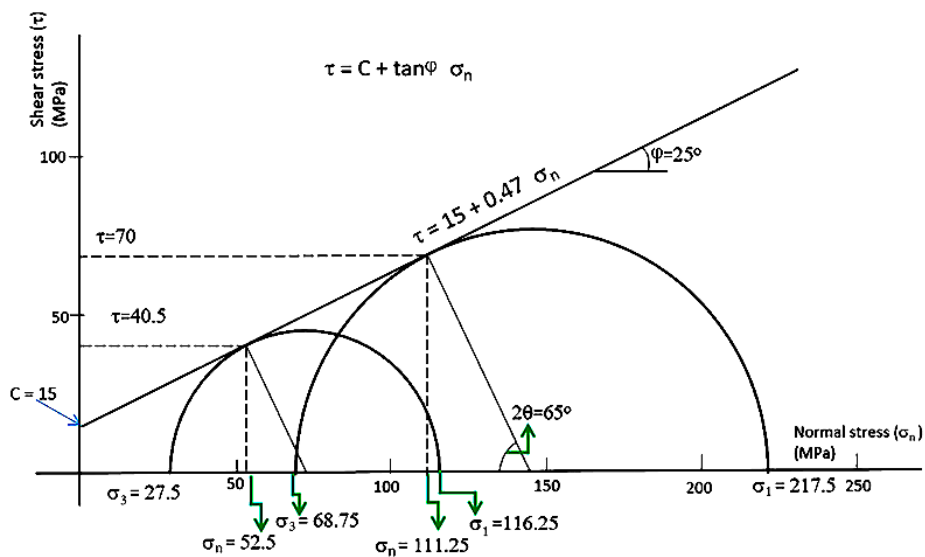
Test #	Principal stresses (MPa)	σ_n (MPa)	τ (MPa)
1	$\sigma_3 = 27.5$, $\sigma_1 = 116.25$	52.5	40.5
2	$\sigma_3 = 68.75$, $\sigma_1 = 217.5$	111.25	70

Limestone
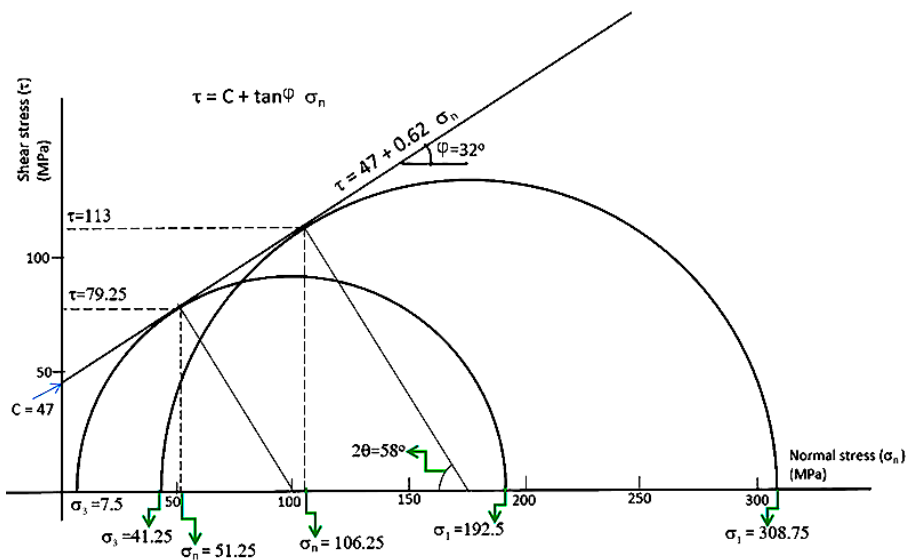
Test #	Principal stresses (MPa)	σ_n (MPa)	τ (MPa)
3	$\sigma_3 = 7.5$, $\sigma_1 = 192.5$	51.25	79.25
4	$\sigma_3 = 41.25$, $\sigma_1 = 308.75$	106.25	113

b) The slopes, φ friction angle, of the sandstone and limestone failure envelopes are manually measured as 25° and 32°, respectively.

c) The measured 2θ values between the shear conjugate fractures are 65° and 58° for the sandstone and limestone, respectively. The angle between the σ_1 and the shear fractures is equal to θ, so these are 32.5° and 29° for the sandstone and limestone, respectively.

d) The critical normal stress (σ_n) and shear stress (τ) that generated the shear fractures in each of the four tests are indicated along the shear and normal stress axes in the Mohr diagrams; the values are also shown in the corresponding tables.

e) The cohesion of each rock corresponds to the value at which each failure envelope intercepts the shear stress axis. The cohesion of the limestone is 47 MPa and is greater than that of the sandstone which is 15 MPa. Consequently, the sandstone can be fractured under lower stress.

f) In the case that both rocks occur in the same geological context and are subjected to the same stress fields, one should expect that the sandstone would have a denser fracture network because milder stress conditions would fracture the sandstone but not the limestone. One possible consequence is that a more densely connected fracture network is expected for the sandstone.

163

The GROUNDWATER PROJECT   © The Authors   Free download from gw-project.org

Anyone may use and share gw-project.org links. Direct distribution of the book is strictly prohibited.

Solution Exercise 4

The minimum principal stress (σ_3) has to be the same value as *T* (tensile strength of the rock) in order for extension fractures be formed. Consequently, joints are formed in the limestone when the value of σ_3 is equal to −27.5 MPa, the tensile strength *T* of the limestone. By the same token, the value of σ_3 for the sandstone should be −6.25 MPa.

The green and red Mohr circles drawn in the Mohr diagrams below represent possible stress conditions under which extension fractures are generated in the limestone and sandstone, respectively.

164
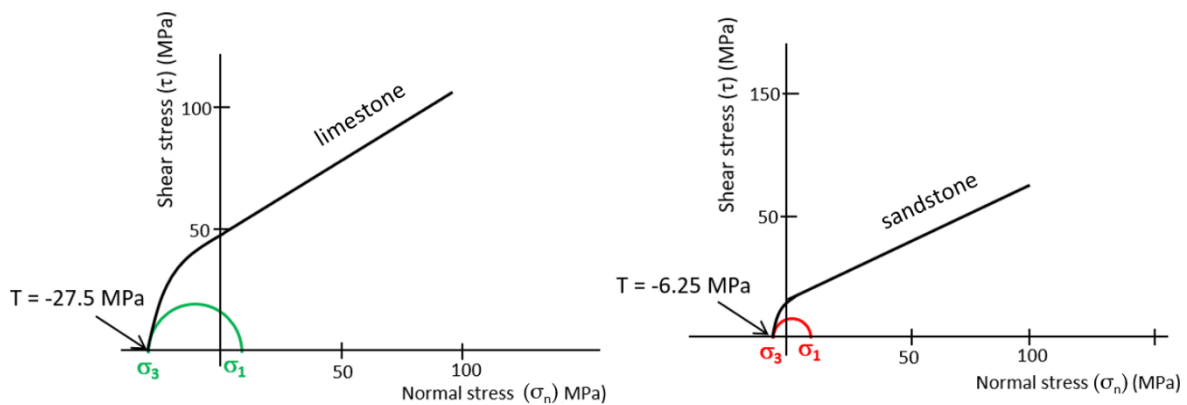
Solution Exercise 5

a) In the case where fluid pressure (p) is present, the Mohr circles would be displaced to the left, as shown in the diagrams below (vertical and horizontal axes are in MPa). The differential stress would remain the same because the fluid pressure is isotropic and reduces all of the stresses, in all directions, by the same amount.
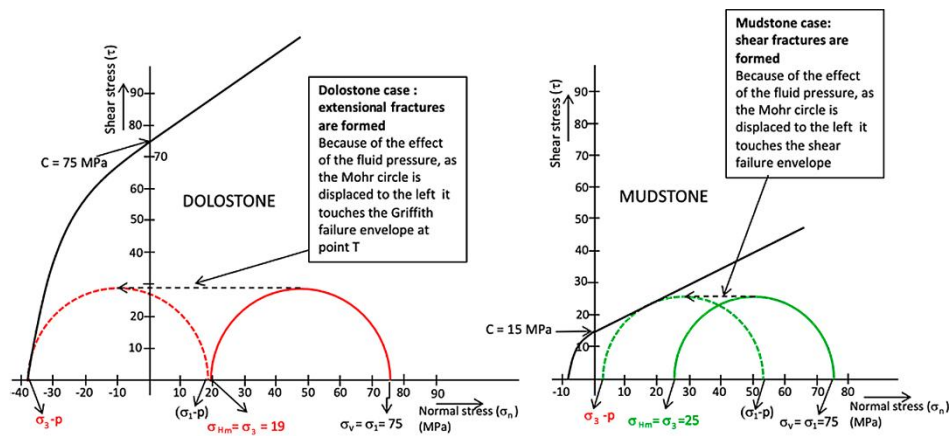
b) If the fluid pressure is high enough, the Mohr circles would be displaced to the left until each one intercepts its own failure envelope. In this situation, extension fractures are formed in the dolostone and shear fractures in the mudstone. The cohesion (C) of the dolostone is higher, so the lithostatic stresses would reach point T of the Griffith failure envelope and joints would be formed. On the other hand, the cohesion (C) of mudstone is lower; under the same lithostatic condition, its Mohr circle would reach the shear failure envelope (Mohr-Coulomb envelope), and shear fractures would be formed.

c) The Mohr diagram demonstrates that specific stress conditions can reach only one of the failure envelopes, so it is not possible to propagate both opening mode and shear mode fractures in the same rock, in a given location, at the same time.

Click to return to where text linked to Exercise 5⤴

Return to Exercise 5⤴

Solution Exercise 6

a) Mohr circle number 1 intercepts the shear failure envelope. Thus, under this stress condition, shear fractures will be formed. The image below shows drawings of the faults that are formed under the stress conditions represented in the Mohr diagram and table to their right. The Mohr circle shows only the stress magnitude and, in this case, is related to the formation of shear fractures (faults); the fault orientation (strike and dip) depends on the tectonic regime and on the stress orientation as specified in the table.
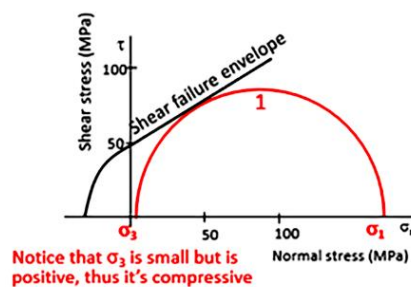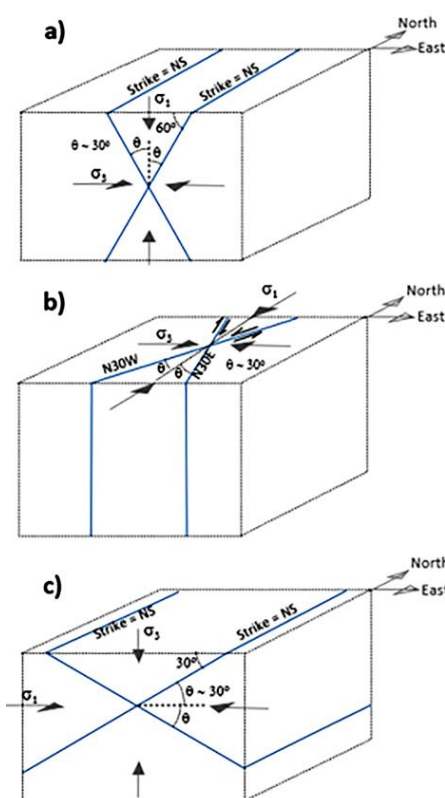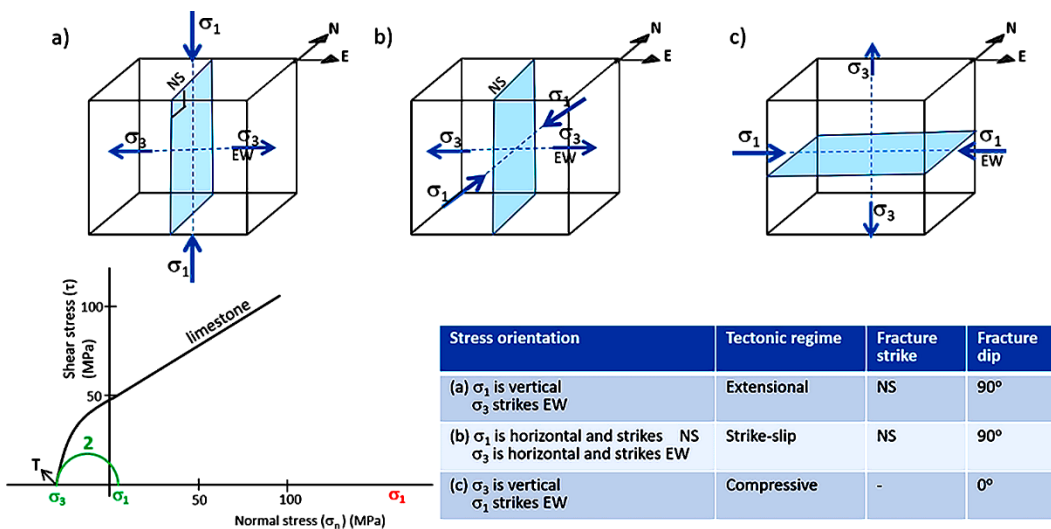

Stress orientation	Tectonic regime	Fracture strike	Fracture dip
a) σ_1 is vertical σ_3 is horizontal and strikes EW	Extensional	NS	60°
b) σ_1 is horizontal and strikes NS σ_3 is horizontal and strikes EW	Strike-slip	N30W and N30E	90°
c) σ_3 is vertical σ_1 is horizontal and strikes EW	Compressive	NS	30°

- When σ_1 is vertical, the tectonic regime is extensional and normal faults are formed. The normal faults must be perpendicular to σ_3 and, consequently, they strike NS. As with all of the shear fractures, the faults make an angle of ~30° with σ_1 and form a conjugate pair of faults dipping ~60°, toward either E or W as shown in part (a) of the above image.

- When both σ_1 and σ_3 are horizontal, σ_2 is vertical and the tectonic regime is strike-slip, i.e., strike-slip faults are formed. As is the case with all of the shear fractures, the faults make an angle of ~30° with σ_1, which is horizontal and strikes NS. Therefore, the directions of the conjugate strike-slip faults are N30W and N30E and they are approximately vertical (dip ~90°) as shown in part (b) of the above image.

166

The GROUNDWATER PROJECT   © The Authors   Free download from gw-project.org

Anyone may use and share gw-project.org links. Direct distribution of the book is strictly prohibited.

- When σ_3 is vertical, the tectonic regime is compressive and thrust faults are formed. The direction of the thrust faults is perpendicular to the direction of σ_1 and the corresponding normal faults strike NS. As with all of the shear fractures, they form a conjugate pair, each making an angle of ~30º with σ_1; their dip is ~30º, toward either E or W as shown in part (c) of the above image.

b) Mohr circle number 2 intercepts the failure envelope at point T (i.e., it means that $\sigma_3 = T$); thus, extension fractures (joints) will be formed. The image below shows drawings of the joints that are formed under the stress condition represented in the Mohr diagram and table shown below the drawings. The Mohr circle shows only the stress magnitude that, in this case, is related to the formation of extension fractures (joints). The joint orientation (strike and dip) depends on the tectonic regime and on the stress orientation as specified in the table.

Stress orientation	Tectonic regime	Fracture strike	Fracture dip
(a) σ_1 is vertical σ_3 strikes EW	Extensional	NS	90º
(b) σ_1 is horizontal and strikes NS σ_3 is horizontal and strikes EW	Strike-slip	NS	90º
(c) σ_3 is vertical σ_1 strikes EW	Compressive	-	0º

- When σ_1 is vertical, the tectonic regime is extensional. Joints are perpendicular to σ_3 (which is horizontal and strikes EW). Therefore, they are vertical and strike NS as shown in part (a) of the above image.
- When σ_2 is vertical, the tectonic regime is strike-slip. Joints are perpendicular to σ_3 (which is horizontal and strikes EW). Thus, they are vertical and strike NS as shown in part (b) of the above image.
- When σ_3 is vertical, the tectonic regime is compressive. Joints are perpendicular to σ_3 and, consequently, are horizontal as shown in part (c) of the above image. The existence of a vertical and negative (tensile) σ_3 is possible when fluid pressure is present; this is usually possible at some depth. When horizontal fractures are formed close to the ground surface (down to ~100 m depth), they are usually sheeting joints as explained in Section 3.6.

In both extensional and strike-slip regimes, joints are vertical. One can distinguish between the two regimes when plumes are present on the joint surface. The axis of the plume is parallel to σ_1 (as shown in Figure 33 and in the image presented in the solution of Exercise 8). Consequently, when the plume axis is horizontal, the tectonic regime is of the strike-slip type and when the axis is vertical, the regime is extensional (examples are shown in the photographs of Exercises 8, 9 and 11).

168
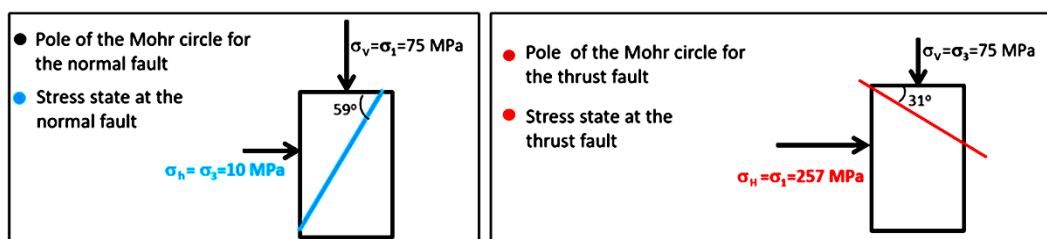
Solution Exercise 7

a) The Mohr circles drawn below are related to the formation of normal faults (blue) and thrust faults (red). The vertical stress is the weight of the rock column and is given in Exercise 14 as 75 MPa at the depth of 3,000 m.

   For the normal fault, the vertical stress σ_v corresponds to σ_1 (the maximum principal stress). When drawing the circle to find the stress state under which normal faults will form, we hold σ_v constant at 75 MPa and draw a circle to the left of the maximum principal stress, experimenting with its radius until it just intersects the failure envelope, then complete the blue circle in the image below down to the x-axis to determine the value of the horizontal stress (σ_3) and in this case $\sigma_3 = 10$ MPa.

   In the case of a thrust fault, the vertical stress σ_3 (is the minimum principal stress) so we hold σ_v constant at 75 MPa and draw a circle to the right of the minimum principal stress, experimenting with its radius until it just intersects the failure envelope so that thrust faults will be formed, then complete the red circle in the image below down to the x-axis to find the value of $\sigma_H = \sigma_1$, in this case 257 MPa.
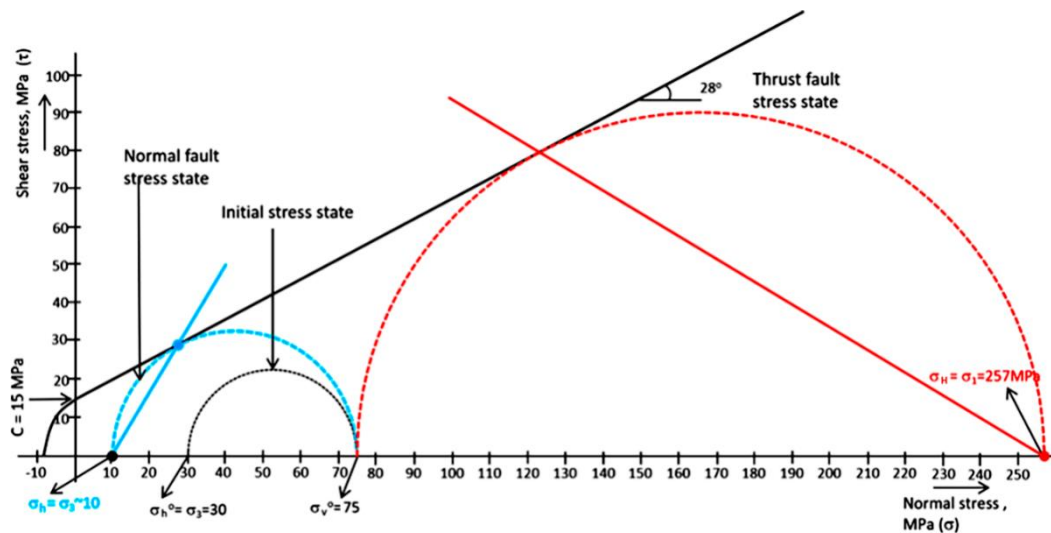
b) The dip of each fault is found either by measuring the angle of the blue (normal fault) and red (thrust faults) lines with the horizontal, or by the geometric relationships with φ. So, the dip of the normal fault is $45 + \varphi/2$ and that of the thrust fault is $45 - \varphi/2$, values that are $59°$ and $31°$, respectively.

c) The graph in Exercise 14c shows that, close to the surface, the in-situ average horizontal stress can be as large as 3.5 times the vertical stress. This situation extends from the ground surface down to depths of around 500 to 600 m, the depth range in which most aquifers are located. A consequence of this fact is that we can expect that the structures related to the compressive tectonic regime, either faults (dips around 30° or less) or joints (horizontal), will occur more frequently at shallower depths. Consequently, subhorizontal preferential pathways are expected to be more common at shallower depths.

Solution Exercise 8

a) The fracture shown in the photograph of Exercise 7a is depicted in the block diagram below. The very presence of the striae lineation on the face indicates propagation through shear. The dip of 60° and striae lineation parallel to the dip of the fracture are consistent with normal faults, which are generated in the extensional tectonic regime; this implies that σ_1 is vertical. In this regime, σ_3 is perpendicular to the direction of the fault, or N50W, and σ_2 is parallel to its direction.
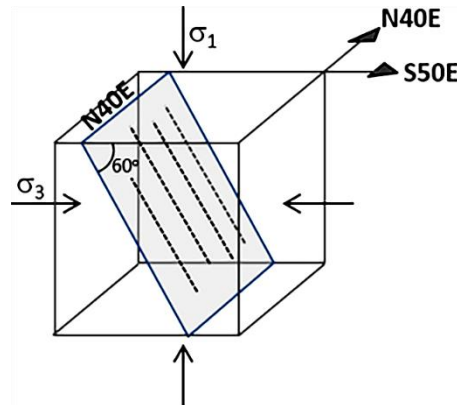

b) The fracture shown in the photograph of Exercise 7b is depicted in the block diagram below. The subvertical dip (88°) and the striae lineation on the face, almost parallel to the direction of the fracture, are consistent with strike-slip faults (propagated by shear) generated in the strike-slip tectonic regime. Thus, both σ_1 and σ_3 are horizontal and σ_2 is vertical. The direction of σ_1 depends on the movement sense of the fault. The small steps, transversal to the striae, imply a dextral movement (Petit, 1987) and the block to the right of the fault could have moved toward the observer, as shown in the block diagram. Therefore σ_1 is N70W and σ_3 (perpendicular to σ_1) is N20E. This is one possible interpretation and more field data would be necessary to confirm it.
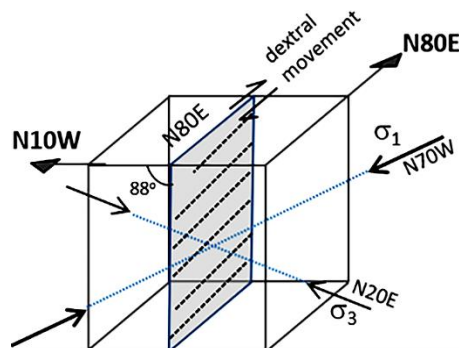
c) The fracture shown in the photograph of Exercise 7c is depicted by the block diagram below along with its striae lineation. The fracture presents two typical characteristics of faults (propagation by shear) generated in the compressive regime: a dip of 30° and striae lineation parallel to the dip of the fracture. In the compressive tectonic regime, σ_1

is horizontal and perpendicular to the direction of the fault. This means that the σ_1 direction is NS, σ_3 is vertical and σ_2 is parallel to the direction of the fault (EW).
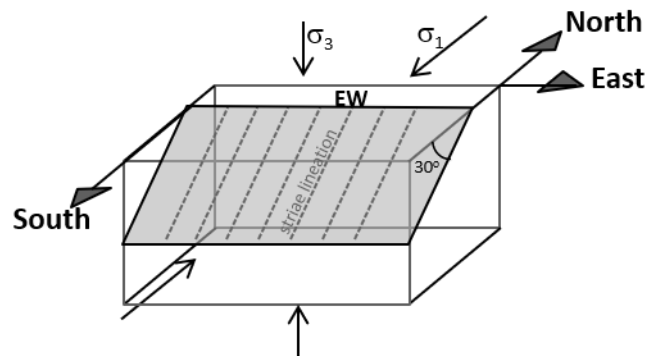
The exercise includes the statement "striae lineation is assumed to be formed at the same time as the fracture, i.e., the striae lineation was not formed by reactivation." This premise is reasonable because in each of the three faults illustrated by the photographs in exercise 7 both the fracture dip and the orientation of the striae lineation were consistent with a specific tectonic regime. The lack of this type of consistency, for example horizontal striae on fractures dipping 30º or 60º, would indicate reactivation.

Solution Exercise 9

a) The image below (modified from Dunne & Hancock, 1994) shows the orientation of the principal stresses with regard to a joint that bears a plume with a horizontal axis. The N30W/90 fracture bears a plume on its surface, which indicates that it propagated through the opening mode; thus, it is a joint. Because joints are perpendicular to σ_3, this stress is horizontal and strikes N60E. The axis of the plume is horizontal and, given that σ_1 is parallel to it (as shown in the image below), this stress is horizontal and strikes N30W. Because both σ_3 and σ_1 are horizontal, these fractures were formed under a strike-slip regime.
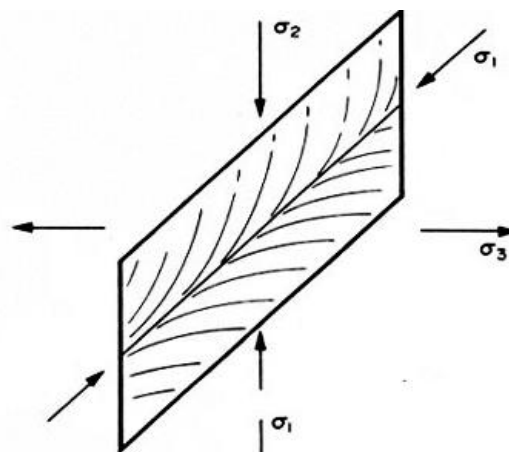
b) The EW/42SW fracture has a dip that is closer to the one of the thrust faults. However, the typical dip of these faults is 30° or less. So, more data, such as surface features (plume or striae, for example) and/or fracture pattern (conjugate or parallel) are needed in order to know the propagation mode, the principal stresses and the tectonic regime that produced this fracture.

c) It is not possible that both fracture sets have been formed during the same tectonic event, as the N30W/90 fracture was formed in the strike-slip regime and fractures of intermediate dip do not fit into any type of fracture pattern that is generated by that regime (Figure 30).

Solution Exercise 10

The N62E/74SE fracture bears a plume which indicates that it propagated through the opening mode; therefore, the fracture is a joint (extension fracture) and σ_3 is perpendicular to it, close to horizontal and striking at around N30W. Exercise 8 shows that σ_1 is parallel to the axis of a plume, so σ_1 should approach vertical. This implies that the tectonic regime is extensional (σ_1 is vertical and σ_3 is horizontal). However, the typical dip of joints of the Andersonian extensional regime is vertical. Thus, assuming that σ_1 is vertical, the fracture makes an angle of ~15° with this stress. This implies that it is a hybrid fracture, formed by both opening and shear modes.

Solution Exercise 11

a) The drawing below shows two conjugate fracture sets typical of the extensional tectonic regime. The two fracture sets have the same strike, around N45E, and a similar dip value, around 75°, but one set dips toward NW and the other toward SE. This pattern is typical of the conjugate fractures generated in the Andersonian extensional tectonic regime (Figure 30). They exhibit mutual abutting relationships (spots indicated by the black circles in the drawing below); the set that dips toward NW may abut against the set that dips toward SE, and vice versa. This means that these fractures were formed in the same tectonic event, which is consistent with the conjugate pattern.
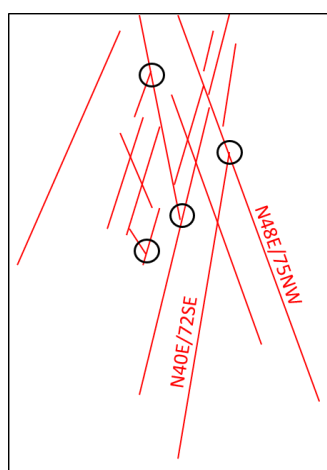
b) In the extensional regime, σ_3 is horizontal and perpendicular to the direction of the shear fractures (or normal faults). Therefore, its direction is N45W, σ_1 is vertical and σ_2 is parallel to the direction of the conjugate fractures. The typical dip of normal faults is around 60°. In this case, both sets dip at around 75°, meaning that 2θ is approximately 30°. This indicates that they are hybrid fractures formed simultaneously through shear and opening modes.

c) This fracture pattern provides connectivity. The fact that the fractures were formed by both shear and opening implies a larger fracture aperture than if they were formed only by shear. However, this applies to the time period when they were formed. In order to know whether the apertures are large at present would require systematic observations searching for evidence of groundwater flow (weathering, water leakage and vegetation) along these fractures and/or conduction of hydraulic tests. The intersections of the two fracture sets are horizontal and increased horizontal channel flow along these intersections may be significant for groundwater flow in the aquifer.

Solution Exercise 12

a) The dip of set 1 and the presence of striae lineation parallel to its dip are consistent with faults of a compressive regime; thus, they propagated through shear mode. In a compressive regime the maximum principal stress (σ_1) is horizontal and strikes perpendicularly to the direction of the faults; this corresponds to an average direction of N70W for σ_1. Also, σ_3 is vertical and σ_2 is parallel to the direction of fracture set 1.

b) Fracture set 2 bears a plume, which indicates a propagation by the opening mode, so the fracture is a joint; it is subvertical and, consequently, σ_3 is horizontal and strikes N45E (perpendicular to the direction of the fracture set). Subvertical joints can be formed by both extensional and strike-slip regimes. The axis of the plume, although irregular, is approximately horizontal, so σ_1 is likely horizontal and in the same direction as the fracture. Therefore, the associated tectonic regime is of the strike-slip type.

c) The existence of active fluid flow along the fractures of set 1 is indicated by the presence of vegetation, oxidation and, mostly, by the weathering of the rock. The surfaces of fracture set 2 are oxidized but, considering that the oxidation process can take place on any surface that is exposed to the atmosphere, this flow evidence is likely not as reliable as weathering of the rock. Based on the flow evidence (weathering, vegetation, and oxidation), it is likely that set 1 has higher K when compared to set 2; thus, set 1 is probably a preferential pathway for groundwater flow. Set 2 crosscuts set 1 (upper part of photograph (a) in Exercise 11), providing a connected network. Subhorizontal fractures of set 1 could form aquifer intervals that may be vertically connected by set 2. The extent of these connections depends on the persistence and density of set 2 fractures.

Solution Exercise 13

The same direction and high dips toward opposite senses are typical characteristics of conjugate fractures formed in the extensional regime; both the acute angle between the veins (around 10°), and the infilling of the fractures indicate that these are conjugate hybrid fractures simultaneously propagated by opening and shear. In this tectonic regime, σ_1 is vertical and σ_3 is horizontal and perpendicular to the direction of the conjugate fractures. In this case, the direction of σ_3 is N20W.

Click to return to where text linked to Exercise 13↥

Return to Exercise 13↥

Solution Exercise 14

Although the weathering indicates flow along the sheeting joints, it is reported in the literature that the hydraulic conductivity of horizontal joints tends to decrease considerably with depth. This happens because the vertical stress (weight of the rock column), which acts directly on the horizontal fracture as a normal stress, increases with depth and causes a gradual decrease of the joint aperture. The sheeting joints themselves are closely spaced within the first tens of meters from the ground surface. However, they tend to disappear below depths of 100 m.

Click to return to where text linked to Exercise 14↥

Return to Exercise 14↥

Solution Exercise 15

The image below schematically synthesizes the traces of the three subvertical fracture sets on the horizontal rock exposure described in Exercise 15.
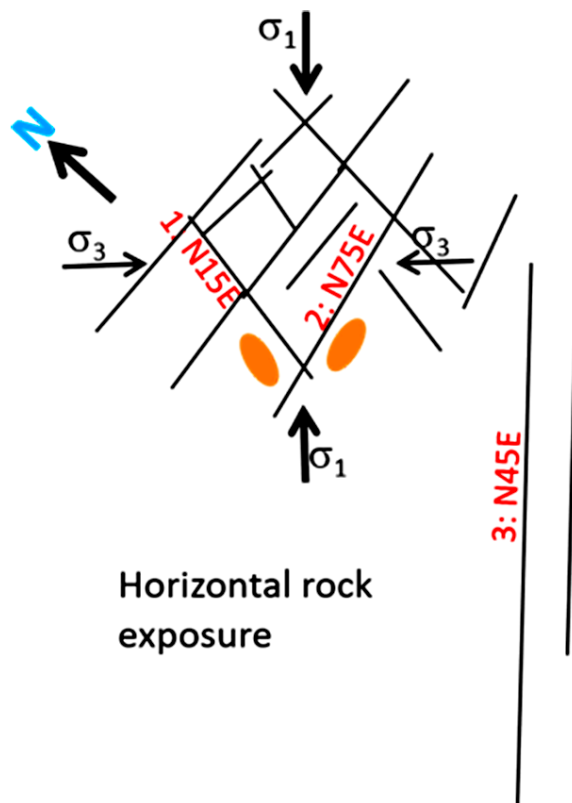
Fracture sets 1 and 2 occur in a consistent association forming a conjugate pattern of vertical fractures typical of the strike-slip tectonic regime. The 60º angle between them indicates they are conjugate fractures propagated by shear.

In the strike-slip regime the maximum and minimum principal stresses, σ_1 and σ_3, are both horizontal; the former is parallel to the bisector of the conjugate fractures, which strikes N45E, and the latter is perpendicular to σ_1 and its direction is N45W.

Fracture set 3 is comprised of persistent parallel fractures, which indicates that they are probably joints (opening mode fractures) that propagated perpendicular to σ_3. Thus, the direction of this stress at the time the joints were formed was N45W. This orientation is consistent with the stress field that generated sets 1 and 2. Thus, it is reasonable to think that all three sets were generated under the same tectonic event (same tectonic regime and stress orientation). However, conjugate fractures and joints cannot be formed precisely at the same time because σ_3 must be positive to form the conjugate sets 1 and 2 and negative to form set 3. This implies that the stress magnitude was variable during that tectonic event.

Fracture set 3 is persistent; and this coupled with the variable directions of sets 1 and 2 favors connectivity. Although set 3 is comprised of joints, presumably of greater aperture at the time they were formed, data on flow evidence would need to be collected in order to determine if this set currently bears significant groundwater flow. Systematic collection on flow evidence also needs to be performed for the other fracture sets.

Solution Exercise 16

All the necessary information to answer the questions of this exercise can be found in Figure 10, Figure 21 and Figure 30 of this book. The image below illustrates all three fracture sets in one block diagram with respect to their orientation and the stresses at the time of their generation.
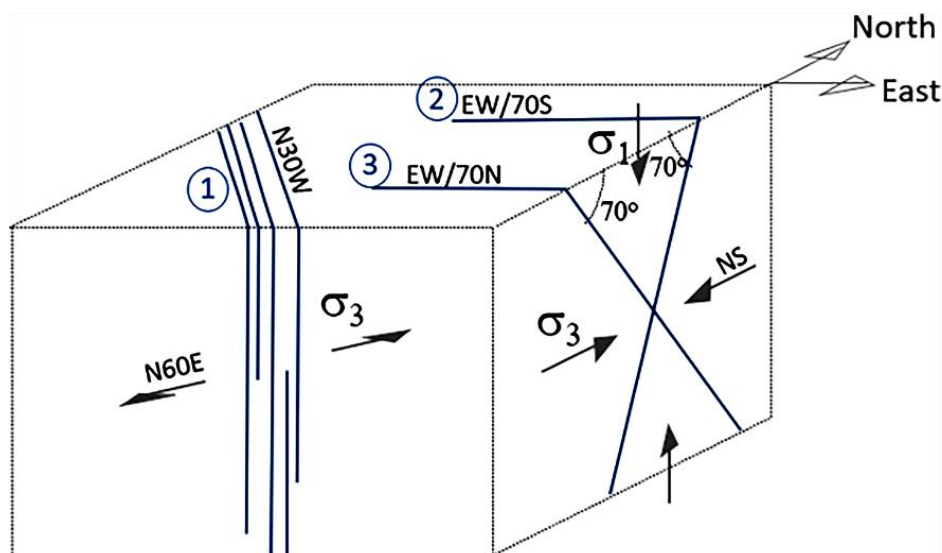
a) The parallelism of the fractures of set 1 (average orientation = N30–35W/ 85NE) and the associated dikes indicate an opening propagation mode. The dikes were emplaced because of the space created by the opening mode.

b) Joints are perpendicular to σ_3, so this stress at the time the NW joints were formed must have been horizontal. This is consistent with both extensional and strike-slip regimes.

c) The minimum principal stress σ_3 is horizontal and, because it has to be perpendicular to set 1, it must strike N60E on average. The available information is not enough to know whether the maximum principal stress, σ_1, was either horizontal (strike-slip regime) or vertical (extensional regime).

d) Sets 2 and 3 form a typical conjugate pattern of the extensional regime because they have the same direction (EW) and dip around 60–70° in opposite senses (set 2 dips toward south and set 3 toward north). So, sets 2 and 3 are faults that have propagated through shear.

e) In the extensional regime, σ_3 is horizontal and perpendicular to the strike of the faults, which means that σ_3 strikes NS. In addition, σ_1 is vertical and σ_2 is horizontal and parallel to the strike of the faults.

f) Fracture set 1 was formed by the opening mode. However, this alone cannot be taken as an indication of a larger present-day aperture. On the other hand, the weathering of the dikes that infill the fractures of set 1 is an indication that flow along those fractures

is currently taking place. Thus, K of set 1 is likely larger than the K of sets 2 and 3 because the surfaces of the latter are fresh and do not show any other evidence of flow. This means that greater K can be expected along the direction N30W. As the fracture zones of set 1 are vertically persistent (>80 m), the groundwater flow system may be well connected. The orientation and persistence of the three fracture sets favor connectivity. However, the spacing of set 1 fracture zones can be as large as tens of meters. The prediction of where these zones are and how they control preferential flow paths is a challenging task.

Click to return to where text linked to Exercise 16⤴

Return to Exercise 16⤴

Structural Geology Applied to
Fractured Aquifer Characterization
                                 Amélia João Fernandes, Alain Rouleau, and
                                       Eurípedes do Amaral Vargas Jr.

Solution Exercise 17

a) Fracture sets 1 and 2 have the same average direction, N20E, and dip toward opposite senses, NW and SE, respectively. These characteristics alone resemble both the conjugate fractures of thrust and normal faults. However, these sets are approximately perpendicular (they make an angle of roughly 80° to 90°) to each other and this is an indication that they do not form a conjugate pair.

Set 1 is formed by parallel fractures as shown in the photographs of Exercise 17, although the dip varies by around 20° from line 1 to line 2. The parallelism is a pattern typical of joints formed by the opening mode, but the dips do not fit any of the Andersonian tectonic regime. Consequently, none of the stresses that generated set 1 are vertical. As we have seen, joints have to be perpendicular to σ_3, so set 1 was generated perpendicularly to a σ_3 that dips around 45° toward S70E.

Fracture set 2 is also formed by subparallel fractures, so we assume that they are also joints. At the time of the formation of set 2 (average orientation = 20E/40SE), σ_3 dipped around 50° toward N70W.

The subvertical dips and subhorizontal striae lineation of set 3 (average orientation = N70W/88SW) are both consistent with strike-slip faults of the strike-slip tectonic regime where σ_2 is vertical. The presence of gouge zones (the original rock was finely ground) indicates that the deformation was intense. The shear sense is not known, so we can only say that σ_1 is horizontal and can be either ~N40W, in the case where the faults are dextral, or ~N80E, in the case where they are sinistral.

b) Sets 1 and 2 abut against each other, and the σ_3 necessary to generate set 1 is perpendicular to the one that generated set 2. Both characteristics together suggest that they were formed by a single tectonic event in which the σ_3 orientation probably alternated with the orientation of σ_2. This is similar to the gridlock joint pattern, although in this pattern both joint sets are vertical and the tectonic regime is Andersonian.

The fact that sets 1 and 2 cut through set 3 is, by itself, an indication that they are younger. The deformation caused by the faults of set 3 is intense and forms a gouge. Thus, if sets 1 and 2 were older, they would have been strongly disturbed by the faults.

c) The three fracture sets provide a well-connected fracture network due to the following characteristics: set 1 is formed by closely spaced and persistent fractures (the fractures continue beyond the rock wall exposures), with frequent fracture zones; fractures of set 1 are well connected to sets 2 and 3, as they are approximately orthogonal; and all sets occur in both lines. Weathering along fracture set 1 as shown in photograph (a) of Exercise 17 is evidence of flow in present time. This

182

suggests that flow could predominantly take place along set 1 fractures. Because of the low dips of the fractures of this set, it is likely that an important horizontal flow component toward WNW (dip sense of set 1) takes place. A thorough analysis of the flow evidence of all the fracture sets should be carried out in order to develop a more complete understanding on the preferential flow paths.

Regarding groundwater extraction, this location seems to have a favorable potential. The low dips of set 1 and 2 increase the probability that vertical wells will intercept a large number of fractures, mainly those of set 1 because of its density. This situation improves the chance of intersecting high-*K* fractures.

12 Notations

$1/v$ Poisson's number (m) the inverse of Poisson's ratio [$M^0L^0T^0$, dimensionless]

C cohesion or intrinsic shear strength of material [$ML^{-1}T^{-2}$]

CDZ composite deformation zone

C_f cohesion or intrinsic shear strength along-foliation feature [$ML^{-1}T^{-2}$]

DDZ distributed deformation zone

E Young's modulus [$ML^{-1}T^{-2}$]

e fracture aperture [L]

e_v vertical compression [LL^{-1}, dimensionless]

FPF foliation parallel fracture

g gravitational acceleration [LT^{-2}]

h depth [L]

ISF intermediate to high dip fracture

K hydraulic conductivity [LT^{-1}]

k permeability [L^2]

K_f fracture hydraulic conductivity [LT^{-1}]

LDZ localized deformation zone

MPa megapascal [10^6 Pascals]

N number of fractures per unit length [L^{-1}]

ρ density [ML^{-3}]

p fluid pressure [$ML^{-1}T^{-2}$]

R_1 Riedel shear [same sense of movement]

R_2 Riedel shear [opposite sense of movement]

SFF single fracture fault

SHF subhorizontal fracture

S_{Hmax},   maximum horizontal stress [$ML^{-1}T^{-2}$]

SVF subvertical fractures

S_z vertical stress [$ML^{-1}T^{-2}$]

T definition depends on context, fluid flow - transmissivity [L^2T^{-1}]

T definition depends on context, material property - tensile strength [$ML^{-1}T^{-2}$]

t_f intrinsic transmissivity [L^3]

TFZ throughgoing fracture zone

v Poisson's ratio [$M^0L^0T^0$, dimensionless]

v   Darcy flux [L^2T^{-1}]

z depth [L]

Δh hydraulic head gradient [LL^{-1}, dimensionless]

μ dynamic viscosity [$ML^{-1}T^{-1}$]

φ friction angle [°]

σ_1 maximum principal stress [$ML^{-1}T^{-2}$]

σ_2 intermediate principal stress [$ML^{-1}T^{-2}$]

σ_3 minimum principal stress [$ML^{-1}T^{-2}$]

σ_h horizontal stress [$ML^{-1}T^{-2}$]

$\sigma_h°$ initial horizontal stress [$ML^{-1}T^{-2}$]

$\sigma_{h\ dol}$ dolostone horizontal stress [$ML^{-1}T^{-2}$]

185

$\sigma_{h\,mud}$ mudstone horizontal stress $[ML^{-1}T^{-2}]$

σ_n normal stress $[ML^{-1}T^{-2}]$

σ_v vertical stress $[ML^{-1}T^{-2}]$

$\sigma_v°$ Initial vertical stress $[ML^{-1}T^{-2}]$

τ shear stress $[ML^{-1}T^{-2}]$

θ angle between shear fracture and σ_1 $[°]$

13   About the Authors

Dr. Amélia João Fernandes obtained a Bachelor of Science degree in geology, completed a Master of Science thesis on ductile deformation of Precambrian rocks, and completed a Doctor of Philosophy thesis at the University of São Paulo-USP, Brazil on brittle deformation and the production of wells in fractured aquifers. She joined the Geological Institute in 1988 as a researcher and had sabbatical leaves in Canada at the universities of Waterloo, Québec at Chicoutimi, and Calgary. She has mostly dedicated herself to the application of structural geology in the characterization of fractured aquifers, carrying out and coordinating projects mainly in the context of Precambrian crystalline rocks and Cretaceous basalts. In addition, she also teaches and advises graduate students at the Geosciences Institute-USP. She has increasingly been dedicating herself to the transfer of knowledge on groundwater to the watershed committees of the state of São Paulo, Brazil.

Dr. Alain Rouleau obtained a Bachelor of Science degree in engineering geology and completed a Master of Science thesis in structural geology, both at Laval University in Québec City. He was a geological consultant for a few years before completing his Doctorate at the University of Waterloo in 1984 with a thesis dealing with fracture characterization and groundwater flow modeling in hard rock. After two years conducting research at Environment Canada, he joined the University of Québec at Chicoutimi (UQAC) in 1986 as a professor, where he has been teaching, servicing communities, and conducting research. He has participated in field research on five continents. As emeritus professor at UQAC since 2016, he continues to pursue research in hydrogeology and fracture system characterization in rock. Current endeavors also include efforts to make hydrogeological knowledge widely available and effectively used in environmental and land management issues.

Dr. Eurípedes A. Vargas Jr. graduated in civil engineering at São Carlos School of Engineering, University of São Paulo. He subsequently obtained a Master of Science degree in geotechnical engineering at the Catholic University in Rio de Janeiro. In 1975, he joined the Faculty of the Department of Civil Engineering at the same university. In 1977, he was admitted in the Rock Mechanics Section of the Royal School of Mines of Imperial College, London, to pursue a Doctor of Philosophy program in rock mechanics, which he completed in 1982. The research topic of his dissertation was numerical modeling of coupled hydromechanics problems in fractured media. Upon returning to his position at Catholic University in Rio de Janeiro, besides teaching basic rock mechanics courses, he has continued to conduct research in experimental and numerical topics in rock mechanics, with particular interest in the analysis of hydromechanics problems in fractured media. Current research also includes modeling the genesis of geological structures such as faults and joints.

Please consider signing up for the GW-Project mailing list to stay informed about new book releases, events, and ways to participate in the GW-Project. When you sign up for our email list it helps us build a global groundwater community. Sign up↗.

Modifications to Original Release

Changes from the Original Version to Version 2

Original Version: April 13, 2023, Version 2: April 17, 2023

Specific changes:

page iii, publication date corrected from 2022 to 2023

Changes from Version 2 to Version 3

Version 2: April 17, 2023, Version 3: April 18, 2023

Specific changes:

page numbers refer to the pdf of version 2

page 92, first image, under the circle to the right, changed "equal area stereogram" to "equal angle stereogram"

page 94, first image, under the circle to the right, changed "equal area stereogram" to "equal angle stereogram"

A